CERN 89-10
ECFA 89-124
Volume 2
24 November 1989

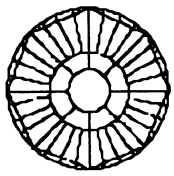

ECFA STUDY WEEK

on Instrumentation Technology for High-Luminosity Hadron Colliders

PROCEEDINGS
VOL. 2

Editors: E. Fernandez
G. Jarlskog

ECFA/CERN/CICYT/EEC Workshop
held at
Universitat Autonoma de Barcelona, Bellaterra, Barcelona, Spain
14-21 September 1989

ISSN 0007-8328
ISBN 92-9083-017-4

ABSTRACT

The main aim of the present ECFA Study Week on 'Instrumentation Technology for High Luminosity Hadron Colliders' was to review the progress made after the La Thuile Workshop (1987) and to critically evaluate which of the detection methods and data handling structures could be suitable for luminosities in the 10^{34} cm^{-2} s^{-1} range. The Study Week was sponsored by the Universitat Autonoma de Barcelona, the Comision Interministerial Ciencia y Tecnologia of Spain, CERN, and the Commission of the European Communities. It attracted 220 participants, including 35 from industry and good representation from groups planning experiments at the SSC. The various conveners gathered many excellent and original contributions, which led to intense discussions. Subjects covered include the use of scintillating fibres; silicon, gaseous, and crystal detectors, particle identification; readout and data acquisition systems. A separate session dealt with the contributions of industry to this kind of research.

CONTENTS

Volume 1

Volume 2

Session 6

GASEOUS DETECTORS

Gaseous Track Detection at Future Supercolliders

J B Dainton
Department of Physics
Oliver Lodge Laboratory
University of Liverpool
P O Box 147
Liverpool L69 3BX, UK

Abstract

The use of gaseous detectors for charged track detection and reconstruction are considered at the new supercolliders SSC and LHC. The problems associated with the proposed high luminosity and bunch crossing structure of these machines are elucidated for operation of gaseous drift chambers with different cell geometries and long memory times. The usefulness of arrays of such devices as charged particle spectrometers is considered. The inclusion of transition radiation X-ray detection in a hybrid charged track spectrometer with electron identification is discussed.

1 Introduction - the Task

Most experimental physicists might subscribe to figure 1 as their picture of hadron supercollider physics and its sustaining motivation during the long years of experimental preparation. At large angle, that is high p_T, new physics, characteristic of the new energy scale at these machines, is expected. It will come with low rate and in the central phase space region. If we are prepared to extend our polar angular range to below $\sim 30^\circ$ (beyond $\sim 150^\circ$) there may still be surprises in the physics of old quanta (W's, Z's, quarks and leptons) in new phase space. Such physics will come with a significantly larger rate than hitherto available at present day colliders. Below $\sim 5^\circ$, that is resting in peace in the beam pipe, will be the immense rate of archaeological physics of the late 1960s and 1970s.

This experimentalists' picture assumes a terrifying reality in the high luminosity of a supercollider, $\sim 10^{33}$ cm^{-2} s^{-1} at SSC and, may be, even $\sim 5 \times 10^{34}$ cm^{-2} s^{-1} at LHC. With 100 mb of inelastic pp interaction cross section and a mean number ~ 7 charged particles per unit of rapidity y per minimum bias event, the event characteristics which a detector must handle are best summarised by the lines of fixed rapidity in figure 1 between which roughly uniform numbers of charged secondaries are to be found. More specifically Hanson [1] has simulated typical interesting events - examples are in figures 2. Clearly charged track detection, even in a magnetic field of 2 T, is a challenging business in which it is unclear to what extent one attempts to reconstruct all tracks within one's geometrical acceptance.

With figure 2 in mind, a way of proceeding is to adopt the philosophy that charged track detection at a supercollider must be capable of *at least* assisting with the identifi-

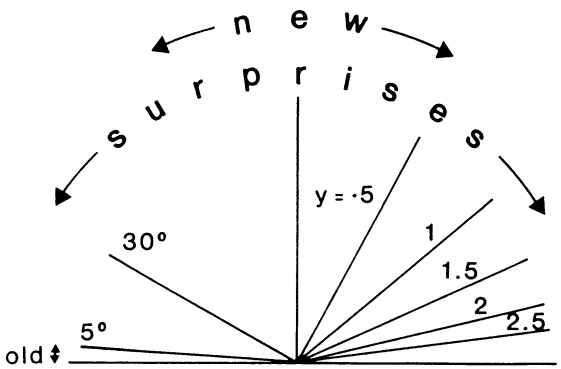

Figure 1: Experimentalists' picture of physics at the SSC: with respect to the beam axis lines of different polar angle and lines of different rapidity y are drawn: minimum bias event rates are roughly uniform in y.

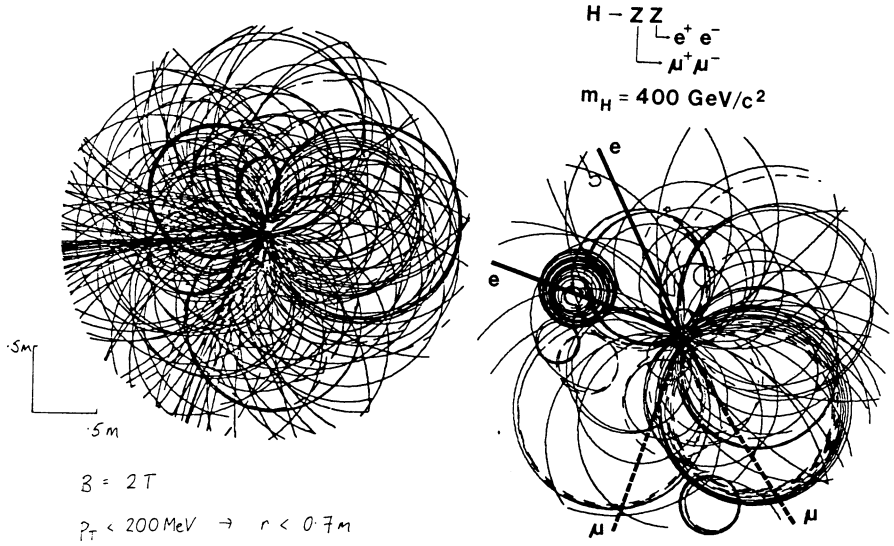

Figure 2: $r-o$ views of a 2-jet event and a Higgs event at the SSC.

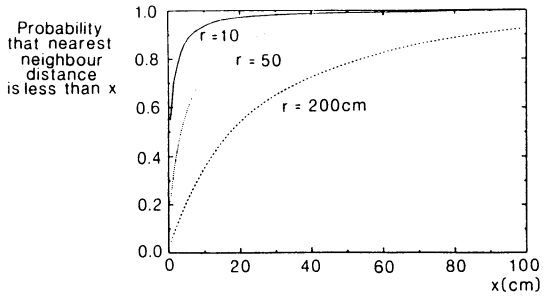

Figure 3: Distance to nearest neighbour in 3D of 1 TeV jet fragments.

cation and reconstruction of both quarks (i e jets) and leptons. In isolation from other sources of signal, both of these tasks are eminently achievable in principle with gaseous detectors. Figure 3 [2] summarises the spatial extent of 1 TeV jets at different distances from the production vertex in 1.5 T. Beyond 50 cm from the production vertex (i e the interaction point) a large fraction of jet fragments have their nearest neighbour more than 2 mm away, or equivalently $\sim 20\%$ of hits are lost due to overlap (within 2 mm) of hits. The current generation of gaseous drift chambers achieve 2 mm adjacent track resolution with analysis of flash digitised output, so the reconstruction of TeV jets beyond 50 cm from their point of production looks plausible. If jet fragments can be reconstructed, lepton reconstruction follows if candidates can then be tagged with calorimetry or muon filter, or possibly with track detector pulse profile analysis if transition radiation (TR) energy deposition can occur.

Success at both jet and lepton identification, and therefore by inference the inclusion of charged track reconstruction, will be a powerful handle in disentangling the physics in an SSC or LHC experiment. This is not the place to list in detail the reasons why. They are all summarised well in the old adage for tracking - "imagine events from one's experiment without it" [3].

The realism of achieving effective charged track reconstruction depends not only on the individual precision achievable with gaseous detectors but also on the feasibility of constructing large arrays of such wires capable of achieving the necessary momentum resolution for tracks which have been adequately recognised. A good rule of thumb is that at SSC or LHC one will want to be sure of determining the charge on a 1 TeV track (when, for example, it is an isolated lepton). This implies a momentum resolution of ~ 0.3 TeV^{-1}. Figure 4 [4,5] show the momentum spectrum and momentum resolution with a realistic magnetic spectrometer covering the central track detector (CTD), $30^\circ < \theta < 150^\circ$, and forward track detector (FTD), $\theta < 30^\circ$ and $\theta > 150^\circ$, regions of a magnetic detector. The task is not impossible.

Whatever array of proportional wires is used, the complexity of the events is not the over-riding consideration. The immense interaction rate ($\sim$ 100 MHz) due to 100 mb of inelastic pp cross section at 10^{33} cm^{-2} s^{-1} (or greater) implies that chamber operation without impossibly large operating current is only possible beyond $\sim$ 50 cm

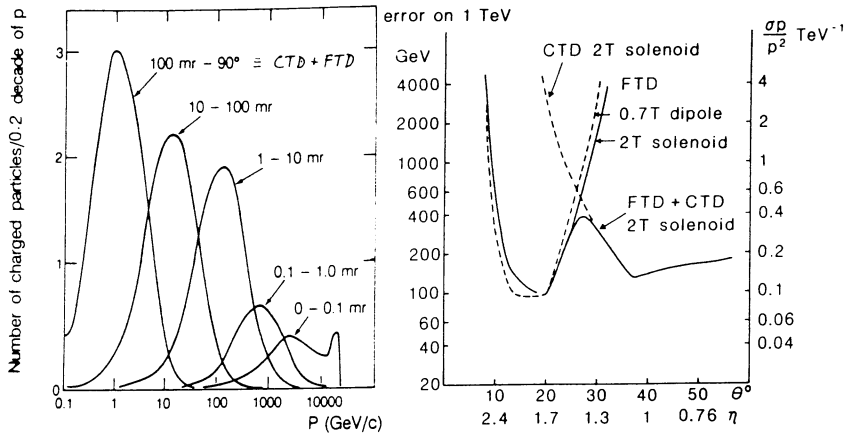

Figure 4: Momentum spectrum of secondaries from minimum bias events at SSC for different polar angle ranges and momentum resolution for two different magnetic field configurations using realistic arrays of gaseous wires. The latter are oriented so as to optimise the result: contributions are shown separately from the "forward" region (FTD) with transverse wires and the central region (CTD) with axial wires: the geometry of the wires is consistent with the operation of proportional wires at a supercollider of luminosity 10^{33} cm^{-2} s^{-1}.

(or further) from the beam [6]. Figure 5 shows the radiation exposure due *only* to pp interactions in bunch crossings at the SSC [4]. It neglects the familiar backgrounds from beam-gas, beam-wall, beam-halo, halo-wall, and halo-detector interactions, together with synchrotron radiation and secondary particle albedo. As we shall see, operating 50 cm from the beam with no additional shielding in a luminosity of $\sim 10^{33}$ cm^{-2} s^{-1} is just about possible for the operation of gaseous detectors as we conceive them today. Closer in than 50 cm is not considered any further here.

The experimental environment is further complicated by the bunch structure of SSC and LHC. Table 1 summarises and compares the essential operating characteristics of

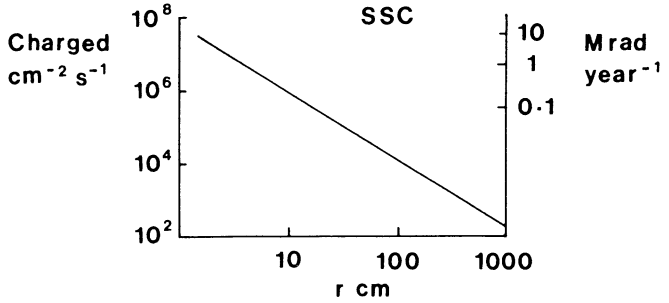

Figure 5: Radiation exposure as a function of radial distance from the interaction point at SSC due to pp interactions.

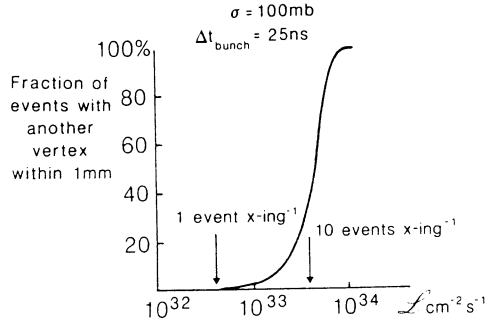

Figure 6: Fraction of events with another vertex within 1 mm as a function of supercollider luminosity assuming 25 ns bunch crossing interval.

machine	bunch x-ing interval	$\mathcal{L}$ cm^{-2} s^{-1}	σ_{inel}	CMS energy
LEP	25 μs	10^{32}	20 pb to 20 nb	$\geq$ 140 GeV
Tevatron	3 to 0.4 μs	(0.2 to 5) $\times$ 10^{31}	100 mb	1.8 TeV
HERA	96 ns	10^{32}	$\sim$ 100μb	314 GeV
LHC	25 to 5 ns	(0.1 to 5) $\times$ 10^{34}	100 mb	$\sim$ 16 TeV
SSC	15 ns	10^{33}	100 mb	$\sim$ 40 TeV

Table 1: Basic operating characteristics of present and future storage ring supercolliders.

the present and next generation of (storage ring) colliders. The jump down to bunch crossing intervals of 96 ns at HERA from the μs at $\epsilon^+\epsilon^-$ colliders has already forced the development of technology capable of handling data from such closely spaced bunch structures, "pipelining" in the trade[1] [7,8]. At SSC and LHC life is at first sight even harder. We can expect a mean number of $\sim$ 1.5 interactions per bunch crossing at 10^{33} cm^{-2} s^{-1}. In terms of spatial confusion of events Albrow [9] first pointed out figure 6 in which one cannot help but conclude that for luminosities greater than 10^{33} cm^{-2} s^{-1} physics may just be impossible with any detector which cannot "turn off" hits from unwanted tracks in both wanted and unwanted events.

The task for tracking is thus clear: to reconstruct enough of the charged track topology, possibly with the help of external calorimetry and muon filter, of events so as to identify and measure the topological structure of partons and leptons in each event. This has all to be achieved in by far the most hostile environment yet confronted, namely that of high event multiplicity confused further by the complications of extremely high lumi-

[1] It is interesting to realise that this sort of bunch structure is hardly novel. Similar conditions have been handled many times in fixed target experiments.

nosity and high bunch crossing rate. If gaseous detectors are to be used because of their proven track record and more significantly because of their inherent electron identification capability, then the conditions demand that the closest that the detectors may ever be placed to the interaction point is radially ~ 50 cm.

2 Proportional Wires at Supercolliders

The viability of any tracking system with wires operating in proportional mode depends both on the lack of confusion due to overlap of track hits, quantitatively specified by "occupancy" and taken to be the mean number of hits whose primary ionisation is still to be collected on the sense wire, and on the operating current in the experimental environment. If we assume the operating characteristics of the SSC summarised in Table 1 above (which means an average of 1.5 interactions per bunch crossing) together with a uniform distribution of a mean of $\bar{\imath}$ charged secondary tracks per unit of rapidity for minimum bias events, i e a distribution

$$\mathrm{d}n_{track} = \frac{\bar{\imath}}{2\pi}\mathrm{d}y\mathrm{d}o \tag{1}$$

then the average rate of charged particle hits in a solid angle $\mathrm{d}\Omega$ takes the form

$$\frac{\mathrm{d}n^{hit}_{wire}}{\mathrm{d}t} = \frac{\bar{\imath}}{2\pi}\mathcal{L}\sigma_{inel}\frac{\mathrm{d}\Omega}{\sin^2\theta} \tag{2}$$

It is convenient to work in terms of layers of detector, such as a cylindrical wire plane of a o symmetric CTD with wires supported parallel to the beam axis, or the plane defined by wires transverse to the beam axis at fixed z (the co-ordinate along the beam axis) for which the o symmetric configuration is with the wires strung either radially or in a cobweb structure. Then each o symmetric plane subtends a certain range or acceptance in rapidity. Using equation 1 and in terms of

- no. of wires exposed to the secondary charged particle flux per layer : N_{wire}
- no. of ion pairs per minimum ionising particle (mip) in a drift cell : N_{ion}
- acceptance bite in rapidity of this detector layer : Δy
- maximum drift time of the drift cell (ns) : T_d
- gas gain at the wire surface : G

we can write expressions for the average number of hits per drift cell per pp interaction

$$< n^{hit}_{wire} >= \frac{\bar{\imath}\Delta y}{N_{wire}}. \tag{3}$$

the average hit rate per wire (s^{-1})

$$< \frac{\mathrm{d}n^{hit}_{wire}}{\mathrm{d}t} >= \frac{\bar{\imath}\Delta y}{N_{wire}}10^8. \tag{4}$$

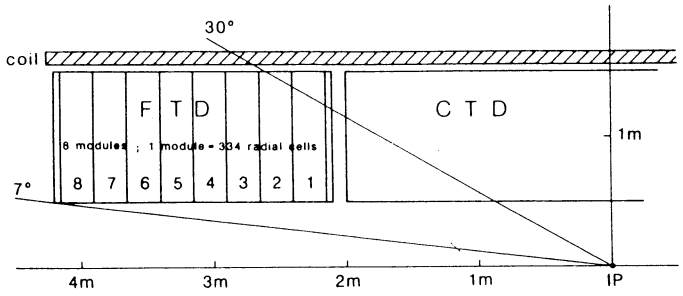

Figure 7: Schematic layout of a gaseous tracking system in SSC/LHC.

the average total occupancy of each drift cell

$$< n^{hit}_{wire} >= \frac{0.7\Delta y}{N_{wire}}T_d(ns). \tag{5}$$

and the current drawn per sense wire (μA)

$$I_{wire} = \frac{11G\Delta y N_{ion}}{N_{wire}}10^{-5} \tag{6}$$

where each charged track is assumed to cross the wire plane only once. To keep both mean occupancy *and* mean current low requires short maximum drift times T_d, large numbers of sense wires N_{wire}, small acceptance in rapidity Δy, the lowest possible track ionisation N_{ion}, and low gas gain G. In terms of construction and operation of gaseous drift chambers these restrictions at the SSC or LHC imply much more severe constraints than present generation drift chambers have to meet. Nevertheless, as we shall see, these constraints do not appear to be impossibly severe.

To get a feeling for the meaning of the above in an SSC/LHC environment consider the putative, and only schematic, layout of track detectors of figure 7. Geometrically the divide between CTD and FTD is at $\sim 30°$ and, together with the (presently achievable) spatial resolution ($\sigma_{pt} \sim 100$ μm), is what was used to calculate the track momentum resolution in figure 4 [5]. If we assume drift cells can be built with $N_{ion} = 100$ (about 1 cm of a common Ar based mixture at 1 bar), and $G = 2 \times 10^4$ (about half the operating gas gain of contemporary drift cells), then for the CTD wires (uniformly distributed in o with length $\simeq$ 4m, $\Delta y \simeq 2.8$ at the inner radius of 50 cm) and for the FTD wires (if strung radially uniformly distributed in o with length $\simeq$ 1m, $\Delta y \simeq 1$) we find the results summarised in Table 2. Tolerable current drawn per sense wire is the most severe requirement. It is hard to imagine a proportional wire operating reliably and drawing more than ~ 0.5 μA - in itself that means that ionisation collection alone on each wire is generating ~ 1 mW at 2 KV before one even considers read-out electronics!

For a sense wire current of less than ~ 0.5 μA we are thus forced to assume that in azimuth o a CTD requires at least 1232 sense wires per layer (at fixed r), that is a sense to sense spacing of 2.5 mm - a maximum drift length 1.25 mm! - at the inner radius

	CTD	FTD
sense wire current (μA)	$\frac{616}{N_{wire}}$	$\frac{220}{N_{wire}}$
mean occupancy $< n^{hit}_{wire} >$	$\frac{2T_d(ns)}{N_{wire}}$	$\frac{0.7T_d(ns)}{N_{wire}}$
irradiation [C (cm wire)$^{-1}$ year^{-1}]	$\frac{100}{N_{wire}}\frac{1}{\sqrt{r^2+z^2}}$	$\frac{100}{N_{wire}}\frac{z}{r}\frac{1}{\sqrt{r^2+z^2}}$
maximum irradiation [C (cm wire)$^{-1}$ year^{-1}]	$\frac{2}{N_{wire}}$	$\frac{1.94}{N_{wire}}$

Table 2: Estimated operating characteristics of a proportional wire in a CTD and an FTD at the SSC as a function of N_{wire} the number of wires per detector plane and T_d the maximum drift time: a CTD axial wire of 4 m length at a radial distance of 50 cm and an FTD transverse wire strung radially $50 < r < 150$ cm at $z = 200$ cm are assumed both operating with a gas gain of 2×10^4 in drift cells yielding 100 primary ion pairs.

of 50 cm (7.5 mm at an outer radius of 150 cm). If one can even contemplate such a small cell dimension as in any way realistic, this implies an immense spatial density of wires which, for many reasons, is probably too large for a CTD built along the lines of present day central detectors. A way out of this nightmare is possible if one can alter one, some, or all of the parameters listed above, though each change brings added complication. For example reducing the acceptance Δy, that is length, of each wire is possible, but at the price of an increased number of read-out channels and greater mechanical complexity if the same acceptance is to be maintained. It might be possible to reduce sense wire gas gain G and/or primary ionisation N_{ion} with sufficiently sensitive and noise free electronics, but presumably at increased cost. The situation is in fact even worse than these considerations reveal in an axial magnetic field where low momentum tracks may spiral - so called "loopers". In figure 2 one can see such tracks causing multiple hits at a particular radius.

In contrast, for the FTD (with transverse wires) at least 440 equally spaced sense wires are necessary if we restrict the operating current per wire to less than 0.5 μA. If these are to be strung radially (one of many possibilities) this amounts to a sense wire spacing of ~ 7 mm at the inner radius of 50 cm (21 mm at an outer radius of 150 cm), which is a somewhat easier task than in the central region though still daunting in terms of the total numbers, $\sim$ 44000 sense and a similar number of field (potential) wires. There is also no added complication of "loopers" in an axial magnetic field.

Of course the choice of 0.5 μA maximum current per wire is arbitrary. If one believes that one can operate with larger currents then the number of drift cells can decrease. However even if operation is foreseen as possible at larger instantaneous current, gaseous proportional wires age. A canonical rule of thumb is that wires will be dead due to

deposits of dielectric polymer after having laboured in electron avalanche to the tune of ~ 1 C cm^{-1}, though certain alcoholic vapours added to taste to the gas mixture can prolong life and certain choices of wire material can shorten it [10.11]. The chemistry seems to be complicated and not completely understood. With this rule of thumb in mind, equation 2 can be turned into Coulomb exposures $\frac{dQ}{dz}$ (CTD) or $\frac{dQ}{dr}$ (FTD) in C cm^{-1} year^{-1}, where an operational year is taken to be 10^7 s. For a CTD axial wire at radius r:

$$dQ = \frac{11 \times 10^{-12}\mathcal{L}\sigma_{inel}GN_{ion}}{N_{wire}}\frac{dz}{\sqrt{r^2+z^2}} \tag{7}$$

and for an FTD radial wire at beam axis co-ordinate z

$$dQ = \frac{11 \times 10^{-12}\mathcal{L}\sigma_{inel}GN_{ion}}{N_{wire}}\frac{z}{r}\frac{dr}{\sqrt{r^2+z^2}}. \tag{8}$$

Using the wire parameters above we find the exposures shown in Table 2. The wires die first at the points closest to the interaction point (for CTD $r = 50$ and $z = 0$ cm, for FTD $r = 50$ and $z = 200$ cm): there is a useful lifetime for the putative wire arrays considered above in the SSC luminosity of 10^{33} cm^{-2} s^{-1}. In the proposed LHC luminosity of $\sim 5 \times 10^{34}$ cm^{-2} s^{-1} life looks impossible.

Given that the monumental wire assemblies (CTD $N_{wire} \sim 123200$ and FTD $N_{wire} \sim$ 44000 for $I_{wire} \sim 0.5$ μA) mentioned as examples above are both mechanically feasible and operationally sound, their efficacy as track detectors in the high multiplicities characteristic of SSC/LHC physics relies on tolerable drift cell occupancy so that track recognition is a feasible task.The total occupancies of the CTD and FTD drift cells depend on the time it takes to collect the track ionisation, that is on the drift velocity. Using equation 5 and expressing the maximum drift *time* in terms of the maximum drift *length* d cm and the drift velocity v_{drift} (μm ns^{-1}) we find

$$< n^{hit}_{wire} >= \frac{0.7\Delta y}{N_{wire}}\frac{d}{v_{drift}}10^4. \tag{9}$$

Obviously the fastest possible gas is desirable, but commensurate with adequate digitisation frequency to maintain acceptable track spatial resolution.

Commonly used gases based on argon mixtures have drift velocities (e g 50 : 50 Ar:C_2H_6 with $v_{drift} \sim 50$ μm ns^{-1}) such that for a CTD maximum drift length of 0.75/0.25 cm (a drift cell memory time of 11/4.33 SSC bunch crossings) in an outer/inner radius drift cell, we find an occupancy of $\sim 25\%/\sim 8\%$. Thus the tiny CTD drift cells chosen to avoid excessive current draw have occupancy which is not a problem even with a conventional gas mixture.

The FTD and its transverse wires are a more interesting calculational exercise. Taking radial wires, and thus wedge shaped drift cells, the maximum drift length varies with r. Occupancy integrates up over the variable maximum drift length to be given in terms of the axial co-ordinate z and the inner and outer radii r_1 and r_2 cm of the wire by (v_{drift} in μm ns^{-1})

$$< n^{hit}_{wire} >= \frac{7000\pi z}{v_{drift}.N^2_{wire}} \ln\frac{(2z+r_2)(2z-r_1)}{(2z-r_2)(2z+r_2)}. \tag{10}$$

For the transverse radial wires discussed above and quoted in Table 2 this gives an occupancy of $\sim 30\%$ with a conventional argon based gas mixture. Using a fast gas (e g Ar/Xe and CF_4 with $v_{drift} \sim 120\ \mu m\ ns^{-1}$ [12.13]) this can be reduced to 12%.

It appears then that gaseous proportional wires are a feasible way of building a realistic charged track detector for $r > 50$ cm at a supercollider with luminosity no greater than $\sim 10^{33}\ cm^{-2}\ s^{-1}$. The major constraint is the need for a realistic operating current: total charge collection. leading to wire ageing. and wire hit occupancy. giving rise to impossibly complex pattern recognition problems. are then not prohibitive. In the central region ($|y| \leq \sim 1$) very small drift cells are necessary (~ 2.5 mm sense wire spacing) which makes for extremely difficult mechanical construction over the required lengths (~ 4 m). Outside the central region. again with $r > 50$ cm and where transverse wires are the most effective solution. the task is significantly less demanding.

3 Technological Signposts to the Future

Encouraged by the viability of gaseous proportional wires at a supercollider and not discouraged by the magnitude of the task necessary for a suitable charged track detector. it is timely to consider some contemporary developments which may hint at technological ways forward.

The high track multiplicities demand that future supercollider track detectors build on the proven essentials of present day devices. These all accept that the best way of ensuring the easiest and most efficient pattern recognition is to arrange sense wires in groups so as to provide easily recognisable. localised track segments [3.14]. Then track recognition builds on linking track *vector* segments. each of which carry both spatial and directional information. The pioneer of these vector detectors was MarkIII at SLAC [15] and subsequently MarkII [16] and CDF [17]. The latter was the first vector chamber to tilt its drift cells so that the sense wire planes were no longer radial in an attempt both to compensate for Lorentz angle of drift and so as to ensure that every track crossed a sense wire plane at least once [3.14]. Then in a collider environment where drift cell memory is more than one bunch crossing. track segments which are spatially ambiguous to within a "jog" of at least one bunch crossing interval can be lined up unambiguously within a cell. This advantage is exploited in anger in Zeus and H1 at HERA (figure 8).

As discussed above before any of these features of contemporary central detectors (CTD's) can be considered at SSC/LHC. a way has to be found of miniaturising the drift cells. An encouraging signpost comes from the D-zero vertex detector which includes all the features of a vector drift chamber but without tilted cells (figure 9) [18]. The by now familiar demands of tolerable operating current and cell occupancy lead to small cell dimension in the flux close to the interaction vertex. The inner maximum drift length is 3.6 mm. Excellent resolution is obtained with a slow gas (1 bar DME) and 100 MHz flash digitisation which establishes that the mechanical support of the necessarily large wire density is possible with adequate precision despite the enhanced electrostatic stresses. It seems that it is possible to have drift cells of few mm dimension in a precision mechanical structure containing a few thousand wires. Can we extrapolate this to much

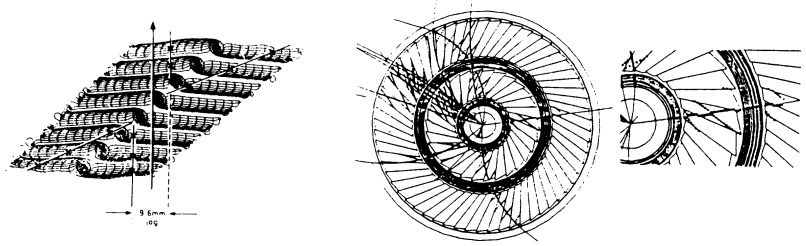

Figure 8: Simulated digitisations and parent tracks in a Zeus and H1 cell showing how a background track from an earlier HERA bunch crossing fails to produce a collinear track segment.

larger dimension and a hundred thousand wires? Apart from the maintenance of accuracy over a much larger volume. the stronger end-plates required for mechanical stability of the wires will have to exploit new lightweight materials if calorimetry and other track detection is not to be compromised by excessive passive absorber material.

This end-plate problem can be alleviated if the wire support can be redistributed throughout the CTD volume. The idea of the Multi-Drift Module (MDM) of Sauli [19] does so by grouping wires together in a hexagonal matrix structure of modules each supported by lightweight C-fibre composite envelopes (figure 10). Each drift cell is very small (1.45 mm radius) and 70 are grouped together in one envelope. Whether such a high density of wires can be maintained mechanically stable over the typical (~ 4 m) lengths required in a collider CTD without additional support is unclear.

The immense task of wire support and assembly in a realistic supercollider CTD using MDMs can be eased a little by resorting to "straw tubes" in which each sense wire is inside an aluminised mylar cathode forming a miniature cylindrical proportional counter [20]. Each sense wire or a group of sense wires plus cathodes is now a self-supporting structure in which mass production by a precision manufacturing process is envisaged. Tests of 4 mm diameter straws have already shown excellent operating characteristics with a fast CF_4 and isobutane gas mixture [21]. Simple ideas for space point read-out (drift co-ordinate plus perpendicular direction along the wire) from straws by means of a spiralling aluminium topology on the cathode wait to be tried. Long straws suitable for a CTD (≤ 4 m) remain completely unproven both mechanically and as efficient and accurate detectors until a considerable R and D program is carried out. Given adequate benevolence by funding agencies. this may happen over the next two or three years [21].

One advantage of gaseous detectors at supercolliders is the inherent possibility of using them both for track reconstruction and electron identification. The X-ray sensitivity of proportional wires means that electron identification can be achieved at high momenta (100's of GeV) by detection of transition radiation (TR). generated when ultra-relativistic charged particles cross suitable dielectric interfaces [22]. The possibility of a hybrid detector in which it is possible to reconstruct and identify electrons (and positrons) with

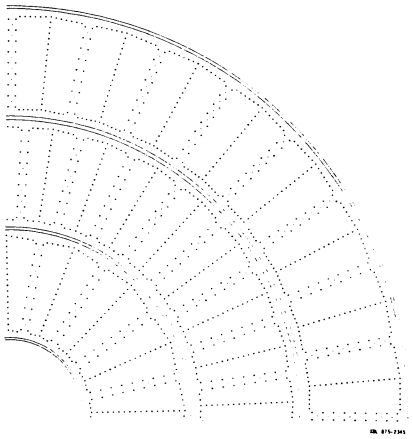

Figure 9: $r - o$ view of a quadrant of the D-zero vertex detector: each of three layers is staggered relative to the others in o: a double plane of potential wires is used in each cell for improved isochronicity and two-track separation.

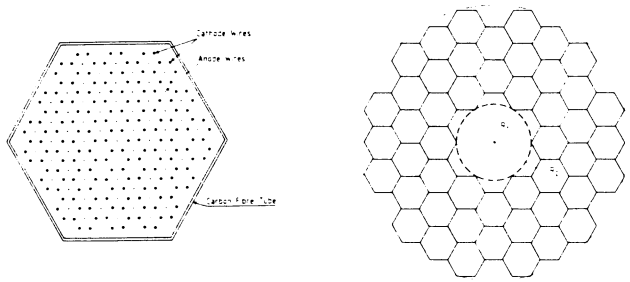

Figure 10: Schematic of assembly of Multi-Drift Module (MDM): a single module is shown as an array of hexagonal drift cells supported in a C-fibre hexagonal tube; also shown is a putative array of MDMs forming a high precision, high rate detector.

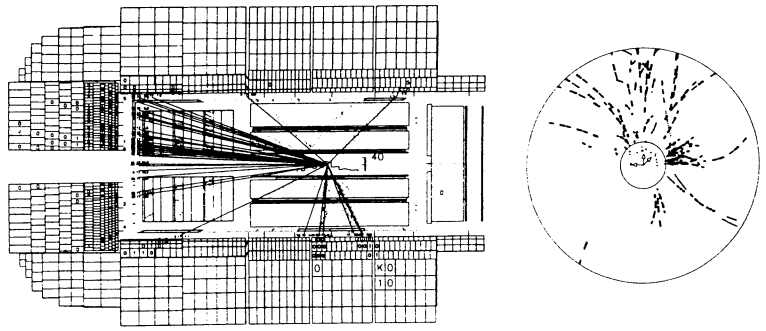

Figure 11: Simulated electron proton interaction in the H1 detector at HERA: a high multiplicity of hadronic fragments going forward (proton direction) are visible in the forward track detector (FTD) in which hybrid track reconstruction and electron identification is possible. Also shown is the $r - o$ projection of hits in the FTD.

a typical drift chamber spatial precision of 100 μm is clearly a powerful proposition for supercollider physics. Dolgoshein and Fabjan [23.24.25] have proposed that the low material content of straw tubes be exploited for TR X-ray detection by embedding them in a matrix of foam which has excellent TR generating capability. With multi-threshold hit electronics one would thus be able to "turn off" track hits with low pulse height, that is "turn on" interesting electron track candidates both for triggering and for easier track finding in interesting events. Calculations indicate that hadron rejection of 10^{-2} may be achievable for track momenta up to $\sim$ 100 GeV.

An interesting alternative approach to electron identification in complicated high multiplicity events in already under way at HERA [26.27]. In the forward (proton beam) direction the H1 experiment includes transition radiator and detectors as an integrated part of a powerful forward track detector (FTD). Efficient multi-track reconstruction is achieved with a combination of radial wire and planar wire drift chambers in the layout apparent in figure 11.

The radial wire chambers provide accurate track segment reconstruction by means of drift and charge division ($\sigma_{ro} \sim 100$ μm and $\frac{\sigma_r}{r} \sim 2\%$) in wedge shaped transverse drift cells (figure 12). The "front window" of each radial chamber is carefully designed so as to optimise X-ray transmission. Thus sampled pulse height analysis using the 12 sense wires provides electron identification on an accurately reconstructed track combining the discrimination possible with both TR and $\frac{dE}{dx}$.

This technique of detecting the X-rays on one or more sense wires in a vector drift chamber cell has one further advantage over the use of straw tubes - track segments are reconstructed accurately so that the major background to $\frac{\pi}{e}$ discrimination, hadronic knock-on immediately upstream of the gaseous volume, can be eliminated with some efficiency by direct observation spatially. Prototype tests have been extremely encour-

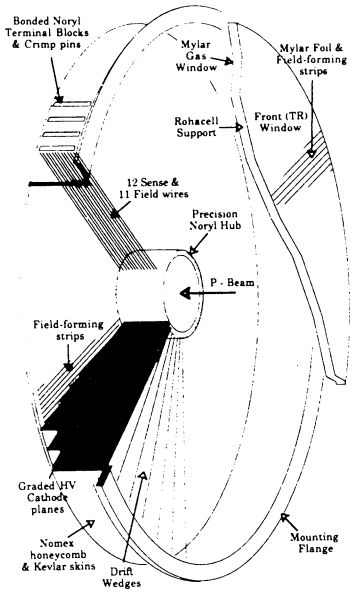

Figure 12: Exploded view showing the principle of construction of a radial wire drift chamber for the H1 FTD. The flat "saucepan" like structure supports radial wires strung between an inner hub and the outer radius. The upstream window of the chamber is designed to maintain the drift accuracy (transverse to the incident particle) while simultaneously having the best possible X-ray transmissivity for detection of transition radiation.

aging if a dilute X-ray sensitive gas is used (Xe:He:C_2H_6 30 : 40 : 30): figure 13 shows the drift co-ordinate spatial precision and the $\frac{e}{\pi}$ discrimination simultaneously obtained. The feasibility of radial sense wires for track reconstruction outside the central region of a supercollider detector has already been mentioned above. The efficacy of this technique, which exploits the uniform ionisation response of the radial wedge drift cells due to both charged track $\frac{dE}{dx}$ and TR X-rays, at a supercollider with a much higher wire density and lower track ionisation yield and gas gain remains to be proven [21].

As has already been discussed, the most effective charged track detector at a supercollider must use a gas mixture with large drift velocity and thus fast digitisation of drift time for the best possible results. For many years we have known how to "speed up" argon and xenon based gas mixtures by adding organic components, so called "quenchers", like methane CH_4 and ethane C_2H_6. Figure 14 shows the dramatic effect of a 10% admixture of methane to pure argon at 1 bar. The drift velocity increases dramatically and its dependence on applied electric field changes. The reason is straightforward. Organic molecules cool the drift of the electron ionisation because they have large inelastic (ro-

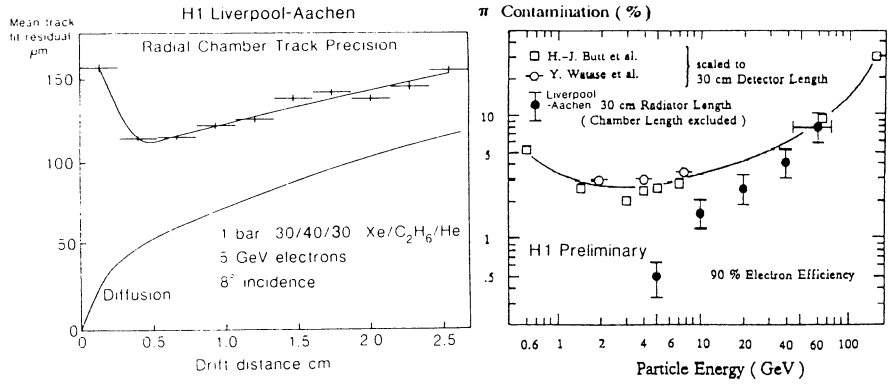

Figure 13: Measurements of the spatial precision and of the $\frac{e}{\pi}$ discrimination in a radial drift chamber prototype using a dilute Xe based gas mixture suitable for X-ray detection.

tational and vibrational excitation) electron scattering cross sections. Thus the energies of electrons in the drifting ionisation swarm are kept low enough so that the electron scattering by the noble gas constituent (Ar or Xe) is in a region of the scattering cross section corresponding to the Ramsauer Townsend minimum.

Figure 15 shows a compilation of electron cross sections in xenon and the organic gas CF_4 where the inelastic contributions at the energy corresponding to the Ramsauer dip are unusually large [28,29]. Measurements in xenon CF_4 mixtures are shown in figure 14 where one can see factors of up to 5 increase in drift velocity with increasing concentrations of CF_4 [30]. Provided the materials used for mechanical construction of chambers for a supercollider are not attacked chemically in any way by CF_4, and this may be a big "provided", it seems that speeding up the drift cell operation by similar factors may be possible, and moreover whilest also maintaining X-ray detection efficiency.

4 Conclusion

For hadron supercolliders with luminosities no greater than $\sim 10^{33}$ cm^{-2} s^{-1} the use of gaseous drift chambers operating in proportional mode seems possible beyond $\sim$ 50 cm from the interaction point. Furthermore, they have distinct advantages:

- relative cheapness per unit volume
- flexibility of geometry
- technology established in past and present fixed target and collider experiments
- multiplicity of purpose - space point determination and electron/hadron discrimination

Because these advantages assume greater significance at supercolliders, gaseous drift chambers will be important parts of experiments at such machines. However before that can happen, a considerable program of research and development is necessary, and is indeed now beginning, to overcome the considerable problems in their exploitation.

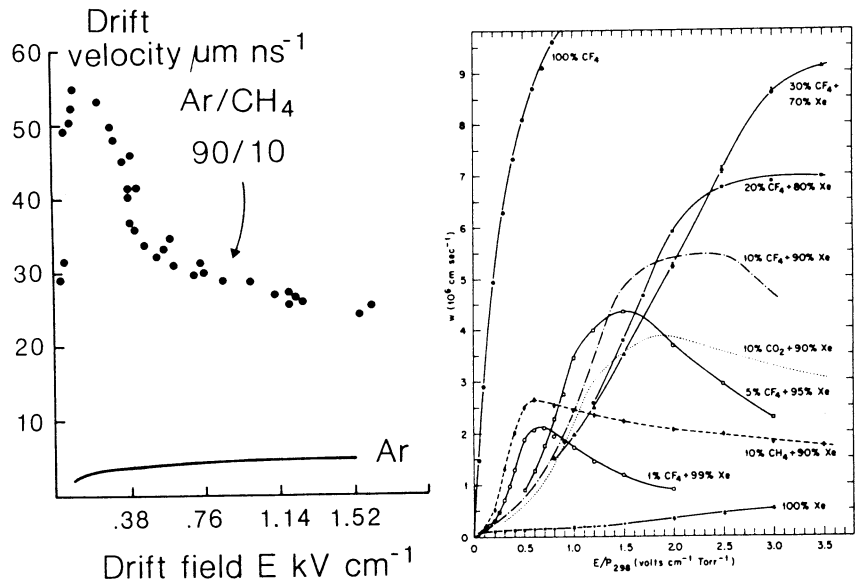

Figure 14: Measurements of a) the drift velocity of electrons in pure argon and in a mixture of argon and methane (Ar:CH_4 90:10) showing the dramatic effect of a small admixture of organic gas, and b) of the drift velocity of xenon CF_4 gas mixtures showing the dramatic changes due to small admixtures of the latter.

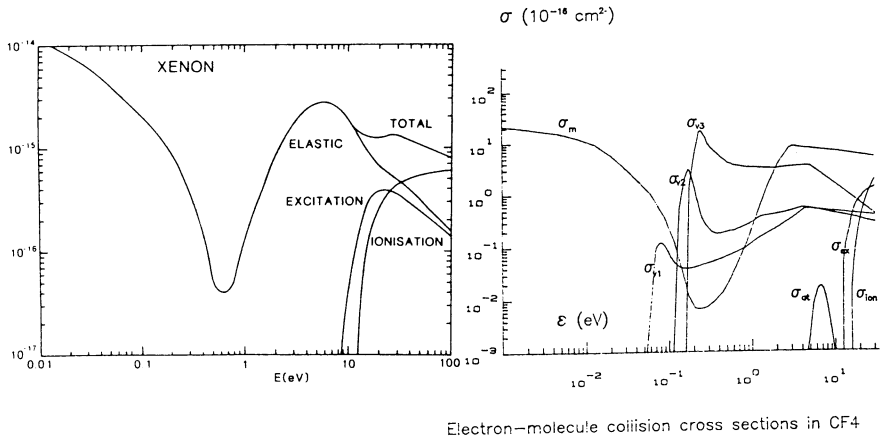

Figure 15: Compilation of electron-atom/molecule cross sections as a function of incident electron energy for xenon and CF_4 showing the large inelastic contributions from the latter at energies close to the Ramsauer Townsend minimum in xenon.

These problems are associated with *both* the physics of the new energy scale *and* the difficult experimental environment to be found at supercolliders. None of them seem insurmountable so that it is reasonable to foresee the gaseous drift chamber continuing as the backbone of experimentation in high energy physics for many years to come.

I wish to acknowledge the influence of very many people on this presentation and to thank them. In particular I am grateful to my colleagues in the H1 experiment in Liverpool, RAL, Aachen and DESY with whom it continues to be a pleasure to work, from whom I have learnt much, and without whom none of the H1 radial wire chambers and TR would have been possible. I thank organisers and participants of supercollider workshops in the US and in Europe with whom and where respectively I have learnt much of the work presented here. If any is misrepresented here then it is entirely of my own making. I also wish to thank the organisers of this study week, and in particular Fabio Sauli who organised session P6, for their invitation to take part in the meeting and for their forbearance in tolerating my rather truncated attendance due to other commitments.

References

[1] G G Hanson. "Report of the Wire Chamber Group", to appear in *Proceedings of the Workshop on Tracking Systems for the SSC, TRIUMF Laboratory, Vancouver, Canada, ed W Frisken, July 24-28 1989*

[2] P Burrows and G Ingelmann. "Jet Characteristics at TeV Energies", in *Proceedings of the Workshop on Physics at Future Accelerators, La Thuile and Geneva, ed. J H Mulvey, January 1987* CERN 87-07

[3] J B Dainton. "Tracking in a High Multiplicity Environment", in *Proceedings of the XXIV International Conference on High Energy Physics, ed. R Kotthaus and J H Kuhn, Springer Verlag, Munich 1989 p 1229* and references therein

[4] G G Hanson *et al.* "Report of the Large Solenoid Detector Group" in *Proceedings of the Workshop on Experiments, Detectors, and Experimental Areas for the Supercollider, ed. R Donaldson and MGD Gilchriese, Berkeley 1987 p 340*

[5] J B Dainton. "A Forward Charged Track Detector at LHC/CLIC", in *Proceedings of the Workshop on Physics at Future Accelerators, La Thuile and Geneva, ed. J H Mulvey, January 1987* CERN 87-07

[6] D H Saxon. "Summary Report of the Working Group on Vertex Detection and Tracking", in *Proceedings of the Workshop on Physics at Future Accelerators, La Thuile and Geneva, ed. J H Mulvey, January 1987* CERN 87-07

[7] H1 Collaboration. H1 Technical Proposal. *DESY*

[8] Zeus Collaboration. Zeus Technical Proposal. *DESY*

[9] M Albrow, quoted in D H Saxon, "Summary Report of the Working Group on Vertex Detection and Tracking", in *Proceedings of the Workshop on Physics at Future Accelerators, La Thuile and Geneva, ed. J H Mulvey, January 1987* CERN 87-07

[10] J Kadyk, "Wire Chamber Ageing", to appear in *Proceedings of the Workshop on Tracking Systems for the SSC, TRIUMF Laboratory, Vancouver, Canada, ed W Frisken, July 24-28 1989*

[11] S Majewski, "Properties and Limitations of gaseous detectors at High Fluxes", *these proceedings*

[12] L G Christophorou *et al.* Nucl. Instr. and Meth. **163** 141 (1979)

[13] L G Christophorou *et al.* Nucl. Instr. and Meth. **171** 491 (1980)

[14] D H Saxon, Nucl. Instr. and Meth. **A265**, 20 (1988)

[15] J Roehrig *et al.* Nucl. Instr. and Meth. **226**, 319 (1984)

[16] G G Hanson, Nucl. Instr. and Meth. **252**, 343 (1986)

[17] R L Wagner, Nucl. Instr. and Meth. **A265**, 1 (1988)

[18] A R Clarke *et al.* Nucl. Instr. and Meth. **A261**, 420 (1987)

[19] R Bouclier *et al.* Nucl. Instr. and Meth. **A265**, 78 (1988) and references therein

[20] H Ogren, "Straw Tubes at the SSC", to appear in *Proceedings of the Workshop on Tracking Systems for the SSC, TRIUMF Laboratory, Vancouver, Canada, ed W Frisken, July 24-28 1989*

[21] D Blockus *et al.* "SSC Detector Subsystem Proposal - Central and Forward Tracking with Wire Chambers", SSC PC-024, October 1989

[22] B Dolgoshein, Nucl. Instr. and Meth. **A252** 137 (1986) and references therein.

[23] B Dolgoshein, "Particle Identification at Future Supercolliders", *these proceedings*

[24] V Chernyatin *et al.* LAA Proposal to investigate the development of a Transition Radiation detector for a hadron supercollider, CERN 1989

[25] S Ahlen *et al.* "Proposal to develop an integrated high-rate Transition Radiation Detector and Tracking Chamber for the SSC", SSC PC-011, October 1989

[26] G A Beck *et al.* "Radial Wire Chambers for the H1 Forward Track Detector at HERA: Design, Construction and Performance", to appear in *Proceedings of the Wire Chamber Conference, Vienna, Austria, February 13-17 1989*, to be published in Nucl. Instr. and Meth.

[27] H Graessler *et al.* "Simultaneous Track Reconstruction and Electron Identification in the H1 Radial Wire Drift Chambers", to appear in *Proceedings of the Wire Chamber Conference, Vienna, Austria, February 13-17 1989*, to be published in Nucl. Instr. and Meth.

[28] S Biagi, University of Liverpool, private compilation of data

[29] T Yamashita *et al.* "Measurements of the Electron Drift Velocity and Positive Ion Mobility for the Gases containing CF_4", paper submitted to the Wire Chamber Conference, Vienna, Austria, February 13-17 1989, KEK 88-133

[30] M K Kopp *et al.* Nucl. Instr. and Meth. **201** 395 (1982)

TRACKING WITH WIRE CHAMBERS AT HIGH LUMINOSITIES*

GAIL G. HANSON
Indiana University, Bloomington, Indiana 47405 USA
and
Stanford Linear Accelerator Center, Stanford University,
Stanford, California 94309, USA

Abstract

Radiation damage and rate limitations impose severe constraints on wire chambers at the SSC. Possible conceptual designs for wire chamber tracking systems that satisfy these constraints are discussed. Computer simulation studies of tracking in such systems are presented. Simulations of events from interesting physics at the SSC, including hits from minimum bias background events, are examined. Results of some preliminary pattern recognition studies are given.

1. Introduction

The primary motivation for the SSC is the expectation that it will lead to new discoveries, such as Higgs bosons, supersymmetric particles, heavy W's or Z's, new heavy fermions, or composite particles with masses in the TeV region. Such particles would be produced in the central rapidity region, that is, over $\pm$ 3 units of rapidity, and would decay to high-p_T electrons, muons, or jets, often with large missing transverse energy due to undetectable neutrinos. In order to fully investigate the physics opportunities in this regime, a general-purpose detector which includes charged particle tracking is needed.

Tracking at the SSC at the full design luminosity, $\mathcal{L}$, of 10^{33} cm^{-2}s^{-1} is expected to be a difficult problem. The limitations imposed by rates and radiation damage have been described by the previous speaker [1]. Once the wire chambers can be shown to survive, the dominant constraint is the combination of occupancy and double-hit resolution. Single events from new physics at the SSC have many (several hundred) charged particle tracks and are further complicated by curling tracks in a magnetic field, photon conversions, hits from events from out-of-time bunch crossings, and multiple interactions within the same bunch crossing [2]. We have begun studies using computer simulation to establish how well one can find tracks in complex SSC events.

* Work supported by the Department of Energy, contracts DE–AC03–84ER40125 and DE–AC03–76SF00515.

2. Wire Chamber Requirements

2.1. Constraints of the SSC Environment on Cell Design

Limitations on wire chamber tracking detectors at the SSC are imposed by radiation damage, current draw, chamber lifetime, gain reduction from large particle flux, hit rate, occupancy and pattern recognition. Of these, the most severe is probably current draw since this determines survivability in the SSC environment. For wires parallel to the beam direction in a central tracking system, current draw per wire, I, for a layer of wires of length L at radius r is given by

$$I = \frac{n_c w h \sigma \mathcal{L} G e \alpha L}{2\pi r^2} \quad , \tag{1}$$

where n_c is the average charged particle multiplicity per unit of rapidity (7.5), w and h are the width and height of the cell (assumed to be equal), e is the electron charge, and σ is the inelastic cross section (100 mb). The ionization rate, α, in the gas is assumed to be 100 electrons/cm, and the gas gain, G, is assumed to be 2×10^4, which is rather low. A layer of 4 mm wide cells at a radius of 50 cm covering $|\eta| < 1.5$ (L = 213 cm) will draw 0.52 μA/wire. The limit of acceptable current draw before breakdown will occur is about 1 μA/wire. For the above example, the collected charge over a chamber lifetime of five years (5×10^7 s) would be 0.12 C/cm, where the limit is about 1.0 C/cm. However, this calculation includes only the particles produced in an interaction and must be increased by a factor of 2–4 because of curling tracks in a magnetic field, converted photons, and albedo particles leaking out of the front face of the calorimeter. An extra safety margin may be obtained by splitting the length of wire needed to cover the entire rapidity range in the middle or increasing the minimum radius at which the tracking system operates at the full design luminosity.

Straw tube chambers are a natural candidate for a small cell design. The straws are typically made of aluminized polyester film (Mylar) or polycarbonate (Lexan) with wall thicknesses of about 30 μm. Several layers of straw tubes can be glued together to form superlayers which would be rigid, mechanically stable structures. Within each superlayer the layers can be staggered by half the cell width in order to allow hits from out-of-time bunch crossings to be rejected and resolve left-right ambiguities, as illustrated in fig. 1. By dividing the chamber into superlayers, locally identifiable track segments can be obtained at the pattern recognition stage. The track segments can then be linked to form tracks. There must be a sufficient number of layers in the superlayers to provide redundancy.

Since cell widths are constrained to a few mm, vector cells (jet cells) in the central tracking region are not practical. However, in the forward tracking region ($|\eta| \gtrsim 1.5$), the radial wire chamber may be an excellent candidate [1, 3]. The current draw per

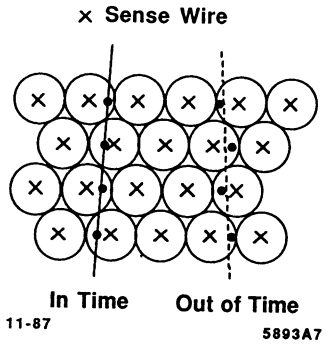

Fig. 1. Layers of straw tubes in a superlayer with every other layer staggered by the straw tube radius. A single in-time track will appear as a series of hits on the wires on alternate sides of the track. The left-right ambiguity is easily resolved locally. A track from an out-of-time bunch crossing will produce hits which are displaced from possible tracks by at least 16 ns in drift time.

wire for a radial wire chamber is given by

$$\frac{d^2Q}{dr\,dt} = \frac{n_c\,\sigma\,\mathcal{L}\,G\,e\,\alpha\,h}{r\,N_{cell}} \quad , \tag{2}$$

where h is the distance between sense wires in a wedge and N_{cell} is the number of wedges azimuthally. The current draw is inversely proportional to the radial position along the wire. For $h = 4$ mm and 335 wedges, the current draw is $(2.9 \times 10^{-7}$ C/s)/ r(cm), which integrates to 0.3 C/cm/5 years at a radial position of 50 cm. For a radial wire chamber there is no increase in current due to curling tracks in a magnetic field.

Other possible problems for wire chambers at the SSC were considered at the Vancouver SSC Tracking Workshop [4]. Space charge effects should not be a problem for straw tube chambers because the drift distance is so small and are probably not a problem for radial wire chambers. The current draw causes about 1 mW of power dissipation in the gas of a single straw, but this can probably be handled by adequate gas flow. The neutron and photon albedo were estimated to increase the current draw by about 20%. The calculation should be done more carefully, and we should also look at the effects for existing tracking chambers in front of calorimeters.

2.2. Measurement of the Coordinate Along the Wire

The three conventional methods for measuring the coordinate along a wire are charge division, small-angle stereo, and cathode strips (or pads) running perpendicular to the wires. A fourth, less conventional, method is the time-difference method which probably has similar resolution to charge division, but may be worth further consideration.

Charge division, at best (high gas gain $\sim 10^5$), gives a resolution of about 1% of the length of the wire. Since the wires in an SSC tracking system would be quite long (3–6 m) in order to cover the required rapidity range, the resolution would be only 3–6 cm. Since low gas gain is needed to reduce current draw and increase chamber lifetime, the resolution in an SSC tracking system would be even worse. Also, charge division requires electronics readout at both ends of the wire which increases the complexity of a system with a large number of wires. For these reasons charge division does not appear to be a practical method for measuring the coordinate along the wire in an SSC tracking system.

Small-angle stereo ($\sim 3°$) wires typically give a resolution in the coordinate along the wire of a few mm (the drift distance resolution divided by the stereo angle). The same electronics for time measurement can be used for all wires. In a system of superlayers of straw tubes, every other superlayer might be small-angle stereo. However, in complex SSC events it may be difficult to associate the hits on stereo wires with the correct tracks. The H1 radial wire chambers use charge division plus planes of crossed wires to resolve ambiguities. For the SSC, "stereo" wires at a small angle to radial may work to determine the coordinate along the radial direction.

Cathode strips or pads perpendicular to the wire direction can give a resolution of better than 1 mm. They might be included on the outer surfaces of the superlayers in the central tracking system to aid in bunch assignment and reducing stereo ambiguities and in front of the calorimeter in the forward tracking system. However, they present added electrical and mechanical difficulties, as well as increasing the number of readout channels.

2.3. Momentum Measurement

The minimum requirement for momentum resolution based on physics criteria is that the sign of the charge for electrons should be measured for $p_T \leq 0.5$–1.0 TeV/c, or $\sigma_{p_T}/p_T \leq 0.30 p_T$ (TeV/c). To obtain this momentum resolution in a robust manner, one can scale from existing detectors, such as Mark II and CDF. One then finds that for a magnetic field of 2 Tesla and a tracking inner radius of 50 cm, we need an outer radius of about 1.8 m to obtain the required momentum resolution for non-beam-constrained momentum fits. It has been found that the momentum resolution is generally worse than the ideal due to systematic errors in positioning, imperfect pattern recognition, and lost hits in complex events in large tracking systems. Of course, we would really like to achieve better than the minimum requirement for

momentum resolution, for example, in order to reconstruct invariant masses involving high-momentum muons. We can improve on the above momentum resolution by using beam-constrained fits where appropriate, trying to improve the spatial resolution for the large tracking system, and by including a few layers of silicon detectors with very precise spatial resolution at small radius inside the wire chamber system. Such silicon systems still require considerable R&D to show that they will work reliably in the SSC environment and achieve the calculated momentum precision.

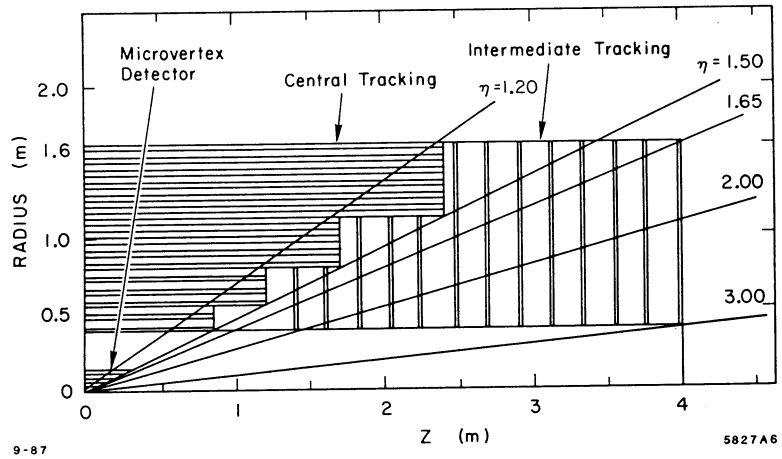

Fig. 2. Schematic view of the central and intermediate tracking systems in the Large Solenoid Detector (from ref. [5]).

2.4. Examples of SSC Tracking Systems

A large solenoid detector based on more-or-less "conventional" technology was discussed at the 1987 Berkeley Workshop [5]. Calorimetry and tracking are located inside a large superconducting solenoid with 2 Tesla field. The tracking detector design for the Large Solenoid Detector was divided into central tracking ($|\eta| \lesssim 1.2$) and intermediate tracking ($1.2 \lesssim |\eta| < 2.5$). The central tracking system was assumed to be built of superlayers of straw tubes of radii from 2 to 3.5 mm parallel or nearly parallel to the beam direction. Every other superlayer is small-angle stereo. Two options for intermediate tracking were considered: planes of parallel wires and radial wire chambers. A schematic view of the tracking system in the Large Solenoid Detector is shown in fig. 2.

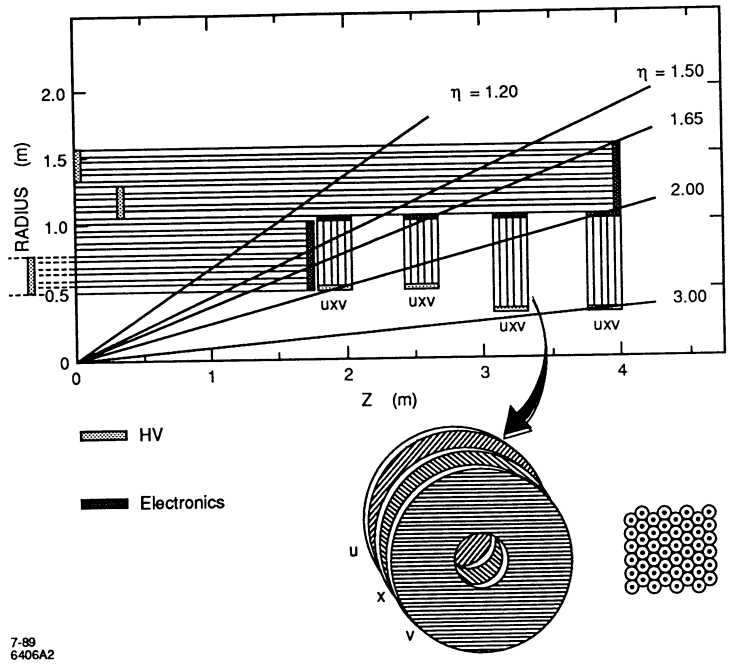

Fig. 3. Schematic view of a solenoidal detector tracking system capable of measuring p_T in the outer superlayers for $|\eta| \lesssim 2$. The tracking system for $2 < |\eta| < 3$ consists of planar superlayers of straw tubes.

In a solenoidal detector with geometry as in the Large Solenoid Detector, the momentum resolution becomes very large near $|\eta| \sim 2$, so in reality one can hope to measure only track positions at the entrance to the calorimeters for larger $|\eta|$. On the other hand, one can use the outer superlayers to measure p_T, for example, for the trigger, for $|\eta| \lesssim 2$. In principle (see sec. 3.3), we know how to do this for wires parallel to the beam direction. This leads to the idea of extending the axial wires to cover this area. Also, position measurement for $2 < |\eta| < 3$ can be accomplished with planar superlayers of straw tubes. Track segments can be found in the superlayers in a manner similar to the central tracking. The wires in these superlayers would run alternately at $\pm$ 45° to each other (u, x, v). A tracking system incorporating these

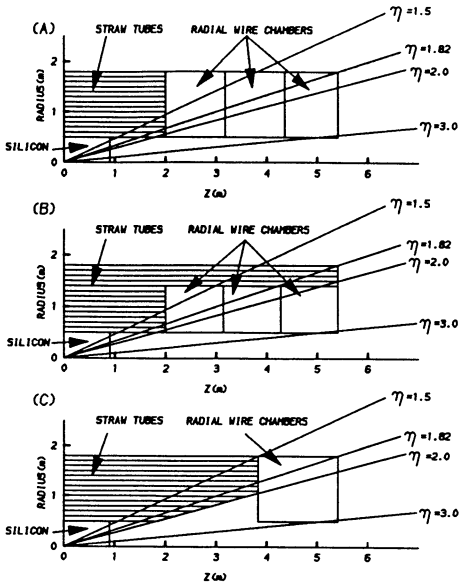

Fig. 4. Various options for combining central tracking with radial wire chamber modules. All have 50 cm inner radius, 180 cm outer radius and length sufficient to cover $|\eta| < 1.82$ with all tracking layers and $|\eta| < 2.0$ with momentum resolution degraded by no more than about a factor of two. (a) Axial wires covering $|z| < 2.0$ m and radial wire chambers covering $|z| > 2$ m. (b) Axial wires covering $|\eta| < 2.0$ in order to find high-p_T track segments for the trigger. (c) Tracks cross only one boundary between central and forward tracking, except at $|\eta| = 2.0$.

ideas is shown in fig. 3.

Figure 4 shows three options for combining central tracking with radial wire chamber modules for forward tracking. We would like to be able to construct high-p_T track segments for the trigger. If we can understand how to accomplish this with radial wires, then the tracking systems shown in figs. 4(a) or (c) would be preferable because they do not require such long wires.

3. TRACKING SIMULATION

3.1. Simulation of a Central Tracking System for the SSC

The SSC tracking system design used for this simulation was based on that for the Large Solenoid Detector [5], described in sec. 2.4, although it is quite general and can be used for any system of cylindrically oriented sensing elements. The simulation has been described in detail elsewhere [6–9]. Briefly, we used ISAJET [10] to generate events from interesting physics processes, such as high-p_T two-jet events or Higgs boson production, and from inelastic scattering background, for which we used minimum bias events. We used the GEANT3 [11] general-purpose detector simulation package to simulate the interactions of the particles with the detector. The particles interact in the 8% of a radiation length of material due to straw tube walls, wires, and gas (the material was assumed to be distributed uniformly throughout the tracking volume), including photon conversion and multiple Coulomb scattering. The digitizations consist of a wire number and a drift time, calculated from the distance of closest approach of a track to a wire using a drift velocity of 50 μm/ns, for each track in each layer. Background from inelastic scatterings in the same and out-of-time bunch crossings is included by superimposing the digitizations from minimum bias events from the number of bunch crossings as determined by the resolving time of the straw tube cell. The double-hit resolution is equal to the cell width, that is, only the earliest hit on a wire is kept.

3.2. Results of the Simulation

Figure 5(a) shows a simulation of a two-jet event with $p_T > 1$ TeV/c in the Large Solenoid Detector, and fig. 5(b) shows an enlargement of the same event in the outer two superlayers in the area of the dense jet. Figure 5(c) shows the earliest hits in the cells for the tracks shown in fig. 5(b). Hits from background events and converted photons are not shown in fig. 5.

Figure 6 shows the same event as in fig. 5, but with no magnetic field. In figs. 5 and 6 we can observe that the hits form identifiable tracks in the outer superlayers with a 2 Tesla field, but with no magnetic field the tracks are less easily resolved. The 2 T field, however, produces many curling tracks which obscure the high-p_T tracks to some extent, particularly in the inner superlayers.

Figure 7 shows an event from Higgs boson production, $pp \rightarrow HX$, with the Higgs decaying to Z^0Z^0 and each Z^0 decaying to e^+e^- or $\mu^+\mu^-$. We used a Higgs mass of 400 GeV/c^2. For these events we used the full simulation as described in the previous section. We generated $\sim$ 200 such events, which we used for further studies of hit loss and pattern recognition.

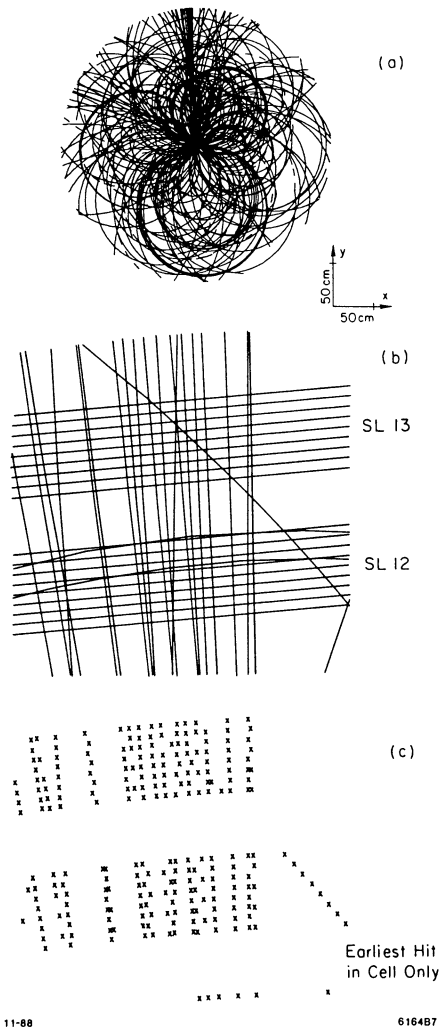

Fig. 5. (a) Two-jet event from ISAJET with $p_T > 1$ TeV/c in a 2 Tesla magnetic field in a detector of the geometry of the Large Solenoid Detector. There are 223 particles with $p_T > 200$ MeV/c and $|\eta| < 1.5$. Converted photons and background from minimum bias events are not shown. (b) Enlargement of the event in the outer two superlayers in the area of the dense jet at the top of the detector. (c) Earliest hit in each cell for the tracks shown in (b).

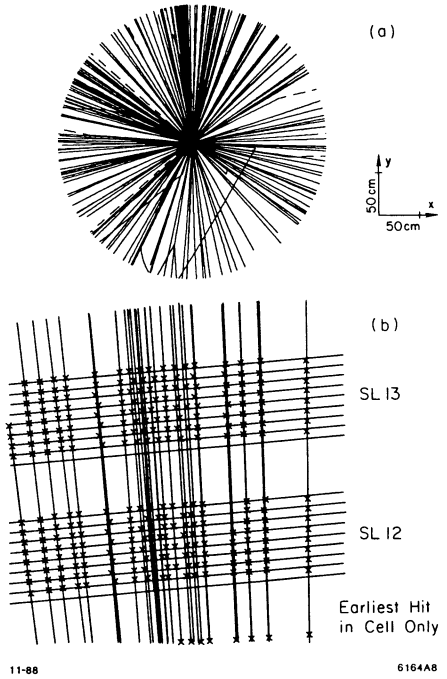

Fig. 6. (a) Same two-jet event from ISAJET as shown in fig. 5, except with no magnetic field. (b) Tracks and earliest hit in each cell in the enlargement of the event in the outer two superlayers in the area of the dense jet at the top of the detector.

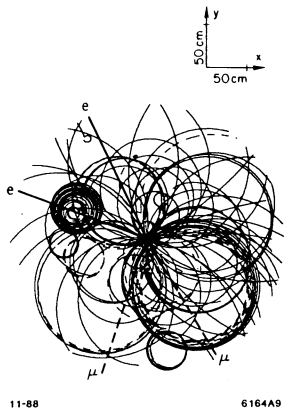

Fig. 7. Example of a Higgs event in the simulated central tracking system. The leptons from the Higgs decay are indicated by the heavier lines. Converted photons and other interactions with the material are included.

The fully-simulated events, including adding digitizations from minimum bias background events and removing digitizations within the double-hit resolution, had 12,000 - 30,000 digitizations in the central tracking system. On the average 57% of the digitizations were due to minimum bias background events. For all tracks $(11.6 \pm 0.7)\%$ of the digitizations were lost because of the double-hit resolution, and the loss was about the same in all superlayers. For the leptons from the Higgs decay an average of $(7.3 \pm 0.6)\%$ of the digitizations were lost with the worst losses being in the inner superlayers.

We are now beginning to include intermediate tracking in the simulation. Figure 8 shows a projection in the direction along the beam line of a simulated Higgs event in a detector similar to that shown in fig. 3.

3.3. Pattern Recognition

We began working on pattern recognition algorithms in order to examine our original design goals of finding track segments in superlayers and removing hits from out-of-time bunch crossings. The algorithm for finding track segments was the following:

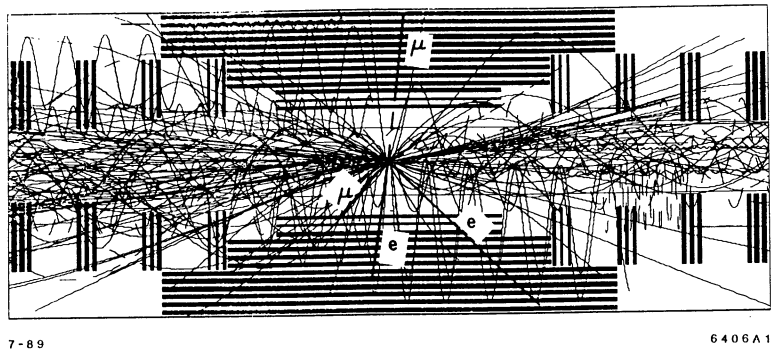

Fig. 8. Example of a Higgs event in a projection along the beam direction. The central tracking system is the same as that shown in fig. 2 and the intermediate tracking system is that shown in fig. 3. The leptons from the Higgs decay are indicated by the heavier lines. Converted photons and other interactions with the material are included.

1. In each superlayer we identified "roads" containing hits. There are two parameters which can be varied: the width of the road and the number of hits required on the road. We used a width of five wires and required three or more hits out of eight possible.

2. We required that at least one of the hits be in a layer with the opposite wire stagger from the others so that the left-right ambiguities could be resolved.

3. We required that the hits be consistent with a straight line to within an error based on the spatial resolution and in the process resolved the left-right ambiguities.

Figure 9(a) shows all of the digitizations for the event shown in fig. 7, including those from minimum bias background events. Figure 9(b) shows only those digitizations which are included in segments. Keeping only those digitizations which form segments cleans up the events considerably. Figure 9(c) shows the tracks from the original event in the outer five superlayers in the region around the muon at the lower right. Figure 9(d) shows all of the digitizations in the event in the enlarged region (the digitizations are displayed at the locations of the hit wires). Finally, fig. 9(e)

shows only those digitizations which form track segments; here, the left-right ambiguities have been resolved, the drift times have been converted to distances, and the digitizations are displayed at the positions of closest approach of the tracks to the wires. One can clearly identify the muon track, and most of the extra hits have been removed.

Next, we applied our segment-finding algorithm to the e and μ tracks from Higgs boson decays. We defined two classes of segments: a "good" segment was one with at least five hits from a lepton track and no other hits, and an "OK" segment was one with at least five hits from the lepton track and one hit from another track. The effects of hits from other tracks remain to be studied; we plan to compare measured momenta with produced momenta in future work. With these definitions, we counted the number of segments found for each lepton track.

The distribution of the number of good segments for the e's and μ's in the Higgs events is shown in fig. 10(a). The corresponding distribution of total (good or OK) segments is shown in fig. 10(b). We see that the lepton tracks from Higgs decay have an average of about 8 good segments and 10 total segments out of 13 possible. Typically 30–50% of segments were good in the inner superlayers, increasing to almost 80% for the outer superlayers. When OK segments are counted as well, 50–60% of segments are accepted for inner superlayers and over 80% for outer superlayers.

After finding the hits in roads, we can find the coordinate along the wire from the displacement of nearby axial and stereo roads. We can then correct the drift times for the propagation time along the wires and determine the bunch number from the time offset which gives a straight line. We will test this procedure in future simulation work.

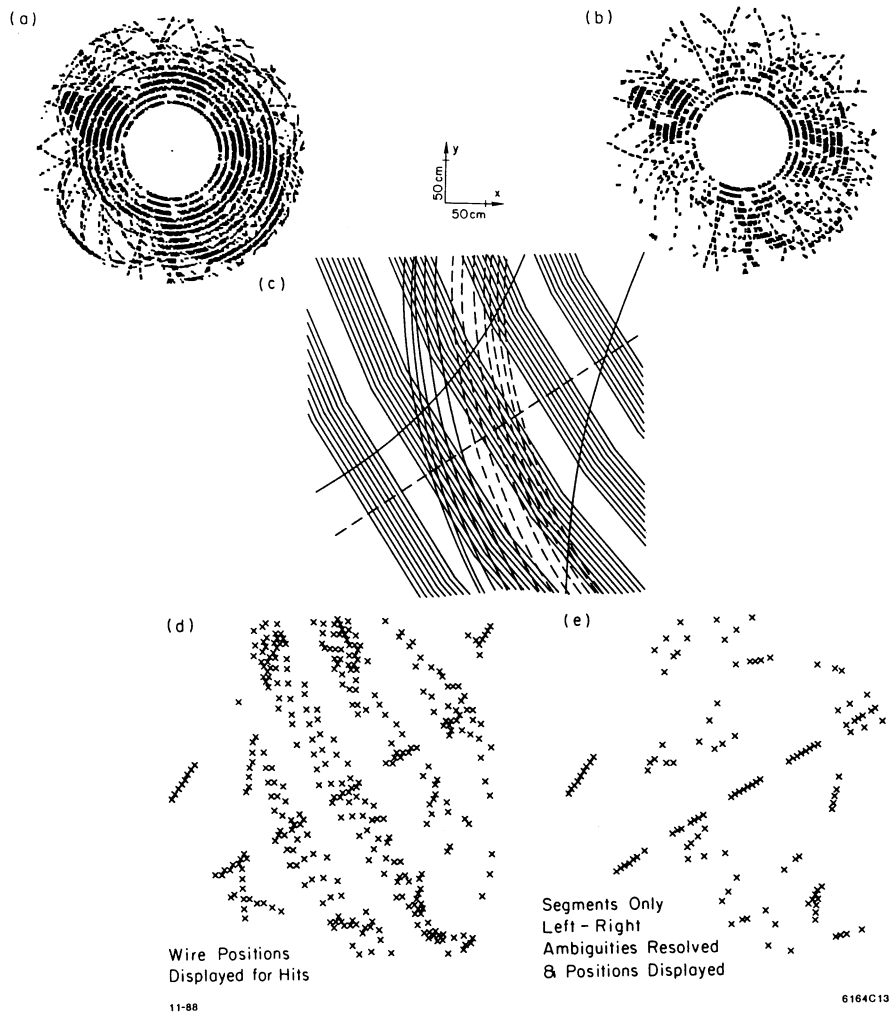

Fig. 9. (a) All of the digitizations for the Higgs event shown in fig. 7, including those from minimum bias background events. (b) Digitizations for this event which are included in track segments, as defined in the text. (c) Tracks from the original event in an enlarged region in the outer five superlayers in the region around the muon at the lower right. (d) All of the digitizations in the event in the enlarged region of (c) [the digitizations are displayed at the locations of the hit wires]. (e) Digitizations which form track segments in the enlarged region. Here, left-right ambiguities have been resolved, drift times have been converted to distances, and digitizations are displayed at the positions of closest approach of the tracks to the wires.

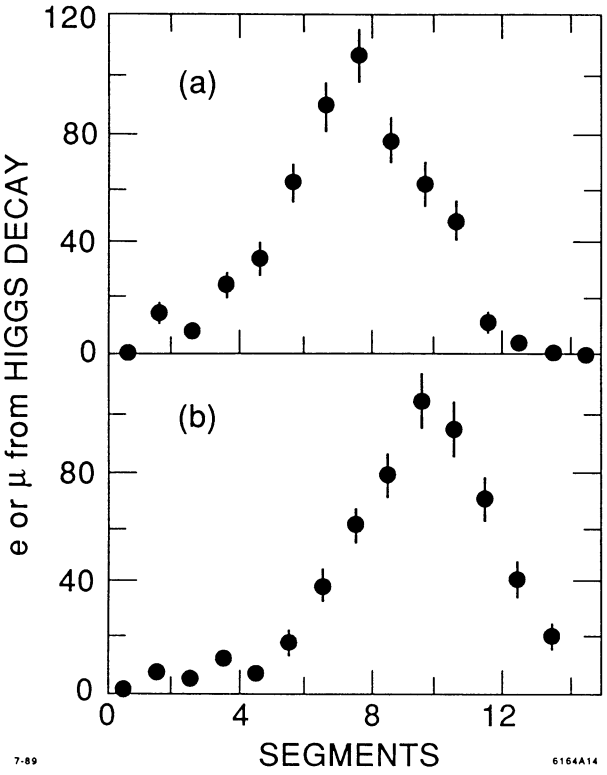

Fig. 10. (a) Distribution of the number of good segments out of 13 possible for the e's and μ's from the Higgs decays. (b) Distribution of the number of total segments (good or OK) for the leptons from the Higgs decay.

4. CONCLUSIONS

We have shown that an SSC tracking system design based on a pattern recognition strategy of finding track segments in superlayers appears to provide a powerful means of finding tracks in complex SSC events, even in an environment of multiple events from several bunch crossings. So far, detailed simulations have verified the concepts developed over several years for SSC tracking detectors. An algorithm for finding track segments such as that described here could be used in the trigger for high-p_T tracks. Depending on the effects on the physics analyses, we might envision making this requirement at the processor level, reading out only the hits that form track segments or even just the segments themselves.

We will apply similar procedures to the simulation of radial wire chambers. Two major conceptual questions arise:

1. How can the coordinate along a radial wire be found? Do we need to use crossed planes of wires to resolve the ambiguities?

2. Can high-p_T track segments for the trigger be found quickly using radial wire chambers?

Wire chamber tracking systems for high luminosity ($\leq 10^{33}$ cm^{-2} s^{-1} at the SSC) pp colliders look feasible. However, wire chamber tracking systems will probably not survive at a luminosity of 5×10^{34}.

ACKNOWLEDGMENTS

We would like to thank the organizers of the Study Week and our hosts at the Universitat Autonoma de Barcelona for providing such a stimulating environment. We gratefully acknowledge the support of the U.S. Department of Energy Program for Generic Detector Research and Development for the SSC.

REFERENCES

[1] J. B. Dainton, "Gaseous Track Detectors at High Luminosity Colliders," and references therein, in these Proceedings.

[2] D. G. Cassel, G. G. Hanson *et al.*, "Report of the Central Tracking Group," in *Proceedings of the 1986 Summer Study on the Physics of the Superconducting Supercollider, Snowmass, CO*, 1986, eds. R. Donaldson and J. Marx, p. 377.

[3] G. A. Beck *et al.*, "Radial Wire Drift Chambers for the H1 Forward Track Detector at HERA: Design, Construction and Performance," *Proceedings of the Wire Chamber Conference, Vienna, Austria, February 13–17, 1989*, to be published in Nucl. Instr. and Meth.

[4] G. G. Hanson, "Report of the Wire Chamber Group," to appear in *Proceedings of the Workshop on Tracking Systems for the SSC, TRIUMF Laboratory, Vancouver, Canada, July 24–28, 1989.*

[5] G. G. Hanson, S. Mori, L. G. Pondrom, H. H. Williams *et al.*, "Report of the Large Solenoid Detector Group," in *Proceedings of the Workshop on Experiments, Detectors, and Experimental Areas for the Supercollider, Berkeley, CA*, 1987, eds. R. Donaldson and M.G.D. Gilchriese, p. 340.

[6] G. G. Hanson, B. B. Niczyporuk and A. P. T. Palounek, "Wire Chamber Requirements and Tracking Simulation Studies for Tracking Systems at the Superconducting Supercollider," *Proceedings of the Wire Chamber Conference, Vienna, Austria, February 13–17, 1989*, to be published in Nucl. Instr. and Meth., SLAC–PUB–4860.

[7] G. G. Hanson, B. B. Niczyporuk and A. P. T. Palounek, "Triggering and Data Acquisition Aspects of SSC Tracking," *Proceedings of the Workshop on Triggering and Data Acquisition for Experiments at the Supercollider, Toronto, Canada, January 16–19, 1989*, p. 55.

[8] G. G. Hanson, M. C. Gundy and A. P. T. Palounek, "Tracking with Wire Chambers at the SSC," to appear in *Proceedings of the 4th Pisa Meeting on Advanced Detectors, La Biodola, Isola d'Elba, Italy, May 21–26, 1989*, SLAC–PUB–5041.

[9] A. P. T. Palounek, "Simulating a Central Drift Chamber for a Large Solenoid Detector at the SSC," SLAC–PUB–4787.

[10] F. E. Paige and S. D. Protopopescu, "ISAJET 5.30: A Monte Carlo Event Generator for pp and $\bar{p}p$ Interactions," in *Proceedings of the 1986 Summer Study on the Physics of the Superconducting Supercollider, Snowmass, CO*, 1986, eds. R. Donaldson and J. Marx, p. 320. (The current version of ISAJET is 6.12.)

[11] R. Brun, F. Bruyant, and A. C. McPherson, *GEANT3 User's Guide*, CERN DD/EE/84–1.

A New Gaseous Detector for Tracking : the Blade Chamber

The LAA-LAD Group

G. Ambrosi[d], T. Barillari[c], R. Battiston[d], F. Bergsma[a], D. Boscherini[b], G. Bruni[b], H. Castro[e], A. Contin[a], S. De Pasquale[b], J. Galvez[e], P. Giusti[b], J.C. Labbé[a], G. Laurenti[a], G. Levi[d], G. Maccarrone[b], D. Mattern[a], R. Nania[b], V. O'Shea[b], F. Rivera[e], M. Schioppa[e], A. Sharma[e], G. Simonet[a], G. Susinno[c], M.C.S. Williams[a] and A. Zichichi[a].

a) CERN, Geneva, Switzerland
b) University of Bologna and INFN Bologna, Italy
c) University of Calabria and INFN Cosenza, Italy
d) University of Perugia and INFN Perugia, Italy
e) World Laboratory, Geneva, Switzerland

Abstract

As part of the LAA project at CERN a prototype of a streamer-chamber has been built in which a blade, instead of a wire, is used as the amplification electrode. A big advantage is that the blade can be bent to follow a curve so that a chamber can be built with cells ideally matched to the geometry of the experiment. Moreover a blade is very rugged, it can withstand severe mechanical shock and also it is resistant to damage by sparks. The drift-time has been measured and a spatial resolution of 250 μm has been achieved. Left right ambiguity can be solved by measuring the charge asymmetry on the walls. The coordinate along the blade is read by external pickup strips.

Introduction

The "Large Area Devices" (LAD) group of the LAA project at CERN is devoted to R & D for muon detection at a future multi-TeV hadronic collider. Results reported in this paper are a part of the LAA-LAD work. In a hadron collider muon measurements in the forward and backward directions are of fundamental value. In these regions muon spectrometers require toroidal magnetic fields. In a toroidal field polar coordinate readings are desirable to improve trigger capability and momentum measurements. Our problem is: how can we build a circular cell? The idea being investigated is whether we can use a blade, instead of a wire, as the amplification electrode in a chamber working in the limited streamer mode. This is an adaption of a cell design already in use for X-ray spectroscopy [1,2]. There are several advantages with this technique. One is that a blade is very rugged, it can withstand severe mechanical shock and also it is resistant to damage by sparks. Another advantage is that it can be bent to follow a curve so that a chamber can be built with cells ideally matched to the geometry of the experiment. The problem with a blade is that the high field region needed for the avalanche process is only at the tip of the blade. We therefore have to find a geometry such that the primary electrons are drifted to the high field region.

Geometry of the cell

The cross section of the first chamber that we built and tested is shown in figure 1. The blade is 20 μm thick steel (this is commercially available as a shim material). The blades are spaced 10 mm apart. Between each blade there is a wall of 0.5 mm steel, which supports a roof made of copper clad p.c. board, located 15 mm above the tip of the blade. The walls and the roof are conducting

[6] G. G. Hanson, B. B. Niczyporuk and A. P. T. Palounek, "Wire Chamber Requirements and Tracking Simulation Studies for Tracking Systems at the Superconducting Supercollider," *Proceedings of the Wire Chamber Conference, Vienna, Austria, February 13–17, 1989*, to be published in Nucl. Instr. and Meth., SLAC–PUB–4860.

[7] G. G. Hanson, B. B. Niczyporuk and A. P. T. Palounek, "Triggering and Data Acquisition Aspects of SSC Tracking," *Proceedings of the Workshop on Triggering and Data Acquisition for Experiments at the Supercollider, Toronto, Canada, January 16–19, 1989*, p. 55.

[8] G. G. Hanson, M. C. Gundy and A. P. T. Palounek, "Tracking with Wire Chambers at the SSC," to appear in *Proceedings of the 4th Pisa Meeting on Advanced Detectors, La Biodola, Isola d'Elba, Italy, May 21–26, 1989*, SLAC–PUB–5041.

[9] A. P. T. Palounek, "Simulating a Central Drift Chamber for a Large Solenoid Detector at the SSC," SLAC–PUB–4787.

[10] F. E. Paige and S. D. Protopopescu, "ISAJET 5.30: A Monte Carlo Event Generator for pp and $\bar{p}p$ Interactions," in *Proceedings of the 1986 Summer Study on the Physics of the Superconducting Supercollider, Snowmass, CO*, 1986, eds. R. Donaldson and J. Marx, p. 320. (The current version of ISAJET is 6.12.)

[11] R. Brun, F. Bruyant, and A. C. McPherson, *GEANT3 User's Guide*, CERN DD/EE/84–1.

A New Gaseous Detector for Tracking : the Blade Chamber

The LAA-LAD Group

G. Ambrosi[d], T. Barillari[c], R. Battiston[d], F. Bergsma[a], D. Boscherini[b], G. Bruni[b], H. Castro[e], A. Contin[a], S. De Pasquale[b], J. Galvez[e], P. Giusti[b], J.C. Labbé[a], G. Laurenti[a], G. Levi[d], G. Maccarrone[b], D. Mattern[a], R. Nania[b], V. O'Shea[b], F. Rivera[e], M. Schioppa[e], A. Sharma[e], G. Simonet[a], G. Susinno[c], M.C.S. Williams[a] and A. Zichichi[a].

a) CERN, Geneva, Switzerland
b) University of Bologna and INFN Bologna, Italy
c) University of Calabria and INFN Cosenza, Italy
d) University of Perugia and INFN Perugia, Italy
e) World Laboratory, Geneva, Switzerland

Abstract

As part of the LAA project at CERN a prototype of a streamer-chamber has been built in which a blade, instead of a wire, is used as the amplification electrode. A big advantage is that the blade can be bent to follow a curve so that a chamber can be built with cells ideally matched to the geometry of the experiment. Moreover a blade is very rugged, it can withstand severe mechanical shock and also it is resistant to damage by sparks. The drift-time has been measured and a spatial resolution of 250 μm has been achieved. Left right ambiguity can be solved by measuring the charge asymmetry on the walls. The coordinate along the blade is read by external pickup strips.

Introduction

The "Large Area Devices" (LAD) group of the LAA project at CERN is devoted to R & D for muon detection at a future multi-TeV hadronic collider. Results reported in this paper are a part of the LAA-LAD work. In a hadron collider muon measurements in the forward and backward directions are of fundamental value. In these regions muon spectrometers require toroidal magnetic fields. In a toroidal field polar coordinate readings are desirable to improve trigger capability and momentum measurements. Our problem is: how can we build a circular cell? The idea being investigated is whether we can use a blade, instead of a wire, as the amplification electrode in a chamber working in the limited streamer mode. This is an adaption of a cell design already in use for X-ray spectroscopy [1,2]. There are several advantages with this technique. One is that a blade is very rugged, it can withstand severe mechanical shock and also it is resistant to damage by sparks. Another advantage is that it can be bent to follow a curve so that a chamber can be built with cells ideally matched to the geometry of the experiment. The problem with a blade is that the high field region needed for the avalanche process is only at the tip of the blade. We therefore have to find a geometry such that the primary electrons are drifted to the high field region.

Geometry of the cell

The cross section of the first chamber that we built and tested is shown in figure 1. The blade is 20 μm thick steel (this is commercially available as a shim material). The blades are spaced 10 mm apart. Between each blade there is a wall of 0.5 mm steel, which supports a roof made of copper clad p.c. board, located 15 mm above the tip of the blade. The walls and the roof are conducting

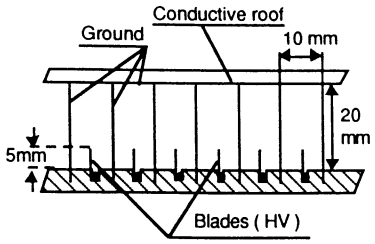

Figure 1. Cross section of conductive roof blade chamber

and are at ground potential. The blade is at positive high voltage and is readout via a 1nF decoupling capacitor. We fill the chamber with pure isobutane and find that we can achieve

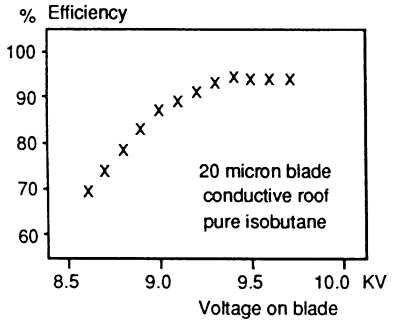

Figure 2. Detection efficiency versus high voltage on the blade

full efficiency. The plot (figure 2) shows the result for particles perpendicular to the roof of the chamber. Due to the dead area introduced by the thickness of the walls we only expect 95% efficiency. If we change the shape of the cell, such that the roof is lower (closer to the blade), we get a lower efficiency as primary electrons produced by tracks close to the wall are not drifted to the high field region. Many alternative designs have been attempted in order to optimise the detector performances. The current chamber, shown in figure 3, consists of a 30 μm thick blade with a 4mm blade distance. The roof is made of an insulating Kapton foil and is located 6mm above the tip of the blade. With this geometry the roof is charged and the field lines are bent (figure 4). As a consequence, primary electrons liberated near the wall are drifted to the high field region, even though the roof is close to the blade. Furthermore this design allows a reduction of the cell size shortening the maximum drift-time. An insulated roof also allows an easy placement of pickup strips. These are located on the outside of the roof and are used to determine the position of the streamer along

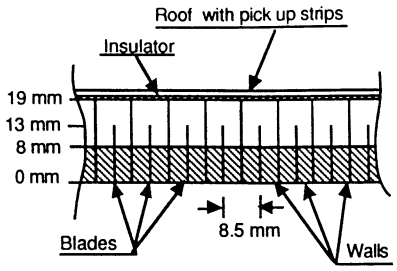

Figure 3. Cross section of insulating roof chamber

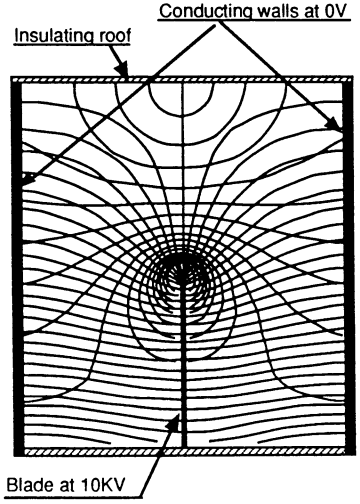

Figure 4. Field and Equifield lines for a Blade chamber cell

the length of the blade. We filled with pure isobutane. The remainder of this report describes results obtained with this chamber.

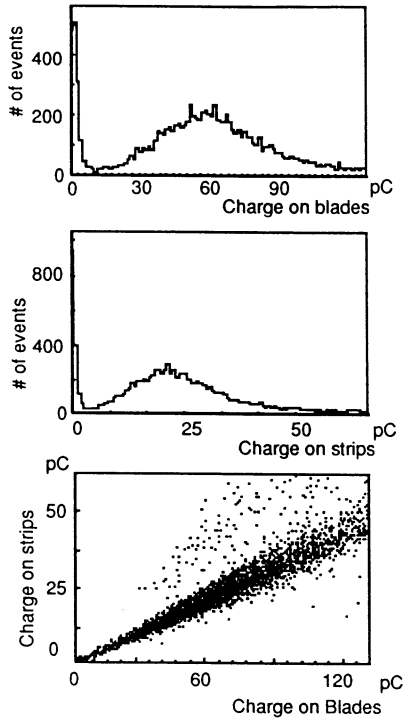

Figure 5. Charge spectrum on blades, strips and their correlation

Test Set-up

The chamber was mounted between two drift chambers. These chambers are equipped with wires in the x and y direction. The active area is 15 x 15 cm^2. Three scintillation counters are used to select through going tracks. This set-up was used to test the blade chamber with cosmic rays and with a pion beam of 3.5 GeV at CERN PS. Figure 5 shows the charge spectrum of the signal observed on the blades, on the sum of the strips and the correlation between the two. The main features are that the signal is large and there is a very strong correlation. The reason for this correlation is that the streamer can only grow in the direction away from the tip - towards the roof (where the pickup strips are located). This is different from the case of a wire, where the streamer can grow either towards or away from the pickup strips located on one side of the chamber.

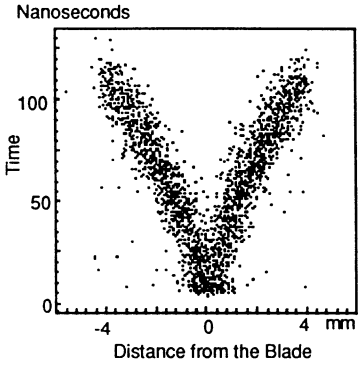

Figure 6. Particle distance from blade versus time of blade signal

Resolution

We reconstruct tracks using the auxiliary drift chambers and plot the distance from the blade versus the time of the blade signal. This is shown in figure 6. The left-right ambiguity can be solved using the charges measured on the walls. When a cell fires the charges induced on the delimiting walls are found to be different. We define a charge asymmetry A :

$$A = (Q_R - Q_L) / Q_M$$

where Q_R, Q_L are the charges on the right and left wall respectively and Q_M is the average of the two. The sign of A is found to be related to the left or right position of a track. This asymmetry is shown in figure 7. The two peaks are related to the left right position of the tracks. In fact one peak disappears when, by

means of external chambers, only tracks on one side of the blade are selected.

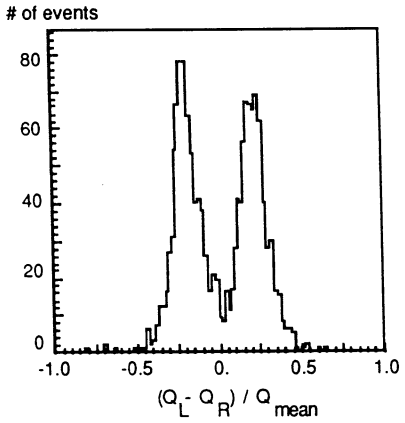

Figure 7. Asymmetry of charge collected on walls

We use this method to solve the left right ambiguity and then the drift time measurement is used to determine the position inside a cell. A spatial accuracy of 250 μm has been achieved (figure 8). It should be noted that this is an upper limit because the contribution of the external chambers and multiple scattering are still included in the residuals.

The coordinate along the blade was measured by means of pickup strips. These were 11 mm wide. Due to this width most of the induced charge was collected by one or two strips. With this limited distribution the centre of gravity algorithm does not produce a good result. We have defined a quantity called Y_{share} as follows:

$$Y_{share} = Q_1 / (Q_1 + Q_2 - Q_3)$$

where Q_1 is the charge on the strip with the largest signal, Q_2 the charge on the neighbouring strip with the larger pulse height and Q_3 the charge on the other. The minus sign in front of Q_3 is used to reduce the effects of cross talk, but its contribution is in any case very small. A histogram of Yshare is shown in figure 9. Solving the left-right ambiguity on the basis of which of the neighbours has the higher charge we obtain a resolution of σ = 380 μm (figure 10). Again it should be stressed that this is an upper limit.

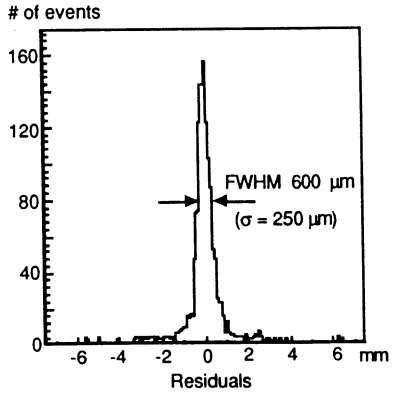

Figure 8. Residuals of coordinate measured by drift time

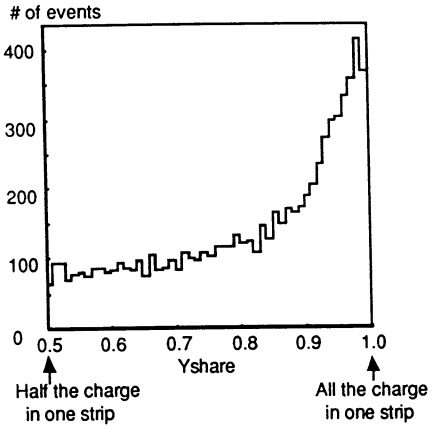

Figure 9. Yshare Distribution

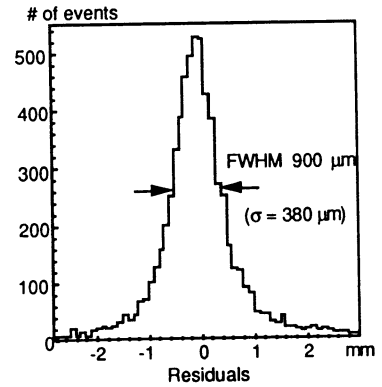

Figure 10. Residuals of coordinate measured by pickup strips

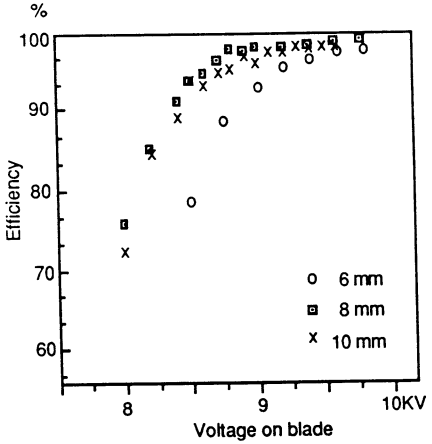

Figure 11. Efficiency of blade chamber for various blade to roof distances

Efficiency and Rate Dependence

We have investigated various cell geometries during the beam test in order to learn the optimal cell design. In figure 11 we show the efficiency for 3 different blade tip to to roof distances. The full geometric effiency is 96% due to the finite thickness of the walls. Another investigation that we are performing is the dependence of the chamber on the rate. We can operate the chamber above 90% efficiency at fluxes of 700 particles / cm^2, this is shown in figure 12.

Conclusion

We have shown that the blade chamber works with full efficiency for minimum ionizing particles with good spatial resolution.

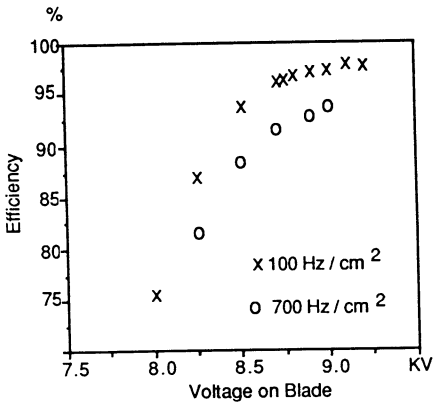

Figure 12. Efficiency of blade chamber for different particle flux

We can solve the left-right ambiguity with charge asymmetry measurement on the walls. During the last beam test we also tested a chamber built with curved blades. This chamber worked extremely well. This technique allows us to build detectors with very small limitations in the geometry, with high mechanical reliability; requirements needed for the construction of Large Area Devices for μ detection at a future multi-TeV hadron collider.

Future Developments

Further work is needed on the effect of particle rate on the chamber efficiency and resolution. We have also started the construction of large scale prototype, it will have curved cells.

References

[1] J. Ballon, V. Comparat and J. Pouxe, Nucl. Instr. and Meth. 217 (1983) 213-216.

[2] J.H. Duijn, C.W.E. Van Eijk, R.W. Hollander and G.W. Sloof, Nucl. Instr. and Meth. A273 (1988) 541-543

Preliminary Report on a Planar Surface Chamber Working in Limited Streamer Mode

LAA Large Area Devices Group
CERN, Geneva
Switzerland

Presented by
D. Mattern and M.C.S. Williams

Abstract

This report outlines the very preliminary work that we are doing to investigate whether we can build a chamber with lines or other types of patterns on a insulating surface. The usual problem with this approach is that the insulator gets rapidly charged and makes it impossible to obtain a high enough field to work with gas gains in the proportional or limited streamer mode. However, with our surface patterns we reach a **steady state with very high gas amplification.** We are using **anode structure widths of typically 300 µm**, which can be easily obtained in a printed circuit board production line. We will discuss the measurements being done with three different chambers and give an outline of the continuing studies.

Introduction

The purpose of the LAA large area devices group is to find a suitable detector for µ-detection at future hadron colliders.

Many people have had the desire to build a chamber by 'printing' the lines on an insulator, using the techniques of printed circuit boards or some similar technology. In fact there have been successes. Neumann[1] et al. built a chamber where they attached wires onto a resistive foil and obtained efficiencies of 85%. Recently Oed[2] followed by others [3,4] have built a device with 10 µm wide lines, with 200 µm pitch evaporated onto a glass plate. They have obtained a gas gain of 10^3 and 10^4.

This was the starting point of our investigation. We decided to scale up their device and have lines of 100 µm width etched onto standard Kapton and epoxy sheets with a pitch of 1 cm.

Set-up and results

Our first surface is shown in *figure 1*. Basically it is a series of parallel copper lines etched onto a Kapton foil. They are alternately cathode and anode. The anode lines are 100 µm wide, with a wider section at the tip of 300 µm to reduce corona discharge problems at the ends. This surface we installed into a gas tight box through which we flowed pure isobutane. We connected the anode lines (via a transformer and diode box, as a protection against sparks) to a x5 LeCroy amplifier (LRS 335L) and then to a Tektronix 2440 digital oscilloscope. We irradiated the box with a ^{57}Co source (130 keV γ's) and applied a positive high voltage to the anodes. At 6 kV we started to observe signals. Immediately after applying

the high voltage to the surface many signals were observed, but the rate quickly dropped within a few minutes to a **steady rate still correlated with the source.**

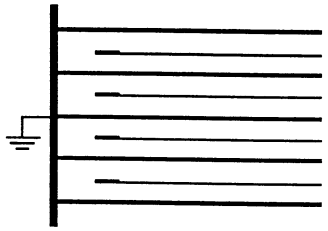

figure 1: First attempt, showing sensitive tips

Further work showed that only the tips of the 300 µm section of the anode lines remain active, i.e. giving a signal in this steady state mode.

Our initial understanding of this effect came from our work with blade chambers [5]. In figure 4 of the contribution to this conference concerning blade chambers, we show the field and equifield lines of a blade chamber. The field is highest at the tip. All field lines are in the surface of the paper. An insulator has the property that no field line ends on it (if they do, then a free electron or positive ion would be attracted to the surface changing the potential so that field lines no longer end on the surface). Thus if we could, by some magic means, insert a sheet of insulator parallel to the plane of the paper, the field should be undisturbed. This is not a true representation of the field of our printed device as the field has to be considered in three dimensions, however it is a useful way of visualising the potentials on the surface. This means that in the steady state the tip of the anode is still surrounded by a nonlinear field **on the surface.**

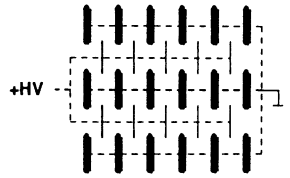

figure 2: Second surface chamber, dotted lines are on second layer

With this analogy in mind we constructed our second surface shown in *figure 2*. If the basic cell of this surface was a cross-section of a blade chamber, then the field on the surface should be as shown in the figure from [5].

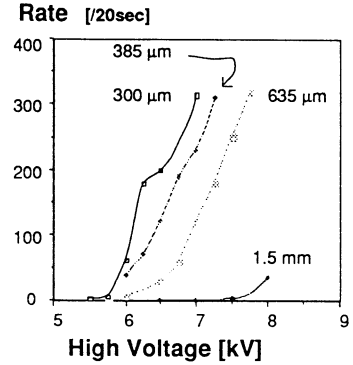

figure 3: Counting rate vs. HV for various anode line widths with ^{57}Co source

We made various similar patterns with different anode line widths. Using a discriminator/scaler set-up to quantify the results, we found a similar behaviour for different

width lines, except for needing a higher voltage for wider lines. We found that lines even as wide as 1.5 mm also give signals. However with the anode-cathode spacing used on this surface, sparking occured at several hundred volts above this point. The results for the various line widths are shown in *figure 3*. We show the time dependence of the counting rate in *figure 4*.

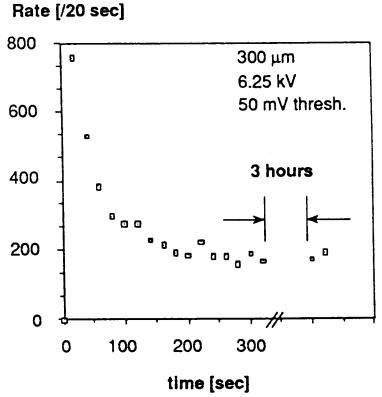

figure 4: Rate vs. time with ^{57}Co source

This rate drops for the first 5 minutes and is then stable giving the same rate after three hours. The rate is effectively zero without the source. We have tested the 300 µm wide lines of this chamber in a 5 GeV/c pion beam. We could measure the position of the through-going particle with a set of external drift chambers. In *figure 5* we can see points in a plane perpendicular to the beam for particles that give a valid 'stop' signal to the TDC. It is easy to see that the sensitive region is located only at the tips of the anodes. The TDC spectrum is shown in *figure 6*. It is compatible with the assumption that we do have drift of electrons in the gas .

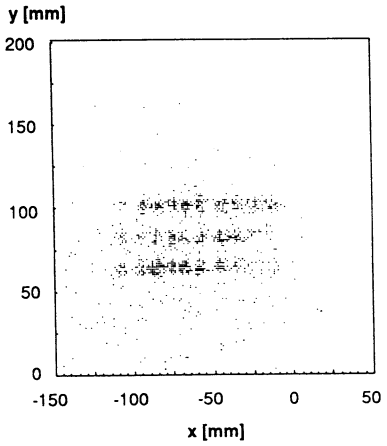

figure 5: Minimum ionizing particles crossing foil chamber

Another strong indication of this can be seen, when we apply a cut on the drift time excluding drift times greater than 100 ns: we cut the tracks that are furthest from the tips. The y-projection of *figure 5*, also with this time cut, is shown in *figure 7*.

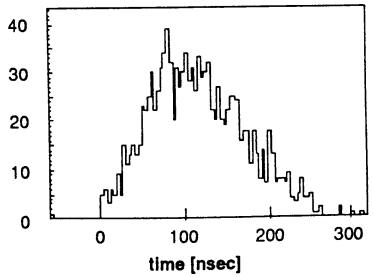

figure 6: Drifttime spectrum . Measured with beam particles.

Encouraged by these results we decided to make a plane of 'tips', i.e. the anode is just a small circle. This is favorable because

we avoid the inefficient part (the lines) of the anodes. Since we need to connect a voltage to it, and to read out the pulses, these spots

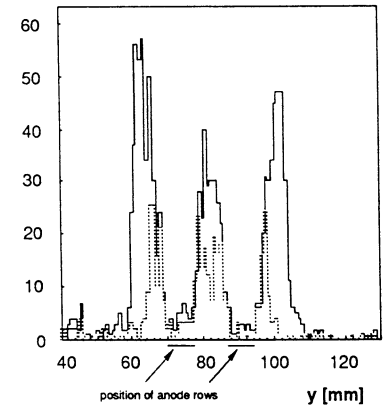

figure 7: Y-projection with time cut (dashed line)

are through-plated to lines that run on the back side. The diameter of this hole is 0.5 mm with a pitch of 10 mm. These holes

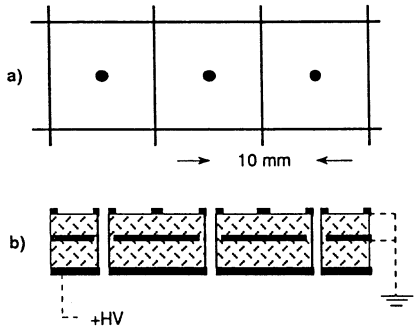

figure 8: The hole chamber: a) top view, b) cross section

we surround with a square cathode grid made of 300 µm lines. In order to control the charging of the surface we inserted a ground plane in between. This plane comes within 1 mm of the plated through hole. We show this design in *figure 8*.

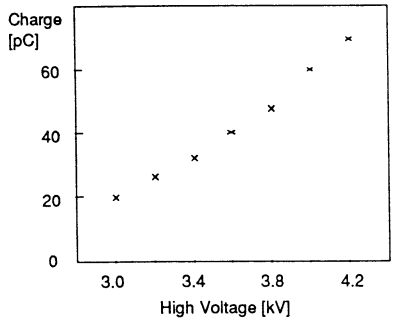

figure 9: Charge vs. High Voltage with ^{57}Co source

We mounted a ground plane 4 mm above this surface and installed it inside a gas box filled with 3:1 Ar/Isobutane.

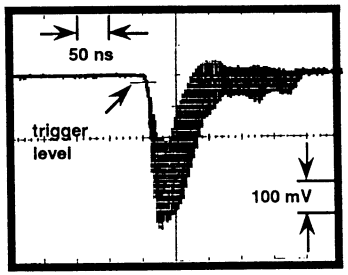

figure 10: Envelope of hole chamber signals (^{57}Co source)

In *figure 9* we show the average charge of the signals observed from this surface versus high voltage. One can see that the signals are large and increase with high voltage. Our digital oscilloscope displays the maximum and minimum signal that satisfy the

trigger (i.e. the envelope). This is shown in *figure 10* . One can see that even though the trigger is set at 25 mV the smallest signal has a peak at 200 mV. It seems that either we grow a streamer or not. Another interesting point is to test wether we are able to observe the positive ions coming from the gas amplification process. We coupled our digital oscilloscope directly to the ground plane above this surface with a 1 MΩ input impedance. The averaged pulse is shown in *figure 11.* Initially there is a large charge induced by the growth of the streamer, and the slow increase of the signal for 80 μs is compatible with mobility data for positive ions and the assumption of positive charge moving towards the cathode. Further work is in progress on the investigation of this surface.

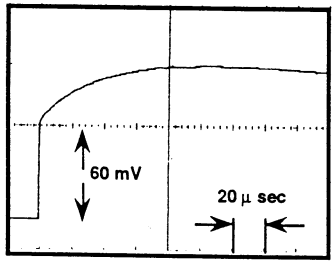

figure 11: Drift of positive ions. measured with ^{57}Co source

Advantages of the design

There are many advantages of such a chamber. One goal is to produce a large area detector with this method. If we can find some simple pattern that works with a reasonable efficiency for minimum ionising particles, then one can imagine printing sheets or rolls of it, and then using it somewhat like wall paper. Another big gain could be that it would be very easy to make a geometry that suits the experiment. No longer is one bound by straight stretched wires or flat surfaces. Furthermore we have been using somewhat standard printed circuit techniques to generate our surfaces. 250 μm lines are a standard line width in this business. This would lead to highly automated and simple chamber construction.

Aim and future work

These studies have only just begun. We have shown that we can have a surface that produces large pulses and that this surface works in a repeatable and stable way. Obviously the goal is to produce a chamber that is 100% efficient for minimum ionising particles,with a good position resolution.

Acknowledgement

We want to thank the people of the CERN Printed Circuit Workshop and especially its leader Mr. Gandi. We enjoyed the excellent quality of the boards they delivered to us. G. Ambrosi and D. Hatzifotiadou took some of the measurements presented here.

References

[1] M.J. Neumann, T.A. Nunamaker IEEE Trans. on Nucl. Sci. 17(3),43-49 (1970)
[2] A. Oed, Nucl. Instr. and Meth. A263 351-359 (1988)
[3] F. Angelini et al., INFN-PI/AE 89/2
[4] F. Hartjes et al. CERN/EF/4330 R/FU/ed
[5] LAA Blade Chamber, this conference

The Honeycomb Strip Chamber

Harry van der Graaf
Gerard Faber*
Paul Rewiersma
Joop Buskens

NIKHEF-H, Kruislaan 409, 1098 SJ Amsterdam, The Netherlands

* now at ETH, Zürich/CERN

A new detector is proposed for the accurate measurement of the position of charged particle tracks; it uses the principle of strip-segmented cathode readout and it has an extremely low weight since it is constructed merely out of foil. Multiplexers are used to reduce the readout electronics to a quantity which allows integration on the chamber: the costs of the electronics and the volume of the cables is therefore a fraction of that of a comparable drift chamber.

Introduction

Experiments at the future hadron colliders are likely to include the detection of muons; identification could be done by placing planar track detectors behind hadron absorbers (calorimeters), while the measurement of muon momentum would require the accurate determination of the track curvature due to the magnetic field [L*, EMPACT]. The latter is realized in the L3 experiment at LEP, CERN [L3]. Here the muons are deflected by a magnetic field of 0.5 T; the diameter of the magnet is 12 m and its length is also 12 m. The muons, created in the Z_0 decay in the center, have a curved trajectory which is measured by three coaxial cylindrical detectors with diameters of 6, 9 and 12 m, respectively. Effectively one measures the deviation from a straight line (fig. 1).
For the accurate measurement of muon momenta in LHC/SSC experiments the following differences show up:

- The maximum momentum is a factor 10 higher; the bending power BL^2 of the magnet and the space resolution of the muon detectors should be sufficient to reach the required momentum resolution.
- The detection of muons in the forward region is relatively important;
- The counting rate may be much higher and will certainly be much higher in the forward region; ambiguity in track positions should be avoided. The short bunch rate (20 - 40 ns) requires an instantaneous event labeling.

Some calculations have been made on what the consequences will be for such a new detector. If one requires a muon momentum resolution of 2 % at 300 GeV and an outer diameter for the hadron calorimeter of 9 m then the following figures and quantities are obtained:

total muon chamber surface:		3000 m^2
spatial resolution	inner layer:	30 μm
	middle:	20 μm
	outer:	30 μm
relative layer alignment:		better than 10 μm

A system of drift chambers and alignment systems has been proposed which could satisfy these demands [Becker]; the chambers need to be equipped with planes of 32, 64 and 32 sampling wires in order to reach the spatial resolution. The high weight of such chambers and the demands of alignment stability lead to complicated support structures. They require a large number of channels consisting of a preamp, discriminator, TDC and connecting cables. Moreover, existing TDCs like LeCroy type 1879 can not be applied because of a too large random error in the common stop. Application of FADCs would solve this problem but the costs would be too high.

The Honeycomb Strip Chamber (HSC)

Principle. The HSC is a proportional chamber with strip-segmented cathode readout [Cha, Gatty, Gra1, Gra2, Gra3]. A charged particle leaves a track of electron-ion pairs of which the electrons drift towards the anode wire and the ions (much slower) to the cathode planes. The electrons cause an avalanche at the wire; after this the ions created in the avalanche drift towards the cathode planes. This causes a negative charge on the avalanche wire and positive charges on the cathode planes and, if present, adjacent wires. The sum of the positive charges is equal to the negative charge on the avalanche wire. The shape of the charge distribution on the cathode planes is an exclusive function of the geometry of the chamber if the avalanche size is small [Gra3].
By splitting the cathode planes in mutually insulated strips perpendicular to the wires, the charge distribution results in a charge for each strip; from the distribution of the signals of three adjacent strips nearest to the avalanche the position of the avalanche in the direction of the wire can be accurately obtained.

Honeycomb Chambers. The chamber will consist merely out of foil. Using well known etching technology one can obtain kapton foil with copper strips. The foil can be folded into a ribbon surface such that the folding lines are perpendicular to the strips (fig.2).
Two of those ribbon foils form the 'honeycomb' cells as shown in fig.3:
A stack of these layers form a stiff honeycomb shown in fig.4.
In the center of each cell an anode wire is to be strung. The foils would then need to have conducting strips on both sides in order to surround the wire. This results in an unacceptable capacitance between an oppositional upper and lower strip of a foil; since the strips of two foils associated with one cell are connected there would exist a strong capacitive coupling between all strips that have the same X coordinate (see fig. 7 for the coordinate system). This would create a poor signal/noise ratio and much cross talk.

This 'vertical' strip capacitance can be reduced using foil with strips on only one side in the geometry of fig. 5. Each elementary layer of fig. 3 is covered with a flat insulating foil which acts as base for a next layer. This layer is shifted by half the cell pitch. Wires are strung only in the hexagonal cells. The inherent dead space can be reduced to a minimum by reducing the horizontal distance between active cells within a layer.
As a consequence one needs a stack of at least two layers in order to have a full efficient track detector. In fact, there are still a few tracks with angle $\theta = 60^{o}$ which will never be detected using this geometry. This can be solved by an additional relative shift between groups of chamber layers.
The Z coordinates of a track can be determined by the recording of the hit pattern of the anode wires in the hexagonal cells. One could also add chamber layers with a strip direction perpendicular to the existing ones.
The details of the geometry of the chamber will depend very much on the application.
At the open sides of the honeycomb cells an end cover must be fixed. It has the following functions:

- it defines the shape and pitch of the honeycomb cells at their open ends;
- it acts as support for the wire: it has a hole for a shrink pin;
- it carries a reference surface having a well defined distance to the strips;
- it acts as gas inlet or outlet;
- it covers potential regions of high electrical fields to prevent HV breakdowns;
- it stiffens the chamber;
- it guides the load forces of the chamber supports;
- it carries the weight of the on-board electronics;
- it supports the cables

The end pieces should be light and have a small volume in order to limit the dead space. The chamber under construction has end pieces of square aluminium tube for each chamber layer; more layers can be glued together to form a rigid, self-supporting unit. Holes are drilled through the end cover tube and a plastic plug is inserted. The plastic plug carries a shrink pin which fixes the wire. The tube distributes the chamber gas over the honeycomb cells. Grooves are machined to guide the honeycomb foil on its position at the aluminium tube and to provide for a good gluing surface.

The Readout System

In recent years much progress has been made in reducing the volume and power consumption of an electronic unit with given specifications. A better understanding of chamber (mis)behavior resulted in efficient protection circuits; a good test procedure reduces the probability of malfunctioning to a very low level. Furthermore, very small and powerful microprocessors and FADCs are now available for low prices. Finally, recent large scale experiments have experienced major problems and limitations due to the huge quantities of cable; solving the problems associated with the total weight and volume and the diversification in cables and connectors have consumed much manpower.

For these reasons virtually all electronic circuits will be located on the chambers. The functions of these systems are:

- to amplify the signals from wires and strips;
- to digitize the ratios of three strip signals
- to form a digital hit pattern of the wires;
- to produce a fast trigger signal for each individual chamber layer;
- to calibrate the preamp/ADC combinations;
- to provide test facilities;
- to monitor: chamber alignment, temperature, local magnetic field;
- to provide communication with the outside world.

Some functions of the electronics are discussed below in more detail:

Amplification of wire and strip signals. The strip signal amplifiers will be mounted at the end of their own strip. A printed circuit board may transport the output signals to the box containing the signal processors.

Digitizing the ratios of the charge signals from the strips. The principle is explained in detail in [Gra4]. The circuit is shown in fig. 6. Each strip has a (charge sensitive) preamplifier followed by a

discriminator. An avalanche on an anode wire causes induced charge signals on the strips. The discriminator associated with the strip having the largest signal will be activated first. By means of a logic circuit this strip is selected; only the output level associated with this strip becomes 'active'.
At each charge amplifier output there are three analog switches; using these the output signals from the charge amplifiers can be connected to three lines called Q_{left}, Q_{middle} and Q_{right}. An active output of the logic circuit results in the connection of three adjacent strip charge signals with the three signal lines. A priority encoder produces a digital number for the 'middle' strip: these form the most significant bits of the avalanche coordinate.
The signals Q_{left}, Q_{middle} and Q_{right} are converted by Flash ADCs (FADCs); the FADCs do not have a fixed reference signal but the signal Q_{middle} is used instead. The outputs of the FADCs are therefore straight digital figures for the charge ratios Q_{left}/Q_{middle} and Q_{right}/Q_{middle}. These two figures, to be transmitted to the outside world, allow an accurate calculation of the avalanche position using a look-up table.

A fast trigger signal. The output of a wire signal discriminator could be enabled to give a direct signal to the outside world. A typical time resolution of this signal is 20 ns; if there are 16 layers of active cells a resolution of 10 ns can be obtained. A hit pattern from all the wires of a chamber provides accurate Z coordinate information of the track. If this information is used in off-line analyses the time resolution may be reduced to 5 ns. The chamber could then be applied for time-of-flight measurements for bunch identification and discrimination against cosmic rays.

Calibration and test of preamp/ADC combinations. A typical strip pitch is 5 mm: a determination of an avalanche position better than 100 μm requires the interpolation of a factor 50. A high quality preamp is therefore needed. By means of resistor adjustments using laser beams differences of individual preamps can be canceled. This may be expensive and it may not be necessary if a good calibration provides for the knowledge of the gain differences.
Calibration pulses on one or more wires would result in equal signals on all strips simultaneously due to the capacitive coupling between wires and strips. Two adjacent selected preamp channels could be connected to one of the FADCs (this requires a remote control ability of the latches at the discriminator outputs). The relative gain of the preamps is proportional or inverse proportional to the output of the FADC.
If this calibration method is used cross talk between strips and between other parts deeper in the electronics may have influence on the measured

relative gains. Perhaps a better method would be the injection of charge pulses using an accurate capacitor per strip and a multiplexer which allows pulsing of any possible combination of strips.

Monitor tasks. In some applications the position of the chamber must be accurately known. A proven method is the 'monitored survey' RASNIK system [Duinker]. The electronics of this system could be integrated with the rest of the system. Other monitoring tasks are the local measurements of the temperature and the magnetic field.

Communication with the outside world. There are only digital signals between a chamber and the outside world; they consist of a group of fast timing signals and a group of FADC data and monitor data. The use of fiber light guides would permit a high data rate without interference while the cable volumes remains small. There should be a two-way communication link to provide the control of test and calibration systems. Due to the simple cabling the chamber and its readout system could be tested during installation.

Spatial resolution

In order to study the spatial resolution of a chamber consisting of one layer of honeycomb cells a Monte Carlo simulation program has been written. It has the following sequence:

1 generate a muon track through a hexagonal cell with a specific φ, θ and Z coordinate (see fig. 7);

2 calculate cross points of the track with the cell walls;

3 generate spots of primary interaction between muon and gas according specific probability [Ader];

4 calculate or generate for each primary interaction the energy of primary electron, the total charge of the associated secondary electrons and the position of the centre-of-gravity of the secondary electron cloud [Ermi];

5 generate the avalanche charge for each secondary electron according specified distribution [Alkha], [Curran];

6 calculate the charge signals on the strips assuming specified chamber geometry [Gra4];

7 generate preamp noise on the charge signals;

8 calculate the track position from the charge signals.

Fig. 8 shows the resolution as function of φ for two cell radii. The influence of preamp noise is not included. The differences are therefore only caused by the statistical fluctuations in the size and quantities of the clusters of secondary radiation. The RMS of the differences is a direct measure for the intrinsic spatial resolution of a hexagonal cell. At $\varphi = 0^o$ the resolution is 35 μm due to the non-zero energy of primary electrons (∂-rays). Angle θ does not have influence on the resolution.
If we can limit the angle of incidence φ to 5°, then the resolution due to the fluctuation of the centre-of-gravity of the secondary electron distribution has the maximum value of 70 μm.
We calculated the permissible preamp noise which would increase the resolution to a maximum of 100 μm. Assuming a gas gain of 50.000, a charge collection fraction of 0.3 [Gra4], a strip pitch of 5 mm, a strip width of 4 mm and a cell radius of 5 mm it was found that the equivalent input preamp noise should be limited to 5000 e- RMS. This limits the length of the chamber; the capacity of a strip for this geometry has a value of 220 pF m^{-1}.

The influence of magnetic field. If a magnetic field is applied with field lines into the direction of the strips, the electrons will no longer drift along their local electrical field line. The Lorentz force causes the electron to follow a track which makes an angle with the zero B field track. This is called the Lorentz Angle.
Fig. 9 shows the effect of the magnetic field: it results in an effective additional angle of incidence which is bad for the resolution. There is also a systematical error associated with the Lorentz angle;
if the center of the track within the cell differs from Y = 0 the Lorentz angle will shift the X coordinate of the center of gravity of the avalanche. The influence if the magnetic field can be canceled by a rotation of the chamber around the Z-axis equal to the Lorentz angle.
Since the electrical field is not constant in the chamber (E :: 1/R) the Lorentz angle will vary and complete canceling of the angle by a tilt is not possible. The compensation is the best if the tilt equals the local Lorentz angle at the cathode plane; in particular the outer secondary electrons contribute to the deterioration of the spatial resolution.

Low Lorentz angle gases. The HSC will have to be able to operate in high magnetic fields. In order to limit the tilt of the chamber a low-Lorentz gas should be used. A mixture of argon and CO_2 is a good non-flammable

candidate [Ma,Coyle]; some ethane may be added to improve the operation at high gas gain. The drift velocity should be high enough in order to reach the needed time resolution.

Conclusions, Status and Future Developments

If the Honeycomb Strip Chamber performs as expected then it has the following advantages compared to drift chambers:

- high accuracy per sampling layer;
- low cost of electronics;
- no trigger required; it provides timing signals;
- small cable quantity;
- simple gas system; no exotic or flammable gases or special purities are required;
- broken wires only disable a chamber layer;
- extreme low weight.

In the design of the detector one has, however, to limit the angle of incidence φ to 5 °. The Lorentz angle requires a tilt of the chambers; this causes a dependency of the X coordinate on the Z coordinate and inhibits the inversion of the magnetic field. A high gas gain is required for a sufficient signal/noise ratio of charge signals.
At NIKHEF-H a method to fold foils has been developed; the first honeycombs have been made. A test of a working prototype is foreseen in the first half of 1990.
Mass production requires an intensive study of foil stability in variable conditions like temperature and humidity. The quantity of foil with strip conductors may exceed 100 km; etching technology will be too slow and accurately printing of conducting tape should be considered instead. The total number of wires requires automatic wiring of chamber layers.

References

[Ader] M. Aderholz et al.: Nucl. Instr. & Methods 118 (1974) 419

[Alkha] G.D. Alkhazov: Nucl. Instr. & Methods 89 (1970) 155-165

[Becker] U.Becker et al.: Accurate measurements of high momenta muons. Nucl. Instr. & Methods vol. A263 -1 (1988) 14-19

[Cha] G. Charpak et al.: Nucl. Instr. & Methods 148 (1978) 471-482

[Coyle] P.Coyle et al.: Nucl. Instr. & Methods A273 (1988) 862

[Curran] S.C. Curran et al.: Phil. Mag. 40 (1949) 929

[Duinker] P. Duinker et al.: Some methods and tools for testing and optimizing proportional wire chambers.
Nuclear Instruments & Methods vol. A273, no. 2-3, 15 Dec. 1988, p.814-819

[EMPACT] M. Marx: An Alternative Approach to a High P_T SSC experiment.
SSC/CDG Physics Dept. and SUNY, Stony Brook. SSC-219, May 1989.

[Ermi] V.C. Ermilova et al.: Nucl. Instr. & Methods 145 (1977) 555-563

[Gatty] E. Gatty et al.: Nucl. Instr. & Methods 163 (1979) 83- 92

[Gra1] Thesis: Signal Development & Processing in MWPCs. University of Technology 1986, Delft, The Netherlands

[Gra2] H.v.d.Graaf, J.P.Wagenaar: A calculation in three dimensions of the induced charge on the electrodes of a MWPC. Nucl. Instr. and Meth. 217 (1983) 330-334

[Gra3] H.v.d.Graaf, J.P.Wagenaar: Numerical results from calculations in three dimensions of the induced charge in MWPC's. Vienna Wire Chamber Conference Issue Nucl. Instr. and Meth. (October 1986).

[Gra4] H.v.d.Graaf, J.P.Wagenaar: A novel, two dimensional, fast, low cost and accurate readout system for MWPC's. Nucl. Instr. and Meth. 217 (1983) 357-359

[Hanson] G.G. Hanson et al.: Wire chamber requirements and tracking simulation studies for tracking systems at the SSC.
SLAC-PUB-4860, February 1989

[L3] B. Adeva et al.: Nucl. Instr. and Meth. A277 (1989) 187-193

[L*] Meeting on preparation a proposal for R&D for L*. ITEP, Moscow, September 9-13, 1989.

[Ma] C.M. Ma et al.: Drift Velocity and Drift Angle Measurements.
M.I.T, Lab. for Nuclear Science Report Nr 129 October. 22, 1982

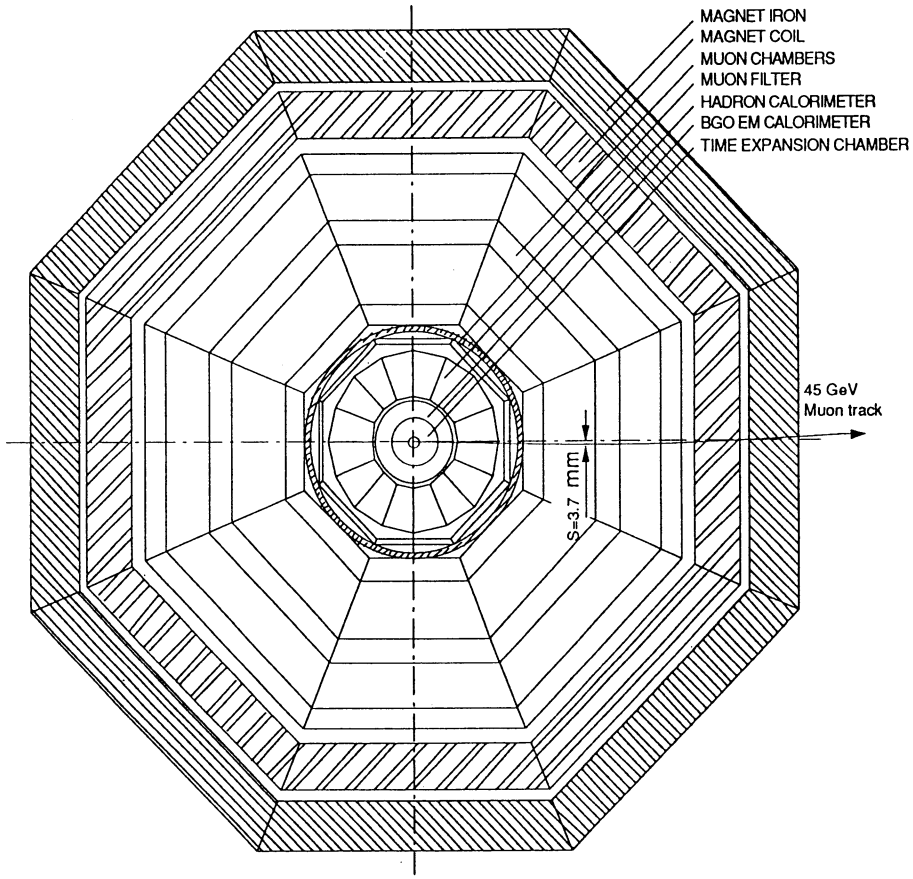

Fig. 1 The L3 detector. Starting from the interaction point: vertex detector, EM calorimeter (BGO), hadron calorimeter, muon filter, muon chambers, magnet coil, magnet return yoke. The track of a deflected muon of 45 GeV has a sagitta of 3.7 mm.

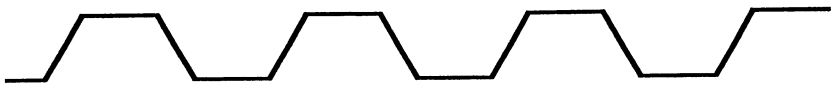

Fig. 2 Folded foil. The strips have a direction perpendicular to the folding edges.

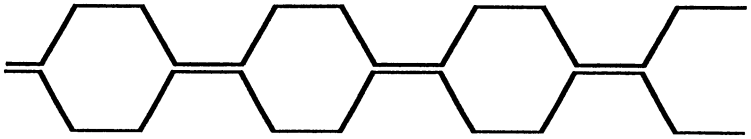

Fig. 3 Honeycomb cells made from two folded foils of fig. 2.

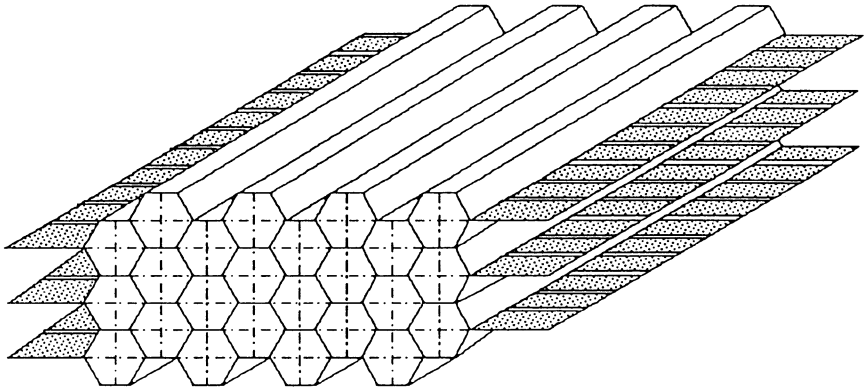

Fig. 4 Multi-layer honeycomb; the mutual strip capacitance is too high. This cell configuration is a good alternative for 'straw chambers' [Hanson]

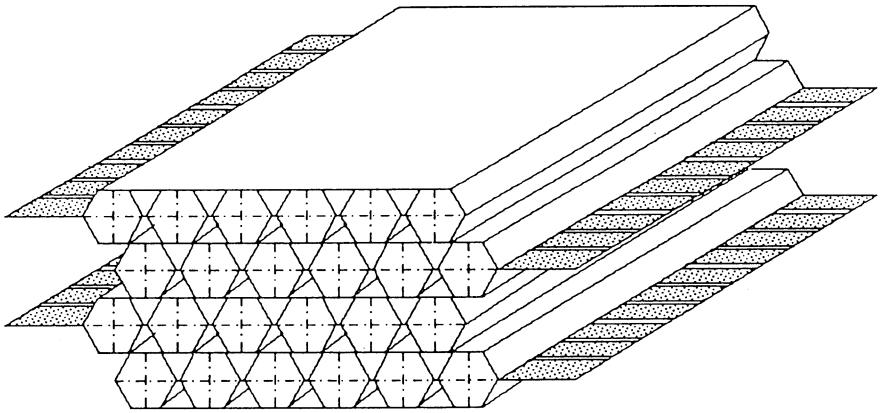

Fig. 5 Multi-layer honeycomb with intermediate foil.

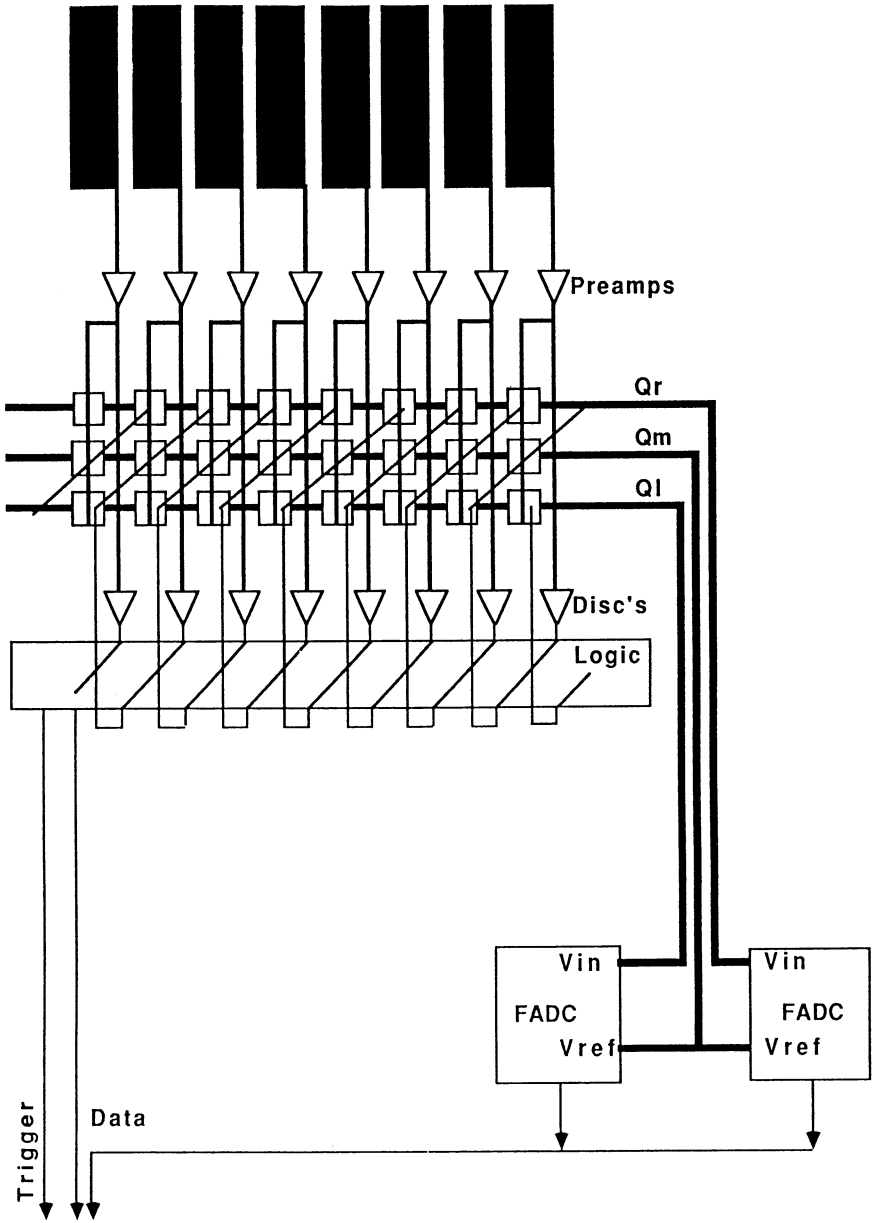

Fig. 6 Principle of readout system

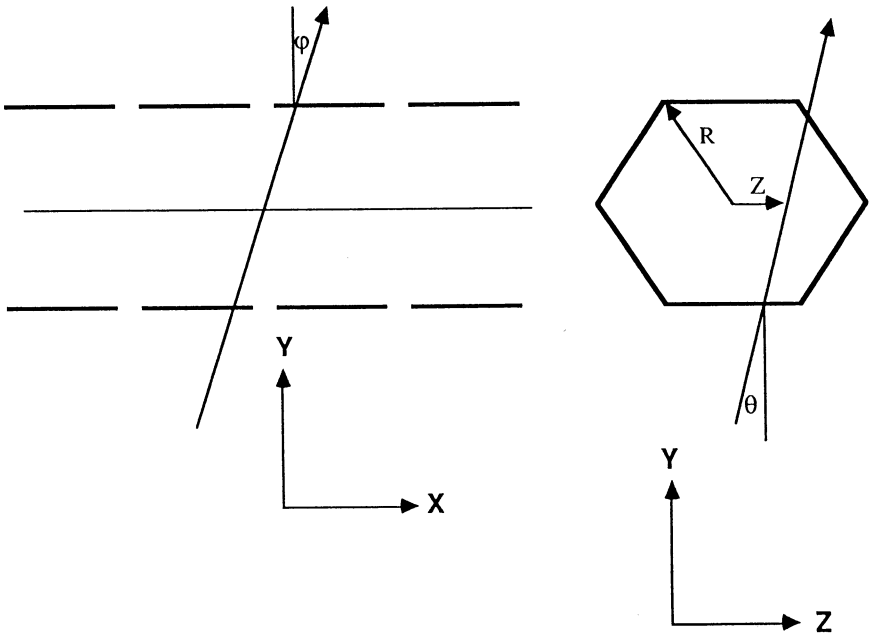

Fig. 7 The coordinate system; muon track through honeycomb cell.

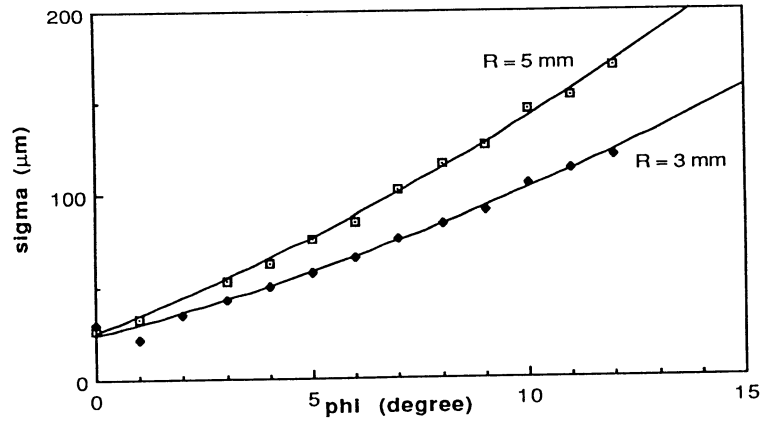

Fig. 8 Spatial resolution of a honeycomb cell as a function of the angle of incidence φ. Shown for cell radii R = 3 and R = 5 mm.

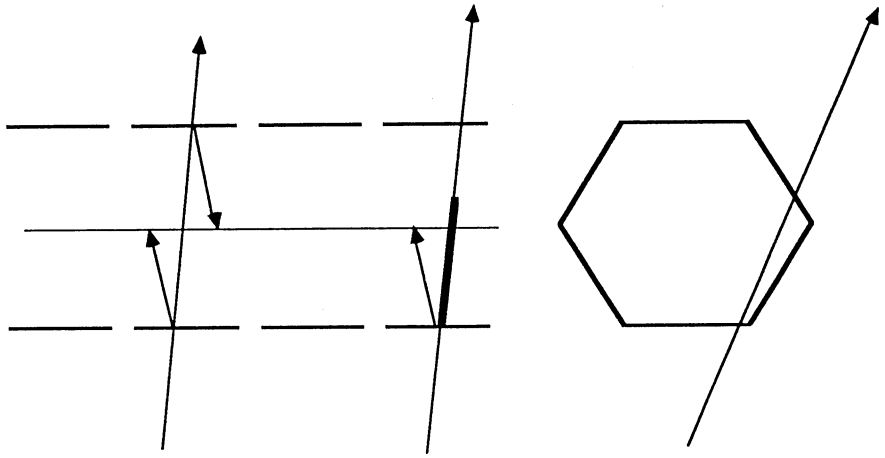

Fig. 9 The effect of a magnetic field: the Lorentz angle. The right hand track does not cross the cell symmetrically; the center of gravity of the avalanche is therefore shifted and a systematical error occurs. This error can be corrected for if the Z coordinate of the track is known from the pattern of hit anode wires.

Recent tests with a gaseous microstrip chamber

Oct 30, 1989

F. Hartjes, B. Hendriksen, J. Schmitz and F. Udo
NIKHEF-H Amsterdam

Abstract

This paper presents a recent measurement using a pulsed UV laser carried out on a microstrip gasdetector as introduced by Oed[1]. The measurement demonstrates that the rms value of the systematic error in the position measurement amounts 6.7 μm for a simple averaging routine and that a further reduction is certainly possible.

1. Introduction

In a gaseous wire chamber, the anode spacing can not be made smaller than about 1 mm because of the appearance of problems with electrostatic instability. By replacing the anode wire plane by metal strips deposited on an insulating surface, it is possible to pass this limit. This method is applied for the gaseous microstrip chamber, a detector with a very small anode spacing, which can be produced using a photolythographic technique. Oed [1] introduced this idea and showed it to work excellently as a detector for low-energy alpha particles and protons. For the measurements presented here we used an insulating plate of which one surface side was covered with alternately anode and cathode strips. The static electric charge on the anode which is needed for the gas gain, was induced by a negative voltage on the cathode strips. The anode pitch was 200 μm. The drift field was generated by a conductive plate positioned parallel to the substrate. Fig. 1. shows a cross-section of the device perpendicular to the strips. An electron cloud liberated in the gas above the substrate, for instance by the passage of a minimum ionizing particle, can be distributed by diffusion while drifting towards the substrate over at least 3 anodes. Whether this process really takes place depends among others on the relation between the transverse diffusion in the gas and the anode pitch. The distribution over more strips enables the calculation of the center of gravity of the original ionization cloud from the charge collected by each strip. As the gas gain is very stable like discovered already by Oed, an accurate position determination will be possible in this way. The electric field between anode and cathode is very high, so nearly all the field lines from the anode end into the adjacent cathode strips. Therefore the positive ions created in the avalanche close to the anode are almost completely collected by the cathodes. Because of the high dipole field the collection of the ions takes place in a short time, the poisoning of the drift space is avoided. As a consequence, the rate capability of this detector is very high [2].

To investigate systematic effects in the position accuracy of the chamber, a scan parallel to the substrate was made with a UV laser beam. It appeared that the systematic error in the measured position of the laser track as calculated by simple averaging of the charge distribution deviated less than 6.7 μm from a fitted straight line.

2. Set-up

A microstrip plate[1] with the same strip layout as described in [3] was used for the test. The pitch of the anode strips was 200 μm, the width of the anode and cathode strips was 10 and 90 μm respectively. The plate was made of 1.5 mm thick glass on which a conductor of 0.6 μm gold was deposited. A detail of the actual strip layout is given in fig. 3. The drift volume above the plate was terminated at 10 mm from the plate by a cathode plane held at -1000V. The anode strips were grounded and the cathode strips were mostly operated at about -500 V. The chamber was placed in a gas-tight box containing mixtures of argon, ethane and carbondioxide as a counting gas. The anodes were connected via a 50 cm long

[1] Manufactured by 'SRON', Utrecht, The Netherlands

twisted pair cable to integrating amplifiers with a sensitivity of 1V/pC. The signals were read out via shaping amplifiers with a time constant of 200 ns by CAMAC ADC's.

3. Measurements

The measurements were done by directing a weakly focused laserbeam (f = 350 mm, Ø = 7 mm) into the counter along the direction of the strips. Focussing of a diffraction limited beam using these parameters produces an ionisation track of 3 cm long and 20 - 40 μm wide. Using a mixture of 76% argon and 24% ethane, the ionisation was distributed over 4 - 5 strips. When the ethane was replaced by carbondioxide, the ionisation was almost completely confined in one strip. The ideal mixture could thus be made by carefully tuning the amount of carbondioxide. A distribution over just 3 anodes like shown in fig. 2. was obtained with 84% argon, 5% ethane and 11% carbondioxide. For this mixture, a scan was made using a remotely controlled stage of the confined ionization spot perpendicular to the strips and parallel to the substrate. Fig. 3. shows the plot of the charge collected on each strip and averaged over 25 laser shots as a function of the beam position along the substrate. The peak value of the amplitude is not completely constant for each strip. Calibration of the electronic chain changed the picture but yielded no substantial improvement. The center of gravity was determined for each measured value of X by a simple averaging over all the strips having an amplitude greater than 5% of the peak amplitude. The result of the calculation is shown in fig. 4. As can be seen, the measured points almost perfectly match a fitted line. A small area of 15 strips was used covering a total width of only 3 mm. Therefore, the drift paths were converging towards the strips. As a consequence, the distance between the peaks in fig. 3 is somewhat bigger than the anode pitch and for the line in fig. 4 a quadratic fit had to be used. The difference between the fitted line and the measured points is plotted in fig. 5. The figure shows that in the plotted curve an oscillation can be distinguished of which the period is related to the anode pitch. This phenomenon indicates that the rather low systematic errors with a rms of 6.7 μm can be further reduced by a more elaborate routine for the calculation of the center of gravity. The irregular behaviour of the curve for values of X greater than 1.5 could be caused by edge effects.

The high voltage operation was often troublesome. In the event of sparking a conductive layer was deposited which required disconnection of the anode strip. The effect appeared to be absent in pure ethane, but the problem with damage or even interruption of the sparking strip remained.

4. Conclusion

The measurements shown above indicate that the center of gravity of confined ionization clouds can be localized with neglectable systematic errors. Because of the very stable gas gain, statistical errors are expected to be kept at a minimum: close to the limit determined by the limited number of primary electrons. The resolution for minimum ionizing particles will depend also on another parameter: the angle of the track. Because of the irregular Landau distribution, the center of gravity of the ionisation induced by a particle will differ in general from the middle of the track. The error caused by this phenomenon is therefore

expected to increase rapidly with the angle of incidence. The gas mixture is in principle not critical, provided that the transverse diffusion is kept at the required level. This constraint inhibits for instance the use of pure di-methyl-ether. Eventual problems with damage in the event of sparking have to be avoided in future by raising the impedance of the electrodes and by using other materials for the strips at a greater thickness.

References

[1] A. Oed, Position sensitive microstrip proportional counter, Instr. Bulletin no 4, March 1988; Nucl. Instr. and Meth. A263(1988) 351.

[2] F. Angelini et al., A Microstrip Gas Avalanche Chamber with two dimensional read-out; Vienna wire chamber conference 1989 and these proceedings.

[3] F. Hartjes et al., A Prototype Microstrip Gas Detector; CERN/EF/4330R/FU/ed, 13 July 1989.

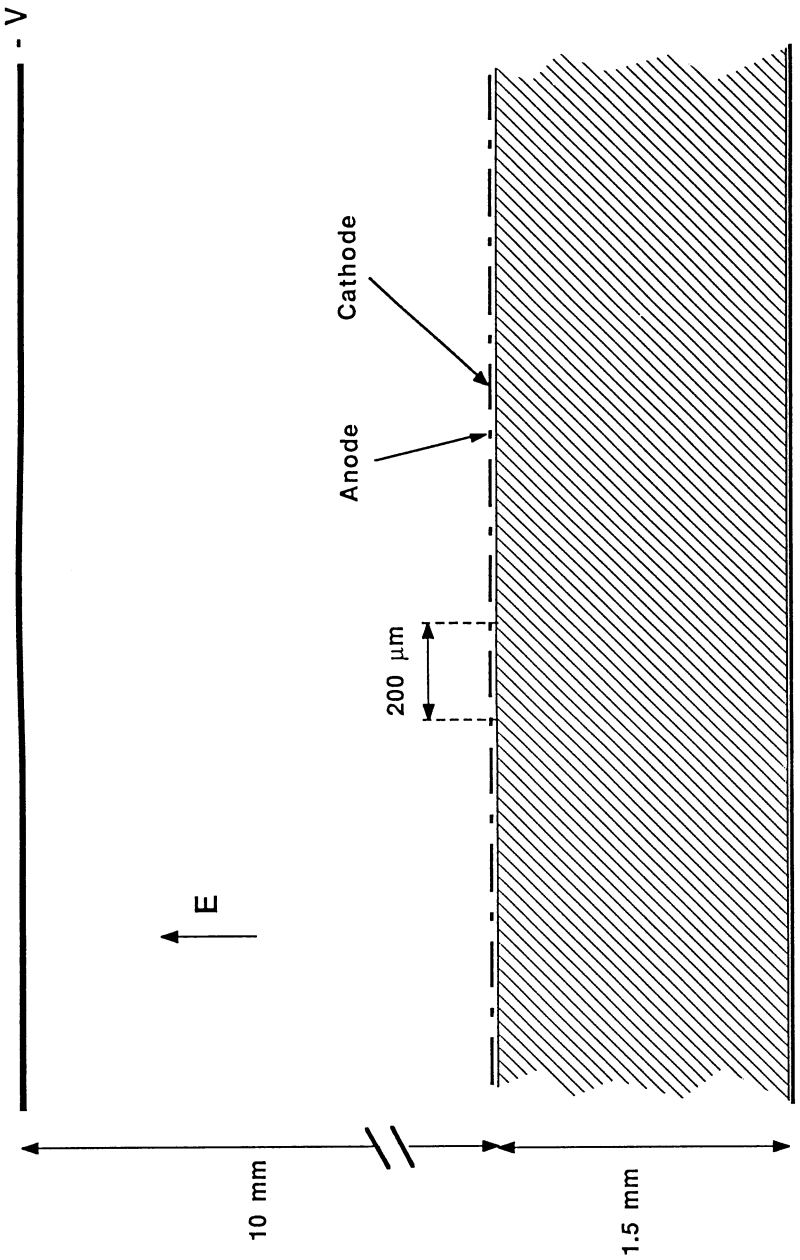

Fig. 1 Cross section diagram of the microstrip plate and driftspace above.

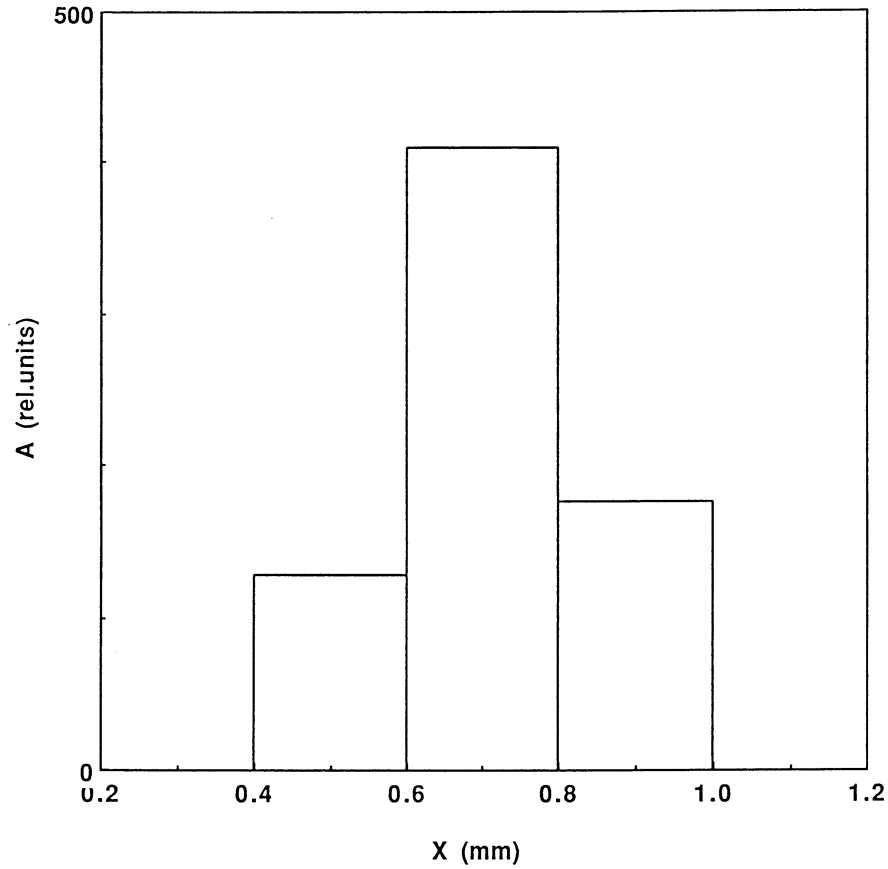

Fig. 2 Example of the distribution of the charge from a thin laser track over three strips. The width of the distribution is completely determined by transverse diffusion.

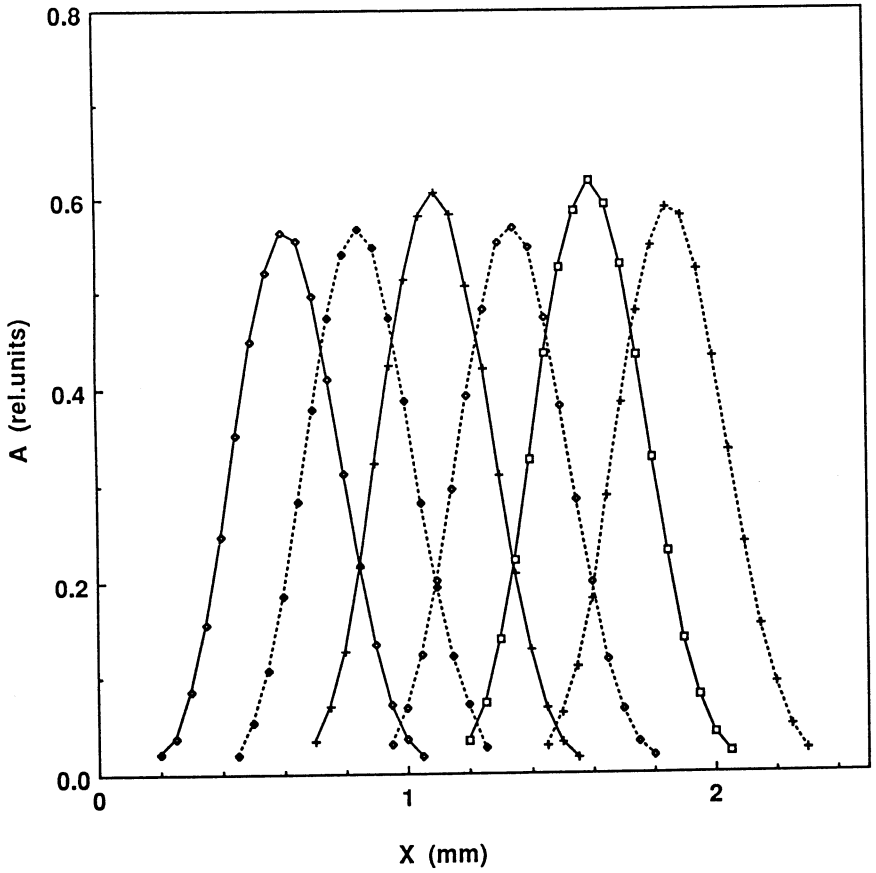

Fig. 3 Plot of the charge (A) collected on each strip and averaged over 25 laser shots as a function of the beam position along the substrate (X).

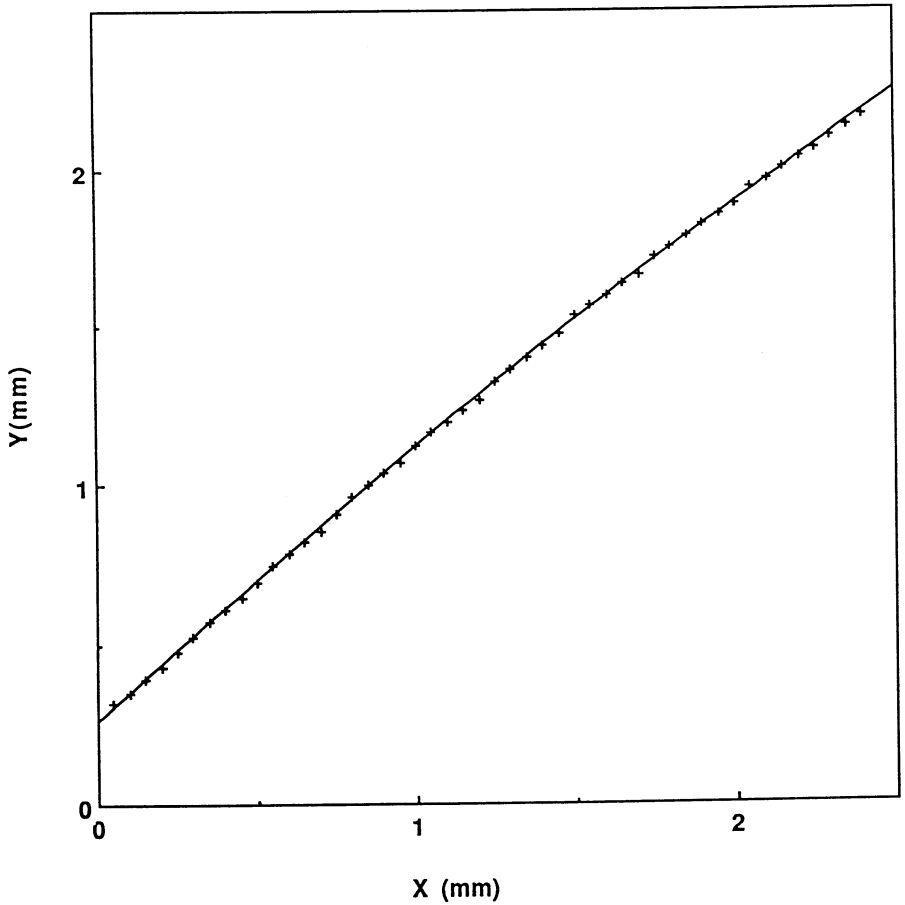

Fig. 4 Center of gravity (Y) of the charge distribution of the laser ionisation versus the beam position (X). The center of gravity was calculated by a simply averaging over all the strips having an amplitude greater than 5% of the peak amplitude. For the plotted line a quadratic fit had to be used because of edge effects in the drift field.

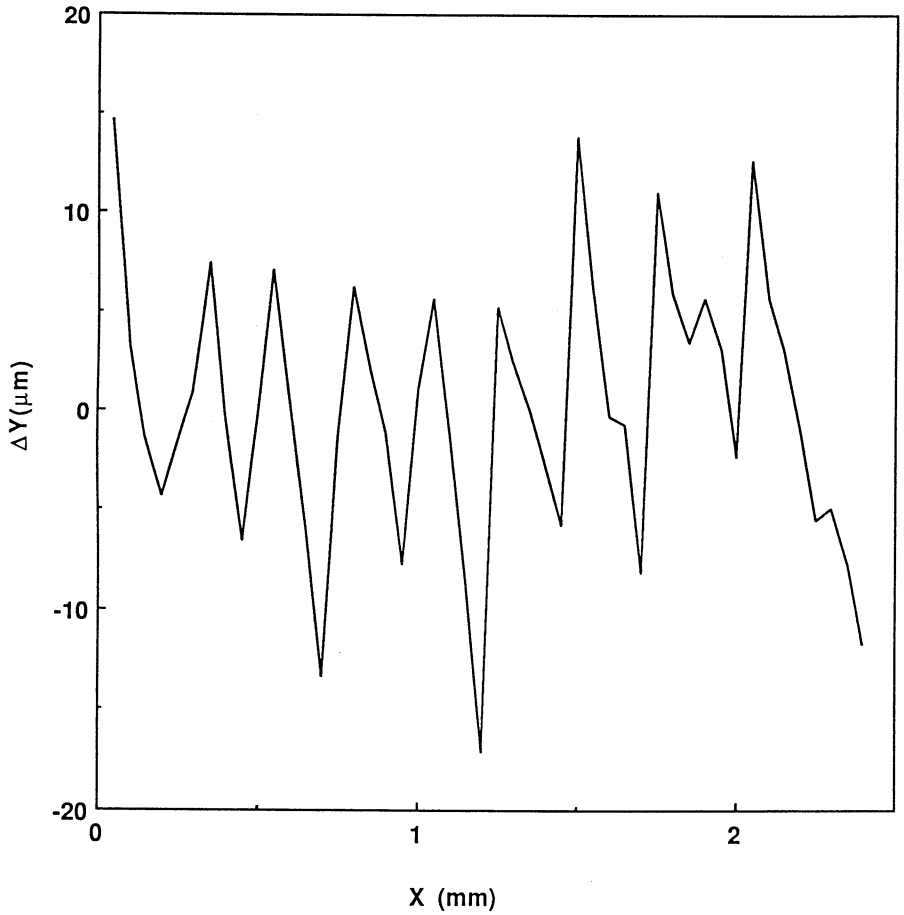

Fig. 5 Plot of the difference (ΔY) between the fitted line in fig. 4 and the calculated center of gravity versus the beam position (X). The rms value of the deviation amounts 6.7 μm.

THE MICROSTRIP GAS AVALANCHE CHAMBER: A NEW DETECTOR FOR THE NEXT GENERATION OF HIGH LUMINOSITY MACHINES

F. Angelini, R. Bellazzini, A. Brez, E. Focardi,
M. M. Massai, G. Spandre, M. R. Torquati.
Sezione INFN di Pisa and Università di Pisa- Italy
and
F. Sauli
CERN, Geneva-Switzerland

Abstract

We present further developments and experimental tests of the Microstrip Gas Avalanche Chamber (MISGAC). This new detector is based on the idea of reproducing intensity and structure of the electric field typical of a MWPC, but on a geometrical scale reduced by a factor 10. This has become possible by using microelectronics technology (electron beam lithography) to define the electric field shaping electrodes. Very good spatial resolution (< 50 μm) and a rate capability > 1 MHz / mm^2 have been measured. We have investigated also the behavior of different electrode geometries and of several gas fillings.

I. INTRODUCTION

There is no doubt that the severe experimental and enviromental conditions at the next generation of high luminosity machines (SSC, LHC, UNK, b-τ factories) pose a tremendous challenge to the gas detectors commonly used for charged particles tracking (wire chambers, drift chambers etc.). The performance of a state of the art gas detector seems limited in spatial resolution, time resolution, rate capability and ageing. Because there is not much room for improvement in these areas, a solution can probably be found only with a drastic change of technology.

In a previous paper [1] we have shown how the use of a microelectronics technology (electron beam lithography) having 0.1 μm accuracy allowed us to construct a gas proportional chamber with a 200 μm anode pitch and a gas gain ≈ 10^4. More recently we have begun a program to study in detail the detector operational characteristics by varying the geometrical parameters such as anode width, anode-cathode gap, far cathode distance etc., as well as varying the gas filling (Ar-Isobutane, Ar-DME, Ar-Xe, Xe-DME, DME). The detector rate capability has also been studied. In this paper, we report on the most recent results of this work.

II. THE DETECTOR STRUCTURE

The detector can be thought of as consisting of two parts: a low electric field region followed by a high electric field amplification region. The drift region (from 3 up to 35 mm) is shaped by a cathode plane ('far cathode') and by the amplification plane. Primary electrons, created in the drift region by the incoming radiation, drift toward the anode and are multiplied in the amplification region around the anode strips.

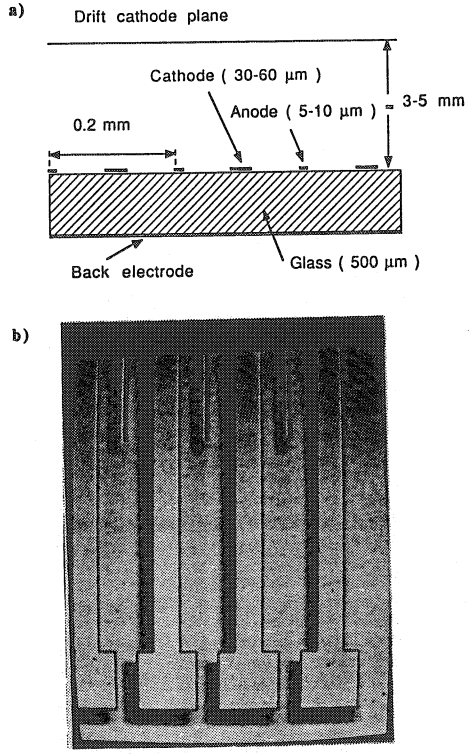

Fig. 1) a) A cross-section of the detector; b) a microphotography of anode-cathode structure.

The high electric field (> to 10^5 V/cm) is obtained by interleaving anode and cathode strips, which were engraved with an electron beam lithographic techniques onto a 0.5 mm thick glass substrate (CSEM-Neuchatel-Switzerland). The precision of this technique is 0.1 μm. The aluminum anode strips have a pitch of 200 μm, are 5 (or 10) μm wide and are 2 μm thick, while the cathodes are 30 (or 60) μm wide. The width and thickness of the anode strips were chosen to have an aspect ratio as round as possible to minimize edge effects. In fig. 1 a) and b) are shown a cross section of the detector and a microphotography of the anode-cathode structure.
The prototype we have built has as 80mm×80mm active area; the back of the glass ('back electrode') can be put at positive or negative potential (with cathodes at ground) to reinforce, if necessary, the field around the anode (see fig. 2).

III. MODELING THE DETECTOR PERFORMANCES

In order to investigate the detector characteristics and find optimum potential settings, the Garfield program (developed at CERN by R. Veenhof) has been used [2]. Even though the original scope of this program was to model chambers made up of thin wires, it is possible to simulate our detector strips by replacing the line electrodes with rows of wires of appropriate diameter (0.1-0.2 μm): the simulation results are meaningful from a distance of at least 5-10 times the wire radius.

Fig. 3 shows details of the equipotential lines in a region close to the anode strips; it is possible to estimate the intensity of the electric field, near the anodes, which is needed to initiate the avalanche process. Fig. 4 shows the drift lines for the electrons released by a ionizing track crossing the detector and fig. 5 shows a detailed view of the drift lines for positive ions in the region between the anode and the cathode strips; almost all of the positive charge is collected by the two closest (60 μm) cathode strips.

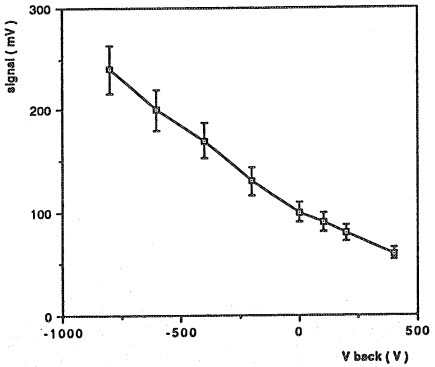

Fig. 2) The signal amplitude as a function of the back electrode potential.

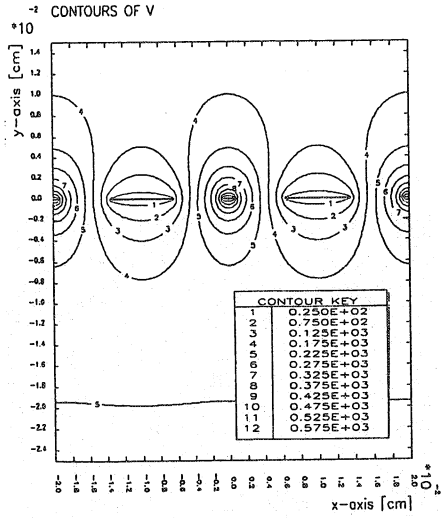

Fig. 3) Details of the equipotential lines in a region close to the anode strips.

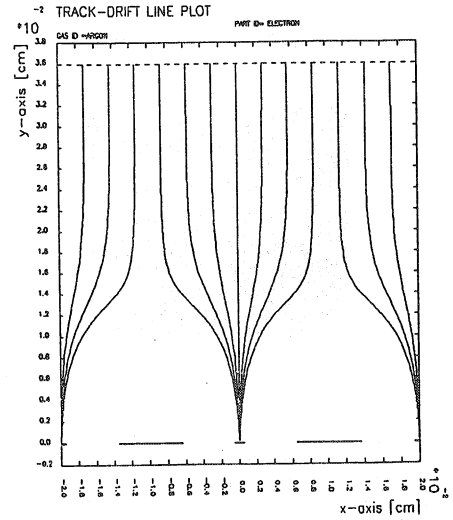

Fig. 4) The drift lines for electrons.

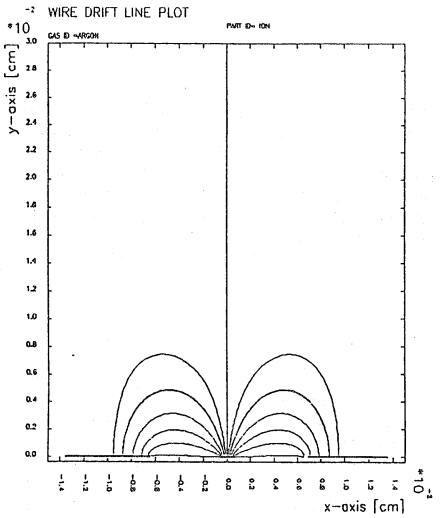

Fig. 5) The drift lines for positive ions.

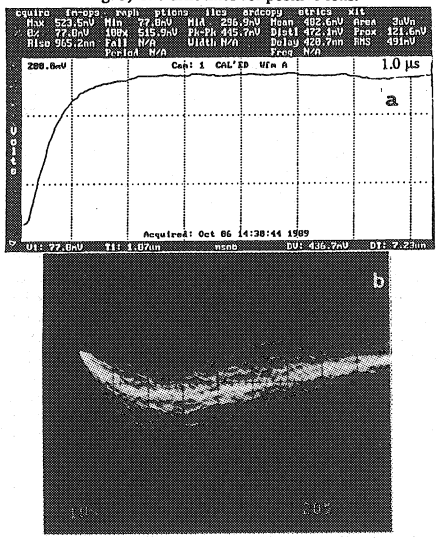

Fig. 6) a) The signal from the anodes observed on a digital oscilloscope (no differentiation); b) the corresponding signals from a standard MWPC observed on an analog oscilloscope.

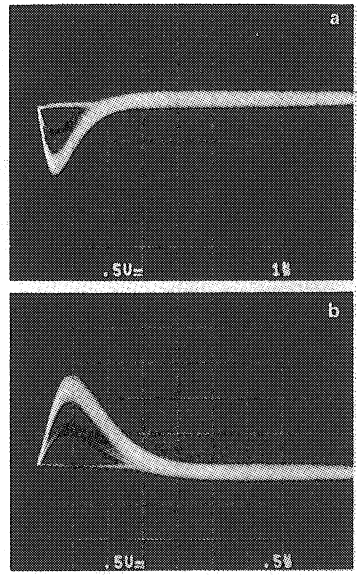

Fig. 7) a) The signal from the anode strips; b) the signal from the cathode strips, with a ^{55}Fe source in Ar-CO_2 mixture (500 ns differentiation time constant).

IV. THE SIGNALS

The structure of the electric field defined by the geometry of anodes, cathodes and far cathode is such that the positive ions are collected mainly by the near cathodes as shown in fig.5.The time needed to collect all the positive charge at the cathode is therefore < 1 µs while in the standard MWPC it is several tens of microseconds (see fig. 6). Depending on the applications, the charge signal can be shaped relatively slowly as in fig. 7 (500 ns differentiation time constant) or can be shaped quickly as in fig. 8 (30 ns differentiation time constant). The signal to noise ratio was ≈ 30 for the fast shaping time constant (^{55}Fe source).

V. THE GAS FILLING

An important goal of our research effort was to explore the range of possible gas filling for this new detector. We started with rather conventional and well known gas mixtures like Argon-Isobutane and Argon-CO_2. With these mixtures we have tested detectors having a 5 or 10 µm anode width and an anode-cathode separation of 60 µm. The maximum gas gain of ≈10^4 was obtained with Argon-Isobutane and a 5 µm anode.

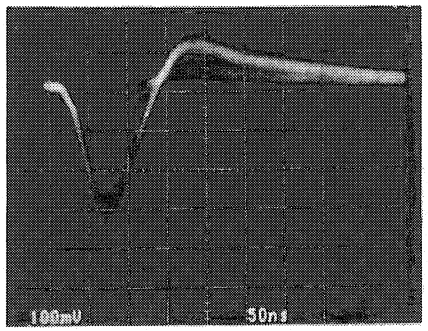

Fig. 8) A signal from the cathodes connected to fast- shaping electronics (τ_{diff} ≈ 30 ns) in a Ar-DME mixture; the S/N ratio is 30.

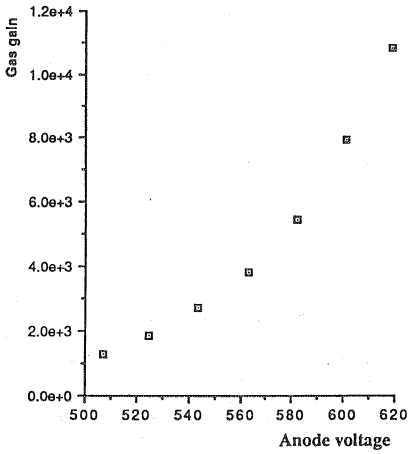

Fig. 9) The gas gain as a function of the potential difference between anode and cathode strips. The anode width was 5 µm and the source was ^{55}Fe.

Fig. 9 shows the gas gain plotted versus the anode voltage in these particular conditions, while fig. 10 shows the pulse height spectrum obtained with an Ar-CO_2 mixture and ^{55} Fe source.

An important point for using this kind of detector in a tracking system at, for example, the next hadron colliders (bunch crossing-time < 40 ns) is to reduce as much as possible the gas thickness, so as to avoid the degrading the spatial resolution at wide angles and to reduce the time to collect the primary electrons (the detector memory). The use of gas with high cluster density and high specific ionization is therefore strongly preferred. Xenon and Dimethil-Ether (DME) are two of the most promising candidates. Xenon has an ionization density of 44 clusters/cm and a total specific ionization of ≈ 300 pairs/cm. DME has an ionization density of 55 cluster/cm and a total specific ionization of ≈ 150 pairs/cm. A microstrip chamber with a 10 µm anode and a anode-cathode separation of 80 µm was tested with Ar-DME, Xe-DME, Ar-Xe and pure DME filling; a standard mixture of Ar-Isobutane was also used as reference. The detector worked well with all mixtures, but with Xe-DME and pure DME an increase of a factor two in the gain was observed. Fig. 11 shows a typical cathode signal when MISGAC was filled with pure DME (^{55}Fe source). Tab. 1 summarizes our experience with the various gas mixtures we have tried.

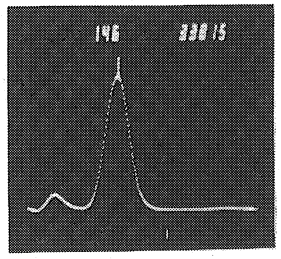

Fig. 10) The pulse height spectrum of ^{55}Fe signals in Ar-CO_2. The FWHM of the 6 KeV peak is ≈ 18%.

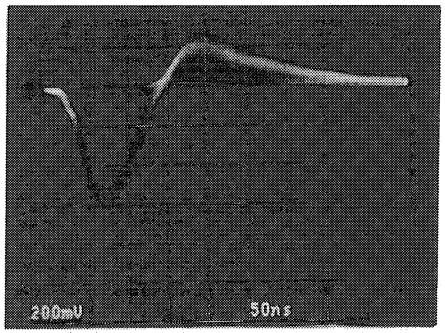

Fig. 11) A typical cathode signal with pure DME (^{55}Fe source).

	good	fairly good	very good
Ar-CO_2	×		
Ar-CH_4	×		
Ar-C_4H_{10}	×		
DME		×	
Ar-DME		×	
Ar-Xe		×	
Xe-DME			×

Tab.1 Summary of the gas results in terms of gain and stability.

VI. COMBINIG A MISGAC STRUCTURE WITH A PPAC

One possible solution to further increase the gain of the microstrip detector is to subdivide the amplification process in two steps. The first stage can be made with a parallel plate avalanche chamber (PPAC) with modest amplification (≈ 10^3)in a uniform electric field (≈ 10 KV / cm).
A significant fraction (0.2+0.3) of the charge produced in the PPAC can be transferred through a stainless steel mesh into the drift region of the MISGAC and finally amplified (≈ 10^3) at the anode strips (see fig. 12). In spite of a more complicate mechanical assembly, this approch has several advantages: i) because the first cluster generated in the PPAC region gives the greatest contribution to the signal, the effective thickness of the detector is reduced to ≈ 0.5 mm; ii) consequently, also the time jitter is strongly reduced.
We have built and tested a combined MISGAC-PPAC structure, which worked satisfactorly with a total gain 5 times greater than MISGAC alone.

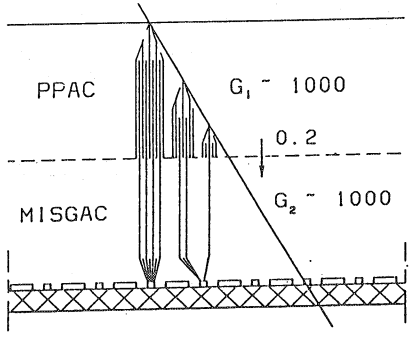

Fig. 12) The electrode structure of the combined MISGAC-PPAC.

VII. THE SPATIAL RESOLUTION

To study the positional sensitivity of the detector, eight consecutive cathode strips were connected using a microbonding technique to eight charge preamplifiers and individually read-out. Fig. 13 shows an example of the single event charge distribution on the cathode strips (^{55}Fe source illumination, 7 mm drift space), while fig. 14 shows the histogram of the centroid of the distribution of fig. 13 when two slits 120 μm wide, 1 cm thick and 500 μm apart were uniformly illuminated with a ^{55}Fe source. The FWHM of the two peaks is much less than 200 μm indicating that the major contribution to the width comes from the slit itself. The spatial resolution can be roughly estimated on the order of 50 μm (RMS), and is dominated in this case by the range of the photoelectrons.

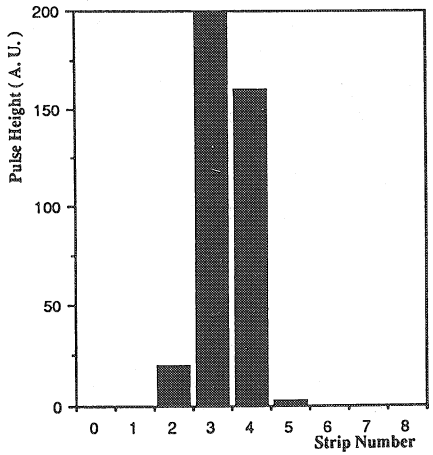

Fig. 13) A cathode pulse height distribution obtained with ^{55}Fe (single event).

VIII. THE RATE CAPABILITY OF THE DETECTOR

One of the most important features of the microstrip detector should be the high rate capability. This comes from two factors: i) the very fine pitch which reduces the incoming flux per wire by at least a factor 10 compared with the standard MWPC and ii) the very short ion collection time (hundreds of nanoseconds instead of tens of microseconds as in the MWPC) which avoids the space charge buildup which usually occurs in the MWPC, at high data rates. Because of space charge buildup which shields the electric field around the wire, the gas gain starts to drop in the standard MWPC at a rate ≈ $5 \cdot 10^3$ particles/s mm^2. To study quantitatively this problem we have illuminated a small area (≈ 1 mm^2) of the microstrip chamber with a very intense beam of 8 KeV X-ray coming from the copper anticathode of an X-ray tube. We observed no gain drop even at the maximum output current of the X-ray tube corresponding to a detector current of 20 nA/cm wire. At this current the measured mean rate was $5 \cdot 10^5$ particles / $s \cdot mm^2$ (see fig 15).The istantaneous rate was at least of factor 4 higher due to the duty cycle of the X-ray tube. Fig. 16 shows an oscilloscope picture of the signal coming from ≈ 1 mm^2 of the detector at rate of a few 10^5 Hz. To study the stability of the detector, the MISGAC was exposed to a flux of 10^5 Hz/ mm^2 for one hour, without any particular problem.

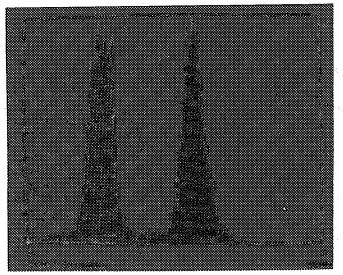

Fig. 14) The histogram of the centroid of the cathode charge distribution obtained with two slits 500 μm apart (^{55}Fe source).

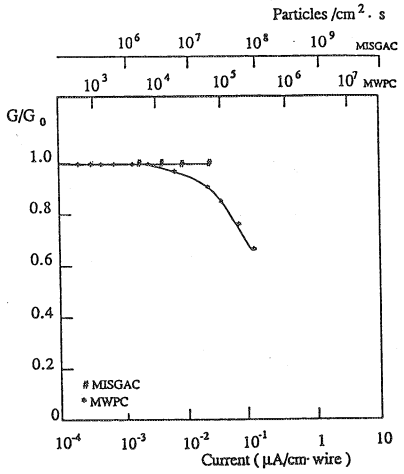

Fig. 15) The relative gas gain versus the wire current and incoming flux for a standard MWPC and MISGAC.

IX. CONCLUSIONS

As we continue to gain are more and more experience on the operation of the microstrip gas avalanche chamber, we become more and more convinced that the coupling of microelectronics technology to the fabrication of a gas detector represents a major step forward for the improvement of the detector performance. Indeed, almost all the characteristics of the detector (spatial resolution, energy resolution, rate capability) are significantly improved over those of the standard MWPC without increasing the cost of the detector (≈ 1$/$cm^2$). The detector works well with all gas mixtures we have tried, including Xenon and pure DME, which are of special interest for the next generation of high luminosity hadron colliders. The only limitation (if such) comes from the gas gain which at the present is limited to ≤ 10^4. Further tests of the performance of the detector with minimum ionizing particles are certainly needed and will be pursued in the future.

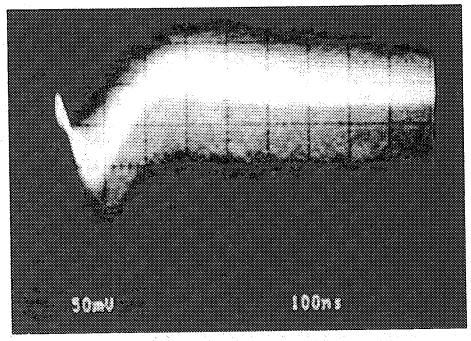

Fig. 16) The signal from the cathode strips when a high intensity flux of 8 KeV X-ray impinges on the detector (rate ≈ 500 KHz/mm^2)

Acknowledgments.
We would like to thank G. De Carolis and C. Magazzù for the efficient technical support.

References

1. F. Angelini, R. Bellazzini et al., Paper presented at 1989 Vienna Wire Chamber Conference, in publication on NIM A.
2. R. Veenhof - CERN Helios note, 1988.

PHOTON FEEDBACK IN MIXTURES WITH LOW PHOTOIONIZATION VAPOURS*

R.S. Ribeiro[1], E.P. de Lima[2], R. Ferreira Marques[1,2], A.J.P.L.Policarpo[1,2] and J.R. da Silva[1]

1- LIP - Coimbra

2- CFRM / INIC - Coimbra

DEPARTAMENTO DE FISICA, UNIVERSIDADE DE COIMBRA, P3000 COIMBRA, PORTUGAL

ABSTRACT

Afterpulse formation in gaseous detectors using mixtures with vapours of low photoionization potential can be a serious drawback for their use in UV detection . In the present work a review is made of the results obtained previously in a cylindrical counter working in SQS mode, concerning the percentage of photon feedback in mixtures of argon-ethane-TEA. Data are also presented concerning the time distribution of afterpulses formed in a MWC, for mixtures of argon-ethane(methane)-TEA, with TEA concentrations up to 30%. These results show that the percentages of photon feedback can be substantially decreased, down to a few percent, with the use of short gates. This is encouraging for the application of this type of readout in UV detection (namely in RICH) as it provides an efficient background rejection mechanism together with an improvement in the spatial resolution, without the need for further amplification.

1 - CYLINDRICAL COUNTER

The aim of this part of the work was to see how the percentage of photon feedback from the gas evolves in a cylindrical counter working in the limited streamer mode (SQS), as we change the concentration of TEA, for anode voltages in the plateau region.

The experimental setup used was a cylindrical counter 29.5 mm diameter and 235 mm long, with the anode wire (100 μm Be-Cu) stretched along its axis. A more detailed description of the apparatus can be found in ref. 1. Tests were made with mixtures of Ar-Eth-TEA with TEA concentrations up to 30%. A ^{55}Fe source was used in all cases.

As explained in ref. 1, the signals due to the photoelectric effect on the detector walls are well localised in time with respect to the first avalanche. So, by using appropriate gates one can count the pulses coming

from the ^{55}Fe source, the time localised afterpulses and the non-localised ones wich correspond to the photoionization in the gas by the light emitted from the avalanche. These three curves are represented in fig. 1 for the argon(20%)- ethane(50%)- TEA(30%) mixture as a function of the anode voltage. From such curves one is able to plot the dependence of the percentage of photon feedback on the anode voltage for each mixture. In order to compare data from different mixtures, these percentages were plotted against the "increment in voltage" , which is the difference between the applied voltage and the voltage that corresponds to the beginning of the plateau. Fig. 2 represents the results obtained for the set of mixtures with 50% ethane.

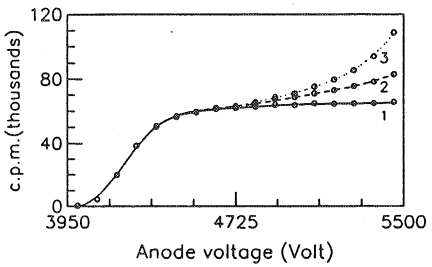

Fig. 1 - The evolution of the counting rate with the applied voltage. 1- primary pulses; 2 - primary pulses plus 'non localized' afterpulses; 3 - primary pulses plus all the afterpulses (ref. 1).

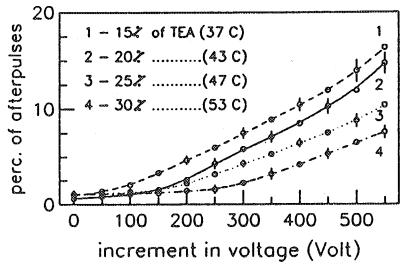

Fig. 2 - The dependance of the percentage of afterpulses arising from the gas on the increment in voltage for Ar - (50%) ethane and several concentrations of TEA (ref. 1).

2 - MULTIWIRE CHAMBER

For this setup the purpose was to study the time distribution of the afterpulses formed in a multiwire chamber working in the SQS mode in mixtures with argon-ethane and argon-methane, as a function of the TEA concentration.

The test setup consisted of a MWC with 40μm gold-plated tungsten anode wires 6mm pitch, 50μm Be-Cu 2mm pitch cathode wires and anode to cathode distance of 7mm. For the measurement of the time distribution of the afterpulses in the neighbouring wires as a function of the anode voltage for the different mixtures, the 5.89 keV X-rays from a ^{55}Fe source were collimated entering the chamber through a 100μm mylar foil. For this geometry no photoelectric effect on the cathodes was observed.

Due to the vapour pressure of TEA at room temperature, it is necessary

to use a thermal bath for the bubbler and heat all the remaining pipes and the chamber to achieve TEA concentrations higher than 7%.

After discrimination the anode signals are fed to a LeCroy CAMAC 2229 TDC which is started (and gated) by the signal of the irradiated wire and stopped by the pulses from the photon feedback on each of the three neighbouring wires; for normalisation purposes the four wire signals are counted by a quad-scaler, with the same gate (500 ns).

For each mixture time distribution measurements were done for three different voltages: one in the middle of the plateau (obtained with the X-rays from the ^{55}Fe source on one wire), another at the end and a last one above the plateau. All results presented here refer to the measurements done at the end of the plateau as the preliminary results of tests made with krypton light indicate that it is a voltage that corresponds to the threshold for a reasonable single photon efficiency.

Fig. 3 shows the time distribution of the pulses due to photon feedback for the argon(35%)-ethane(50%)-TEA(15%) mixture at three consecutive wires (distances of 6, 12 and 18mm). Fig. 4 shows the same distribution on the wire at 6mm for two argon-(50%)ethane mixtures with 15 and 30% of TEA. From fig. 4 we can see that the percentage of afterpulses increases with increasing TEA concentration; this general behaviour is sumarized in fig. 5 for the first 30 ns after the ^{55}Fe streamer as a function of the wire position.

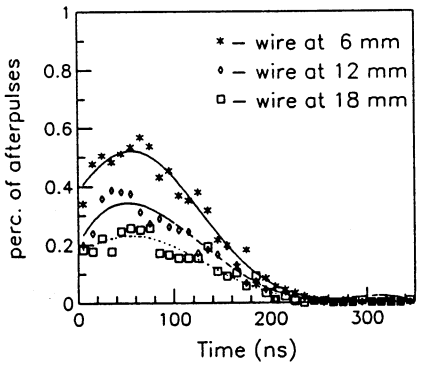

Fig. 3 - Time distribution of afterpulses due to photon feedback in a Ar (35%) - ethane (50%) - TEA (15%) mixture, observed at an anode voltage of 3500 V, for the three wires close to the irradiated one.

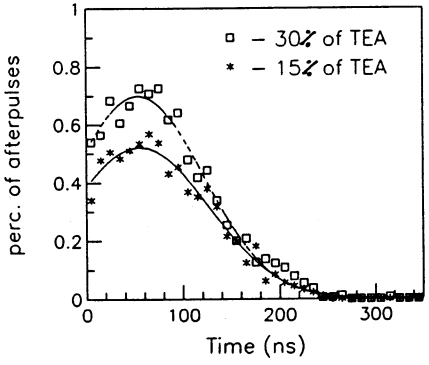

Fig. 4 - Time distribution of afterpulses for the wire at 6 mm from the irradiated one, for two mixtures of Ar-ethane-TEA.

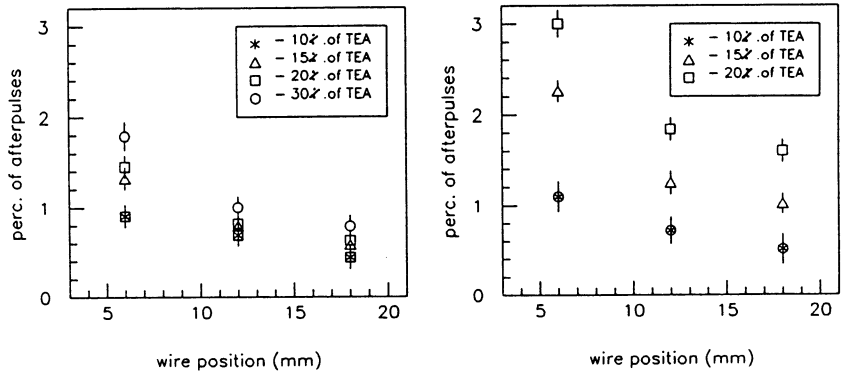

Fig. 5 - Percentual distribution of the afterpulses observed in the three closest wires, for different TEA concentrations in mixtures of: left figure) Ar - ethane (50%) - TEA; right figure) Ar - methane - TEA.

3 - CONCLUSIONS

From the data obtained for the mixtures studied with the cylindrical counter one can conclude that the percentage of photon feedback globally decreases with increasing TEA concentration. In rough terms, this can be explained by dead zone effects: a higher TEA concentration would be responsible for a shorter mean free path of most of the photons responsible for the photoionization in the gas and, consequently, more and more photoelectrons fall in the dead region associated to the primary avalanche.

Conversely, the results from the MWC seem to indicate the reverse behaviour. However, a fact that maybe relevant for the understanding of this problem is the possibility that the dead zone is longer than the anode pitch; so, the photoionization at shorter distances (an effect that cannot be observed in the cylindrical counter) in now clearly seen in the adjacent cell of the MWC. It should be noted that these global percentages of photoionization in the gas are not explained with the short mean free path for ionisation of photons with wavelenght close to the peek of the TEA quantum efficiency . For a better understanding of these phenomena, a measurement of the wavelenght distribution of the light emitted by the avalanches is needed, as well as the time evolution of the dead zone and the efficiency for single photo-electron detection.

The use of short gates (30 ns or so) proved that the SQS mode can be used in a MWC for UV detection with tolerable photon feedback percentages ($\leq$ 2%), allowing their use in particular for RICH appications.

5 - ACKNOWLEDGEMENTS

The authors are grateful to F. Sauli , J.C. Santiard and R. Bouclier for their support.

REFERENCE:

1) R.S. Ribeiro et al. presented at the Wire Chamber Conference '89, Vienna, to be published in Nucl. Instr. and Meth. in Phys. Research.

SUMMARY REPORT ON GASEOUS DETECTORS

Fabio Sauli (CERN, Geneva, Switzerland)

1. INTRODUCTION

Looking at the design of general purpose detectors for high energy, high luminosity colliders (see for example [1,2] , and also contributions to this workshop), one could easily identify two regions that, at the present status of technology, can only be instrumented by some sort of multiwire proportional chambers: the central tracker between, say, 10 and 100 cm from the beam pipe, and the muon detector constituting the outer shell of the assembly+ . The requirements are of course very different; the central detector should have the best possible single and multitrack resolution money can buy, and this in presence of frightening radiation fluxes. Recent improvements in the design of multiwire arrays made of straw chambers or multidrift modules, and some progress in our understanding of the polymerization processes of gases under irradiation give a positive hope (but, I should emphasize, not an absolute certitude) that gaseous detectors could be used safely up to, and maybe above, luminosities of 10^{33} /cm^2.s. A new type of detector, the microstrip proportional chamber, offers a very interesting alternative to the multiwire chambers, and will be described later.

As for the muon detector, the very large surfaces involved imply the use of simple and cheap gaseous devices, such as the plastic tubes already extensively employed for the same purpose in existing setups; a mode of operation at moderate proportional gains (as against the commonly used high gain limited streamer mode) may however be required in order to improve rate capability. Three alternatives to the classic design, the blade, printed circuit and honeycomb chamber, have been presented in the parallel session of this workshop and will be described later in this summary.

2. CENTRAL TRACKING WITH WIRE CHAMBERS

The general operating characteristics and the single and multitrack resolutions one can expect for a central tracker in a high luminosity environment have been extensively discusses by Gail Hanson and John Dainton in the plenary session of the workshop [3,4] . The problems arising at high fluxes, and the possible solutions, are described in the contribution of Stan Majewski [5].

The operating properties of multiwire chambers at high rates are limited by three factors, here briefly summarized together with the obvious steps that can be taken towards improvements:

- Cell occupancy, or probability of two or more tracks to overlap in time so to be confused, or for two or more event to add up within the memory time. The first is determined by the minimum shaping time on the amplifier-discriminator (typically 30 ns), the second by the maximum drift time. The two obvious way to decrease the cell occupancy are to reduce the cell size and/or to use a fast gas.
- Gain reduction due to positive ions accumulating in the cell (space charge). Given that the mobility of ions is sensibly the same for most gases used in proportional counters, one can improve rate capability again decreasing the cell size; indeed, one gains twice: the rate per unit length of anode wire decreases with the wire spacing, and the collection of positive ions is accelerated by the reduced gap anode to cathode.
- Polymerization of the gas under irradiation, or ageing of multiwire chambers. There is some evidence that, with a proper choice of gas and materials, wire chambers may survive several years of use in the central region. Again, a reduction of the cell size, together with operation at the smallest possible gain, will extend the detector lifetime.

+ Two very attractive alternatives, one based on very large arrays of silicon strips and the other on scintillating fibres, seem for the moment unrealistic because of a prohibitive cost and, respectively, because of the unavailability of a suitable image preserving optical delay.

I will briefly describe several detector designs aimed at satisfying the requirements of the central tracker, discussed in this workshop. This being a last-before-lunch talk, I have taken the freedom to use alimentary nicknames for the various detectors, in analogy with a similar terminology used by groups developing scintillating fibre calorimeters.

The *Maccheroni* detector: it consists of a large array of thin cylindrical proportional tubes or straws, similar to those used already by several experiments [6,7] . Individual straws can be organized in layers and superlayers (Fig. 1) in order to improve the pattern recognition capabilities of the detector [2,8] . In the current design, the straws' radius and length are typically 4 mm and 100 cm; reducing the radius while increasing the length to several meters, as required for a SSC or LHC central detector, might be a more severe technological issue that generally assumed. Moreover, the use of thin plastic metallized tubes as cathodes may forbid the use of some interesting gases (mylar, for example, deteriorates quickly in presence of dimethylether). Fig. 2 [9] shows an example of a simulated two-jet event, detected and reconstructed by arrays of straws grouped in superlayers. The pattern recognition properties of the detector are extensively discussed in the quoted literature; the general conclusion is that tracking in the central region is indeed possible in the supercollider environment under rather reasonable assumptions on the detector geometry and resolution.

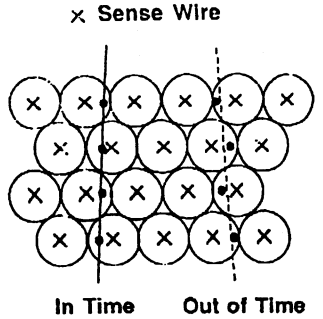

Fig. 1: Rows of straw tubes can be organized in superlayers to improve tracking.

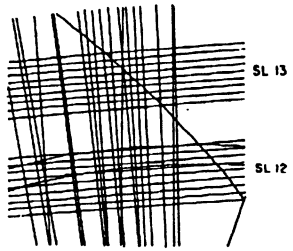

Fig. 2: Detail of the reconstruction of a multitrack event in a straw detector.

The *Cannelloni* detector: a thin envelope stuffed with a large number of independent drift cells. This is the solution based on the multidrift module [10] and adopted for the LAA vertex detector at CERN [11]. Each module (see Fig. 3) consists of a thin carbon fibre envelope, hexagonal in shape, containing a hundred or so independent drift cells, also hexagonal, with an anode wire surrounded by six cathode wires; the cell radius (anode to cathode distance) is 1.4 mm, in order to keep the memory time small. The main design criterion is to position each of the wires within the module with a mechanical accuracy better than 20 μm, thus ensuring that no software corrections are necessary for precision tracking within each module. Average localization accuracies around 60 μm rms have been consistently obtained from the drift time measurement on each wire, using dimethylether as gas fill; tracks are sampled a dozen times in each module. Due to the small size and the high electric field in most of the cell, space charge effects are substantially smaller than in conventional multiwire chambers; Fig. 4 shows a comparison between classic measurements of gain drop versus current or rate in MWPCs, and the same measured with the multidrift module.

The *Fettuccine* detector, also called the microstrip gas chamber. This is a very promising high resolution, high rate gaseous chamber originally proposed a few years ago [12] and then developed by several groups; two papers on the subject were discussed in the parallel session [13,14]. With a photo-lithographic process, thin anodic and cathodic parallel strips are laid down on a 500 μm thick glass substrate, with a 200 μm pitch; an upper cathode seals the chamber and allows to define a region of drift for ionization charges. Fig. 5 [14] shows a typical pattern of alternating thin (10 μm wide) anode strips and wider cathode strips. With a proper gas filling, and applying a few hundred volts between anodes and cathodes, the detector can reach

proportional gains above 10^4 with a surprisingly good energy resolution (15% fwhm for 5.9 keV x-rays). It should be also capable of good localization accuracy, measuring the center of gravity of induced signals on the cathodes (see Fig. 6 [13]) and of high rates, both because of the small pitch and of the short clearing time of ions. Preliminary evidence of these claims was presented at this workshop, but certainly a lot of work has still to be done, particularly to improve the reliability of the detector (rather fragile in case of discharges). Looking at the expected operating performances, one may be tempted to consider the microstrip chamber as a valid competitor with the silicon strip detectors, with a lower price tag by at least an order of magnitude; interestingly, the large scale integrated circuits being developed for solid state devices are very suited to instrument the microstrip chambers.

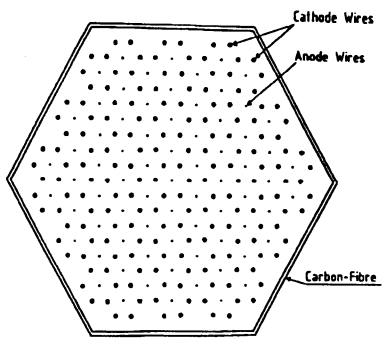

Fig. 3: Schematics of the multidrift module. The envelope is 30 mm in diameter.

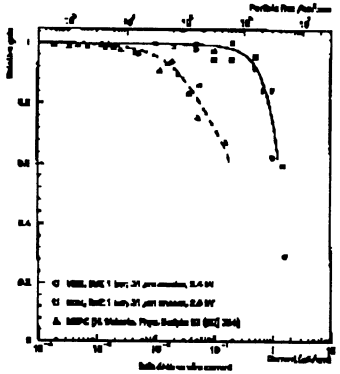

Fig. 4: Rate dependence of gain for a standard MWPC and for the multidrift module.

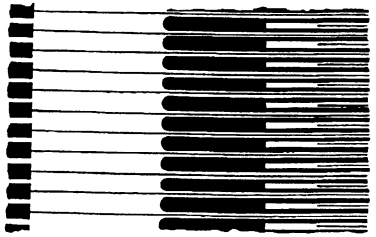

Fig. 5: Alternating anodes and cathodes in the microstrip gas chamber.

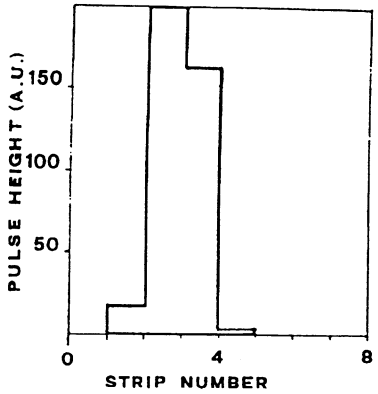

Fig. 6: Charge profile measured in the microstrip. chamber for a single avalanche (200μm pitch)

3. LARGE AREA DETECTORS

Given the requirements on momentum resolution of charged particles, magnetic detectors tend to grow to uncomfortably large sizes at very high energies. Even in the most optimistic estimates, the number of channels required to instrument a muon detector based on multiwire

chambers exceeds 2.10^5, and the corresponding surfaces easily require the acre as unit of measurement. The need to develop cheap and reliable methods of construction for such kind of detectors is obvious. As alternatives to the well established technology of the plastic limited streamer tubes, three new developments have been discussed in the parallel sessions of this workshop.

The *Lasagne*, or blade chamber detector, developed in the framework of the LAA project at CERN [15] consists in a wide and thin metal foil anode, surrounded by cathodes in a box-like geometry (Fig. 7). Under suitable conditions, the gain of the structure (mostly occurring on the tip of the blade) can be pushed to the limited streamer regime; the authors have demonstrated good efficiency for minimum ionizing particles detection, and a spatial resolution (obtained from the drift time) of around 250 μm rms. Moreover, a measurement of charge asymmetry on the two walls of the cell resolves the right-left ambiguity. The advantages of this design are a simplified mechanical construction that does not require to manipulate thin wires, and the possibility to realize geometries other than the planar one, bending the blades and the corresponding cathodes.

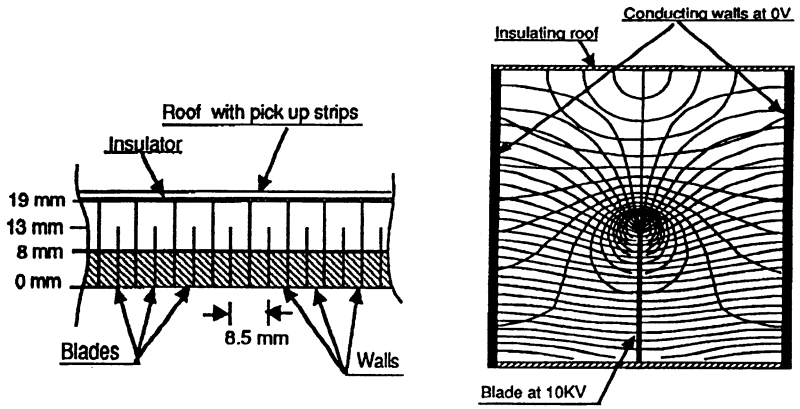

Fig. 7: Schematics and field lines in the blade chamber

The *Tagliatelle* chambers. This is a wildcat approach to the problem of large surface cheap detectors, described by Mattern and Williams [16]; it is based on a strip chamber similar in conception to the microstrip detector previously described, except for the scale, being realized with conventional coarse printed circuit technology. As one would expect for such a structure, the behavior is largely dominated by the charging up processes of the insulating surface between the strips; however, after some "conditioning" time, the authors have demonstrated a stable operation and a decent detection efficiency over extended periods. Moreover, after observing the preferential appearance of large pulses when irradiating the region of the board where anode strips end with a rounded edge surrounded by cathode strips, the authors have built various printed circuit structures where this edge effect is reproduced over all the surface (Fig. 8 and 9); the last one, shown in cross section in the figure, consists of a three-layer printed circuit sheet, with a cellular structure of cathodes on one side, and a metallized hole in the center of each cell serving the function of an anode. A grounded plane is inserted in the middle of the structure, to control charging up of the surfaces. The first results obtained with these structures are very encouraging, and may lead the way to realize flexible, printed-circuit like detectors with arbitrary shapes of the electrodes.

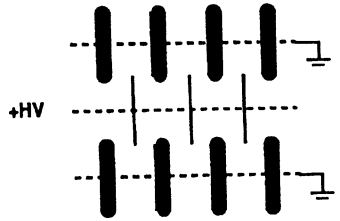

Fig. 8: One of the variants of the printed circuit chamber; dotted lines represent the interconnections on the back plane.

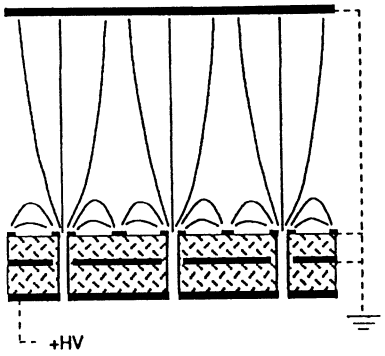

Fig. 9: Cross section of another variant of the printed circuit chamber, with plated-through holes as anodes.

The *Honeycomb Strip Chamber*[*]. This work was presented by Hartjes, in absence of the author who submitted the paper [17]. As shown in Fig.10 the detector is fabricated epoxying together layers of corrugated copper-clad capton foils with a half-hexagonal cross section; after completion of the stack, wires are pulled through the tubes and crimped to suitable end plates. The cathode foils can be striped in order to allow the measurement of the longitudinal coordinate. Although it is not clear yet if such a scheme is competitive with the plastic streamer tubes construction, one obvious advantage in view of high particle fluxes lays in the use of good conductors as cathodes, as against the rather troublesome graphite layers.

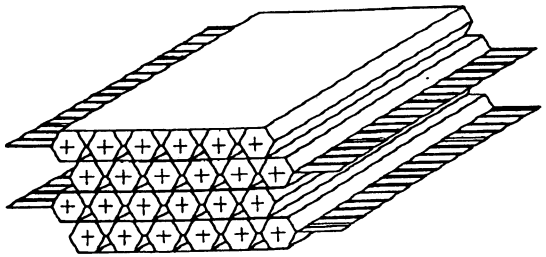

Fig. 10: Schematics of the honeycomb chamber

4. RADIATION DAMAGE OF GASEOUS DETECTORS

It has been known since the very early times of proportional and Geiger counters that prolonged exposure to radiation degrades the operating performances. The noise rate and leakage current tend to increase, and at the same time the gain drops at a given voltage. Visual inspection of a degraded counter shows various kinds of deposits on both anodes and cathodes; the rate of degradation depends from the gas nature, the materials used etc. A summary of the present state of knowledge (confusion?) can be found in Ref. [18]; the major issues of the ageing problem have been discussed by S. Majewski in the plenary session [5].

[*] Despite extensive research in specialized books, I have not been able to find reference to a pasta with hexagonal cross section, proving that there is still space for innovation in Italian cooking.

From the large mass (mess?) of conflicting reports, one can retain the following observations:

- The ageing process is due to the flow of charge generated in the chamber, and depends on the product of rate, ionization losses and gain (although some dependence on gain alone, given the total charge, has been reported). For this reason, the charge flow per cm of wire is a universally adopted unit of measurement.
- The ageing itself is due to the production, under avalanche conditions, of heavy polymers of the gases used in the detector, followed by the formation of insulating deposits on the electrodes.
- While it is recognized that organic gases with high molecular weight (such as isobutane) are particularly efficient in generating polymers, ageing is observed also in non-organic gas mixtures (such as argon-carbon dioxide). This is probably due to the dominant role played by small residual pollutants, present in the gas or produced by outgassing of materials.
- Some pollutants, such as the ubiquitous halogens and various additives used to soften plastic materials, seem to act as catalyzers strongly enhancing the polymer yields.
- Other vapors, such as ethanol and water, play a protective role in the detectors, sometimes (but not always) extending their lifetime by orders of magnitude.
- Secondary effects, due for example to photon emision and reabsorption in the gas, with discharges as possible consequence, may have a catasttrophic effect on lifetime. A study on such processes has been presented in the parallel sessions [19].

Although virtually all experimenters working with proportional chambers regularly report on the appearance or the absence of the ageing process in their particular operating conditions, only two groups have set up a laboratory specialized for the study of polymerization processes (J. Kadyk in Berkeley and S. Majewski in Gainesville). The fundamental importance of encouraging and financially supporting further specific investigations in this field can perhaps be summarized by the following figures. Multiwire chambers have been reported to stop functioning because of ageing any way between a current flow of 10^{-3} and a few Coulomb/cm of wire. At a wire spacing of one mm, a gain of 5.10^4 and a hundred electrons released per track, this gives a range of safe operation between 3 hours and 100 days, for a detector placed at 10 cm from the intersect (where a charged particle flow of 10^6 /cm^{2}s has been estimated). This is clearly too large a range, and in any case too short a survival even in the most optimistic assumption.

If a considerable effort is not put into better understanding of the of proportional chambers, there is no doubt that we will get into the situation depicted in Fig. 11, with radiation quickly cooking all the described detectors installed at the supercollider

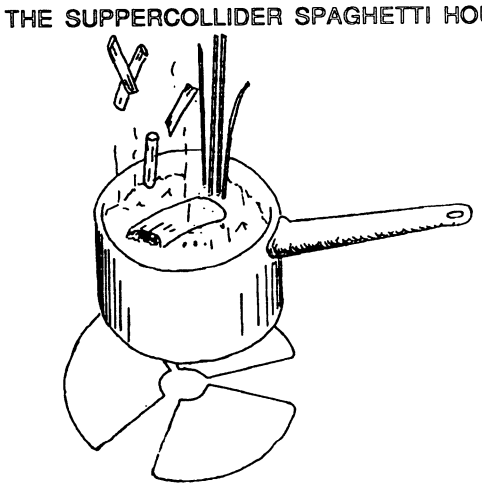

Fig. 11: Radiation-cooking of the various noodle detectors described in the text.

REFERENCES

1. H. H. Williams, *Proc.1986 Summer Study of the Physics of the Superconducting Supercollider* , R. Donaldson, J. Marx, Eds., Snowmass (1986) p. 327.
2. G. G. Hanson, et al., *Proc. Workshop on Experiments, Detectors and Experimental Areas for the Supercollider*, R. Donaldson, M. G. D. Gilchriese, Eds., Berkeley (1987) p. 340.
3. G. G. Hanson, Tracking with wire chambers at high luminosities, *Proc. ECFA Study Week on Instrumentation for High Luminosity Hadron Colliders* , G. Jarlskog, Ed., Barcelona (1989).
4. J. Dainton, Gaseous detectors at high luminosity, *Proc. ECFA Study Week* , Barcelona (1989).
5. S. Majewski, Properties and limitations of gaseous detectors at high fluxes, *Proc. ECFA Study Week*, Barcelona (1989).
6. W. W. Ash et al., *Nucl. Instrum. Methods A 261 (1987) 399*
7. J. Adler et al., *SLAC-PUB-4578 (1988).*
8. R. DeSalvo, *Proc.1986 Summer Study on the Physics of the Superconducting Supercollider,* R. Donaldson, J. Marx, Eds., Snowmass (1986) p. 391.
9. G. Hanson, *Proc.Vienna Wirechamber Conference.(1989).* To be published in Nucl.Insrum. Methods.
10. R. Bouclier et al., *Proc. Vienna Wirechamber Conference (1989).* To be published in Nucl. Instrum. Methods.
11. A. Zichichi, The LAA Project (CERN-LAA/89-1, 1989).
12. A. Oed, *Nucl. Instrum. Methods A263 (1988) 351* .
13. F. Angelini et al., *Proc. ECFA Study Week* , Barcelona (1989).
14. F. G. Hartjes et al., *Proc. ECFA Study Week* , Barcelona (1989).
15. G. Ambrosi, e. al., *Proc. ECFA Study Week* , Barcelona (1989).
16. D. Mattern, M. C. S. Williams, *Proc. ECFA Study Week* , Barcelona (1989).
17. H. v. d. Graaf, G. Faber, P. Rewiersma, *Proc. ECFA Study Week* , Barcelona (1989).
18. *Proc. Workshop on Radiation Damage to Wire Chambers* , J. Kadyk, Ed., Berkeley (1986).
19. R.S.Ribeiro et al., Photon feedback in mixtures with low photoionization vapours, *Proc. ECFA Study Week* , Barcelona (1989).

Session 7

CALORIMETRY BASED ON LIQUID READOUT

Report on Liquid Detectors
Precision EM and Hadron Calorimeters

By the Liquid Detector Working Group

M. Chen, J. Colas, F. Diez-Hedo, T. Doke,
G. Flügge, A. Givernaud, D. Groom, V. Korbel,
B. Mansoulié, K. Masuda, T. Matsuda, J.-P. Mendiburu,
P. Ribatics, E. Shibamura, S. Sugimoto and W. Wallraff

Edited by M. Chen

Table of Contents

I. Introduction.

I-A. Need for Precision Calorimeters

The search for new particles such as the Higgs or a new heavy weak boson at hadron colliders requires high luminosity, which can result in large pile up effects and high radiation damage to the detectors [I-1]. One needs precision calorimeters, with fast response, and radiation-hardness to clearly identify and reconstruct the invariant masses of these particles in their two-γ, or four-lepton, multiply-jet final states. In the case of jets, it is important to have $e\pi$ ratio to be close to 1. To identify leptons or jets for pattern recognition, one also needs good spatial resolution, and three dimensional shower profile.

For example, consider the case of Higgs decaying into four leptons via the intermediate state of a pair of weak bosons. For Higgs mass above 200 GeV, the Higgs decays into energetic particles which sampling LAr or TMP calorimeters could measure to high accuracy. However the rate is very low and one has to consider pile up and trigger problems. For Higgs mass below 300 GeV, one needs as good energy resolution as possible in order to identify the signal and measure the width of the Higgs. When the Higgs mass is very large, even though the width of the Higgs becomes quite broad, larger than a few percent of its mass, one still needs high resolution to reconstruct the invariant masses of some narrow intermediate particles, such as the weak bosons. One such example is shown in Fig. 1 for the reaction:

$$\begin{aligned} p + p \rightarrow & H^o + x, \\ & \rightarrow Z^o Z^o, \\ & \rightarrow \textit{lepton pairs} \end{aligned} \tag{1}$$

and the background contribution from heavy quark decays, i.e. a t quark with mass equal to 100 and 200 GeV, produced via the following reaction:

$$\begin{aligned} p + p \rightarrow t\bar{t} + x \rightarrow & 2W + 2b + x, \\ & \rightarrow \textit{lepton pairs} + x \end{aligned} \tag{2}$$

In Fig. 1a the lepton energy (E) resolution of 4%E with E in TeV has been assumed while in Fig. 1b, a constant resolution of 10% was assumed. We see clearly the importance of having a good resolution in order to reduce the background and to clearly identify the real nature of the process [I-2].

Do we also need high resolution for low energy particles at such high energy machines such as LHC/SSC? For new particles with width less than a few percent of their masses, the signal to noise ratio in general increases with the resolution of the detector until the

[I-1] M.G.D. Gilchriese, Editor, SSC-SR-1035

[I-2] M. Chen *et al.*, MITLNS-163 and p.95 Proceedings of the SSC Berkeley Workshop (1987)

resolution becomes comparable to the widths of the new particles. For instance, for a Higgs mass between 80 and 200 GeV, the best signals are the two-γ and 4 lepton final states (Figs. 2 and 3) via the two Z^o intermediate state. For a Higgs decaying into 4 leptons, one pair of the leptons prefers to have an invariant mass of the Z^o. This leaves little energy (M_{Higgs} - M_Z) for the second pair of leptons. The energy of one of the four leptons can be as low as a few GeV. Therefore very good electromagnetic energy resolution for electron energy of a few GeV is required in order to detect the Higgs boson in its four lepton decay modes, which is one of the most promising signals for the Higgs [I-3]. The better the resolution, the better will be the measurement on the mass and the width of the Higgs. The conclusion is that we do need good resolution for GeV particles.

Fast detectors in general have fewer random background events associated with the trigger and thus less pile up problems. Since more than 40% of the jet energy is expected to be deposited in the EM shower counters, only those hadron calorimeter cells located behind large energy hits in the EM cells are likely to have also large energy hits. Since the chance of picking up random hits due to spurious events (not associated with the trigger) is proportional to the solid angle, a fast EM shower counter can thus alleviate the pile up problem for hadron calorimeter counters situated behind. In this sense, a fast EM counter can help the follow up hadron calorimeter in picking up the relevant hits for jets under heavy background conditions.

Pattern recognition is very difficult at high luminosilty hadron colliders. Therefore one needs measurement of three dimensional shower profile to rid of spurious hits and identify relevant particles. Other properties such as e/π Ratio and pile up problem will be discussed in Chapter II, III and IV for individual detectors and summarized in Chapter V.

I-B. Liquid detectors

We discuss detectors using the following three types of liquids:

1. warm liquids: TMP, TMS, TMG, etc.;
2. cool liquid: xenon;
3. cold liquids: krypton and argon.

For noble liquids listed in items 2 and 3, both ionization and scintillation devices will be considered.

The disadvantage of liquid detectors is obvious: liquid detectors are clumsy; they need purifiers, cryogenics, leak proof containers with precise temperature control to avoid boiling or getting frozen. As scintillators, they do not have internal reflections and how to get the (especially UV) light out has been a difficult problem in the past.

[I-3] J.F. Gunion *et al.*, UCD-87-28; D.A. Dicus et al., MAD/PH/389, 1987; M. Chen *et al.*, MITLNS-166 and contributions to the Snowmass Workshop(1988) on SSC Detectors

On the other hand, liquids have no fixed surface to be damaged. Liquids such as xenon and argon are stable and insensitive to radiation damage, in contrast to all other types of scintillators. They can also be purified and recycled easily, in case of contamination. Liquid detectors can also be divided into fine cells to measure both the longitudinal and the transverse shower development. LAr and TMP detectors have been shown to be linear with $e\pi$ ratio close to be 1.

In comparing with crystal detectors, liquids fill up the entire cell, leaving no clearance near the walls separating the cells. Such clearance causes nonuniformity in energy measurement, dependent on the impact point and incident angle, which will be difficult to calibrate at the LHC/SSC. LAr and LXe saturate at two orders of magnitude higher energy density than crystals like NaI, BGO or BaF_2.

In comparison with gas detectors, liquids produce several orders of magnitude more electron-ion pairs and/or photons per unit length. This larger signals make liquid detectors intrinsically much more precise than gas detector in both energy and position measurements for high energy (hundreds of GeV) particles, where multiple scattering effects become smaller than the resolution of the tracking devices. Because of this much larger number of primary ions/photons, liquid detectors also need less gain, or sometime even no gain, in the amplification of signals, which make them more radiation resistant. Noble liquid detectors can have large signals in the form of both light and ionization. Their energy sum results in superior resolution and linearity, while their timing difference can yield precise space information. Therefore, in principle, liquid detectors can be used both as tracking devices and calorimeters. However in this session, due to limited time and space, we will discuss only the the calorimetry part.

We believe that the disadvantage of liquid detectors can be overcome by well planned engineering designs, while the advantage of liquid detectors are important physical properties of detectors, indispensible at the high radiation environment such as the LHC/SSC. We first discuss LAr ionization calorimeters in chapter II, followed by warm liquid calorimeters in chapter III, then scintillating calorimeters in chapter IV, in the order of the degree of maturity of technology. In chapter V, we discuss the e/π ratio and the pile up problems due to high rates.

II. LAr ionization calorimeters:

Sandwiched liquid argon ionization calorimeters are rather matured technology, where engineering problems concerning container, purifiers, cryogenics, temperature control, etc. have been studied and mostly solved [II-1]. Two new results discussed here are the H1 test beam results [II-2]. and the Helios detector[II-3].

In liquid argon the drift velocity saturates around 5 kV/cm at 5 mm/μs. If liquid argon is doped with 1% CH_4 the drift velocity could rise to 10 mm/μs at 25 kV/cm. Therefore the time response of this type of detector is limited to > a few hundred ns.

The H1 LAr detector uses 2.4 mm Pb/2.8 mm LAr for EM section (1.1 λ) and 5mm Cu/3mm LAr for hadron (6.1 λ) section. In addition, there is a tail catcher with 75mm Fe of 4.5 λ. The properties and the potential of LAr ionization calorimetry with samplings at LHC/SSC has been reviewed by C. W. Fabjan based the H1 and Helios detectors, from which we summarize the following main features:

1. Speed: a gate time of about 200 ns has been achieved and since speed is crucial at high luminosity machines, we will discuss properties of LAr ionization calorimeter always with this short gate of 200 ns unless otherwise specified;

2. Energy resolution and linearity: an intrinsic resolution of 0.4 to $0.5/\sqrt{E}$ has been achieved for isolated hadronic particles, i.e. about 10% at 20 GeV and 5% at 100 GeV;

3. e/π and jet energy resolution.: Typically, $e/\pi = 1.08$ at 20 GeV and 1.01 at 150 GeV for 1000 ns gate time, and $e/\pi = 1.12$ at 20 GeV and 1.07 at 150 GeV for 200 ns gate time, have been achieved with uranium sampling for isolated particles;

4. pile up due to random hits: At a luminosity of $10^{33}cm^{-2}/sec$, a gate time of 200 ns implies that on average there are 20 interactions accompanying each trigger. Using bipolar pulse shaping, it is possible to set the mean energy shift over long periods to be zero, by throwing residue charges away, which will contribute to pile up problems. For individual events, there are also fluctuations due to random hits. This will cause the following problems:

   a. deterioration of energy resolution;

   b. confusion in pattern recognition;

   c. trigger rate;

   d. fake events;

[II-1] N. DiGcomo et al., contribution to this Workshop
[II-2] G. Fluegge, V. Korbel and Ribatics et al., contribution to this Workshop
[II-3] C. Fabyan, contribution to this Workshop.

e. multi-jet invariant mass reconstruction.

We will discuss in greater details on the pile up problems in Chapter V. The R&D on ionization LAr detectors will be discussed together with TMS/TMP detectors in Chapter III.

III. Warm liquid calorimeters:

III-A. UA1 U-TMP test results.

A. U-TMP Calorimeter: [III-1]. The test results of a large U-TMP detector has been presented by Giverwaud. The purification system was described by Fracisco Diez-Hedo. This shows a large warm liquid calorimeter is technically feasible. A position measurement of 2 mm is reached for electrons above 6 GeV. The e/π ratio is found to be dependent on the electric field, changing from 1.15 at 4 kV/cm to 1.0 at 16 kV/cm due to difference in recombination of ions.

The saturation of ionization signals has been measured in tetramethylpentane (TMP). We briefly recall here the importance of saturation effects in calorimetry, with respect to the relative response of a calorimeter to electro-magnetic and hadronic showers (so-called e/π ratio). As has been shown by Wigmans, the e/π ratio depends on a number of parameters which govern the way in which the shower energy is transformed into a useful signal. Among these parameters is the ability of the detecting medium to react to the abundant neutrons in hadronic showers. For example this ability is almost nonexistent in the case of noble liquids, but can be high for hydrogen-rich media. In the latter, neutrons can scatter on free protons, which in turn are very ionizing and thus provide signal. The amount of signal coming from this source depends on the way the detecting medium responds to heavily ionizing particles. In scintillators it is well known that the response is not linear with the deposited energy dE/dx, and can be described by Birk's law:

$$\text{signal} \sim \frac{dE/dx}{1 + kB\, dE/dx}$$

where kB is Birk's constant in cm/MeV.

The results of the measurement is Kb= 0.122±0.010 cm/MeV, which is dependent on the field and angle. The details will be described in II-B.

III-B. TMS/TMP detectors.

TMS is faster than TMP and thus is more suitable than TMP at LHC/SSC. The main problems are safety, saturation, purification, and how high a voltage a practical system

[III-1] A. Giverwaud, F. Diez-Hedo et al., contribution to this Workshop

can be used[III-2]. In TMP and TMS, the velocities increase almost linearly with field and reach 14 and 32 mm/μs at 50 kV/cm, respectively. Recently, the WALIC Collaboration has studied what kind of material can be used together with TMS without contaminating it[III-3]. Vespel (plastic), stainless steel, ceramics and some galsses are found to be compatiable with TMS, while teflon is not. The study is still continuing.

The saturation of ionization signal in TMS/TMP at different angles and electric fields has also been studied by the WALIC Collaboration as presented by B. Mansoulie in this Workshop.

The saturation of ionization signals has been measured in tetramethylpentane (TMP) and tetramethylsilane (TMS) with slow particles (pions, protons and deuterons) at CERN. The complete report of the measurement procedure , analysis , results as well as references can be found in a preprint from LAPP (Annecy, France) : LAPP-EXP/89-08, and has been submitted to N.I.M..

The WALIC collaboration has measured kB in TMP used in an ionization chamber for three different electric field values (4.8 , 8.0 , and 12.0 kV/cm) and five different angles between the incident particle and the electric field (0, 5, 10, 30, 50 degrees); in TMS for 3 electric field values (10 , 20 , 40 kV/cm) and two incidence angles (0 and 20 degrees).

The results are given in the Table below :

kB in TMP (cm/MeV)

Angle	E = 4.8 kV/cm	E = 8.0 kV/cm	E = 12.0 kV/cm
0°	0.128 ± 0.012	0.144 ± 0.024	0.123 ± 0.010
5°	0.116 ± 0.016	0.112 ± 0.021	0.099 ± 0.008
10°	0.079 ± 0.020	0.107 ± 0.017	0.086 ± 0.009
30°	0.073 ± 0.012	0.071 ± 0.010	0.058 ± 0.006
50°	0.058 ± 0.006	0.056 ± 0.008	0.043 ± 0.004

kB in TMS (cm/MeV)

Angle	E = 10.0 kV/cm	E = 20.0 kV/cm	E = 40.0 kV/cm
0°	0.141 ± 0.020	0.101 ± 0.014	0.086 ± 0.009
20°	0.063 ± 0.015	0.044 ± 0.011	0.028 ± 0.009

We observe a clear decrease of kB with incidence angle in both liquids at all fields. The TMP data show no variation of kB with electric field in the moderate range 4.8 to 12

[III-2] Jacques Colas, B. Mansoule/Jean Pierre Mendiburu et al., contribution to this Workshop

[III-3] Jean Pierre Mendiburu, contribution to this Workshop

kV/cm which was accessible for technical reasons. The TMS data show a clear decrease of kB at very high fields.

This results are intended to provide a basis for understanding the e/π response of warm-liquids calorimeters. The WALIC collaboration is now undertaking a thorough investigation of this property by building a large prototype calorimeter with flexibility concerning absorber nature and thickness. This prototype will be exposed to a high energy beam during 1990.

III-C. R&D.

As described earlier, sampling ionization LAr and TMP detectors have been tested using realistic size of test modules and in some cases (D0 and Helios) full size detectors. These devices have demonstrated that the fundamental properties of these detectors have the potential of satisfying the requirements for jet physics in speed (comparable with shadronic shower development time), radiation resistance, energy resolution for high energy jets, linearity and 3-D shower measurement. We list the following common R&D items for ionization LAr and TMP/TMS detectors:

1. tower read-out,
2. study of pile up, See Chapter V for more discussion.
3. magnetic effects,
4. with shorter gate (50ns),
5. uranium versus lead sampling,
6. hermiticity.

In addition, for TMP/TMS detectors, we need to further study the following:

7. purification.
8. material compatibility,
9. safety,
10. practical H.V. for a large system,
11. radiation hardness.

IV. Scintillating calorimeters.

IV-A. Noble Liquid Scintillating Detectors

One promising new type of calorimetry uses scintillating noble liquids [IV-1]. A scintillating liquid xenon detector could serve as a fast, precise and radiation resistant EM shower counter. On the other hand a scintillating liquid argon or krypton calorimeter, read out by layers of the silicon photodiodes and sandwiched with lead/uranium absorbers and doped with small amount of xenon or N_2 to increase the speed of the light signal, could also be used for general purpose hadron calorimeter counters.

Some relevant physical properties of LXe (also LAr), such as the triple temperature (161° K), specific density (3.1), radiation length (2.8 cm), scintillating and ionization parameters etc. are shown in Table I. We see that xenon can be used both as scintillator and for ionization chambers. Other noble liquids such as argon and krypton have lower density and critical temperature, and longer radiation length. They also need doping (e.g. 2% of N_2) to increase the scintillation speed and are thus more difficult to use than xenon.

Many noble liquid detectors of the size of a few hundred cm^3 (for example, see Fig.4) have been built and tested recently. The results have been published [IV-6,7,9,10,15,16,17,19,21,22] in recent years. The following important properties of LXe, satisfying the stringent requirement of high luminosity machines like the SSC/LHC, have been experimentally established and we elaborate on the importance of these properties with respect to the physics at the LHC/SSC:

1. Speed: The drift velocity as a function of field strength of some common liquids are shown in Fig.5. As seen, the fastest known ionization media at low field are noble liquids such as argon and xenon while at high field strength is the TMS liquid[IV-2];[IV-3]; [IV-4];[IV-5]. On the other hand, as shown in Table II and Fig. 6, the scintillation signal of liquid xenon, with a peak wave length of 170 nm, (Fig. 6a) is several orders of magnitude faster than the ionization signal of all of these media in Fig. 5 (under normal conditions, say a drift distance of a few mm and an electric field of a few kV/cm). Fig. 6b, in particular, shows the dramatic contrast in speed between scintillation and ionization signals in a LXe chamber. As seen in Fig. 6a, for

[IV-1] M. Chen *et al.*, Nucl. Inst. and Meth. A267 (1988)43, MITLNS-164, MITLNS-165 and MITLNS-166 and contributions to the Berkeley Workshop (1987) and Snowmass Workshop(1988) on LHC/SSC
[IV-2] Andries Hummel and Werner F. Schmidt, Radiation Research Review, 5 (1974) 199; R.A. Holroyd and D.F. Anderson, Nucl. Instr. and Meth. A236(1985)294-299; S. Ochsenbein SIN preprint (1987); D.F. Anderson, Fermilab, Batavia, IL
[IV-3] A. Giverwaud, Fracisco Diez-Hedo et al., contribution to this Workshop
[IV-4] C. Rubbia and Werner F. Schmidt, UA1; and S. Ochsenbein, SIN, Private Communications
[IV-5] TMG: S. Geer et al., BNL 43155, Aug. 1989.

α particle, 96% (at $t = 0$) of the light output of LXe has a fast decay time of 4 ns and 22 ns for the rest. Therefore with a gate time of 10 ns, one gets most of the light. For relativistic electrons, one gets about 25% of the light with a gate time of 10 ns.

2. Radiation resistant: Each cell of a xenon EM counter (Fig. 10b and c) has the following components:

   a. Scintillating medium: liquids have no fixed surface to be damaged. Liquids such as xenon and argon are stable and insensitive to radiation damage, in contrast to all other types of scintillators. They can also be purified and recycled easily, in case of contamination.

   b. Light detectors: The radiation hardness of surface barrier photo sensors, such as the silicon photodiodes described in IV-B made specifically by us to detect the UV scintillation light of LXe, might improve by about two orders of magnitude, from a typical value of 10^6 rad to 10^8 rad, when they are immersed in cold liquids. This should be tested under realistic conditions.

   c. Reflectors: We use metal UV reflectors such as thin Al foils coated with MgF_2, which is stable and has a UV reflectivity of 80%, fastened onto the container of LXe. They are also immune to radiation damages.

   d. Electronics: This is a general problem for a high luminosity collider. We will not address it here in detail, except mentioning two aspects specific to LXe: first, part of the electronics (pre-amplifiers) could be immersed in cold xenon liquid to reduce leak currents and thus to increase radiation hardness; second, the rest of the electronics could be situated far away from the interaction region. The large light output of LXe results in a large signal to noise ratio. Thus signals can be carried over relatively long distances to avoid radiation damages.

3. Energy resolution and linearity: The size of signals and the dynamical range of some relevant media such as xenon, argon, BaF_2, NaI, BGO, TMS and TMP are shown in Table II. The scintillating light output from liquid xenon [IV-6] is comparable to that of NaI and more than one order of magnitude larger than that of BaF_2. For electro-magnetic showers, liquid xenon, due to its high density, small radiation length (2.8 cm) and high light yield (3.5×10^6 photo-electrons/GeV in 10 ns for electrons, could achieve an excellent r.m.s. energy resolution of better than 1 % for a few GeV electrons/photons, which is important, for example, for the immediate mass Higgs.

   To be specific, with our detector (Fig. 4), for one GeV of energy loss, the scintillating light output from liquid xenon for a beta particle has been measured to be 4×10^7 UV (170nm) photons for a gate width of 150 ns, and 10^7 UV (170nm) photons for a gate width of 10 ns. This is more than one order of magnitude larger than that of

[IV-6] M. Mutterer Nucl. Inst. and Meth. 196(1982)73; A. Hitachi et. al., Nucl. Inst. and Meth. 196(1982)97; K. Masuda et al., Nucl. Inst. and Meth. 160(1979)247.

BaF_2. This large number of photons allows one to use photodiodes, which have no amplification, without being swamped by noise. With a quantum efficiency of 70% (e.g. the silicon photodiodes developed recently by us) and an uniform light collection efficiency of 50%, the number of photo electrons/GeV for beta particles with 10 ns time gate is:

$10^7 \times 0.70 \times 0.50 = 3.5 \times 10^6$ photo-electrons/GeV

The energy resolution at low energies is dominated by the noise of the silicon photodiodes, which has been measured to be 2×10^4 electrons for an area of 50 cm^2 (for three photodiodes in parallel with a total capacitance of 5200 pf). This yields an energy resolution of 1%/E(GeV) due to noise and statistics alone, and also a large signal to noise ratio which is important at LHC/SSC environment, in order to be insensitive to other sources of noise (e.g. due to electronics or uranium).

As seen in Fig. 8, the free electron yield produced by a equivalent minimum ionization particles (mip) in LAr is much larger than TMP. The LXe signals are 3 times bigger than LAr. A typical measured spectrum (Fig. 9) using the ionization liquid xenon detector [IV-7] shows a resolution of 1% at 1 MeV.

Linearity: The measured ratio of light output over energy loss, dL/dE, for relativistic heavy ions (solid dots), fission fragments (open circles) in LAr and LXe is shown in Figs. 7b and c. We see that argon and xenon do not saturate up to an energy loss of 5000 MeV/g/cm^2 (due to relativistic La ions) which is two orders of magnitude better than NaI and BaF_2. Fig. 7a shows that the sum of the scintillating and ionization energy is linear up to 10^4 mip.

4. e/π and jet energy resolution.

   For jets, we need both excellent angular and energy resolutions. The first can be achieved by using calorimeters of high granularity (see items 5. and 6. below) while good jet energy resolution needs careful studies of the delicate compensation effects through nuclear interactions in hadron calorimeters which we will not discuss here, but assume it has been done.

   For an EM shower counter, e/π refers to the relative light output for the same amount of energy loss, E_{loss}, of a high energy electron or pion. E_{loss} is the difference of the incoming particle energy and the total energy of the outgoing charged particles, photons, and neutrons which presumably can be measured by a fully compensated hadron calorimeter situated behind the shower counter.

   There are two main mechanisms which make e/π ratio of many common EM shower counters, such as lead glass, NaI, and BGO etc. (see Table II), to be much larger than one:

[IV-7] E. Aprile et al., Nucl. Inst. Methods A261(1987)519

a. nuclear binding energy loss in deep inelastic hadron-nucleus interactions to break up nucleus. This loss is there for all material;

b. saturation: hadrons produce heavy ions via nuclear interactions. In most common scintillating materials, dL/dE for heavy ions can be significantly lower than that of electrons due to saturation and also due to the fact that sometimes electrons and hadrons excite the same media to different energy levels. The measured values of dL/dE for LAr/LXe are shown in Figs. 7b and 7c. We that LXe saturates at the level of dE/dx about 10000 MeV-cm^2. For comparison, most scintillators, such as NaI, BaF_2 and plastic scintillators, saturate already at dE/dx about 100 MeV-cm^2.

In LXe and LAr, dL/dE for relativistic heavy ions, having much higher density of electrons-ion and thus more light from recombination, is 30-50% larger than dL/dE of electrons. We note that for heavy ions, the electron/ion density produced by ionization, and thus the scintillating light output from recombined ion-electron pairs are even higher in LXe than in LAr (Fig. 7b). LXe also measures the recoil energy of neutrons. These effects compensate well the nuclear energy loss discussed in item a. and should make LXe e/π close to 1;

Thus for a linear and scintillating shower counter such as liquid xenon, we expect that the e/π ratio should be much closer to one than other scintillators such as BaF_2, NaI and BGO etc. Indeed, assuming that the xenon detector is followed by a compensating hadron calorimeter (e.g. uranium-TMS sandwich counter), Monte Carlo calculations have shown that the e/π ratio can be adjusted to be close to one [IV-8] in a short time gate (10ns). We note that most hadron calorimeters achieve e/π =1 only with very long time gate (>100ns) in order to catch slow neutrons.

This e/π ratio should be measured in an array (10x10) of LXe detectors surrounded by compensating hadron calorimeters to confirm the Monte Carlo prediction of e/π being close to 1 for LXe.

5. Spatial resolution. This is useful for the reconstruction of the invariant mass of electron and photon pairs. Since the walls for liquids are only for optical purpose and do not have to support the weight of the liquid, they can be thin and finely divided. There is no clearance between the walls and the scintillating media, as in the case of crystals. Clearance causes large corrections, dependent on the position of the impact point and incident angle of the incoming particle, in the measured shower energy of electrons/photons.

   The noble liquid detectors can be divided into small cells (Fig. 10a) , about 2.2 degrees in both θ and ϕ angles at θ (Fig. 10b) around 90° and the size in θ can be reduced to 1 degree at θ around 10°, corresponding to a pseudo-rapidity interval of 0.03 at θ = 90°, 0.05 at θ = 45° and 0.06 at θ = 15°. For θ < 15°, these detectors could be sandwiched with uranium/lead plates to reduce the equivalent radiation length to about 15 mm (Fig. 10c) . The energy distribution of a 100 GeV electron in such an array of xenon cells, simulated by Monte Carlo program, is shown in Fig. 11. As seen, typically 62% of energy is concentrated in one or two cells. This lateral shower distribution can be used to determine the impact point to better than 2 mm, without having to use complicated corrections dependent on the impact point and angles as in the case of crystals.

6. Measurement of 3-D shower profile. As shown in Fig. 10b, in the central region, 3 layers of silicon photodiodes could measure the energy in the pre-shower, shower maximum and shower tail regions, and in the forward regions 10 layers of photodiodes sandwiched with U/Pb absorbers to shorten the effective radiation length of the detector to 15 mm and make it more compact (Fig. 10c). The charge produced by a mip passing one photodiode is less than 1% of the charge produced by its scintillation light produced in 20 cm of LXe. One could also use 20 layers of photodiodes sandwiched with U/Pb absorbers to further reduce the radiation length. In this case, one could, at a sacrifice of energy resolution at low energies, replace LXe with LAr doped with 2% of N_2 (Fig. 10d). Both transverse and longitudinal shower distributions help to distinguish electrons/photons from hadrons and π^o's.

7. Correlation of Scintillation with Ionization. We note that both scintillation light (fast) and ionization (slow) signals of noble liquids give large outputs. It has been shown that the energy sum yields excellent resolution and linearity (Fig. 7a) while the timing difference between the two signals from a single counter can yield precise spatial information with a resolution better than 30μ (Fig. 12) in the case where incident particles are isolated. Fig. 13 shows the correlation of ionization with scintillation measured by E. Shibamura et al.[IV-9] using a LAr chamber. The measurement of the impact point and the shower profile is valuable to distinguish electrons and photons from hadrons (e.g. π^o's). This will be left for future development, not elaborated further in the present report.

IV-B. R&D.

As described earlier, all of the existing work up to now is based on detectors of about one quarter of the length of a real size cell, which should be about 22 rad. lengths long in order to contain the full shower of a high energy electron or photon. These one quarter length devices have demonstrated that the fundamental properties of Noble Liquid Detectors have the potential of satisfying the stringent requirements of a high luminosity hadron collider in speed, radiation resistance, energy resolution, linearity and 3-D shower measurement. It is necessary to build an array of full size EM shower counters such as

[IV-8] H.S. Chen *et al.*, MITLNS-164 and contribution to the Berkeley Workshop; H. Fesefeldt, PITHA (Aachen) preprint, Nov. 1987.

[IV-9] E. Shibamura et al., Proceedings of ECFA Workshop at Barcelona, Spain, Sept. 1989
References [IV-10] to [IV-19] are listed under Table II.

these shown in Figs. 10b and 10c. which consists of the following major components including photo sensors, UV reflectors and LXe purifier:

1. UV photo sensors to measure the light signals from xenon (170 nm) and argon (130 nm). This is the most important part of the detector and we elaborate here in details:

a. Phototubes: Although phototubes have low noise and high gain, and presently available UV-phototubes could achieve high quantum efficiency for UV light, they are space consuming and difficult to work with in magnetic fields. (Fig. 15 shows the quantum efficiency for phototubes from Hamamatsu: as seen, a quantum efficiency of 35% for xenon with tube type 250M with Cs-Te cathode and MgF_2 window or 250S with Cs-Te cathode and silica window and 22% for argon with tube type 150M with CsI cathode and MgF_2 window are reachable.) Phototubes also need either (UV) transparent windows and/or wave length shifter. Both are difficult to make in large quantity and unstable in nature, often causing drift in gain and/or leaks. We worked hard to eliminate all of these and succeeded finally in doing so, as described in the next paragraph.

b. Our silicon photodiodes: commercially available photodiodes have poor quantum efficiency for UV light, partly because of the thick windows commonly used by commercial photodiodes. To be transparent to UV, the thickness of the window must be much smaller than the wave length of the UV light, which is 170 nm in the case of LXe. Therefore we set out to develop our own devices and have recently successfully made and tested several fast UV sensitive silicon photodiodes with very thin (30 nm presently and maybe as thin as 15 nm in the near future) and thus UV transparent window (Fig. 14). They have a quantum efficiency of about 70% and a shaping time of 10 ns[IV-20]. The noise level for 10 ns shaping time is measured to be 1.5×10^4 electrons for a 25 cm^2 device. It can work directly in the xenon liquid. The relevant properties of this photodiode are summarized in Table IV.

Other candidates, including vacuum and avalanche photodiodes, (e.g. UHVC20 from Valvo, which has thin Al_2O_3 window, a rise time of 0.25 ns, 20 mm diameter and a UV quantum efficiency of 20%), and other efficient photocathodes [IV-21], which could also convert the scintillation light into charge, etc. should also be tested.

The photodiodes described here are compact, fast and suitable to work inside a magnetic field. It greatly reduces the complexity in the construction of the detector by eliminating UV transparent windows and/or wave length shifter. It also allows us to measure the longitudinal shower development. By inserting absorbers behind each photo sensor, one can reduce the effective radiation length of the EM shower counters for the forward regions (Fig. 10c).

[IV-20] T. Doke, Proceedings of ECFA Workshop at Barcelona, Spain, Sept. 1989

[IV-21] e.g. V. Peskov et al., Nucl. Inst. and Meth. A269(1988)149 and T. Ypsilantis, Proceedings of ECFA Workshop on detectors at Barcelona, Spain, 1989

It could also open up the possibility of using many layers of our silicon photodiodes to detect the scintillation light of other noble liquids such as LKr, LAr or liquid scintillators etc., sandwiched with absorbers to further reduce the radiation and the interaction lengths, for EM shower counters (with worse energy resolution at low energies), and for hadron calorimeters. We encourage others who are interested in such detectors to consider this new approach and compare with other more conventional methods.

2. Walls between the cells and UV reflectors: the cell walls are used to reflect UV light, not to support the weight of the liquid. Therefore the walls can be made of thin UV reflecting foils, with small grooves to allow the liquid to flow from cell to cell, causing practically no dead space and no deterioration in energy measurement. A list of UV reflecting material with reflectivity about 80% to 90% is shown in Table V. Due to the strong focusing effect of the tapered cells, the best material is not necessarily the one with the highest reflectivity. One needs to achieve high uniformity in the light collection efficiency along the cell, similar to the case of BGO crystals, in order to achieve the best energy resolution. This can be tested and decided only after a real size tapered cell is available.

3. Purifier: One high performance purification system (to achieve less than a few ppb of impurity) using the phase transition property of NaK (Fig. 16), for Liquid xenon has been studied and is shown in Fig. 17: NaK is very active when dropped as liquid with clean surfaces into LXe, where it turns into solid and absorbs impurities. Solid NaK are then removed from the bottom to the top region (-10° C) to return to the liquid state, stirred to obtain fresh surface to be reused again.

After the full size cells described above are constructed, one can then proceed to carry out the following R&D on the physical properties of the detector:

4. Measurement of the light absorption length of liquid xenon and argon in a tapered cell (see Fig. 10b and Fig. 18) using radioactive isotope sources and vacuum-UV lights, and to measure the dependence of the light output and light absorption on the purity of the liquid [IV-22].

5. Test of radiation hardness of the detector, i.e. photo-cathodes and electronics. We note that the radiation hardness of the silicon photodiodes might improved significantly when they are immersed in a cold liquid like xenon.

6. Design, build and test an array of full size tapered xenon shower counters (Fig. 19), consisting of 3×3 cells at first and later 10×10 cells. Measure the uniformity, energy resolution, linearity, 3-D shower development and the e/π response in intense beams, including pile up and pedestal subtraction due to finite gate width.

[IV-22] E. Aprile et al., Proceedings of ECFA Workshop at Barcelona, Spain, Sept. 1989

IV-C. Conclusion

Precise, compact, fast and radiation-hard detectors are clearly desirable in any detector at the LHC/SSC. Scintillating liquid xenon detectors of a size up to a few hundred cm^3 (i.e 1/4 of the length of a full size cell) have shown that they can satisfy the stringent requirements of the LHC/SSC in speed, resolution, linearity, radiation hardness, 3-D shower measurement, and likely also the e/π ratio. Several large liquid ionization detectors have recently been built successfully. Considering the large difference in speed between scintillation light and ionization (Fig. 6b), one must raise the obvious question: why not also use the scintillation light?

One key technical breakthrough has been made in using fast, windowless UV photo sensors, immersed in the liquid itself, to measure the shower development. It greatly increases the UV light detection capability and reduces the complexity in the construction of the detector by eliminating phototubes, UV transparent windows and/or wave length shifters, and allows us to measure the longitudinal shower development. By inserting absorbers in between two photo sensors, one can make the detector more compact for the forward regions. This new technique for large system EM shower counters for the SSC/LHC should be considered.

IV-D. Comments on the price and availability of xenon

The price for liquid xenon at the US or Europe varies between $ 2000 to 5000/liter. In the U.S.S.R., it is about 1000 Rubles/liter. The production of LXe by two W. German companies, Messer Grieshain and Linde,is about 1200 liquid liters/year. Dr. A. Bondar from Novosibirsk INP told us that the production rate in USSR is about 10 ton (3 m^3) / year and is flexible, depending on the demand. It needs early notification and thus long term planning in order to increase the production significantly.) For the Xenon Olive Detector (Fig.10a), for example, 5 m^3 of liquid xenon is needed.

We note that an ITEP liquid xenon bubble chamber of 0.8 m^3 has been successfully in operation for several years. Another 14.3 m^3 (35 tons) liquid Kr calorimeter, KEDR Detector at VEPP-4M, is under construction and part of it has been tested in beams[IV-23], showing excellent resolution, similar to that of CsI. These developments demonstrate that large noble liquid systems are feasible.

[IV-23] A. Bondar et al., Proceedings of ECFA Workshop at Barcelona, Spain, Sept. 1989

V. Speed, signal/noise, e/π and resolution

V-A. Introduction

As discussed in chapter I, at LHC/SSC, one needs good energy resolution for leptons and for jets in order to reconstruct the invariant mass of new particles, such as the Higgs. The resolution of detectors depends not only on photon or ion statistics as described in Chapter II, III and IV, but also on signal/noise, pile up and e/π ratio.

A significant fraction (about one third with large spread) of the energy of high energy jets is neutral, and in each early collision in a high-energy hadronic cascade, again a large fraction of the energy goes into π^0's and is thereafter lost to hadronic interaction. About half of the jet energy is then deposited in the EM counter of 22 radiation length. Therefore the both the EM and hadron calorimeters need to have the e/π about one in order to measure the jet energy precisely. Pile up and signal/noise ration will further deteriorate resolution. We discuss all these effects in this chapter and point out the present effort is still far from being satisfactory.

V-B. Speed and signal/noise

As described in Chapters II and III, with a gate time of 50 ns the signal-to-noise ratio for a minimum ionizing particle is about 4 for sandwiched ionization LAr detectors and increases linearly with field for TMP and TMS, reaching 6 and 13 respectively at 50 kV/cm. The larger the drift velocity, the larger the peak current and the smaller the signal time. Although liquid ionization calorimeters have been mostly used up to now with slow readout, their signals have a fast rise time. However it is not easy to get this fast component of the pulse out of the calorimeter. In liquid argon the drift velocity saturates around 5 kV/cm at 5 mm/μs. If liquid argon is doped with 1% CH_4 the drift velocity could rise to 10 mm/μs at 25 kV/cm. In TMP and TMS, the velocities increase almost linearly with field and reach 14 and 32 mm/μs at 50 kV/cm, respectively. For ionization systems like LAr or TMP/TMS, the charge collection time is several hundred ns, and to even approach 100 ns involves throwing away charge which then contributes to pile up. For scintillating LXe and LAr (doped with N_2) detectors, the speed is much faster and a 10 ns gate matches well with the beam bunch crossing time of LHC/SSC.

To improve the charge transfer time[V-I], one should

1. Reduce the damping resistor to a few Ωs as in the case of the Helios detector, and the preamplifiers must be on the electrodes to eliminate transmission lines.
2. Reduce the capacitance by connecting the electrodes in series. For this purpose a new connection scheme of the electrodes, the "electrostatic transformer," is presented by

[V-I] J. Colas Proceedings of ECFA Workshop at Barcelona, Spain, Sept. 1989

Colas. This technique reduces the detector capacitance while keeping the number of channels at an acceptable level. Also it allows the use of transmission lines to bring signals from the electrodes to the preamplifiers which could be located in an accessible area.

Assuming 25000 cells covering the pseudorapidity region $-4 < \eta < 4$, the pile up contribution to the error on the transverse energy measurement in one cell has been estimated to be 80 MeV using bipolar shaping, which is adequate for measuring $p_\perp$ of jets. With room temperature liquids, the length of the cables can be short, keeping the added noise at a reasonable level. Contributions to the error on the energy measurement from pile up and electronics noise have been studied in detail. Even on this issue, room temperature liquids (TMS/TMP) are found to be competitive with cold liquid argon, at the expense of a higher gap voltage.

V-C. e/π ratio

A large fraction of the energy in a hadron cascade appears as electromagnetic showers because of π^0 production in early cascades. Because of the small numbers involved, this fraction is subject to large fluctuations. For example, out of 1000 simulated cascades by 50 GeV π^-'s, the broad distribution of the electromagnetic fraction extended from 8 GeV to 45 GeV. [V-2] The mean of the distribution shifts upward with increasing energy; in cosmic-ray airshowers practically all of the energy appears in the electromagnetic channel.

In most calorimeters used in high energy physics, the electromagnetic and hadronic parts of a cascade are detected with different efficiencies. Electromagnetic energy is usually converted to detectable signal very quickly and with greater efficiency. On the other hand a significant amount of hadronic energy is eventually carried by low-energy ($\sim$1 MeV) neutrons, which in their subsequent interactions "hide" energy from detection through nuclear excitation or recoil, deposit energy in ways which cannot be efficiently detected (highly ionizing, short range spallation products and, if hydrogen is present, recoil protons), and deposit energy after a long time (energy goes into a spallation, and the binding energy reappears in (n,γ) reactions after moderation of the spallation or boiloff neutrons in about one hundred ns.

As a result, the level of low-energy hadronic activity in an absorber (as measured by the total yield of $\approx$ 1MeV neutrons, the total number of nuclear collisions above some cutoff energy, the response of a calorimeter when electromagnetic components are excluded, etc.) rises more slowly than linearly with energy. A naïve induction argument yields a power law dependence with an exponent m near 0.85. Simulations with a variety of codes corroborate this result for $E > 10$ GeV. To the extent that this functional form is valid, the ratio of a calorimeter's response to an incident electron to that for an incident hadron

[V-2] D. E. Groom, Fig. 1 from paper in these Proceedings.

is

$$\frac{R_e}{R_h}\left(=\frac{e}{\pi}\right) = \frac{1}{1-(1-\epsilon_h/\epsilon_e)(E/E_0)^{m-1}} ,$$

where ϵ_e and ϵ_h are the calorimeter efficiencies for detecting low-energy electronic and hadronic energy deposition, respectively, and E_0 is a scale factor near 1 GeV. This one-parameter function (if we neglect the slight m dependence) provides a good fit to available test-beam data, and has the correct asymptotic behavior.

The penalties for different detection efficiencies for photons and hadrons are very serious, since the fluctuations in π^0 production worsen resolution in a serious way even for an otherwise ideal calorimeter. A hadron gives a different response than an electron or photon with the same energy, and the response ratio ("e/π") decreases with energy. The response to hadrons is not proportional to their energy; in fact, the response divided by the energy is proportional to the reciprocal of "e/π."

Data concerning the time evolution of hadronic energy deposit are rather sparse. H. Paar has reported at this meeting that 95% of the energy in a lead/scintillator calorimeter appears within 100 ns, while MORSE calculations by Brau and Gabriel [V-3] for a uranium/TMP system (which should be similar) indicate that only 85% of the visible energy has been deposited after 250 ns. Experimental data are complicated by the long signal collection times in systems such as liquid argon. Groom's fits to Helios uranium/liquid argon calorimeter yield relative electron/hadron efficiencies (roughly Wigmans' "intrinsic e/h"; see Groom's paper [V-4] of 1.20, 1.17, and 1.14 for 135 ns, 250, and 500 ns integration times, respectively. [V-5] If the Brau and Gabriel result (for a different system!) were applicable, we might expect the efficiency ratio to be $0.85 \times 1.17 = 1.00$ at very long times. For the D0 test beam results with $\approx 2\mu$s shaping time, Groom finds a ratio of 1.05, and considers the agreement with expectation adequate.

Strategies to make the efficiency ratio close to unity have been widely discussed. These are of three types:

1. Make the integration time long to catch slow neutrons and photons from nuclear fissions. This is not an available strategy at the new hadron colliders; in fact, one must make the integration time as short as feasible, which very likely will be about

[V-3] J. E. Brau and T. A. Gabriel, Oak Ridge National Laboratory Report ORNL/TM-10903 (January 1989).

[V-4] D. E. Groom, SSC Central Design Group Report SSC-227 (July 1989; to be published in *Proc. of the Workshop on Calorimetry for the Superconducting Super Collider,"*, ed. by V. Kelly and M. G. D. Gilchriese, Tuscaloosa, Alabama (to be published, 1989), and D. E. Groom, these proceedings

[V-5] Helios test data: CERN report with "0775 C" stamped on it; H. Gordon et al., "Preliminary Performance Results of the Helios Uranium/Liquid Argon Hadron Calorimeter, 1 Aug 1988

100 ns for hadron calorimeters, and preferable comparable to the beam bunch crossing time of 10 ns for EM counters.

2. Enhance the hadron signal, by using readout media which contain hydrogen and hence "see" neutron energy via proton recoils, and/or use uranium plates, to make more neutrons in exothermic fission reactions. The hydrogen moderator also should help get the signal out faster. The use of uranium has many disadvantages, among them the generation of 2 to 5 times as many neutrons in a situation in which neutrons already present a radiation problem.

   Methods 1 and 2 both require a gate time of at least 100 ns in order to "see" the neutrons. There are 10^{15} interactions/year at the SSC, and 40 times that rate at the high-luminosity interaction region of the LHC. If each trigger contains tens of pile up events, the consequences for pattern recognition, trigger and background problems can be huge. For any system with a gate time much longer than the crossing time, the pile up effect due to random hits must be properly simulated, not only including the mean energy fluctuation due to minimum bias events (m.b.e.) inside a given solid angle (which assumes that the pattern recognition is already properly done), but also the pattern recognition problem itself as well as the trigger and the background problems due to all processes (m.b.e., jets, ...). Piling up tens of events may be tolerable for jet physics, but can be very serious when one tries to reconstruct the invariant masses of jets, bearing in mind that a Z or W boson often decays into 3 or more jets. It is hard to identify and measure the low energy jets, which may contribute little to the total energy but very significantly to the invariant masses because they are likely to be emitted at larger angles.

3. Suppress the electromagnetic signal relative to the hadron signal. This is attractive since it also allow shorted gate time when one does not have to collect all the neutrons. There are two possibilities:

   a. by using "thick" high-Z plates. In this situation electromagnetic energy is preferentially absorbed by inactive parts of the calorimeter. While nonactive high-Z plates always help, the gain is limited. Gabriel [V-6] has examined this possibility for a lead/liquid argon system, with the conclusion that sampling would be far too infrequent if the plates were thick enough to help.

      On the basis of item (3a), Wigmans has conjectured that no totally active calorimeter (NaI, BaF_2 and BGO, etc.) could be compensating. While this might be true, it is still possible that some other material such as scintillating LXe (see 3b.) or a hydrogenous system (e.g. the scintillator $PbCO_3$ containing substantial $Pb(OH)_2$) might be compensating.

   b. by using media which enhance hadron signals. This new way of suppressing the electromagnetic signal has been recently pointed out by M. Chen. There exist well-established experimental data (Figs. 7b and 7c) which show that relativistic heavy fragments (produced from hadron nucleus interaction) give about 30% more scintillation light than electrons for the same amount of energy loss in LAr and LXe. This could offer a natural way of compensating the hadronic "missing" energy. There are two additional advantages: first, the hadron signals are enhansed instead of surppressing the electron signals (4×10^7 photons/GeV), one gets excellent energy resolution even for low energy particles. Second, since the scintillation light signals can be as fast as few ns, we also avoid the problem of long gate time which confronts methods 1. and 2.

      The hadron signals are enhansed in scintillating LXe and LAr because of two competing mechanisms, ionization and scintillation. For heavy nuclear fragments produced in hadronic cascades, the density of ions is much larger than that due to electrons. This results in significant ion/electron recombination and produces more scintillation light and less escaping ions. Liquid argon and xenon also do not saturate up to an energy loss of 5000 MeV/g/cm^2, two orders of magnitude better than NaI and BaF_2 (see IV-B-4).

[V-6] private communication

V-D. R&D

The obvious problem with the above discussion is its qualitative nature. Both CALOR [V-7] and GEANT/GEISHA seem to be able to handle both high-energy cascades and compensation, including its time dependence, and should be used to study the relevant properties of calorimeters. At present, no circuit development proposal which did not include detailed simulation via SPICE or its equivalent would be taken seriously by the community. At the same time, people propose calorimeter development of comparable or greater cost without concurrent simulation. Given the stakes for future detectors, we regard this approach as irresponsible, even at the present state of the art. The implications of this statement for simulation efforts should be obvious. A proper simulation must include the following effects:

1. Define a reasonable gate time;
2. Define a jet algorithm, i.e. the energy and angular cuts for a cluster of hits, under magnetic field influence, to be a jet;
3. Include pile up effects due to all events, not just m.b.e.'s, consistent with the gate and jet definition defined under 1. and 2.. Indeed, the issues of pile up and segmentation are further complicated by the η range in question and the physical size of the calorimeter, particularly for the reconstruction of invariant masses of particles such as top or W mesons [V-8].

[V-7] T. A. Gabriel, J. E. Brau , and B. L. Bishop, Oak Ridge National Laboratory Report ORNL/TM-11060 (March 1989)

[V-8] A.E. Kiryunin, A. M. Moiseev, Proceedings of ECFA Workshop at Barcelona, Spain,

4. Carry out the pattern recognition, which causes most confusion;
5. Consider the trigger problem due to pile up;
6. Reconstruct the invariant masses of heavy particles, such as Higgs, top, etc., using shower Monte Carlos, which allow a W boson to decay into multiple (not just two!) jets. The low energy jet may contribute little to the total energy but a lot to the masses. How to identify these low energy jets for proper mass reconstruction is a crucial part of the pile up problem.

In order to understand the properties of a calorimeter, each of the above effects should be studied in detail separately at first. For example, "e/h" as a *function* of time; jets vs hadrons in a monolithic calorimeter, to see if there is any difference; mass resolution in multijet events to separate resolution from segmentation considerations. After all of these effects are understood in isolation, the ultimate simulation must include all the above effects at the same time, to define the properties of a specific detector. Only then we can claim a certain detector can in principle work at the LHC/SSC environment.

Sept. 1989

Table I

Physical Properties of Liquid Argon and Liquid Xenon*

	LAr	LXe
Atomic number Z	18	54
Atomic mass A	39.95	131.3
Triple point (°K)	83.8	161.3
Density at triple point (g/cm^3)	1.14	2.96
Boiling point (°K) at 1013 mb	87.3	165.0
Density of fluid (g/cm^3)	1.4	3.06
Gas/liquid ratio	784.8	519
Radiation length (cm)	13.9	2.8
Moliere radius (cm)	10	5.6
W-value (eV/ion pair)	23.3	15.6
Fano factor	0.107	0.041
Mobility (m^2/Vs)	0.048	0.22
Oxygen trapping constant (m^2/V)	1.5×10^{-14}	2.0×10^{-14}
Heat capacity C_p (cal/mol K)	10.05	10.7
Thermal conductivity (cal/s cm K) $\times 10^{-3}$	29.9	16.8
Refractive index	1.25	1.41

* from :
"On the Development of Liquid Ionization Detectors as Spectroscopic Instruments" by T. Lindblad et al. Nucl. Instr. and Meth. 215(1983)183

Table II. Properties of some common scintillators and ionization media.

The scintillation light decay times for both the fast and slow components and the ratio of their intensities; the saturation effect, K_B in Birk's law, for both scintillation and ionization outputs; and the light outputs of alpha and beta particles of several common media including BaF_2 in comparison with liquid xenon. T_1, T_2 are the decay time of the fast and slow component and A_1, A_2 their intensities at t=0 respectively.

scintillation	*Liquid Xe*	*BaF_2*	*NaI (Tl)*	*BGO*
fast decay time T_1 (ns)	3 [10]	0.6	250	60
slow decay time T_2(ns)	25-30	620	—	300
ratio A_1/A_2 for β	0.1[10]	0.09	—	0.05
ratio A_1/A_2 for α	25[10]			
rel. output from	0.9 [15,20]	0.008-0.04	1.	0.08
ratio of α/e [10,11]	1.1± 0.2 [10]	0.34 [11]	0.5	0.23 [14]
K_B^{-1} in MeV/cm[12]	50000 [5,20]	– – [13]	3670 [5]	500[8,14]
density (g/cm^3)	3.06	4.89	3.67	7.1
rad. length (cm)	2.8	2.05	2.59	1.12

ionization	*Liquid Xe*	*Liq. Ar.*	*TMS*	*TMP*
rel. output of a mip	12.6[16]	4.6 [17]	1[8]	1.1[3]

references [10] [11] [12] [13] [14] [15] [16] [17] [18] [19]

[10] S. Kubota et. al., Nucl. Inst. and Meth. 196 (82)101, and A242(1986) 291
[11] M.R. Farukhi et. al.,IEEE Trans. Nucl. Sci. NS-18(1971)200.
[12] The output/energy loss, dL/dE, reduces by 50% in Birk's law. See Ref.5.
[13] It is poorly defined since the size of the fast component critically depends on the particle types, such as α,e or heavy ions etc. at a given kinetic energy, see refs. 10 and 11.
[14] J. P. Martin, private communication.
[15] L. Koch and R. Leseur J. Phys. Radium 19(1958)103.
[16] T. Takahashi et.el., Phys. Rev A12(1975)1771; E. Shibamura et. al., Nucl. Inst. and Meth. 31(1975)249.
[17] T. Takahashi et.el., Phys. Lett. 44A(1973)123; M. Miyajima et. al., Phys. Rev. A9(1974)1438
[18] S. Aronson et. al., Fermilab Conf. 86/14-E
[19] M. Miyajima et. al., Nucl. Inst. and Meth. 160(1979)239.

Table III **scintillators**

		Xe	Kr	NaI	BGO	BaF_2	CH
a.radiation length*	[cm]	*2.8*	4.8	2.59	1.12	2.05	42.4
b.absorption length*	[cm]	*55*	61	41	22	30	79.5
c.Moliere radius†	[cm]	*5.6*	7.1	4.4	2.33	3.2	10.5
d.critical energy†	[MeV]	*10.5*	14.2	12.5	10.1	13.5	85
e.density*	[g/cm^3]	*3.06*	2.41	3.67	7.1	4.89	1.03
f.$<\Delta E_{mip}(1cm)>$*	[MeV]	*3.79*	2.96	4.87	9.01	6.6	2.01
g.price per liter$	[SFr]	*3200*	2000	4000	8000	6000	1000

* from "Review of Particle Properties" Phys. Lett. 170B, April 1986

† from "Calorimeters (Total Absorption Detectors) for High - Energy Experiments at Accelerators" by Seigi Iwata DPNU 3-79, February 1979

$ for reference only:

Xe price derived from that demanded at DESY during summer 1987 for small quantities of gas at STP. US prices are significantly higher (x 2 - 3).
Kr price as envisaged for the 35 ton Novosibirsk detetctor.
BGO price for transformation of polycrystalline powder to crystals (L3); raw materials are extra.
CH ≡ organic scintillator of high quality (e.g. NE 110).

Table IV. Properties of the Proposed Silicon Photodiode

Properties	*Si photodiode*
Shaping time (ns)	10 ns
Max. diameter	50mm
Thickness	200μ
Quantum eff.	about 70%
Noise	$1.5x10^4$ e/25 cm^2
Price	about 1 M\$/10^5
Radiation damage	10^6 rad. normal 10^8 rad. in LXe (to be proven)

Table V. Properties of some UV Reflectros for LXe and LAr

Wave length	*Al*	*Al+MgF_2*	*MgO + MgF_2BaSO_4*	
170nm (LXe)	80%	80%	> 90%	90%
130nm (LAr)	35%	80%	> —	85%

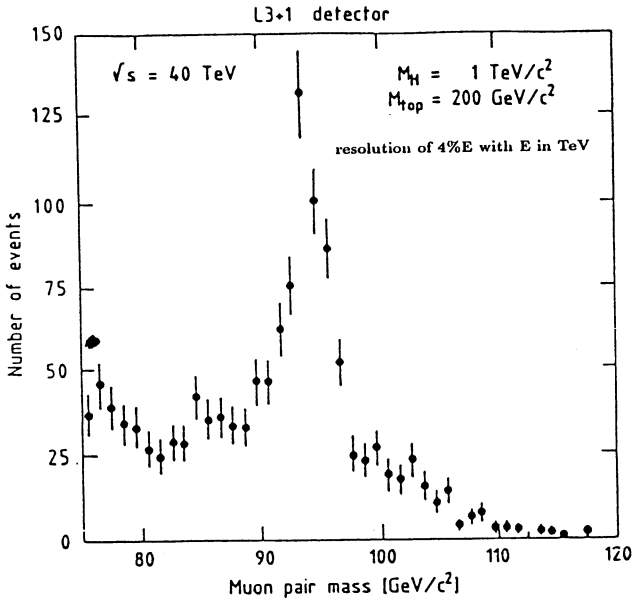

Fig. 1a The reconstructed invariant masses distributions of the dimuons from reactions (1) and (2) with with 1 Tev Higgs and 200 GeV top for the L3+1 detector. The Higgs signal is clearly visi ble above the heavy quark background.

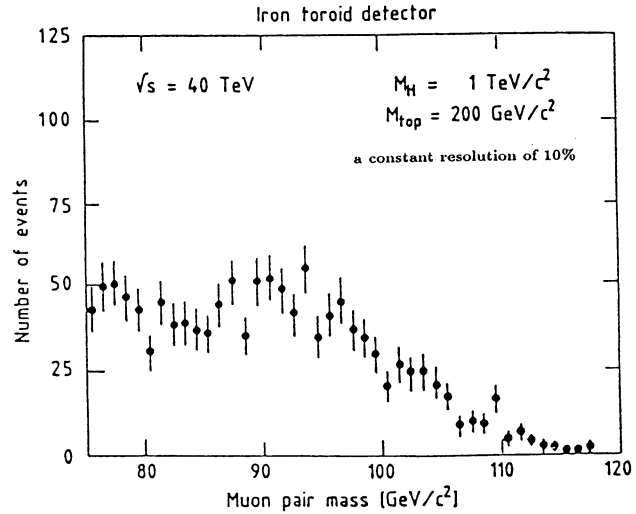

Fig. 1b The reconstructed invariant masses distributions of the dimuons from reactions (1) and (2), same as in Fig. 1a, but with an iron toroid.

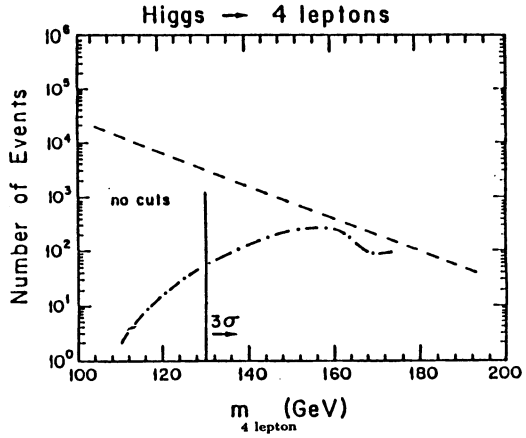

Fig.2 Expected number of events for Higgs → 4 leptons as function of the mass of the Higgs with an integrated luminosity of 10^4 pb^{-1} at $\sqrt{s} = 40$ TeV. The dashed-dot curve is from Higgs for m_t=90 GeV, the dashed curve is the background from QCD. The momentum resolution of each lepton is assumed to be 0.5% which yields a Higgs mass resolution of 0.2%.

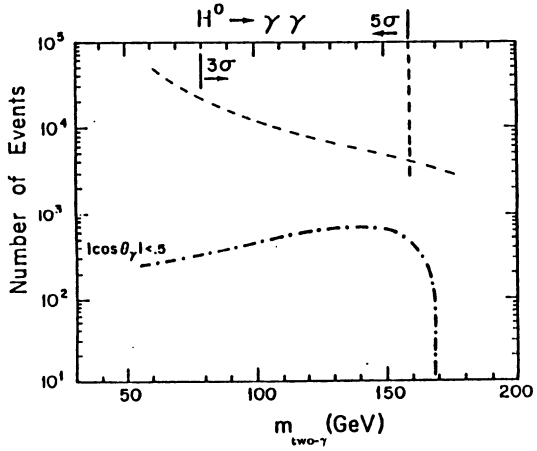

Fig.3 Expected number of events for Higgs → $\gamma\gamma$ as function of the mass of the Higgs with an integrated luminosity of 10^4 pb^{-1} at $\sqrt{s} = 40$ TeV. The dashed-dot curve is from Higgs for m_t=90 GeV [3]; the dashed curve is the background from QCD The momentum resolution of each lepton is assumed to be 0.5% which yields a Higgs mass resolution of 0.3%.

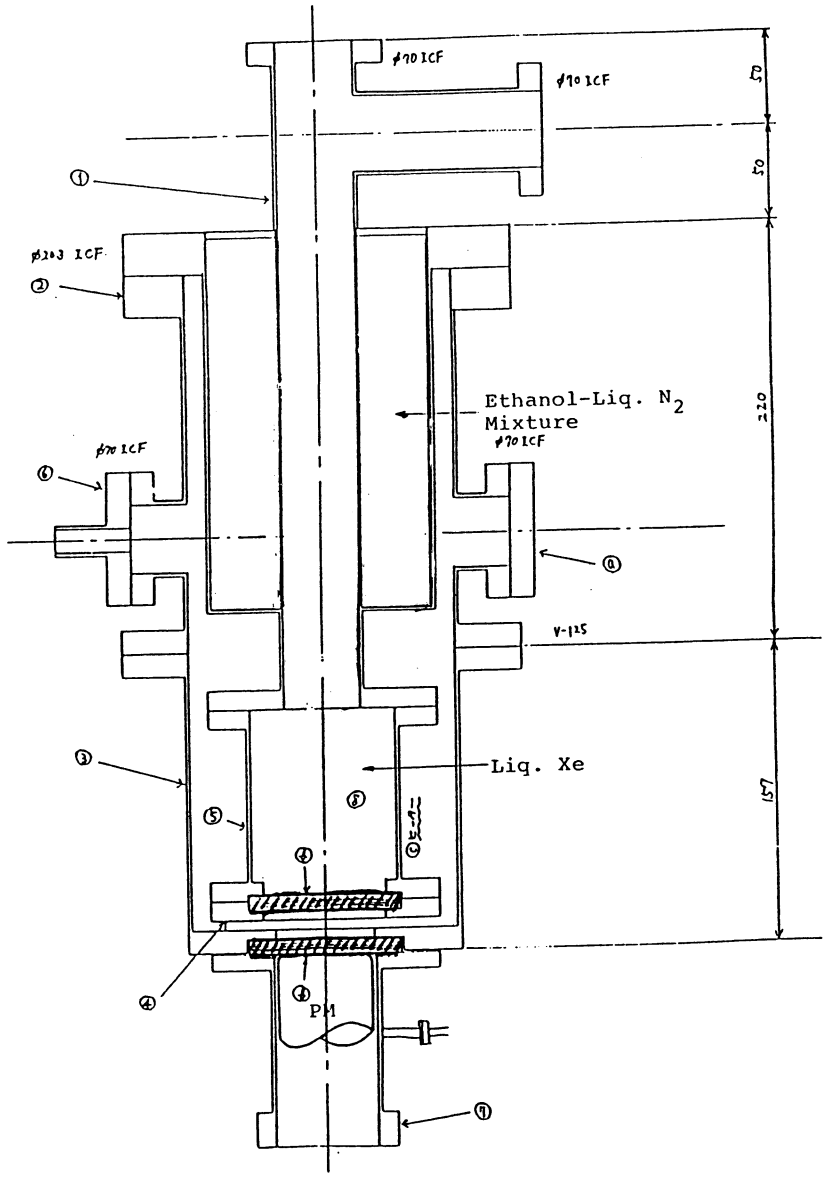

Fig. 4 Scintillating liquid xenon detector built by Doke et al. [20] to measure the reflectivity and light collection efficiency for 170 UV light from xenon. All dimensions are in mm.

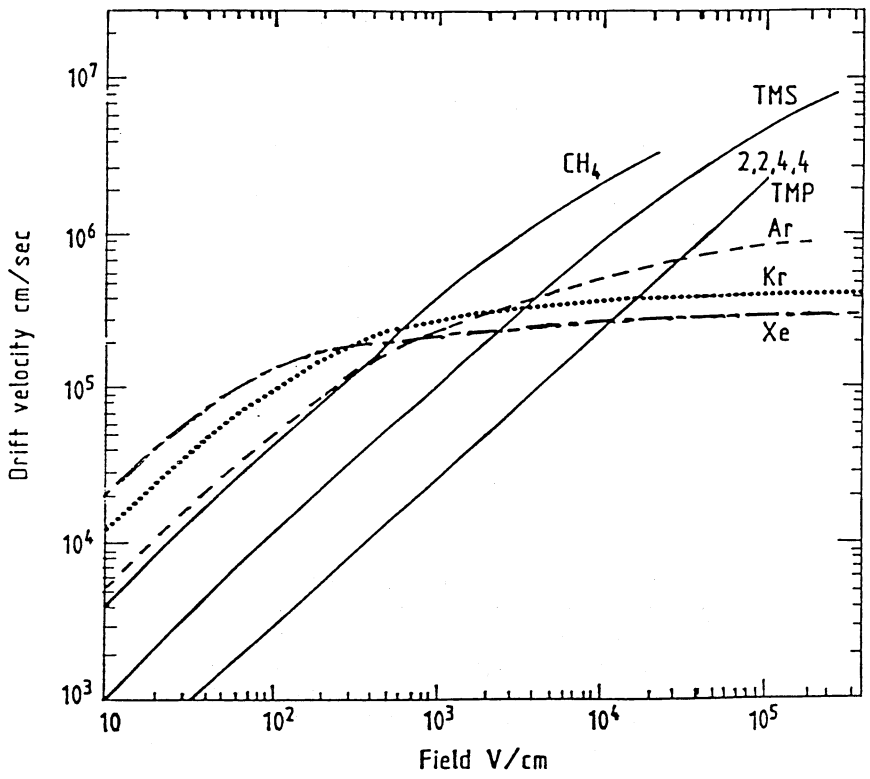

Fig. 5
Dependence of electron drift velocity in liquid noble gases and liquid hydrocarbons on the electric field .

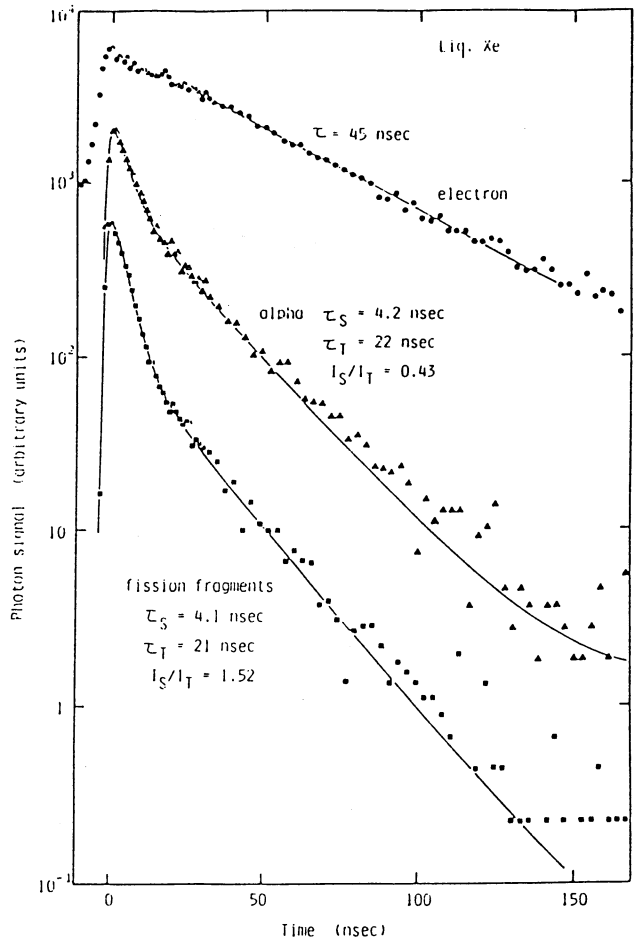

Fig. 6a Decay curves obtained for the luminescence from liquid xenon excited by electrons (●), α particles (▲), and fission fragments (■).

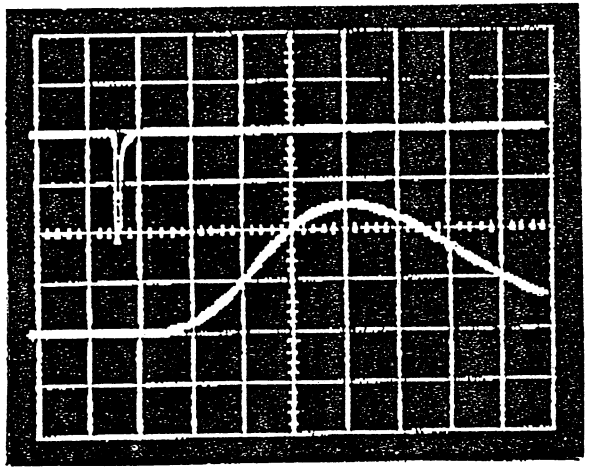

Fig. 6b The scintllating (fast) and ionization (slow) signals (500 mV/div. vertically and 2μs/div. horizontally) from stopping ^{241}Am α particles in a liquid xenon chamber made by E. Aprile et al.[22] The timing difference between the two signals yields a spatial resolution of $< 30\mu$[20].

Linearity of Liquid Argon Detector Scintillation versus Ionization

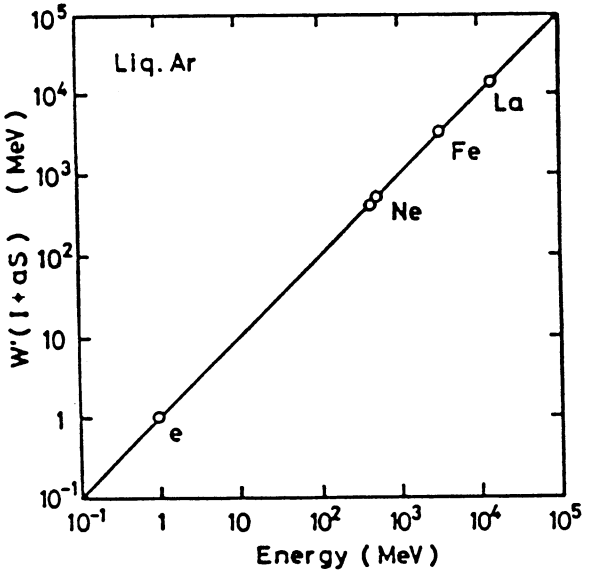

Fig. 7a Relation between the energy absorbed in liquid argon and the amplitude of the sum signal of scintillation and charge in unit of energy.

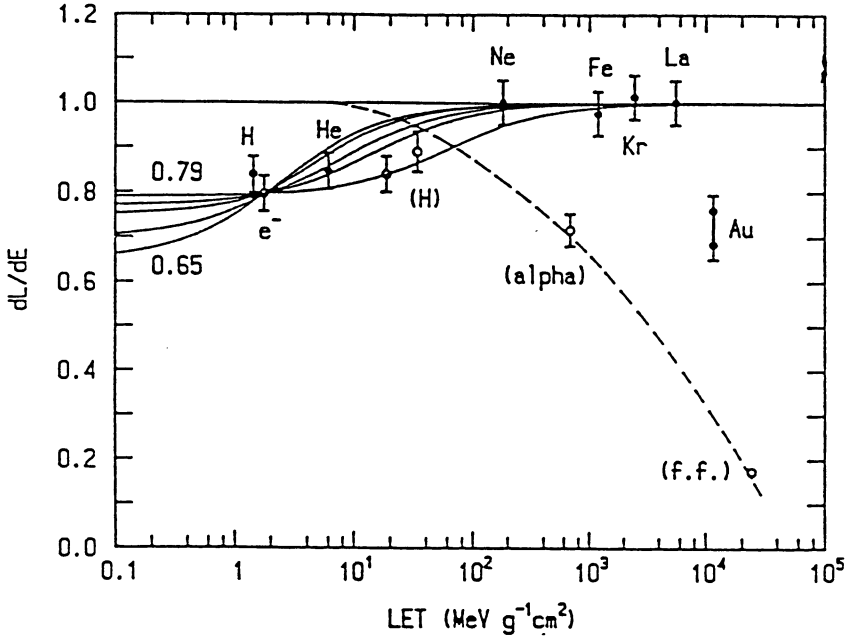

Fig. 7b The measured ratio of light output over energy loss, dL/dE for relativistic ions (solid data points and curves with different fits) and fission fragments (open points and dashed curve), versus dE/dx the energy loss in LAr from Ref.IV-20. LXe or LAr saturates at two orders of magnitude higher energy loss than NaI or BaF_2.

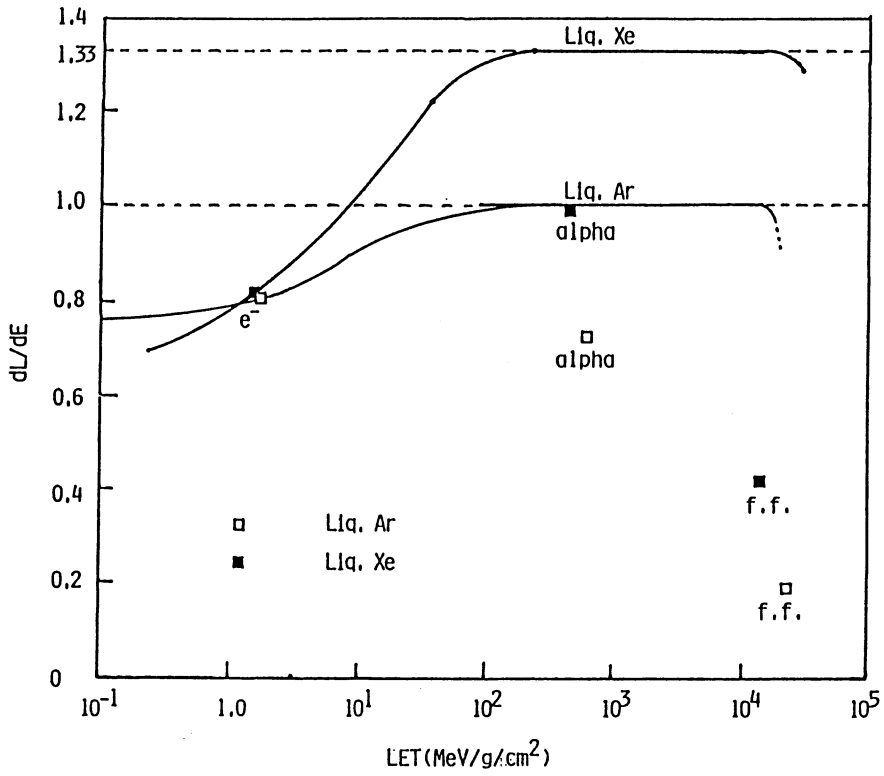

Fig. 7c Similar to Fig. 7b, dL/dE for relatisvistic ions and fission fragments for LXe (solid squares) and for LAr (open squares) versus dE/dx. For heavy ions, the electron/ion density and thus the scintillating light output from recombined ion-electron pairs are higher in LXe than in LAr. LXe or LAr saturates at two orders of magnitude higher dE/dx than NaI or BaF_2.

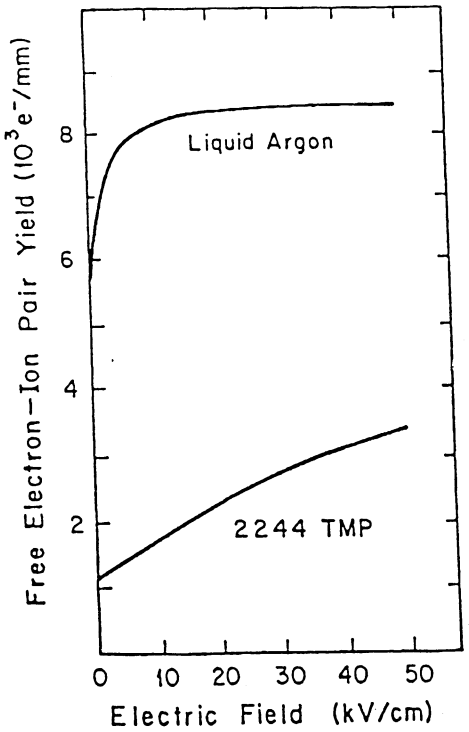

Fig. 8 The free electron yields produced by a minimun ionization particle in liquid argon and TMP as a function of the applied electric field. TMS is about same as TMP while liquid xenon is about 2.5 times larger than liquid argon.

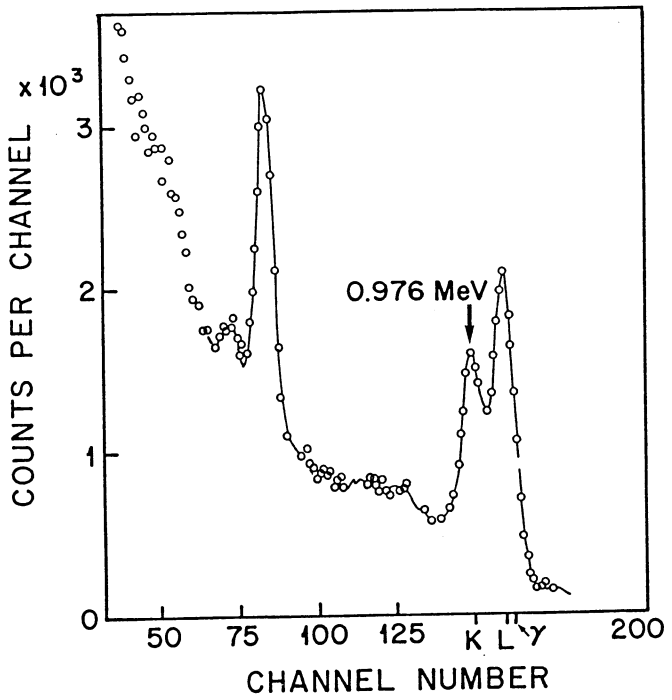

Fig. 9 A typical measured spectrum of ^{207}Bi obtained by a LXe gridded chamber by E. Aprile et al. from ref.22.

EM shower counter: Xe
Hadron: Ar or TMS...

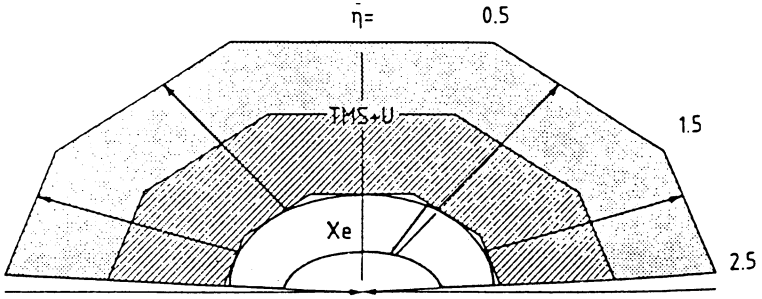

The schematic drawing of the proposed Xenon Ball Detector, showing the cell arrangement of the xenon electro-magnetic shower counter.

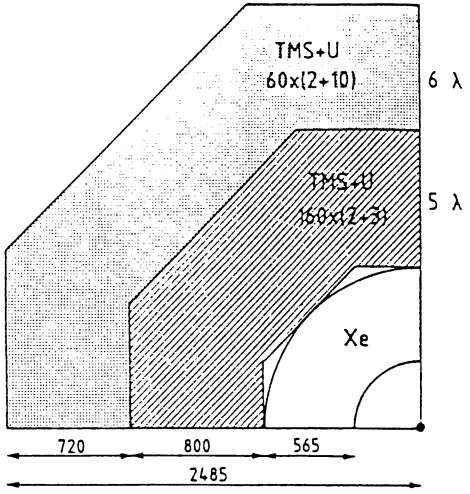

Fig. 10a The R-ϕ projection of the schematic drawing of the proposed Xenon Olive Detector, showing the elctro-magnetic and hadron calorimeter counters.

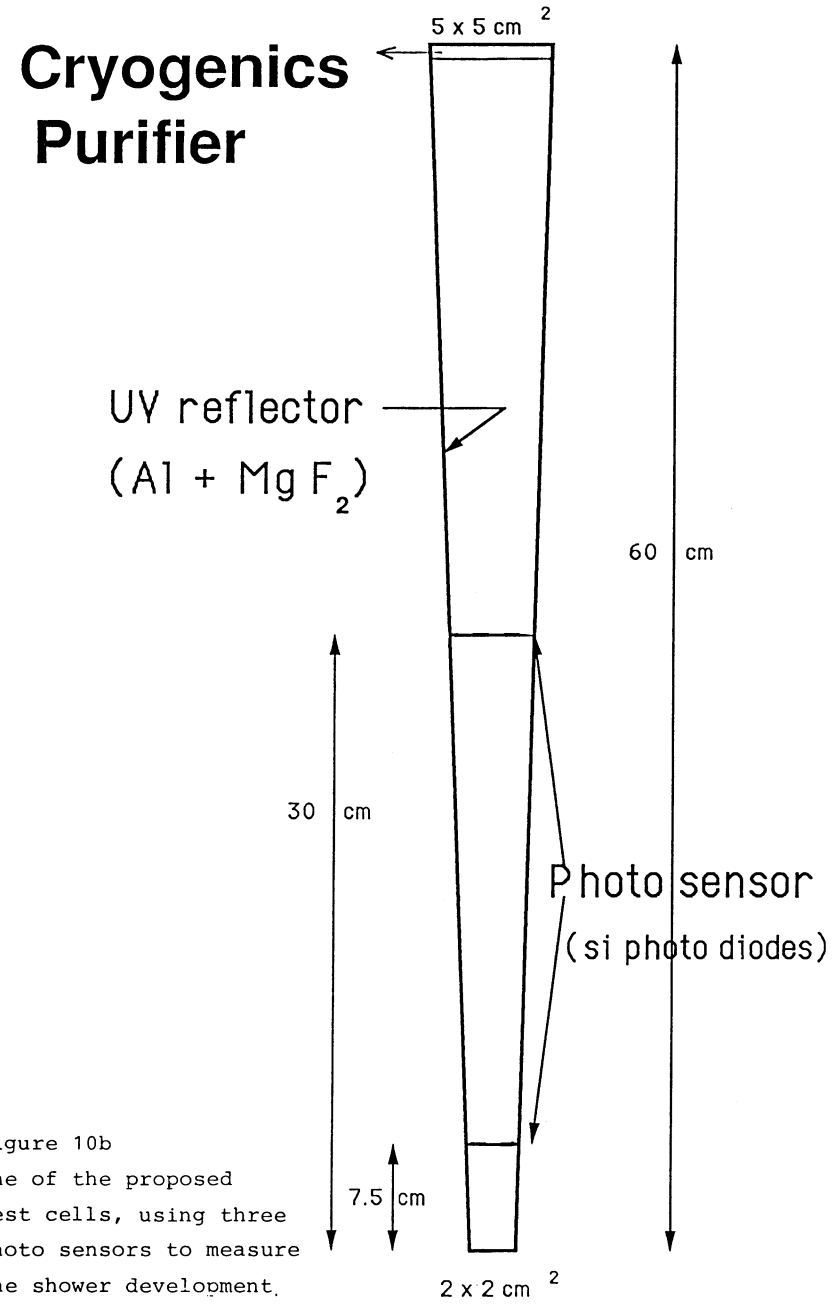

Figure 10b
One of the proposed test cells, using three photo sensors to measure the shower development.

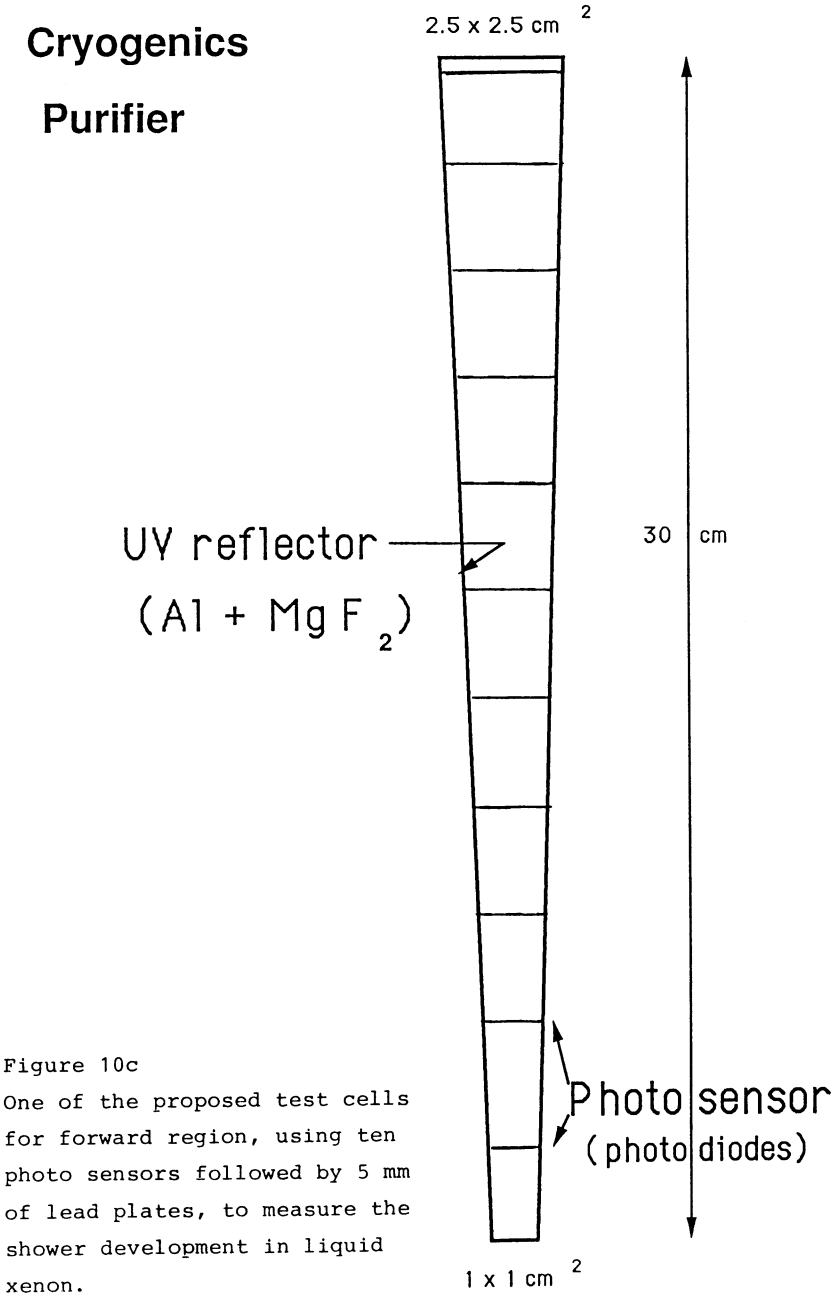

Figure 10c
One of the proposed test cells for forward region, using ten photo sensors followed by 5 mm of lead plates, to measure the shower development in liquid xenon.

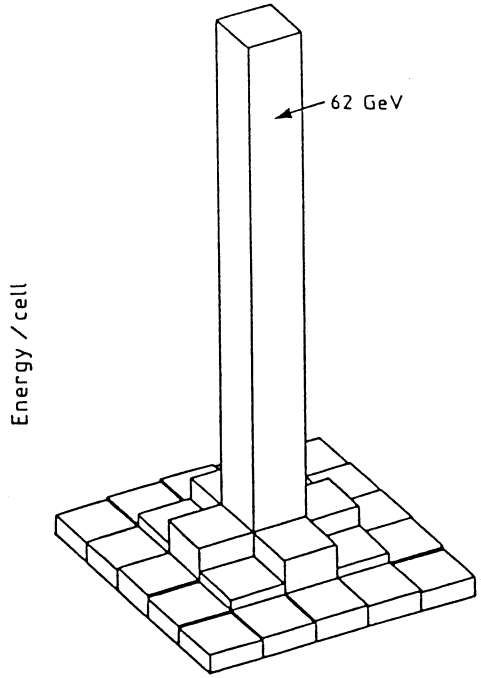

Fig.11 The energy distribution in the xenon detector for a hundred GeV electrons as simulated by the Geant3 Monte Carlo program. Typically more than 62% of the energy concentrates in one or two cells.

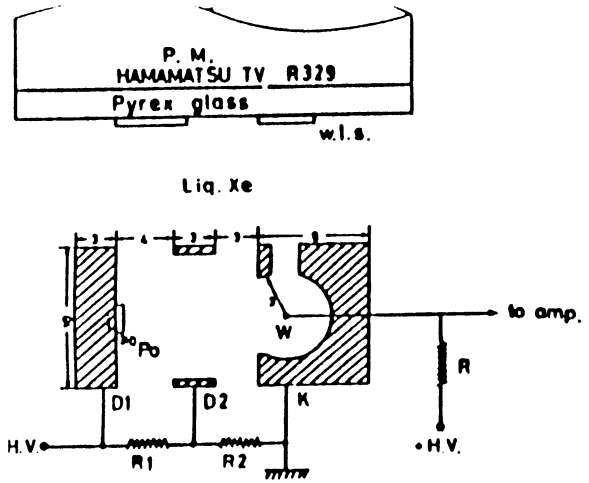

Fig. 12a Schematic cross-section of a small single wire liquid Xenon drift chamber.

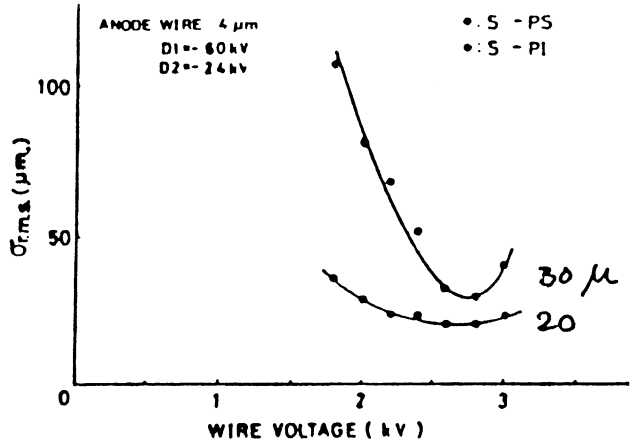

Fig. 12b Spatial resolution (r.m.s.) versus anode voltage by Doke et al.

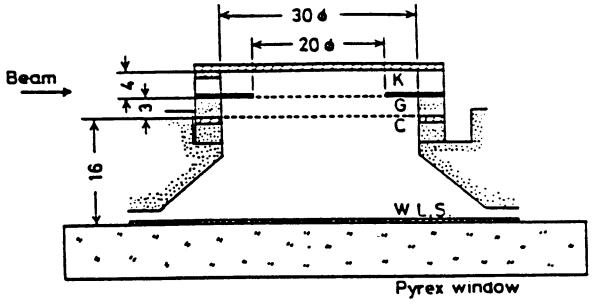

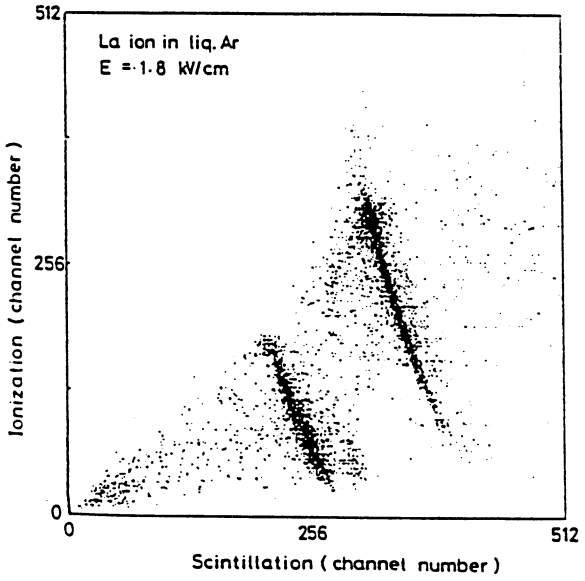

Fig. 13 Correlation between scintillator signal and ionization signal.

Si photo-diode

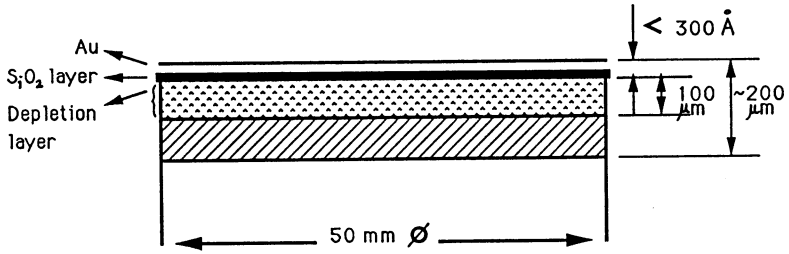

Fig. 14

Schematic Layout of the Silicone Photo-Diode developed by us for liquid xenon detector. It has a shaping time of 10 ns and a quantum efficiency of 70 %. The thin window (30 nm) now is transparent to the UV-light from LXe and it will be further reduced to 15 nm thick.

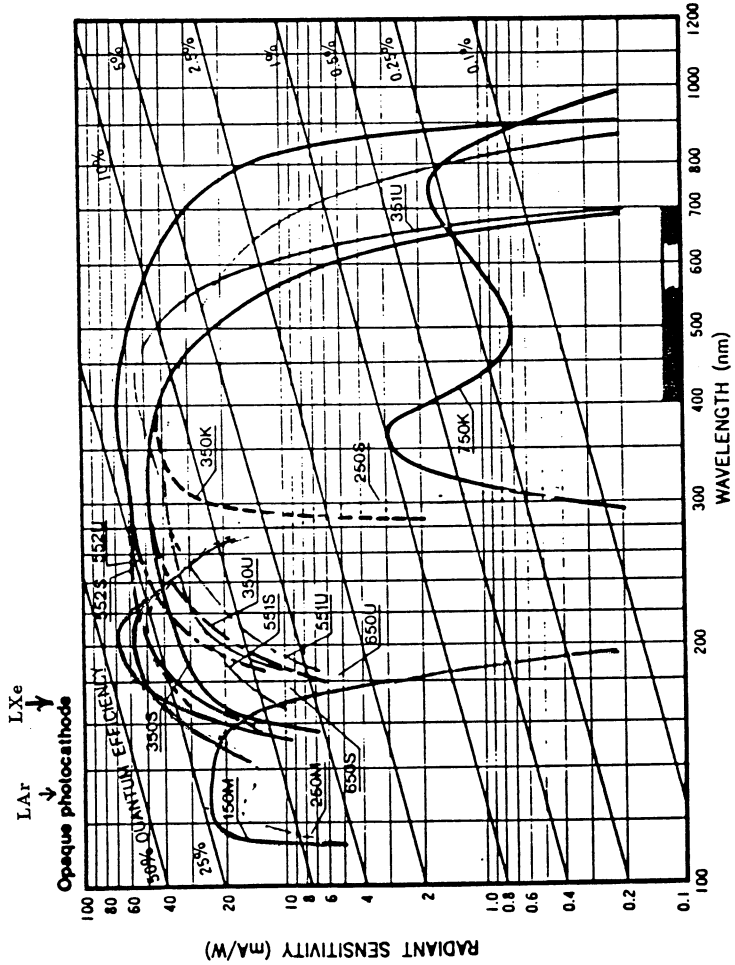

Fig. 15 The quantum efficiencies of some of the presently available photo tubes from Hamamatsu versus wavelength. A quantum efficiency of 25 to 35 % is achieved for LAr (130nm) and LXe (170nm).

From CRC Handbook of Chemistry and Physics(66th ed. 1985-86)

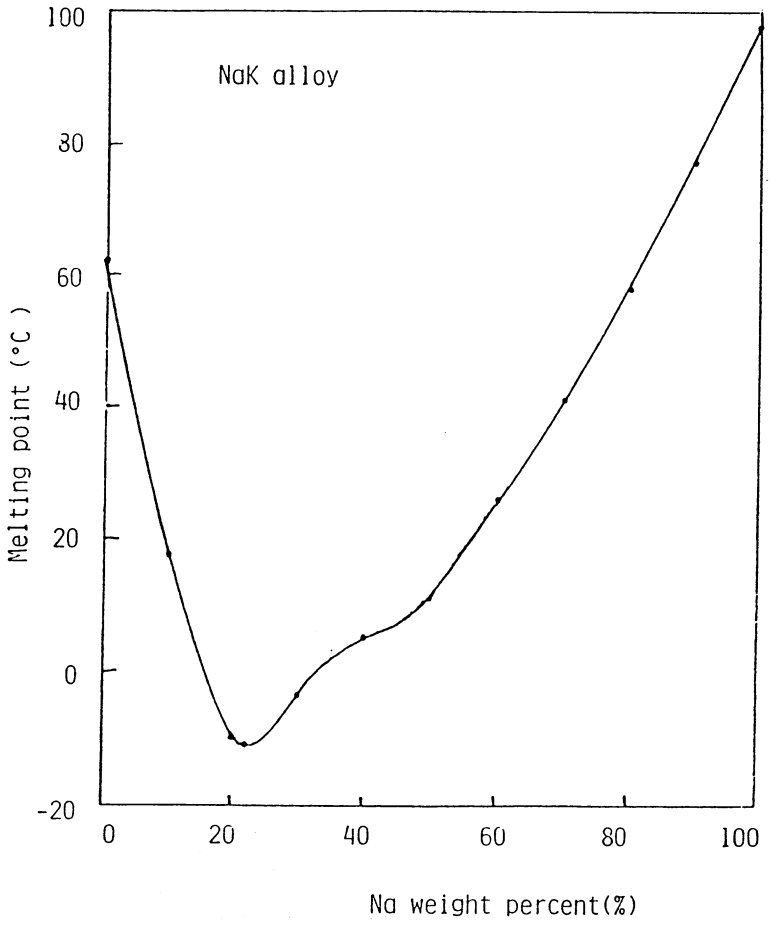

Fig. 16 The phase transition property of NaK alloy versus the % Na weight. Top region is for liquid while bottum is for solid NaK alloy. The operating point for LXe is chosen to be near the minimum, i.e. Na = 21%.

Purification system using NaK alloy:

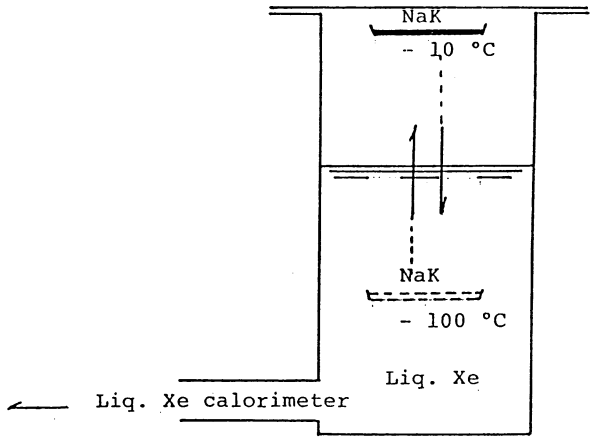

Fig. 17 A high performance (a few ppb of impurity) purification system for LXe detectors. NaK is very active when dropped as liquid into LXe, where it turns into solid and absorbs impurities. Solid NaK are then removed from the bottum to return to liquid state, stired to obtain fresh surface to be reused again.

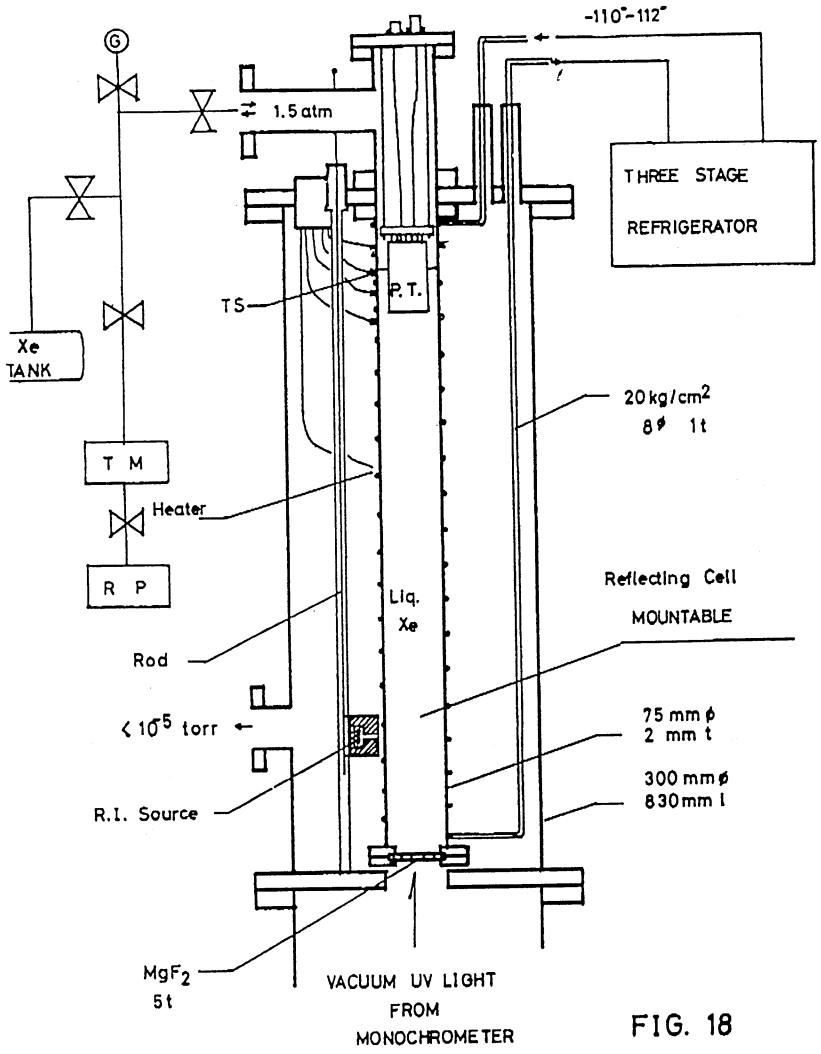
-110°-112°
1.5 atm
THREE STAGE
REFRIGERATOR
TS
P.T.
Xe
TANK
20 kg/cm²
8φ 1t
T M
Heater
R P
Liq.
Xe
Reflecting Cell
MOUNTABLE
Rod
< 10⁻⁵ torr
75 mm φ
2 mm t
300 mm φ
830 mm l
R.I. Source
MgF₂
5t
VACUUM UV LIGHT
FROM
MONOCHROMETER

FIG. 18

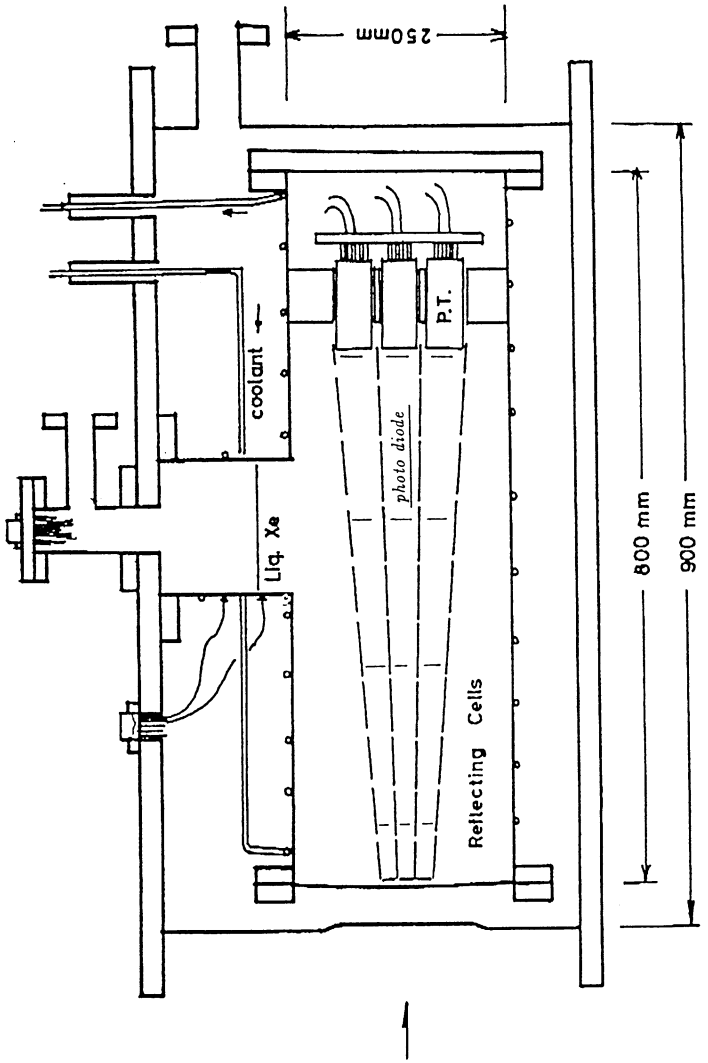
250mm
coolant
P.T.
photo diode
Liq. Xe
Reflecting Cells
800 mm
900 mm

FIG. 19

LIQUID-ARGON CALORIMETRY—ITS POTENTIAL FOR EXPERIMENTATION AT FUTURE HIGH-LUMINOSITY HADRON COLLIDERS

C.W. Fabjan
CERN, Geneva, Switzerland

1. INTRODUCTION

The viability of liquid-argon (LAr) calorimetric techniques in the experimental environment of future hadron colliders is briefly analysed. These machines, such as the Large Hadron Collider (LHC) and the Superconducting Super Collider (SSC), are planned to operate at luminosities up to and exceeding $L \approx 10^{34}\ cm^{-2}\ s^{-1}$. We compare the required and achievable energy resolution with bench-mark figures obtained using practical instruments. Comments on the desirable (i.e. required) temporal performance are made and compared with the state of the art. Some of the major engineering challenges are listed, for which solutions will have to be developed if such instruments are to find a place in an experimental area.

2. ENERGY RESOLUTION: REQUIRED VERSUS PRACTICAL

The calorimetric energy measurement is thought to be the single, most important, spectroscopic tool for the physics programme at these colliders [1]. It requires instruments which must have excellent hermeticity over a large rapidity interval $|y| \leqslant 5.5$, and also 'sufficiently good' energy resolution. There are at least three 'fundamental' (i.e. detector-physics determined) contributions:

i) The intrinsic resolution σ(intrinsic), representing the accuracy on single, low-rate hadrons, for which in large, practical devices $\sigma(\text{intrinsic})/E \leqslant 0.3/\sqrt{E}$ has been achieved [2]. At the LHC/SSC, total or transverse energies will typically be in the few-hundred-GeV regime. A measurement with 10 GeV accuracy would imply an equivalent resolution of $\sigma(E)/E \approx 0.5/\sqrt{E(GeV)}$. Similar resolution requirements are imposed for multijet spectroscopy, e.g. in the study of the reaction

$$\begin{array}{l} pp \rightarrow \text{Higgs} + \text{anything} \\ \quad\quad \big\lfloor\!\!\rightarrow W \rightarrow \text{jet} + \text{jet} \\ \quad\quad \big\lfloor\!\!\rightarrow W \rightarrow 2\ell\,. \end{array}$$

ii) The reconstruction of the energy of a system based on signals in calorimeter cells implies the use of reconstruction algorithms and hence inherently some loss in information. The value of σ(reconstruction) has been studied [3], and a performance of $\sigma(\text{reconstruction}) \approx 10$ GeV for $E \approx 500$ GeV has been estimated.

iii) The temporal signal response of the detector is at the origin of a further contribution to the energy resolution at very high particle rates since, during the 'occupation time' in the detector, on the average more than one particle is recorded [σ(pile-up)]. This contribution will be further discussed in Section 3, where we show that this pile-up contribution can be limited to σ(pile-up) $\leqslant 5$ GeV when operating calorimeters with today's technology at luminosities $L > 10^{33}\ cm^{-2}\ s^{-1}$.

Given the scale set by resolution contributions (ii) and (iii), it is acceptable to aim for values of the intrinsic calorimeter resolution $\sigma(\text{intrinsic})/E \leqslant 0.5/\sqrt{E(GeV)}$, provided this $1/\sqrt{E}$ scaling improvement is applicable over the full energy range of interest, i.e. $E \leqslant 0.5$ TeV. The essential consequence of this requirement is summarized in Fig. 1, which displays σ(intrinsic) for various values of the relative electron-to-hadron response, e/π. As a consequence, it will be necessary to achieve *approximate compensation at the level* $e/\pi \leqslant 1.10$.

In the following we present the measured performance and e/π value for several of the present-generation LAr detectors. Some instrumental parameters are summarized in Table 1. Two of the three devices (D0, Ref. [4]; HELIOS, Ref. [5]) use uranium as the absorber medium, whilst the H1 detector [6] uses lead and copper absorber plates.

Preliminary results obtained in the D0 test are shown in Fig. 2 [4]. The basic performance with respect to e/π is seen to be adequate, $\langle e/\pi \rangle = 1.04 \pm 0.03$, whereas the signal response time of $\lambda \approx 3000$ ns is clearly not adequate for luminosities in the 10^{33}–$10^{34}\ cm^{-2}\ s^{-1}$ range. In view of the interest in 'fast' liquids, the D0 team studied also the effect of using small admixtures of methane to liquid argon, which is known to reduce the drift-time by approximately a factor of 2 at concentration levels of $\leqslant 1\%$ CH_4 [7].

These tests demonstrated that the increased recombination in the Ar/CH_4 system does not present any significant obstacle to using 'fast' LAr ($v_{drift} \approx 1$ cm/μs) in large calorimeter systems (an $\sim 30\%$ loss in signal was observed at 0.5% CH_4 concentration).

To date, the fastest LAr calorimeter is operated by the HELIOS Collaboration at CERN in a Super Proton Synchrotron (SPS) high-energy particle beam [5]. It can be seen from Figs. 3 and 4 that even with the shortest shaping time of $\lambda = 400$ ns, a very good performance [$(\sigma/E) \times \sqrt{E} \leqslant 0.5$ up to $E = 450$ GeV] is obtained. In the next section we will discuss the technical implications of achieving these short (or even shorter) signal response times, and will argue that these values of λ are in an acceptable range.

The H1 Collaboration at HERA was on an entirely different tack. Their calorimeter uses lead and copper plates, instead of uranium, as absorber. This detector is characterized by an exceedingly high granularity (i.e. tower structure with sixfold longitudinal subdivision in the hadronic calorimeter) permitting the shower profile to be measured in detail. This capability suggests the use of an 'energy weighting' procedure [8] that preferentially attenuates 'hot spots' of energy deposits (due to the electromagnetic component in the shower). This method has been tested for *single particles,* and is found to keep the linearity at the 1% level while considerably improving the energy resolution (Fig. 5). Preliminary Monte Carlo calculations indicate that the response to *particle jets* is also much improved, although this has still to be studied more thoroughly [6].

3. TEMPORAL RESPONSE: REQUIRED VERSUS ACHIEVABLE

The key to high-rate operation of calorimeters is the choice of bipolar pulse-shaping [9], so that the pile-up of several events within the sensitive time of the detector *does not, on the average,* produce a net shift in the measurement of a large signal. Pile-up will, however, contribute as noise σ(pile-up) to the overall energy resolution of the detector. The results of several quantitative studies [10] on σ(pile-up) as a function of interaction rate n and shaping time λ are summarized in Fig. 6. It is estimated that this noise contribution should not exceed a few GeV for jet spectroscopy at LHC or SSC luminosities ($n \geqslant 10^8\ s^{-1}$).

Apart from the value of the drift velocity and the charge collection, which determine the electronic noise level relative to the signal level, *the* principal technical limitation is imposed by the

transfer time t_{tr} of the charge from the detector electrodes to the amplifier. The detailed analysis [9] indicates

$$t_{tr} \approx 3.5 \times (L_{cable} \times C_{detector})^{1/2} ,$$

$$t_{tr} \leqslant \lambda/5 .$$

These conditions can be satisfied provided the cable inductance and hence the total cable length L are kept very small: for acceptable values of $\lambda \leqslant 200$ ns, preamplifiers have to be placed in close proximity to the electrodes (< 1 m cable length). This implies that amplifiers will have to be embedded inside the calorimeter and will have to operate at temperatures in the vicinity of ~ 100 K. The latter condition is not a particularly stringent requirement. The vicinity of the electrodes, however, renders the amplifiers almost inaccessible—a problem that could be common to all charge-collecting calorimeters.

4. ENGINEERING DEVELOPMENTS

In the previous sections we showed that the intrinsic performance of LAr calorimetry is commensurate with the required performance at the LHC/SSC. This is to be contrasted with several major, and as yet unresolved, engineering questions, which will need coordinated R&D to demonstrate the viability of LAr calorimetry. Here we list those of main concern:

1) Radiation resistance of active and passive components. This is, of course, the principal problem common to all high-luminosity detectors. For charge-collecting devices, the electronics will have to be embedded in the detector and will therefore be exposed to the particle flux created in the absorber. Before the magnitude of this engineering issue can be adequately addressed, we need to develop a better understanding of all active components that are likely to be placed in this high-radiation environment (preamplifiers, analog storage, trigger electronics, etc.). Radiation-hard electronics is *the* biggest engineering challenge, which the high-energy physics community will have to tackle in collaboration with industry.

2) Readout electrodes. The calorimeters will be characterized by a very high granularity, typical of today's electromagnetic front-sections of advanced calorimeters [4–6]. The feasibility of such a design, satisfying all the requirements (very short cables, excellent hermeticity, etc.), has yet to be demonstrated. As an example of the complexity of readout structures, we show in Fig. 7 a cross-section through a readout gap of the electromagnetic section of the H1 calorimeter: it shows the complex multiboard structure of the electrodes. Its fabrication is a major cost factor, taxing the capabilities of industry.

More recently, the possibility of serial-plate connection was reconsidered [11], offering an alternative to transformer matching. This method may alleviate the otherwise very stringent limits on the length of the cables to the preamplifiers.

3) Cryostats: There is a widespread opinion that the cryogenic vessels required for LAr calorimetry preclude adequate hermeticity, acceptably thin entrance windows, and a minimum of dead space. Whilst awaiting the final results of an adequate engineering evaluation for such a detector, only a few comments will be made:

i) Hermeticity: This is clearly an unresolved issue. In the present generation of detectors, it was not required to the same extent [4, 12]. In Fig. 8 we show, as an example, the SLD solution, which conceptually could possibly evolve into a hermetic design. Similar conclusions have recently been reached by a group [13] who are considering the physics and engineering aspects of a LAr calorimeter optimized for SSC physics.

ii) Thickness of entrance window: I comment on this point by quoting the thickness (90° incidence) of the entrance window for several detectors: D0: $0.9X_0$; SLD: $0.9X_0$; UA1: ~ $0.7X_0$ (TMP, room-temperature liquid!), H1: ~ $0.25X_0$! It does not appear to be a problem.

iii) Dead space for cryogenic insulation: Typically ~ 8 cm are required for purposes of insulation, which will increase the radial dimensions of the detector.

5. CONCLUSIONS

We have repeatedly stressed that the intrinsic performance of today's LAr calorimeters approaches specifications required at our future hadron colliders.

The e/π ratio is adequately close to 1 if uranium is used. Alternatively, energy weighting in very granular devices may permit off-line compensations. The time response requires very short signal connections, with amplifiers located inside the detector. In this way, 'pile-up' contributions may be kept at an acceptable level.

It will be most important to confront some of the major engineering questions head-on, such as radiation-hardness of the electronics, novel concepts of cryostats, and detailed work on readout planes.

I believe that LAr calorimetry may not be the only contender for an SSC/LHC interaction region. However, 15 years of experience with this technique has built up a solid base from which the challenge of these new machines can be faced.

REFERENCES

[1] See, for instance, R.N. Cahn et al., Proc. Workshop on Experiments, Detectors, and Experimental Areas for the Supercollider, Berkeley, 1987, eds. R. Donaldson and M.G.D. Gilchriese (World Scientific, Singapore, 1988), p. 20.

[2] T. Åkesson et al., Nucl. Instrum. Methods **A262** (1987) 243.

[3] T. Åkesson et al., Proc. ECFA-CERN Workshop on a Large Hadron Collider in the LEP Tunnel, Lausanne and Geneva, 1984, ed. M. Jacob (ECFA 84/85, CERN 84-10, Geneva, 1984), p. 167.

[4] S.J. Wimpenny (D0 Collab.), 'Hadron and electron response of uranium/liquid-argon calorimeter modules for the D0 detector', presented at the Int. Conf. on Advanced Technology and Particle Physics, Como, Italy, 1988.

[5] H. Gordon et al. (HELIOS Collab.), 'Performance of the HELIOS uranium/liquid-argon calorimeter', Contribution to the 22nd Int. Conf. on High-Energy Physics, Munich, 1988.

[6] W. Braunschweig et al., 'Results from a test of a Pb-Cu liquid-argon calorimeter, DESY 87-098 (1987).
G. Flügge et al., these proceedings.

[7] E. Shibamura et al., Nucl. Instrum. Methods **A131** (1975) 249.

[8] H. Abramowicz et al., Nucl. Instrum. Methods **180** (1981) 429.

[9] V. Radeka and S. Rescia, Nucl. Instrum. Methods **A256** (1988) 228.

[10] A. Yamashita and K. Kondo, Proc. DPF Summer Study on the Physics of the Superconducting Super Collider, Snowmass, 1986 (AIP, New York, 1987), p. 365.
G.O. Alversson and J. Huston, ibid., p. 368.

[11] J. Colas, Berkeley preprint LBL-27328 (1989).

[12] SLD Design Report, Stanford report SLAC-273 (1984).

[13] T. Adams et al., Status report on an engineering design study of hermetic liquid-argon calorimetry for the SSC, to appear in Proc. Workshop on Calorimetry for the Superconducting Super Collider, Tuscaloosa, 1989.

Table 1
Instrumental parameters for three LAr calorimeters

Collaboration	Ref.	Mechanical parameters	Signal shaping-time λ (ns)	Compensation method	'e/π' (10 GeV)
D0 at the FNAL Tevatron Collider (test device)	4	6 mm ^{238}U, 2 × 2.6 mm LAr	3000	Uranium	≈ 1.08 ± 0.02
HELIOS at the CERN SPS (fixed target)	5	3.4 mm ^{238}U, 2 × 2.5 mm LAr	4000, 1000, 2000	Uranium	≈ 1.13 ± 0.02
H1 at the DESY HERA	6	Electromagnetic part: 2.4 mm Pb/2.8 mm LAr 5-fold longit. segmentation Hadronic part: 5 mm Cu/2 × 1.5 mm LAr 6-fold longit. segmentation		Local energy weighting	'e/π' [weighted] ≈ 1.03

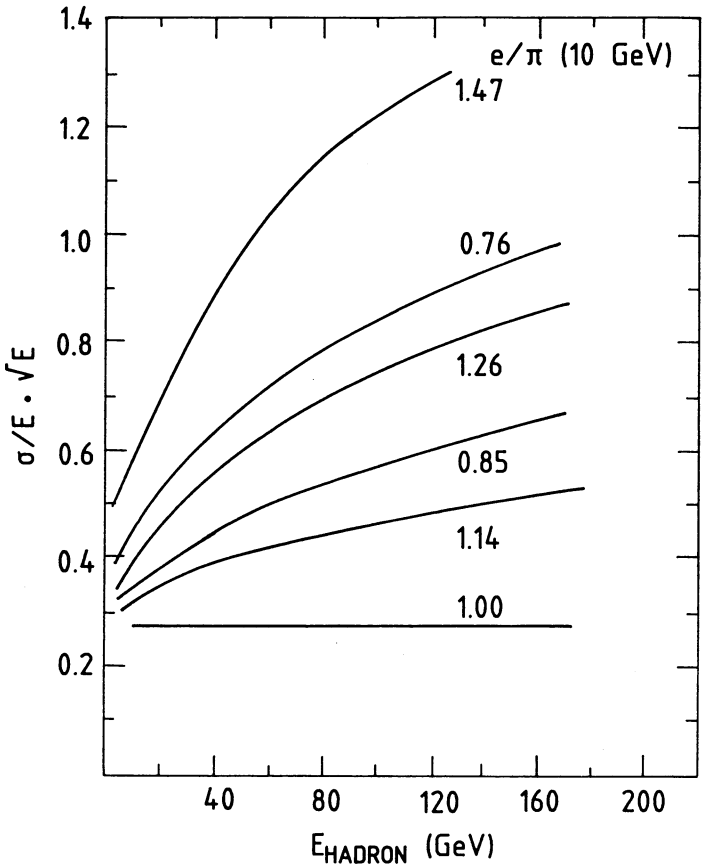

Fig. 1 The intrinsic energy resolution for hadrons as a function of particle energy and various values of e/π. Only for perfectly compensated instruments, $e/\pi = 1$, is the $1/\sqrt{E}$ scaling seen to be strictly true at all particle energies. A requirement for $(\sigma/E) \times \sqrt{E} \leq 0.5$ for energies up to a few hundred GeV imposes limits on e/π, so that $\sim 0.95 \leq e/\pi \leq 1.10$ at 70 GeV.

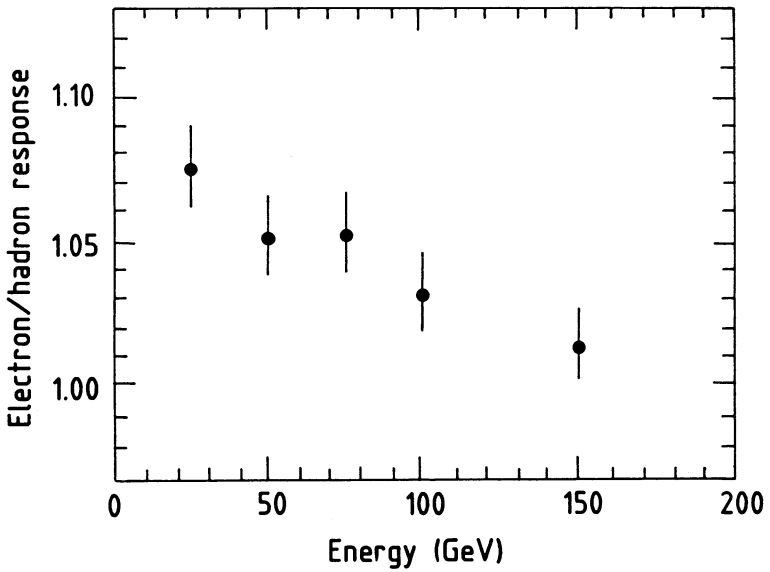

Fig. 2 The value e/π versus particle energy as observed in the D0 test (preliminary result). The signal-shaping time was $\lambda = 3\ \mu s$ [4].

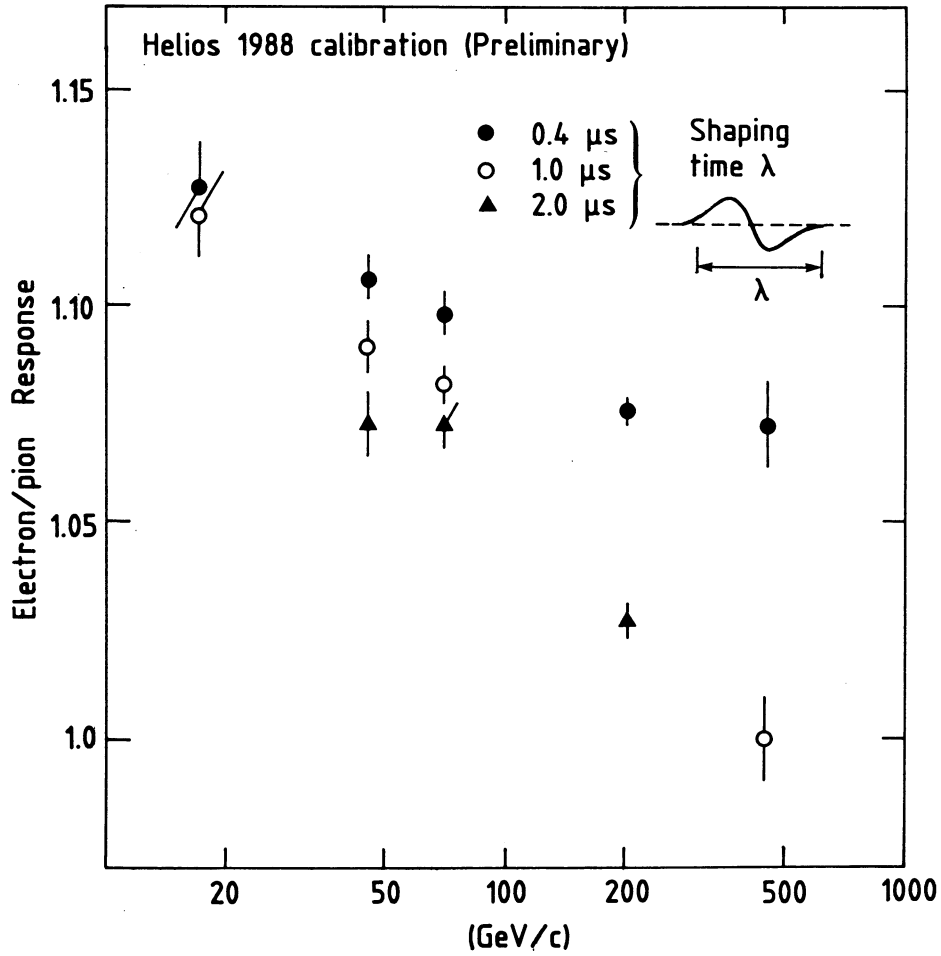

Fig. 3 Electron-to-pion response as a function of particle energy for three different values of the signal-shaping time; HELIOS test [5].

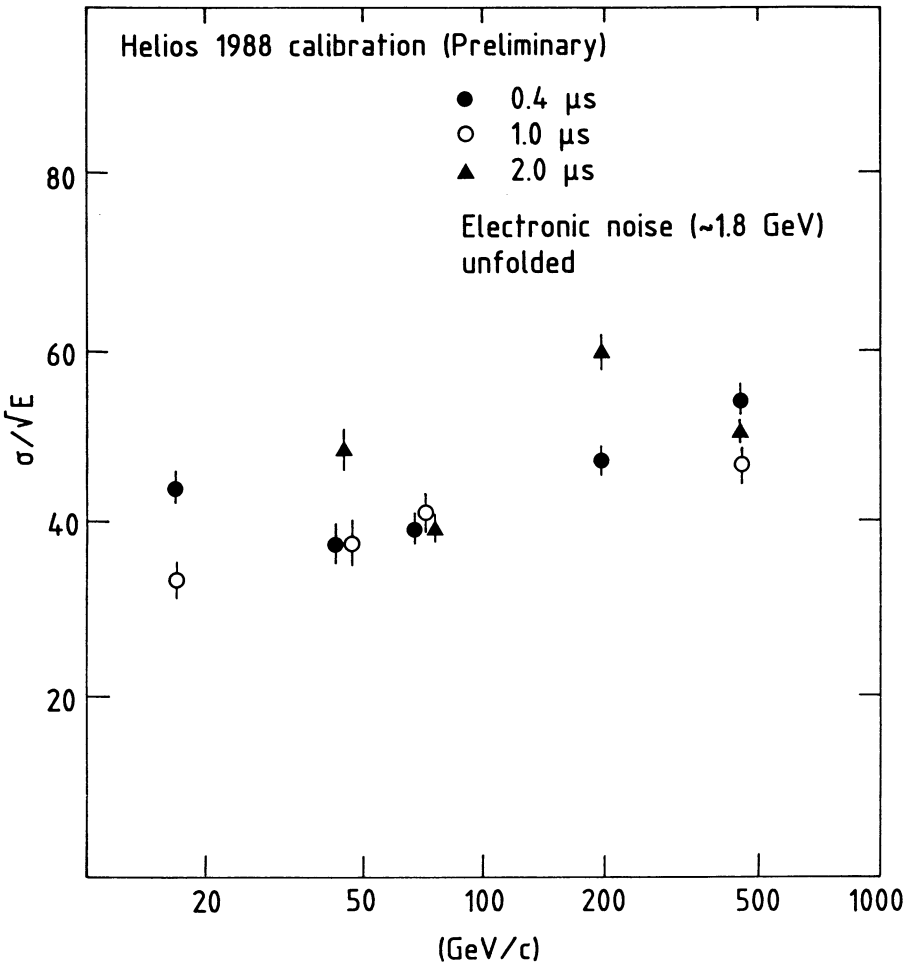

Fig. 4 Hadronic resolution versus particle energy for three different values of the signal-shaping time; HELIOS test [5].

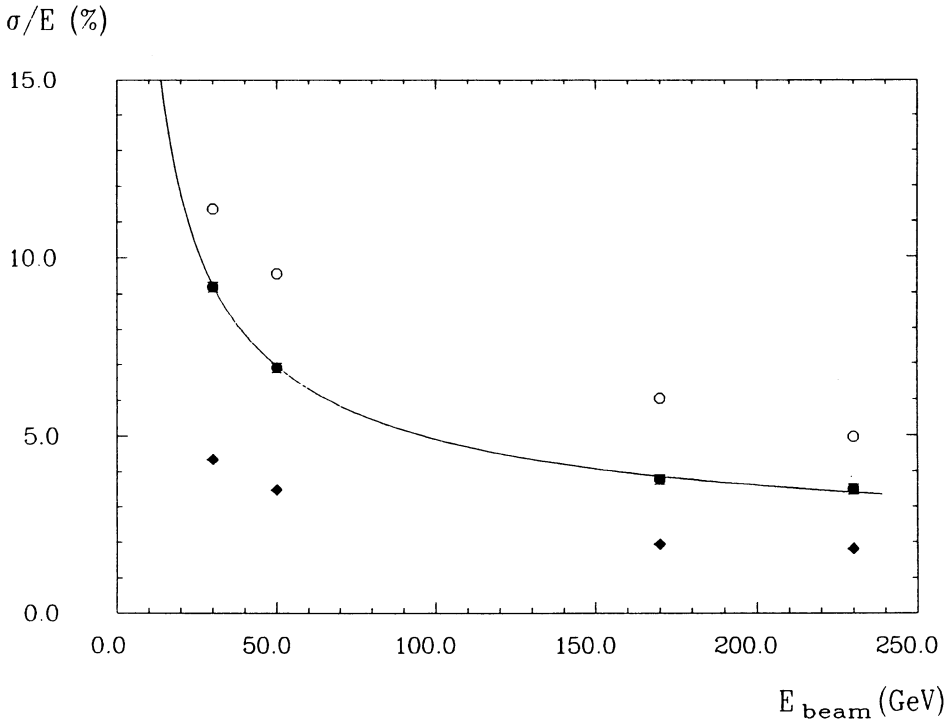

Fig. 5 Energy resolution with no π^0 weighting (open circles) and with π^0 weighting (full squares); sampling fluctuations (full rhombi); H1 test [6].

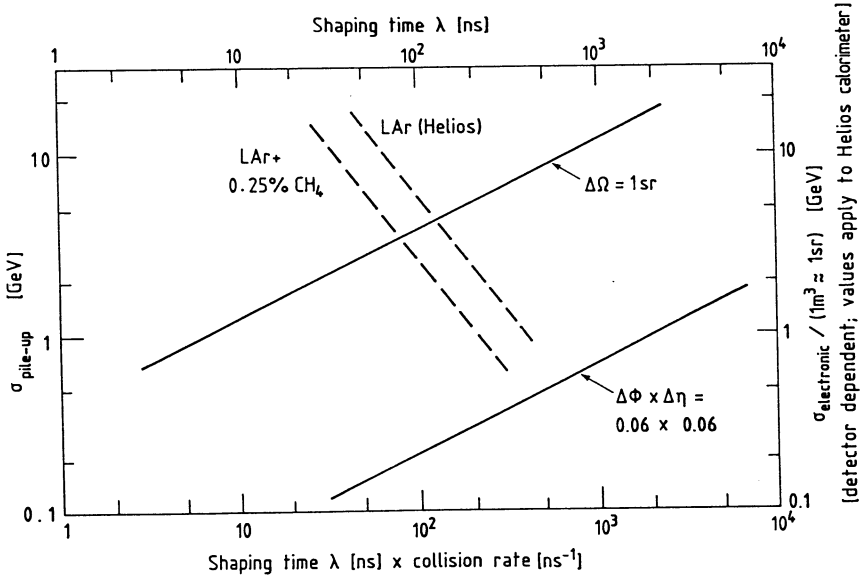

Fig. 6 Estimates (solid lines) of pile-up noise (left ordinate) as a function of the product of shaping time λ and the collision rate n (bottom abscissa), for two different sensitive detector areas. The pile-up noise is compared with the typical electronic noise (as realized in the HELIOS U/LAr calorimeter) (dashed lines) as a function of the signal-shaping time λ (right-hand ordinate and top abscissa).

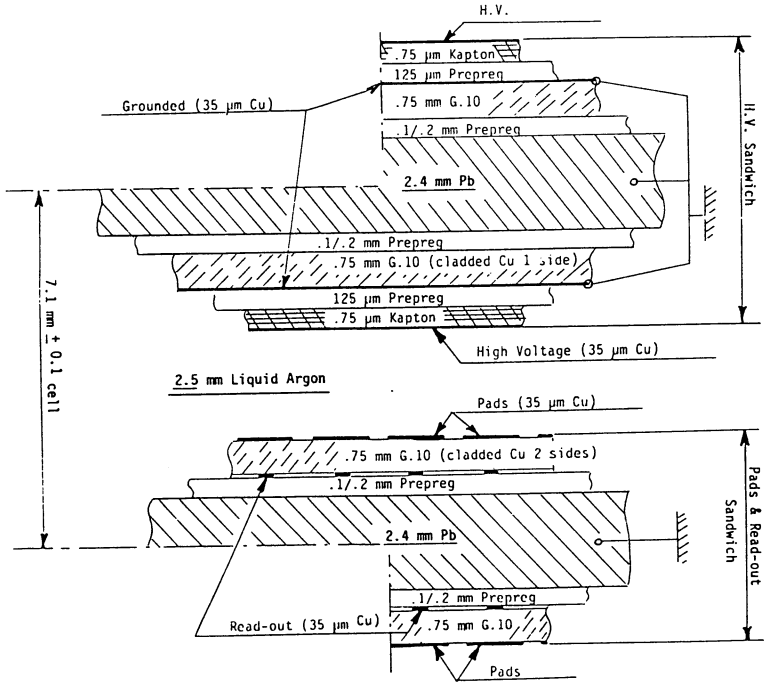

Fig. 7 Cross-section through the readout cell of the electromagnetic part of the H1 calorimeter.

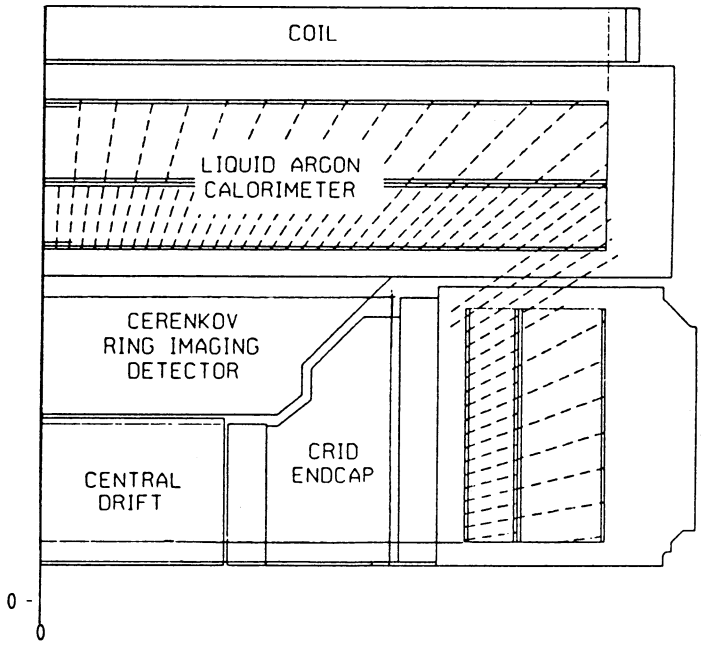

Fig. 8 Cross-section through the SLD detector, showing one possible approach towards hermeticity in LAr hadron calorimetry (Ref. [12]).

Energy Scaling of Low-Energy Neutron Yield, the e/π Ratio, and Hadronic Response in a Calorimeter

Donald E. Groom*
SSC Central Design Group,†
Lawrence Berkeley Laboratory 90-4040, Berkeley CA 94720

1. Introduction

In a high-energy hadron-induced cascade the number of secondaries increases very rapidly as the energies of the interacting particles decrease. In the first few generations π^0's are produced, "bleeding off" a substantial fraction of the energy into electromagnetic cascades. This fraction is sensitive to multiplicity fluctuations in a small number of interactions. It is thus subject to large fluctuations, as shown in Fig. 1. At the end of the cascade particles finally give up their energy to ionization, nuclear excitation, spallation, fission, etc. It is fair to say that essentially all of the signal detected by the sensitive part of a calorimeter is produced by low-energy particles. The part of the energy in a cascade carried by electrons and γ rays is converted to an electrical signal with efficiency ϵ_e, while the "low-energy hadronic activity" is detected with a different efficiency ϵ_h. This efficiency includes saturation effects, energy missed because of a finite gate time, etc. Since most of the physical mechanisms involved in hadron energy loss tend to "hide" the energy, ϵ_h is usually less than ϵ_e. If $\epsilon_e/\epsilon_h = 1$, the system is said to be compensated. If the system is not compensated the scatter shown in Fig. 1 appears as degraded resolution, and, because the fraction of the energy going into the electromagnetic channel increases with incident hadron energy E, the signal size is not proportional to energy. Equivalently, the response to hadrons and electrons of the same energy is different.

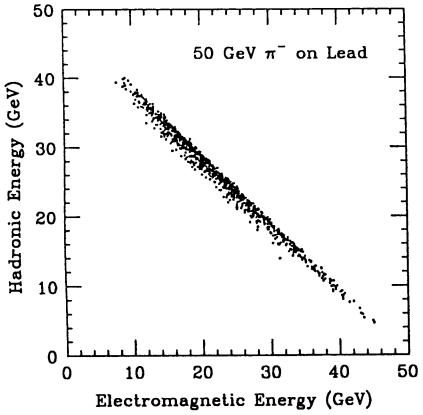

FIG. 1. The energy division of 1000 π^- cascades in lead, as simulated with FLUKA87[1]. "Calorimeter" dimensions are large enough that energy escapes only through the front surface, introducing some scatter in the total.

2. "Low-energy hadronic activity"

There are many measures of the level of low-energy hadronic activity, such as the number of nuclear interactions or the number of neutrons falling below some energy threshold in a simulation. By a simple inductive argument, one may conclude that these scale as E^m, with

$$m = 1 - \frac{\ln\left(1/(1-f_{\pi^0})\right)}{\ln n} .$$

Here n is the mean multiplicity and f_{π^0} the fraction of π^0's in a collision. Because only their logarithms are involved, the slow variation of n and f_{π^0} with energy is of little consequence. The exponent m is about 0.86, as has been corroborated with three cascade simulation codes.

3. The "e/π" ratio in calorimetry

The total response of a calorimeter to an incident hadron with energy E (in Coulombs, or Volts, or GeV) is the sum of the electromagnetic and hadronic contributions:

$$R_h = \epsilon_h E_h + \epsilon_e E_e = \epsilon_h E_h + \epsilon_e (E - E_h) ,$$

where $E = E_h + E_e$. Since $E_h \propto E^m$, it is convenient to introduce a scale factor E_0 so that we can write

$$E_h = E_0(E/E_0)^m = E(E/E_0)^{m-1} .$$

The response to an incident photon or electron is simply $R_e = \epsilon_e$. Dividing this response by R_h after making the above substitution, we obtain

$$\frac{R_e}{R_h}\left(=\frac{e}{\pi}\right) = \frac{1}{1-(1-\epsilon_h/\epsilon_e)(E/E_0)^{m-1}} = \frac{1}{1-a\,E^{m-1}}$$

for the ratio of electromagnetic to hadronic response.

This functional form has two parameters, m and $a = (1-\epsilon_h/\epsilon_e)\,E_0^{1-m}$. R_e/R_h is not sensitive to the value of m in its expected range $0.85 < m < 0.90$. E_0 should be close to 1 GeV for physical reasons, and with this additional assumption ϵ_h/ϵ_e is the same as "the intrinsic e/h" introduced by Wigmans[2]. In any case only a can be obtained from experimental data.

Wigmans[2] has introduced a similar form with logarithmic energy dependence. The two forms are indistinguishable over the range in which test beam data is available, and our values for ϵ_h/ϵ_e (with $E_0 \equiv 1$ GeV) are in agreement with his for e/h. His form does not constrain E_e/E to lie between 0 and 1, nor does it satisfy the physical requirement that R_e/R_h approach unity as the energy increases. Neither form works very well for $E < 10$ GeV, where the sparse data indicates a larger R_e/R_h than might be expected.

To the extent that the above equation is reliable, a measurement of "e/π" at only point, preferably at low energy above 10 GeV, is sufficient to determine the one sensitive parameter. It is also conjectured that the response of a uniform calorimeter to an incident jet is the same as the response to a hadron of the same energy.

4. References

1. P. A. Aarnio, A. Fassò, H-J. Möhring, J. Ranft and G. R. Stevenson, "FLUKA86 User's Guide," CERN TIS-RP/168 (1986); P. A. Aarnio, A. Fassò, J. Lindgren, J. Ranft and G. R. Stevenson, "Enhancements to the FLUKA86 Program (FLUKA87)," CERN TIS-RP/190 (1987).
2. R. Wigmans, Nucl. Instrum. Meth. **A265**, 275 (1988).

* Present Address: Particle Data Group, LBL 50-308, Berkeley CA 94720.
† Operated by the Universities Research Association for the U. S. Department of Energy.

PERFORMANCE OF A UA1 URANIUM – TMP CALORIMETER MODULE

A.GIVERNAUD
CERN, Geneva, Switzerland
(UA1 Collaboration)

Abstract

We present the results obtained from a UA1 U–TMP calorimeter module in a CERN PS test beam, between 1 and 10 Gev, and for several electric fields (from 0.8 to 16 kV/cm). The energy resolutions for electrons and pions are given. We also compare the charge produced by electrons to that produced by pions as a function of the electric field.

1. *THE UA1 UPGRADED CALORIMETER*

The upgraded UA1 calorimeter is discribed in several reports(1,2). The previous lead–scintillator calorimeters are replaced by new ones where the absorber is made of depleted uranium plates interleaved with ionization chambers filled with TMP as active medium. In our design of the calorimeter, the liquid (TMP) is contained in small but very rigid stainless steel boxes. These boxes are assembled and laser welded by industry (UTI). The TMP gap is 1.25 mm, which gives a drift time of 400 ns for an electric field of 10 kV/cm (1250V). In the central barrel ($|\eta| \leq 3.0$) the calorimeter modules are segmented in an electromagnetic part with 2 mm uranium plates and an hadronic part with 5 mm uranium plates. In the forward and very forward regions ($3.0 \leq |\eta| \leq 4.0$ and $4.0 \leq |\eta| \leq 6.0$ respectively) the modules are built with 1 cm uranium plates. The principle of ionization chambers filled with TMP has already been described (3,4); we have also reported on the results obtained with a small U–TMP prototype (5). More recently we have presented the performance of our first full scale module of the central barrel calorimeter (6,7,8). The preparation of the ionization chambers and the TMP purification have been presented at this workshop (9).

2. *THE TEST MODULE*

We are presenting here the results obtained with a module of the very forward calorimeter (10). It consists of 29 uranium plates, each 10 mm thick, interleaved with 30 stainless steel boxes containing TMP; all the 30 chambers have the same dimensions, 551×324 mm². The stack of boxes and uranium plates is pressed between two steel plates, each 22 mm thick. In the test beams, the module is followed by an iron–scintillator calorimeter, similar to the constituants of the old UA1 hadron calorimeter. The test beam set up is terminated by a 1.6 m long iron block, used as a muon filter. As each chamber has 8 electrodes, the module contains a total of 240 electrodes, and it is subdivided in towers of 30 electrodes. A tower is divided in 6 samplings of 5 electrodes each. The readout then consists of 48 channels, the electronics are the standard one designed for the U–TMP calorimeter (11,12).

3. *GENERAL PERFORMANCE*

- **noise** The noise level has been significantly reduced with respect to our previous studies (6,7,8). It ranges from 8600 electrons at 0 Volts to 9900 electrons at 9600 Volts. This increase is due to the uranium noise which grows linearly with the high voltage (from 2600 electrons at 4000 Volts to 4700 electrons at 16000 Volts (13). The chanel to chanel cross talk is about one per mil. From measurements with 7 Gev/c muons, we find a signal to noise ratio of 1.42 ±0.02 at 3200 Volts and 2.00 ±:0.03 at 13600 Volts. We have taken data with electrons (e^-) and pions (π^-) between 1 and 10 GeV/c at the CERN PS. The electric field on the module was 1700 Volts (13.6 kV/cm).

- **electrons** An electron shower is contained in the two first samplings of the module (15 X_0 each), as the pion showers are leaking both on the sides and behind the module. The electron data were taken at 1,4,5,7 and 10 Gev (5000 events each) in the middle of one of the eight towers (tower 2). The energy linearity for electrons is better than 1% above 4 Gev. The energy resolution is well fitted by :

$$\left(\frac{\sigma}{E}\right)^2 = \left(\frac{0.345}{\sqrt{E}}\right)^2 + (0.029)^2$$

where the constant term is deminated by the beam resolution. The noise was found to be negligible.

- **pions** To have the best containment for the pion shower, the beam was hiting the module near by the separation between 2 superposed towers (2 and 4). The data were taken at the same energy as for the electrons, but with higher statistics (10000 events). When summing the signals from 6 towers and without applying any leakage correction, the resolution is well described by :

$$\left(\frac{\sigma}{E}\right)^2 = \left(\frac{0.661}{\sqrt{E}}\right)^2 + \left(\frac{1.572}{E}\right)^2$$

These values of the resolution both for electrons and pions are in good agreement with the calculations using the last version (3.13) of the GEANT Monte Carlo (14):

$$\left(\frac{\sigma}{E}\right)^2 = \left(\frac{0.320}{\sqrt{E}}\right)^2$$

for electrons and

$$\left(\frac{\sigma}{E}\right)^2 = \left(\frac{0.700}{\sqrt{E}}\right)^2$$

for pions. For these calculations we are performing a full shower simulation with tracking all the generated particles in the showers down to 10 Kev.

4. *HIGH VOLTAGE SCAN*

We shot electrons and pions at the same position as discussed above for pions, with different high voltages (from 100 to 2000 Volts) applied on the module. The electron to pion charge collection ratio is shown on Fig.1. We observe that the charge collected in the module exposed to a pion beam increases faster with the electric field than for an electron beam.

On the same figure, we have plotted the results of a calculation using the same GEANT Monte Carlo as before and describing the charge collection by the KRAMERS columnar recombination theory (15--17). We note the good agreement between the data and the calculations. In the framework of this theory this effect is understood to come essentially from the contribution of the low energy, high ionizing protons from the TMP (C_9H_{20}), which are present only in hadron showers. The same calculation, combining the GEANT Monte Carlo and KRAMERS theory gives an absolute prediction of the yield of electrons produced in TMP by alpha particles from an Americium source (5.4 Mev) for electric fields ranging from 2 to 50 kV/cm, in excellent agreement with the measurements (18).

Moreover, we have also noted an improvement of the resolution for pions (σ/E decrases by about 20% from 500 to 2000V), as it does not change for electrons.

5. *CONCLUSION – FURTHER REMARKS*

The measured performance of this very forward module is in good agreement with the expectations. The decrease of the e/h ratio when increasing the high voltage on the module is an important result. This effect is somehow a natural property of warm liquids because they contain a large number of hydrogen atoms. It is also important to note the improvement of the hadron resolution at the same time. New measurements with another very forward modules, at higher energies confirm the present results (19). The fact that these results are well reproduced by a calculation though we need comparison with other data is encouraging since we would have a good tool for developing this kind of calorimeters.

I am very grateful to my collegues of the UA1 collaboration, especially to those working on the U/TMP calorimeter project.

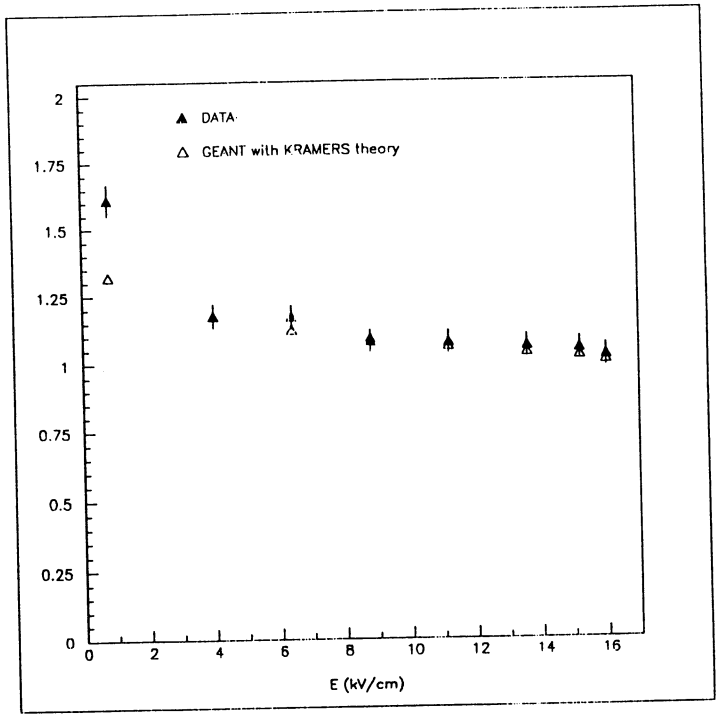

Fig.1: Q(e) / Q(π) as a function of E

References

1. UA1 COLLABORATION, *Design report of a U – TMP calorimeter for the UA1 experiment with ACOL,UA1 TN/86 – 112*

2. C. RUBBIA, *UA1 improvement program: A status report for the SPSC, unpublished (1988)*

3. A. GONIDEC et al, *Calorimetry with room temperature liquids and Uranium, UA1 UTN – 85 – 45(1985)*

4. A. GONIDEC et al, *Ionization chambers with room – temperature liquids for calorimetry CERN – EP/88 – 36(1988)*

5. M.G. ALBROW et al, *NIM A265 (1988) 303*

6. M. KRAMER *Results from a full scale UA1 Uranium – TMP calorimeter module, Talk given at the 5th Wire Chamber Conference, Vienna, 13 – 17 February 1989*

7. A. GIVERNAUD *Performance of a UA1 Uranuim – TMP calorimeter module, Talk given at the Workshop on Calorimetry for the Superconducting Super Collider, March 13 – 17, 1989, University of Alabama, Tuscaloosa, Alabama*

8. F. LACAVA *The UA1 Uranium – TMP calorimeter, project and results from first full scale prototype. Presented at the 4th Pisa Meeting on Advanced Detector, Isola d Elba, 21 – 27 May 1989*

9. F. DIEZ – HEDO *Report to this workshop*

10. F. ALVAREZ – TAVIEL et al, *Nucl. Instr. and Meth. A279 (1989) 114*

11. C. BACCI et al, *Nucl. Instr. and Meth. A273 (1988) 321*

12. C.BACCI et al, *Nucl. Instr. and Meth. A279 (1989) 169*

13. A. CANER et al, *Noise in the supergondolas and very forword modules, UA1 – TN/89 – 09*

14. *GEANT3 Users Guide, CERN DD/EE/84*

15. H.A. KRAMERS, *Physica,18 (1952) 665*

16. A.N. GERRITSEN, *Physica 14 (1948) 381*

17. A.N. GERRITSEN, *Physica 14 (1948) 407*

18. R.C. MUNOZ et al, *J.Chem.Phys. 85 (1986) 1104*

19. C. BACCI et al, *To be submitted to Nucl. Instrum. and Meth. A*

Large scale purifier of Tetramethyl-pentane for the UA1 upgraded calorimeter

F. DIEZ-HEDO
CERN,Geneva,Switzerland
UA1 Collaboration

Abstract: A detailed description of the purification procedure of tetramethyl-pentane established by the UA1 collaboration is presented.

The lifetime of the final purified liquid being typically 100 μs allows its safe use in filling the chambers of the UA1 upgraded calorimeter.

Introduction

The UA1 upgraded calorimeter consists of Uranium plates and thin Ionization chambers filled with a room temperature liquid : Tetramethyl-pentane (TMP) (ref. 1,2). In such a liquid, the electrons from ionization can drift freely in the applied electric field but electronegative impurities will trap these electrons reducing the observed signal. The purity of the liquid with respect to these impurities can be expressed in terms of the "electron lifetime", τ, which is related to the impurity concentration, n_S, and to the electron trapping rate constant, k_S :

$$1/\tau = n_S k_S$$

Fig. 1 shows the charge lost as a function of τ for an ionization chamber of the UA1 calorimeter at the designed voltage. To have a charge lost less than 1%, τ has to be better than 15 μs. Typically after purification we reach lifetimes of the order of 100 μs corresponding to purity levels of around 10 ppb.

Surface cleaning

The high level of purity required of the TMP implies that all surfaces in contact with the liquid have to be treated to avoid any contamination. Materials used are stainless steel (with low carbon content) and ceramics. The cleaning procedure is the following:

- Degreasing in hot detergent.
- Rinsing in demineralised water.
- Bake-out under vacuum ($p < 10^{-5}$ mbar at 950 °C).
- Rinsing in ultrapure water ($\rho = 18.2$ MΩ cm).

- Drying in an ultrapure hot Argon flow.
- Bake-out at 300 °C after assembling.
- Finally a leak test is done on the containers at the level of 10^{-9} mbar l/s.

This procedure has been tested in the calorimeter prototype (ref. 2) built and filled with TMP in 1986. All the lifetime measurements performed from 1986 to 1988 have been compatible with a constant value of 17 μs (ref. 3).

Quality control of the produced TMP

To be sure that a simple method can be applied to purify the large amount of TMP needed for the UA1 calorimeter (12000 l) the following specifications have been required of the TMP produced by Wiley Organics (USA):

- τ of the final product longer than 5 μs.
- Self conductivity less than $10^{-16}\ \Omega^{-1}cm^{-1}$
- Purity better than 99.99 % (in volume).
- Impurities have to be less than 10 ppb measured by gas chromatography
- Tolerable impurities are saturated hydrocarbons
- Non-tolerable impurities are all halogenated compounds and unsaturated hydrocarbons
- Final distillation under vacuum or inert gas (high purity argon) into stainless steel containers (200 l each).

To control the quality of the produced liquid an ionization chamber (lifetime counter) has been developped at CERN (ref. 4) . A side view of the counter is shown in fig. 2.

The ionization is produced by a Ruthenium source (that is a γ and β emiter) and the trigger is provided by a Silicon diode. Fig. 3 shows the Multichannel analyzer spectra obtained with a reference lifetime counter filled at CERN with liquid of $\tau = 5$ μs. Two peaks are observed. One corresponds to the charge collected in the events in which an electron emitted from the source reaches the Si diode after having ionized the TMP gaps. The other one corresponds to the events triggered by an electron coming from a photon conversion in the input window of the Si diode . If the photon is converted in the chamber the conversion electron does not have enough energy to cross the input window of the Si diode. For photon conversion in the input window of the Si diode there is no ionization in the liquid and hence this peak provides the pedestal. The relative position of the two peaks gives the charge and from comparison with the theoretical value the electron lifetime is determined.

For each 200l container a control sample is purified into a Na-K column and transferred into a lifetime counter to measure τ. Typical values larger than 20 μs have been recorded.

Purification of TMP

Once the 200l containers are received at CERN we perform a degassing of the TMP to extract all possible gasses dissolved in the liquid (e.g. Argon). The TMP container is pumped through a condenser (to recover the TMP vapours) with a chemical turbomolecular pump. After each pumping the gas pressure in the container is recorded. This operation is repeated until the pressure stays constant at a value corresponding to the TMP vapour pressure at the container temperature.

The purification is done with the TMP in gas phase (fig. 4). The starting container is maintained at 65 °C (p^{TMP}_{vapour}= 100 mbar) and the clean TMP container at -10 °C (p^{TMP}_{vapour}= 1 mbar). Due to the pressure gradient the TMP vapour is transferred from the starting container through the filter (at 60 °C to avoid condensation) into the clean TMP container where it condenses. Every 10 minutes pumpings through a cold trap are performed on the clean TMP container to pump any non condensable vapour.

The active element in the purification is the filter consisting of a mixture of silica gel and molecular sieves (4A and 13X). Previous to its installation in the purification stations the filters are activated under vacuum ($p < 10^{-5}$ mbars at 350 °C). The input to the filter is a diffuser that leads the TMP vapour to the bottom part of the filter so that the TMP vapour

diffuses through all the active material. The output has a metal sintered filter to avoid any dust coming out of the filter. Two filters are installed in each purification station but only one is used, the second one is ready for use and can be swapped with the other if needed. Typical speed of purification is 1l/h.

Four such stations are now operational at CERN alowing purification of 800 l of liquid each week.

Measurement of the purity of the liquid

After purification a sample of the liquid is transferred into a multiplate ionization chamber (ref. 5). Cosmic rays traversing the chamber are selected and the induced signal recorded by two identical LeCroy 2256 Wave Form Analyzers (WFA).

Knowing the response of the electronics (measured with a Test Pulse) the pulse shape can be calculated theoretically. This is a function of τ. To enhance the signal to noise ratio data are averaged over several events. The lifetime τ is obtained by fitting the theoretical pulse shape to the data.

We use two WFA's; the first one to have detailed information on the rise part of the signal (where the information on τ is contained) and the second one to check the full development of the signal up to 5 ms.

Typically we obtain lifetimes from 100 μs to 500 μs. Fig. 5 shows an example of a fit. The first window shows the fit done with the data recorded by the first WFA up to 500 μs and second window shows the data recorded by the second WFA up to 5 ms. Superimposed is the theoretical pulse shape corresponding to the value of τ fitted in the first window.

Conclusion

The UA1 Collaboration has established a set of procedures allowing the purification of large quantities of Tetramethyl-pentane in which the electron lifetime is typically 100 μs. These procedures have also been succesfully applied to other non polar liquids (TMS, liquid Argon).

Aknowledgments

I am gratefull to all my colleagues at UA1 and especially to D. Schinzel and A. Gonidec who have shown me all I know about liquid purification.

References

1.- Design report for a U-TMP calorimeter for the UA1 experiment with ACOL.
UA1collaboration UA1 TN/86-112
2.- Performance of a Uranium-TMP electromagnetic calorimeter.
M. G. Albrow at al. NIM A265 (1988)303-318.
3.- Long term stability of U-TMP calorimeters.
UA1 collaboration Addendum CERN-EP/87-55
4.- Purity in room temperature liquid ionization chambers
S. Ochsenbein,D. Schinzel,A. Gonidec,W.F. Schmidt
NIM A273 (1988) 654-656
5.- Ionization chambers with room-temperature liquids for calorimetry.
A. Gonidec, C. Rubbia, D. Schinzel,W.F. Schmidt
CERN-EP/88-36

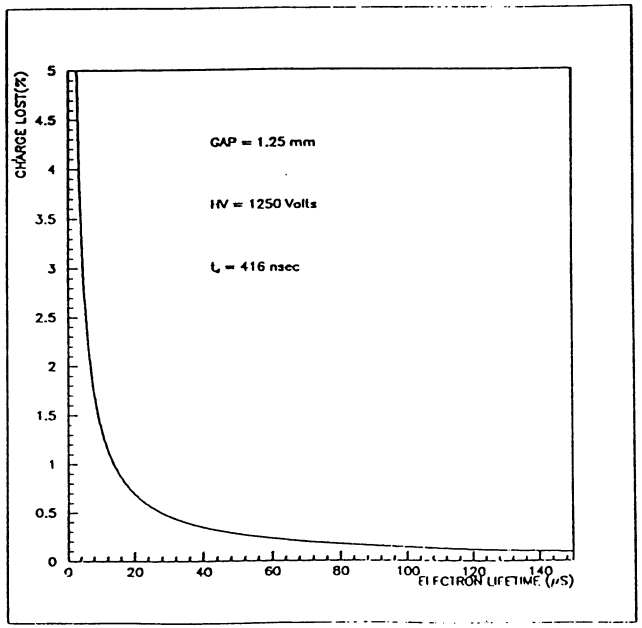

Fig 1

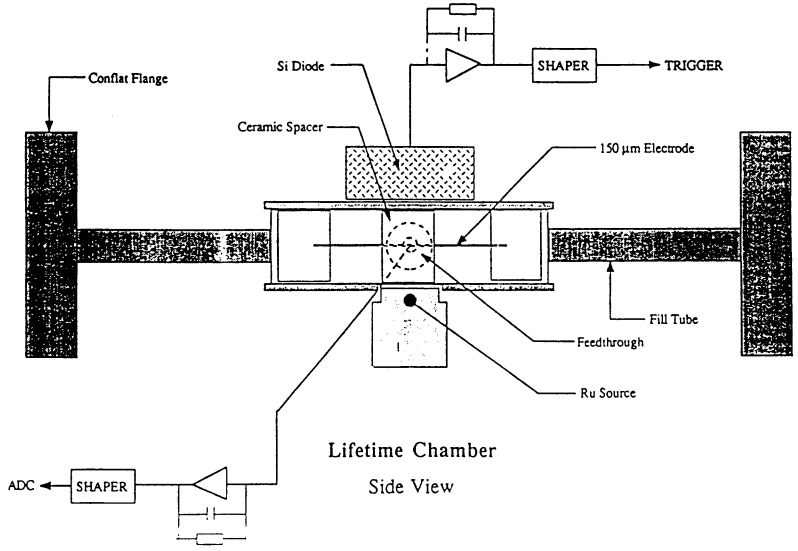

Fig 2

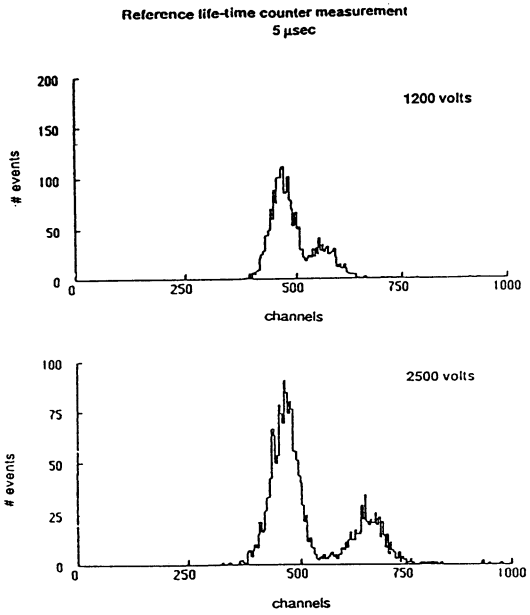

Fig 3

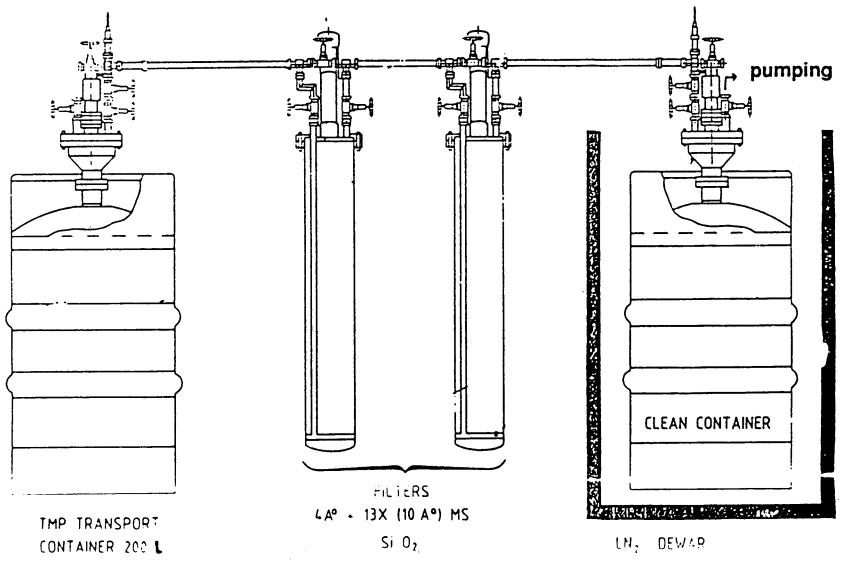

Fig 4

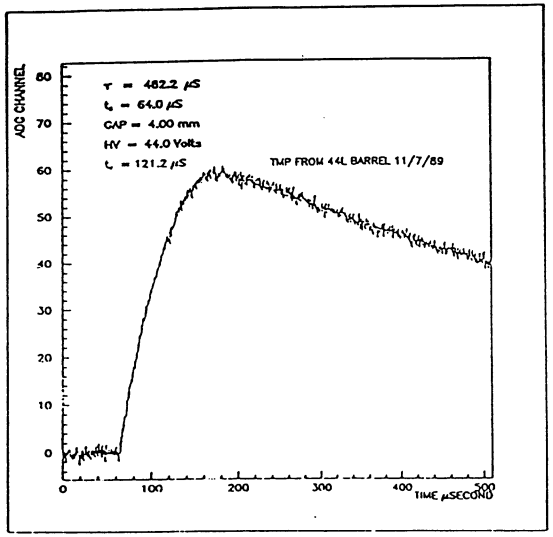

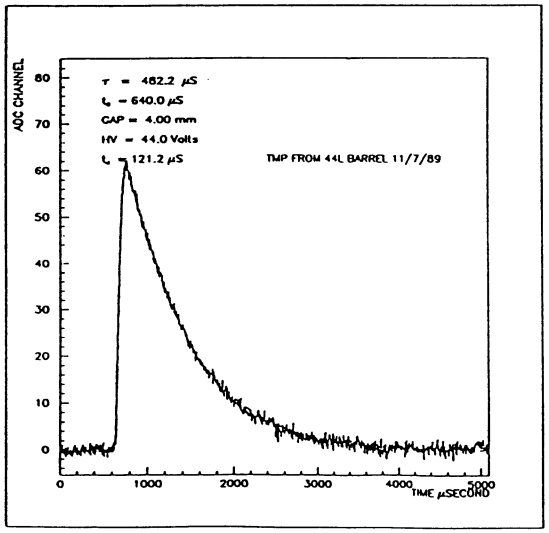

Fig 5

Speed of Response, Pile-up and Signal to Noise Ratio in Liquid Ionization Calorimeters

WALIC collaboration
presented by

J. Colas

L.A.P.P., Annecy-le-Vieux, 74019 France

Summary: Although liquid ionization calorimeters have been mostly used up to now with slow readout, their signals have a fast rise time. However, it is not easy to get this fast component of the pulse out of the calorimeter. For this purpose a new connection scheme of the electrodes, the "electrostatic transformer", is presented and discussed. This technique reduces the detector capacitance while keeping the number of channels at an acceptable level. Also it allows the use of transmission lines to bring signals from the electrodes to the preamplifiers which could be located in an accessible area. With room temperature liquids the length of these cables can be short, keeping the added noise at a reasonable level. Contributions to the error on the energy measurement from pile up and electronics noise are studied in detail. Even on this issue, room temperature liquids (TMP/TMS) are found to be competitive with cold liquid argon at the expense of a moderately higher gap voltage.

1. Introduction

The new generation of high energy hadron colliders (LHC/SSC) presents an experimental challenge for detectors. The short time interval between bunch crossings (≈15 ns) stresses the need for fast devices. Calorimeters will play an important role in these detectors as their resolution improves with increasing energy.

Among the various calorimetry techniques, liquid ionization detectors are strong candidates for their known stability in time and their ease of segmentation. However questions arise : are they fast enough to keep pile up under control ? How large is the electronics noise at the very short shaping times which are required at LHC/SSC ? In a previous paper [1] Radeka and Rescia studied these problems and, based on their experience with the fast liquid argon calorimeter built by the Helios collaboration [2], showed that although non trivial, the use of liquid argon calorimeters at LHC/SSC is feasible if certain constraints are obeyed. A slightly different analysis has also been made by Franzini[3].

This paper revisits these questions with emphasis on the use of room temperature liquids (TMP/TMS). It presents a new technical solution to speed up calorimeter readout and through explicit computation compares performances expected for TMP/TMS and liquid argon.

This work is part of a more general effort by the WALIC collaboration [4] to study room temperature liquids (TMP/TMS) as possible alternative to cold liquid argon as sensitive medium in sampling calorimeters. Room temperature liquids require neither cryogenic equipment nor thermal insulation, resulting in a simpler and more hermetic detector. A detailed study is presently being made to quantify this point. Furthermore, since room temperature liquids are hydrogenuous materials, they may provide a compensated output, that is, a nearly equal response to electromagnetic and hadronic showers, leading to better resolution and linearity over a large energy range, without having to resort to expensive and exotic materials. Measurements on the saturation properties of TMP/TMS which are important for this compensation mechanism to occur have been done by the WALIC collaboration and reported at this conference [5]. A modular hadronic calorimeter, specially designed to study compensation is presently being built and direct measurements will be made in a test beam at Fermi Lab in 1990. These attractive features have to be balanced by the purity requirement of the liquids. If the UA1 collaboration has solved the problem of producing large quantity of very clean liquid where electrons can drift for more than 100 μs [6], too little is known up to now about materials which can be used in direct contact with the liquid. R&D is also going on in that direction.

2. Basic features of the signal formation in ionization chambers

The drift of the ionization electrons in the inter electrode gap of a sampling calorimeter under the influence of an external electric field induces a current signal. Usually, the drift velocity of the ions is so small that as, we will see below, their current pulse can be ignored. Assuming a uniform ionization through the gap, the moving electron charges produce the triangular shaped current pulse shown in figure 1. Its main characteristics are:

i) A fast rise time. Usually the gap size is small and propagation effects can be ignored.

ii) The peak current I_{max} is a function of the density of ionization and of the drift velocity v_d only :

$$I_{max} = G_{fi} \times \frac{dE}{dx} \times v_d$$

where G_{fi} the free ion yield measures the number of electron ion pairs produced per unit of energy loss and dE/dx is the energy loss per unit length in the liquid. Typical values of G_{fi}, dE/dx,v_d and I_{max} are [1,7,8]:

Liquid	dE/dx MeV/cm	G_{fi} 1/100 eV	v_d mm/μs	I_{max} ke/μs
liquid argon@10kV/cm	2.11	3.8	5.0	40.5
TMP@40kV/cm	1.58	2.0	11.6	36.9
TMS@20kV/cm	1.36	1.6	19.6	46.3

iii) The drift-time t_d which is the time an electron takes to cross the whole gap (g). At this point in time the current returns to 0.

$$t_d = \frac{g}{v_d}$$

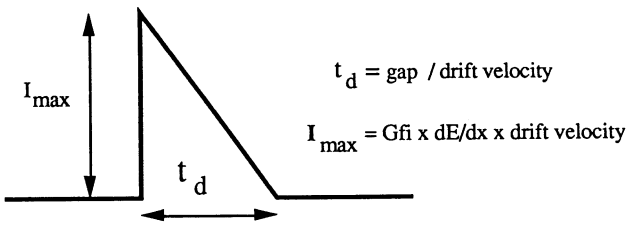

Figure 1 . Induced current waveform in ionization chambers for a uniform energy deposition in the interelectrode gap. t_d is the electron drift time across the gap. G_{fi} is the free electron yield per unit of energy lost in liquid and dE/dx is the energy loss by ionization per unit length.

In most of the existing liquid ionization calorimeter, the drift time is much smaller than the measurement time and the quantity of interest is the total charge collected onto the electrodes :

$$Q = \frac{1}{2} \times I_{max} \times t_d = \frac{1}{2} \times G_{fi} \times \frac{dE}{dx} \times g$$

This will not be the case in an LHC/SSC calorimeter, and the two quantities I_{max} and t_d have to be considered separately. They both depend on the drift velocity. The larger the drift velocity, the larger the peak current and the smaller the drift time. This is why ions with their very low velocities are not detected. Figure 2 shows drift velocities for several liquids as a function of the electric field [1,7] . In liquid argon the drift velocity saturates above ≈ 5 KV/cm. Saturation is less when it is doped with CH4, and even less for room temperature liquids where the drift velocity compares favorably with that of liquid argon at high electric field. For TMP these data are consistent with what has been measured by UA1 [8] and by WALIC up to 25 kV/cm . For TMS, a new measurement [9] indicates an even higher drift velocity above 20 kV/cm.

Three questions then come to mind if we want to build a fast liquid ionization calorimeter :

i) Can we take advantage of the fast rise time of the current waveform to get a fast pulse out of the calorimeter?
ii) Drift time will probably be longer than the 15 ns between bunch crossings. How does that affect the pile-up from one collision to the next one?
iii) What kind of signal to noise ratio can we expect at the small shaping time we want to use at LHC/SSC?

Each of these points will be developed in the following sections.

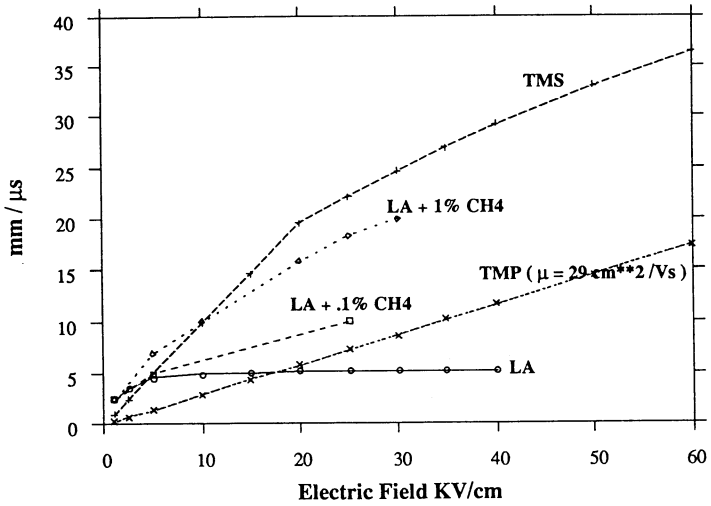

Figure 2. Drift velocities for various liquids as function of the drifting electric field. In room temperature liquids drift velocities saturate at much higher electric field than in liquid argon.

3. Fast Calorimeter Read-out

As discussed in reference 1, the electric characteristics of the circuit formed by the ionization chamber and its preamplifier can be summarized in the schematic of figure 3. The ionization current is forced by the driving electric field to charge the capacitance made up of the detector plates and the electrical connections. This capacitance discharges itself through the self inductance of the connections to the input resistance of the preamplifier which provides the necessary damping.

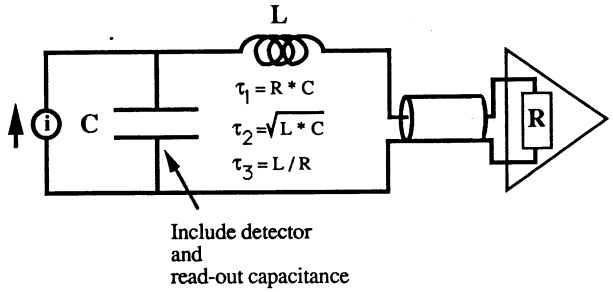

Figure 3. Equivalent circuit of a liquid ionization cell connected to its preamplifier. To damp oscillations, the input impedance of the preamplifier is made resistive and the time constant τ_1 has to dominate over the others. A transmission line connecting the detector cell to the preamplifier does not change the picture if its impedance is matched to the preamplifier input resistance.

Of the three time constants of the circuit :

$$\tau_1 = RC,\ \tau_2 = \sqrt{LC},\ \tau_3 = L/R$$

the first one has to be dominant if one wants to minimize ringing. The critical damping condition is met for $\tau_1 = 2\,\tau_2 = 4\,\tau_3$. The rise time of the pulse [10% - 90%] at the preamplifier level, which can be looked at as the charge transfer time, is then ≈ 2 RC. A transmission line between the detector and the preamplifier if properly terminated by its characteristic impedance, does not change the picture and just acts as delay line. In most of the present liquid ionization calorimeters C is of order 5 nF and R of order 50 Ω which implies a $\approx$ 500 ns charge transfer time. This has to be contrasted with the 15 ns spacing between bunch crossings expected at LHC/SSC.

There are two known ways out to improve the charge transfer time :

i- Reduce the damping resistor. This is for instance the case in the Helios calorimeter at CERN [2], where a ferrite transformer is used to lower the input resistance of the preamplifier to $\approx 3\ \Omega$, leading to a rise time of less than 50 ns [1]. In this case the use of low impedance transmission lines is not practical; they become too bulky and in addition they add too much noise due to their large capacitance. The preamplifiers have to be on the electrodes, as in Helios. The next limitation comes from the self-inductance of the connections. The damping resistor is so small that the time constant L/R is not negligible and oscillations may occur.

ii- Reduce the tower capacitance. If we can keep the tower capacitance below say 300 pF, then a damping resistor of $\approx$75 Ω which gives a charge transfer time of $\approx$ 45 ns is perfectly acceptable from the point of view of speed but also leads to a reasonable impedance for a transmission line. In addition, with a lower tower capacitance, the self inductance of all the connections are less critical than in the previous solution. The standard way to achieve such a reduction in capacitance is by decreasing the pad surface or the number of gaps connected in parallel. This is what will occur in the electromagnetic section of a highly segmented calorimeter. If we consider a segmentation $\Delta\eta \times \Delta\phi = .03 \times .03$ [10], a typical electromagnetic sampling with all gaps connected in parallel will have a capacitance of order 330 pF. There is a large number of towers $\approx$ 40,000 over the interval of rapidity $|\eta|<3$ and an even greater number of preamplifiers $\approx$ 120,000, one per sampling in depth. However such a method applied to the hadronic part of the calorimeter leads to an unreasonable number of channels. Assuming a spatial resolution $\Delta\eta \times \Delta\phi = .05 \times .05$ i.e. 15,000 towers over the whole rapidity region $|\eta|<3$, we would need $\approx$ 75 samplings in depth, i.e. $\approx$ 1,100,000 preamplifiers, to keep the sampling capacitance within the 300 pF limit !

A possible alternative to reduce the capacitance of large hadronic towers is to gang the drifting gaps in series rather than in parallel. This is what we call the electrostatic transformer approach (EST) as it behaves from the preamplifier point of view very much the same as a ferrite-core transformer. The idea is sketched in figure 4, where series connection is compared to parallel ganging, and more fully developed in reference 11. The drawbacks of this solution -- possibly higher high voltage, non uniformity in the gap collection efficiency and increased cross-talk from adjacent calorimeter towers -- are discussed in the next section. In the previous example, using a transformer ratio of 3 would reduce the number of necessary preamplifiers by nearly an order of magnitude.

In conclusion, even if the current coming out of the drifting gaps has a fast rise time, it is non trivial to extract this fast component from the calorimeter due to the capacitive nature of ionization detectors. There is one known way, which has been demonstrated successfully by the Helios collaboration, using ferrite-core transformers

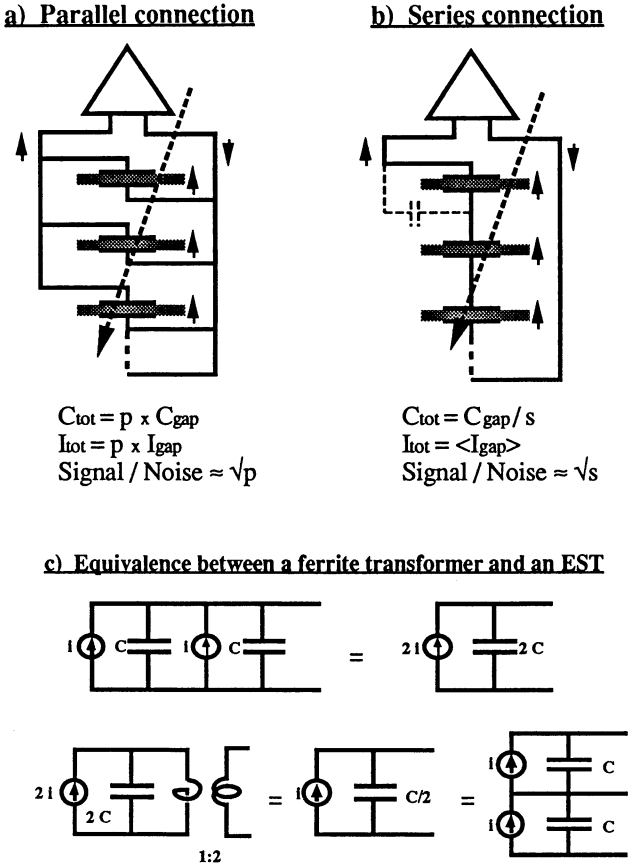

Figure 4. Comparison of the parallel and series connection (EST) of several gaps. In the parallel case, the equivalent current source is the sum of the current in each gap (p in total). The total capacitance seen by the preamplifier is the sum of the capacitance of each gap. A ferrite transformer of turn ratio p transforms this into a current <I> and a capacitance C/p. In the series connection, the equivalent current source is the average current of the gap currents <I>. The capacitance seen by the preamplifier is the gap capacitance divided by the number of gaps in series (s in total) C/s. This much smaller capacitance allows a faster readout. In a mixed scheme, some of the gaps would be connected in parallel and some in series. Note, that in both cases, energy conservation implies that the same signal to noise ratio is achievable.

and preamplifiers close to the electrodes. Another alternative using the EST approach of connecting several gaps in series allows the use of transmissions lines to transport signals from the electrodes to preamplifiers located outside of the calorimeter in an accessible area. To keep the added noise to a reasonable level, these cables should be short (≤ 5 m) which seems feasible in a room temperature liquid calorimeter.

4. The ElectroStatic Transformer.

Two designs of a calorimeter tower are shown schematically in figure 4. In both, absorbing electrodes are separated by liquid sensitive gaps. Ionization electrons produced by shower particules are collected with the help of a large voltage gradient. In other respects the designs are very different. Figure 4a shows the traditional ganging; all the signal gaps are connected in parallel and the individual gap currents are summed. Figure 4b shows an alternative in which the gaps are connected in series. The gap currents are not directly summed but the average signal is delivered on a much higher impedance. And because as seen from the preamplifier this performs the same signal and impedance transformation as the ferrite-core transformer (figure 4c), we have called it the ElectroStatic Transformer (EST). A mixed scheme in which subsets of gaps within a tower are connected in series will probably turn out to be more practical; in all cases, a large reduction in the tower capacitance is obtained. As an example, a typical hadronic tower with 40 gaps of 250 pF each has a total capacitance of 10 nF if all gaps are connected in parallel, but only 0.4 nF if the stack is structured in 8 parallel sets of 5 gaps in series each. In such a scheme, the number of gaps in series plays the same role as the turn ratio in a ferrite-core transformer and has been given the same name: transformer ratio.

4.1 High voltage connection

Figure 4 implies that the d.c. voltages in adjacent gaps of the EST are connected in series. This is conceptually straightforward, but would require an uncomfortably high voltage. In alternative designs, the gaps are decoupled individually so that the maximum voltage is no greater than that across each gap. The example shown conceptually in figure 5 uses metallic tile absorbers imbedded in thin insulating layers. Facing the absorber tiles are metallized pads on the surface of the insulator, resistively connected horizontally to neighbors and eventually to the high voltage source. High voltage decoupling occurs via the capacitances between pads on opposite sides and absorber. Such a structure has the nice features that high voltage is fed in parallel, signal is readout in series and high voltage decoupling is internal to the stack.

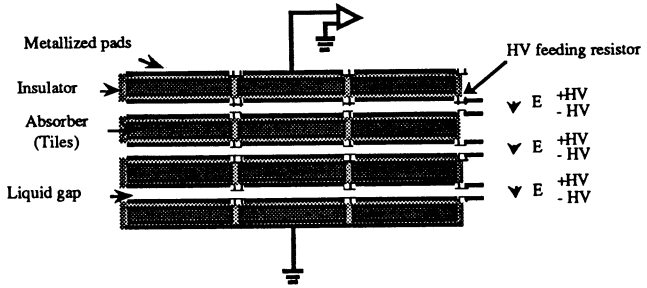

Figure 5. EST design which avoids cumulative high voltage. High voltage is fed in parallel, signal is readout in series. Low inductance high voltage decoupling is internal to each electrode.

4.2 Tower crosstalk.

Figure 6 shows schematically the sources of crosstalk from a central tower to eight surrounding towers. A fraction of the charge produced in each gap is capacitively coupled to neighboring towers. For a large area hadronic tower, this is a small part of the total, i.e. $c/C << 1$; but because the transformer action reduces the total capacitance, the importance of crosstalk increases with the transformer ratio.

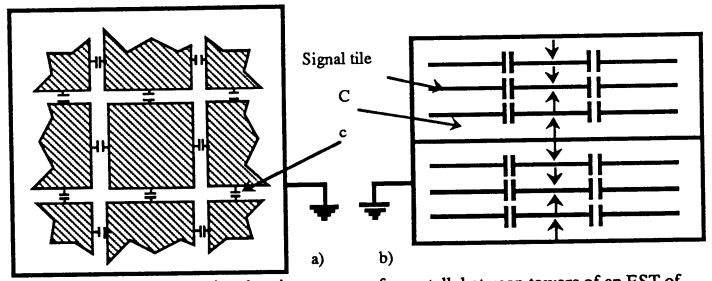

Figure 6. Plan and elevation schematics showing sources of crosstalk between towers of an EST of transformer ratio 2. C is the capacitance of each gap within a tower; c is the coupling capacitance of each tile to a nearest neighbor. Each calorimeter module of many towers is in a grounded container. Within each tower the signal tiles and ground plates are summed along a low impedance transmission line (not shown).

4.2.1 Test set-up

To carefully tevaluate he detailed electrical properties of a calorimeter based on EST, we have constructed the aluminium model of figure 7 and simulate its response assuming that it could be described by the schematic shown in the same figure.

The central reference tower is surrounded by eight neighbors, of which four are nearest neighbors. The entire section of calorimeter is inside a grounded box. Tiles are made of aluminium, 6" x 6" in area and 3/8" thick; sensitive gaps are replaced by air gaps; gap size is fixed at 2mm; these numbers have been chosen to simulate what could be the size of a tower in a realistic hadronic calorimeter. With access from the top, the number of tiles between each signal tiles and the two ground planes is changed in order to vary the transformer ratio n; the number of gaps in the structure is 2 x n; the two sets of n gaps being in parallel. For a transformer ratio of 5 (10 gaps), the structure corresponds to approximately 1/4 the thickness of a high Z tower which is two absorption lengths thick. The crosstalk capacitance c is varied by changing the spacing between towers from 1/16" to 1/2".

The central tile of each tower, which collects the signal from both subsections, is connected to an integrating preamplifier ($\approx 50\ \Omega$ input impedance) by a rod in a hole through the upper subsection. To simulate the entire calorimeter stack (40 gaps) an external discrete capacitance is connected in parallel with the preamplifier input. Current from drifting electrons in any gap of the reference tower are simulated using a high impedance probe inserted through a hole in the lower subsection. The current waveform corresponds to that of the ionization current shown in figure 1 with a drift time of 100 ns. Actually, the probe current flows between a given tile and ground; the effect of a current source in a single gap is obtained by taking differences.

EST Aluminium model

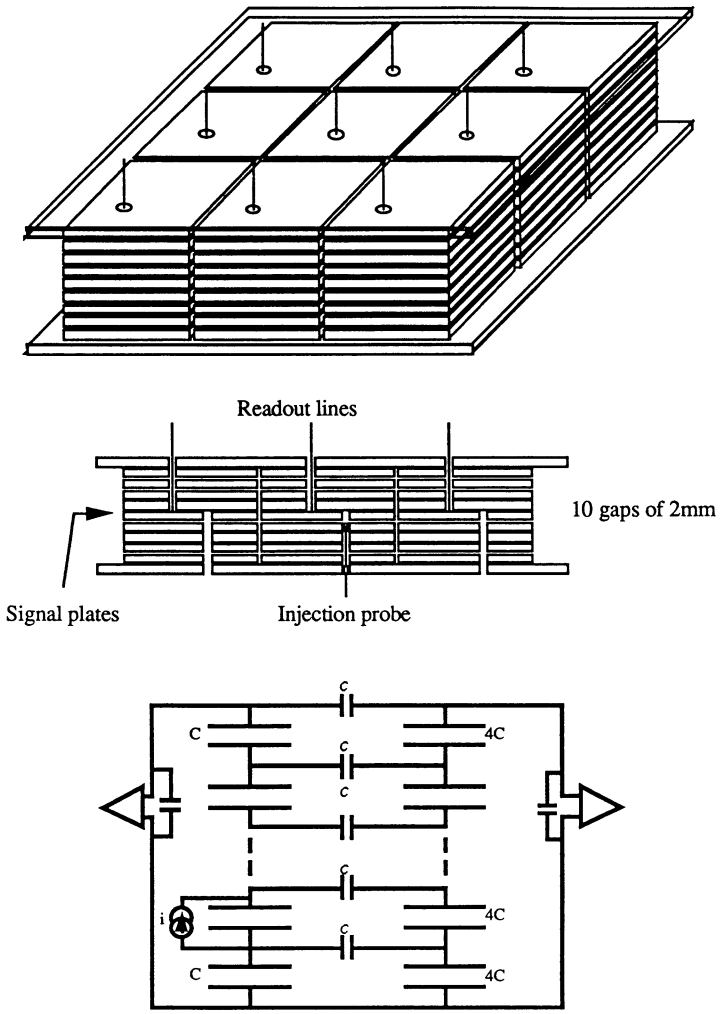

Figure 7. Aluminium model to study the EST pulse properties. The set-up consists of nine towers. Each tower is made up of two parallel sets of gaps; each set with 1 to 5 gaps. Aluminium tiles are 6"x6" in area and 3/8" thick; sensitive gaps are filled with air; gap size is fixed at 2mm; tower spacing can be varied from 1/16" to 1/2" to study the influence of the coupling capacitance. The electrical schematic shown is used to simulate the pulse response of the model. The gap capacitance C is 100 pF; the coupling capacitance c is 15 pF.

4.2.2 Measurement results

All measurements on the aluminium model are well reproduced by the simulation of the electrical circuit in figure 7. This simple circuit diagram enables us to understand what's going on and to extrapolate to other configurations. The main results can be summarized as :

i- The tower capacitance decreases as the transformer ratio increases; this translates into a much faster rise-time at the preamp-output, from ≈ 1μs when all gaps are in parallel to less than 50 ns for a transformer ratio of 5 (see figure 8b where pulse rise time is actually dominated by the input signal 100 ns drift time).

ii- Whatever the injection gap and the tower spacing, summing the 9 towers we get the total charge injected. Crosstalk means loss of localization not of energy.

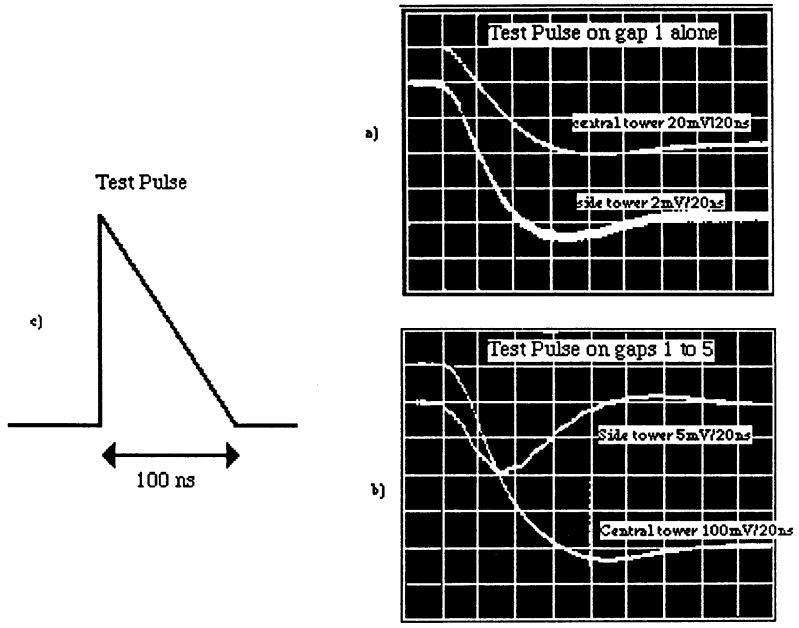

Figure 8. Preamp output pulses of central and side towers when the test pulse shown in c) is fed into the structure. Transformer ratio is 5, and tower are spaced by 1/8". In a) gap 1 only is pulsed; in b) all gaps 1 to 5 are pulsed together.

iii- Crosstalk in the adjacent towers behaves in two qualitatively very different ways whether a signal is sent in only one gap or whether the same signal is applied to all the gaps. Figure 8a shows the preamplifier outputs of the reference tower and of a side tower when only one gap (that which is closer to the ground plate) is pulsed. Tower spacing is 1/8" and transformer ratio is 5. The crosstalk signal tends to a non zero value at large time. On the contrary, crosstalk tends to zero when all gaps are pulsed identically (figure 8b). This feature is well reproduced by the simulation and can be understood considering that in the case of equal currents in all gaps, no charge can accumulate at the intermediate tiles and that the only source of crosstalk is the non zero input impedance of the preamplifiers which produces a short pulse at small time.

Analytic analysis of the electric circuit of figure 7 shows that crosstalk depends on the ratio c/C of the coupling capacitance to the gap capacitance. Results obtained with this air gap model are then valid for a liquid calorimeter. This tells also that the larger the tile area (~ C) compared to its perimeter (~ c), the better. The domain of validity of this scheme is well matched to large hadronic towers.

To be quantitative, let's define crosstalk as :

$$\chi = \text{signal in one side tower / sum over the 9 towers}$$

where signal is measured at 200ns. Crosstalk measurements for two tower spacings are compared with the simulation results in the table below :

Injection in gaps #	χ (1/4" spacing) measured	χ (1/8" spacing) measured	χ (c/C = .15) computed
1	.065	.10	.095
1-2	.055	.09	.085
1-2-3	.045	.075	.067
1-2-3-4	.027	.047	.040
1-2-3-4-5	0.	0.	0.

Note that the coupling strength c/C = .15, which enables us to reproduce the 1/8" spacing measurements, corresponds precisely to the estimated side capacitance between adjacent towers (16 pF / 100 pF) for that spacing.

In addition, as expected, crosstalk values decrease when transformer ratio is decreased. The table below shows, for various transformer ratios and two tower spacings, the measured crosstalk when the gap closer to the ground plate is pulsed. Again, although not shown,measurements results agree well with simulation.

transformer ratio	χ (1/4" spacing)	χ (1/8" spacing)
5	.065	.100
4	.045	.070
3	.027	.045
2	.013	.017

The same data enables us to study variation in the collection efficiency of the gaps ganged in series. Let's define ε_i the collection efficiency of gap i as :

$$\varepsilon_i = \frac{S_i}{\frac{1}{n}\sum_1 S_j}$$

where Si is the signal when gap i is pulsed alone, n is the transformer ratio and gap 1 is that closer to the ground plane. Measurements for a 1/4" spacing yield :

gap #	n = 5	n = 4	n = 3	n = 2
1	.73	.78	.87	.93
2	.76	.86	.95	1.07
3	.88	1.02	1.18	-
4	1.12	1.34	-	-
5	1.52	-	-	-

To interpret these numbers, let's consider a case where the gap currents are equal and compute the sensitivity of the output signal S to a variation of current i in gap k. It is easy to find out that we have :

$$\frac{\Delta S}{S} = \frac{\Delta i}{i} \times \frac{\varepsilon_k - 1}{n-1}$$

For instance, a 10% variation of the current in gap 1 relative to the average current in 5 gaps connected in series, change the output signal by only .7%. Through fluctuations in the longitudinal shower development, this effect will slightly degrade the energy resolution of the calorimeter. In a model where in all gaps, the current is the same in average, but fluctuates independently in each gap, the error introduced by the non uniformity in the gap collection efficiency is zero on average but gives rise to an additional fluctuation :

$$\frac{\sigma(S)}{S} = \frac{\sigma(i)}{i} \times \frac{\sqrt{\sum_{l=1}^{n} (\varepsilon_l - 1)^2}}{n}$$

The error on the output signal fluctuates as the current in each gap but the fluctuation is reduced by an amount which varies from ≈ 20 for a small transformer ratio of 2 to ≈ 7.5 for a transformer ratio of 5. Hence, this contribution to the energy resolution is probably negligible. Nevertheless, a detailed shower simulation must be made to have quantitative numbers.

This first study of the EST gives promising results. It indicates that crosstalk will be small even for relatively large transformer ratios, provided that the series connection is over a length small compared to a shower length, the ionization signal will then be nearly equal in all gaps. The effect of the variation in gap collection efficiency on the energy resolution has to be better quantified but is probably acceptable at least for hadronic calorimeters where the EST approach is the most useful.

5. Signal processing and pile-up.

When after ≈ 15 ns, the next collision comes in, electrons drifting in the ionization gap are not all collected. These remaining electrons induce some pile-up from one event to the next. This can be zeroed on average if the time averaged value of the output signal is zero using AC coupling for instance. However, there is still a random fluctuation in the base line which will affect the energy measurement.

To be quantitative, let us consider a preamplifier with an exponential rise time with a time constant $T_m/2$. This preamplifier is AC coupled to remove any DC shift in the base line but this is achieved with a much longer time constant of several microseconds. The preamplifier output P(t) is processed through one or the other of the two following filters :

$$F_1(t) = P(t) - P(t-T_m)$$
$$F_2(t) = P(t) - 2P(t-T_m) + P(t-2T_m)$$

Time 0 is the crossing time. T_m the measurement time is the time where the signal is measured. Figure 9 sketches the different waveforms. As explained in reference 1, the idea behind filter 2 is that if T_m is much smaller than the drift time, this processing will cancel the tail of the pulse.

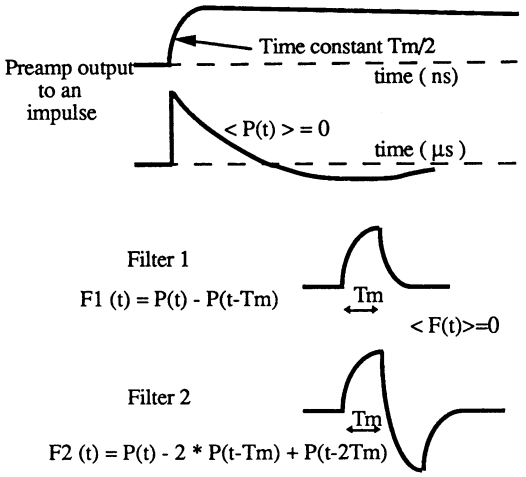

Figure 9. Preamplifier and filter waveforms used to estimate pile-up and signal to noise performances.

The response at time T_m of the filter F to a triangular shaped current wave form originating at time t_i is:

$$S(t_i) = \int_{t_i}^{\min(t_i+t_d,T_m)} (1-\frac{t}{t_d}) \times F(T_m-t) \times dt$$

The probability for a cell to be hit is : $p=\frac{L\times\sigma\times N_p}{N_{cell}}$

L, the luminosity, is assumed to be $10^{33}cm^{-2}s^{-1}$, σ the cross-section is 100 mbarn. Each of the particles (N_p =100 in average) has a mean energy $<E_t>$ of 0.5 GeV. The calorimeter is assumed to have 25 000 cells (Ncell) which correspond to a segmentation $\Delta\eta \times \Delta\phi = .05 \times .05$ over the whole rapidity region $|\eta|<4$.

The average value of pile-up: $p \times <E_t> \times \sum_{t_i<T_m} S(t_i)$ is zero as advertised above because $<P(t)>$ is zero.

In the limit where the probability p for a cell to be hit is small, the random fluctuation in the base-line of this cell has an R.M.S. :

$$<E_t> \times \sqrt{p \times \delta \times \sum_{t_i<T_m} S(t_i)^2}$$

where δ is the time between bunches : 15 ns.

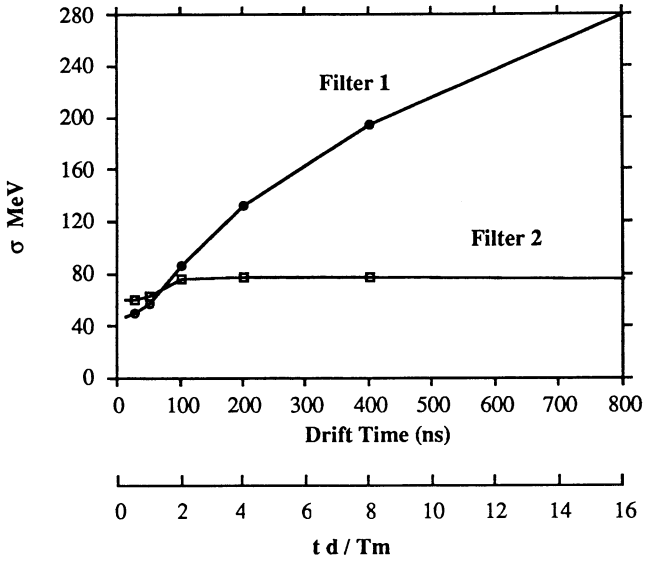

Figure 10. Pile up contribution to the error on the transverse energy measurement in a single cell as a function of the drift time. The strong bipolar shaping is quite effective at reducing the pile up for long drift times. Both filters are similar for short drift times : less than twice the measurement time.

Assuming a measurement time T_m of 50 ns, figure 10 gives the estimated noise contribution to the transverse energy from pile-up as a function of the electron drift time t_d in liquid. Filter 2 does its job of canceling the tails of the pulse. The contribution to the noise is constant at ≈ 80 MeV for each calorimeter cell. This not true for filter 1

where to keep pile up at an acceptable level, we have to stay at short drift times $t_d/T_m < 2$.

In summary, long drift time is not a real problem for pile-up. Tails can be effectively removed by fast bipolar shaping. However as we will see below, the price to pay is a noise increase of ≈ 1.7. So if possible it is better to stick to a moderate drift time, i.e. a drift time less than or equal to twice the measurement time; there the simpler shaper #1 is quite adequate from a pile-up point of view and gives a better signal to noise ratio.

6. Signal and electronics noise in liquid ionization calorimeters

6.1 Minimum ionizing particle signal.

When a minimum ionizing particle (M.I.P.) goes through the calorimeter, each gap gives a triangular current pulse as explained in 2 with a peak current I_{max}. This pulse is processed by the filters defined in section 5. the signal collected is :

$$Q_{collected} = N_{gap} \times I_{max} \times S(0) = N_{gap} \times I_{max} \times T_{eff}$$

The filter response at time Tm to a particle crossing the gap at time 0 : S(0) (see section 5) can be looked at as an effective integration time T_{eff}. Its value is shown in figure 11. For a measurement time T_m large compared to the drift time t_d the effective integration time is $t_d/2$. the factor 2 reflects the triangular shape of the current pulse. If however, as will happen in an SSC calorimeter T_m is small compared to t_d then T_{eff} approaches the measurement time T_m but does not quite get to it due to the finite rise time of the preamplifier pulse. At this point, the signal does not depend any more on the size of the gap.This occurs for a drift time greater than about twice the measurement time.

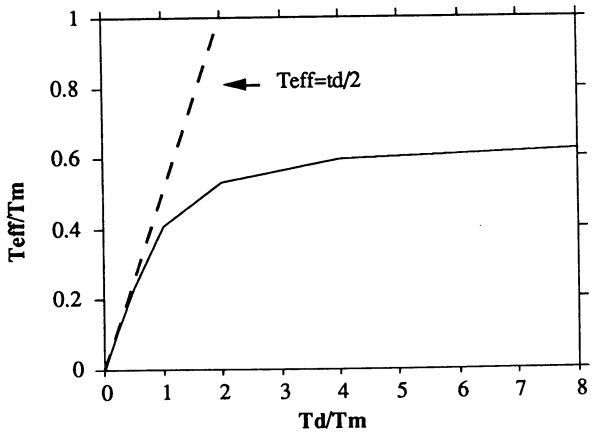

Figure 11. Effective integration time for a given measurement time T_m as function of the drift time. The effective integration time is long enough to get the whole charge (td/2) only when the drift time is small compared to the measurement time. In the other extreme, the effective integration time approaches a constant set by the measurement time and does not depend upon the gap size any more.

6.2 Noise

Electronic noise at fast shaping time is dominated by the series noise of the input FET of the preamplifier. For a given preamplifier, it is well known that this noise is proportional to the capacitance which loads its input. If we optimize the preamplifier to the detector then the optimal noise goes like the square root of the detector capacitance C_D. More precisely, following reference 1

$$ENC = \frac{4}{\sqrt{3}} I_s \sqrt{kT} \sqrt{\frac{\tau_A}{T_m}} \sqrt{C_D}$$

τ_A is the amplifier time constant and is of order 2 ns. I_s is the series noise integral :

$$I_s = \sqrt{T_m \int_0^{\infty} F(t)^2 \, dt}$$

For filter 1 I_s is 1.52 and 2.57 for filter 2. As mentioned in section 5 the strong bipolar filter #2 is noisier by ≈ 1.7 than filter #1.

6.3 Signal/Noise and optimum gap thickness

Let's now consider a calorimeter with a fixed thickness of liquid L subdivided in a number of gaps each of a variable width g. The number of gaps, Ngap, is L/g. In an hadronic calorimeter, the capacitances are large and we will neglect the capacitance of the connections in this computation which aims mainly at comparison. For a pad surface area A, the detector capacitance C_D is (all gaps connected in parallel)

$$C_D = \alpha \times N_{gap} \times \frac{A}{g}$$

where α= 14.2 pF/m for Liquid Argon and 17.8 pF/m for TMP/TMS taking into account the difference in dielectric constants.

Collecting previous results, the optimum signal to noise ratio reads :

$$\frac{S}{N} = \beta \times I_{max} \times \left(\frac{T_{eff}}{T_m}\right) \times T_m^{3/2} \times \sqrt{\frac{L}{A}}$$

β is 2.5 $e^{-1}\sqrt{\frac{s}{m}}$ for liquid Argon with filter #2 and 3.8 $e^{-1}\sqrt{\frac{s}{m}}$ for TMP/TMS using filter #1.

The only gap dependence is through the ratio T_{eff}/T_m which as noted in section 6.1 tends to a constant as soon as the gap is wide enough that the drift time is more than twice the measurement time. On the other hand, minimization of pile-up and of the sampling fluctuations require a small gap. As a reasonable compromise, we choose a liquid gap such that $t_d = 2\ T_m$. For sake of illustration, for a 50 ns measurement time this would correspond to a 0.5 mm gap for liquid argon (as advocated in ref. 3), 1.2 mm gap for TMP at 40 kV/cm, 2 mm for TMS at 20 kV/cm.

Note also, as already underlined in section 2, that the signal to noise ratio depends on the peak current I_{max} and not on the total charge. Figure 12 shows a comparison of peak current for various liquid as a function of the drifting electric field. For room temperature liquids data at low electric field are from Holroyd [7]. Values of

G_{fi} at higher fields have been obtained using the Onsager relation given in [8]. At 50 kV/cm TMP has the same peak current as liquid argon. The cross-over between liquid argon and TMS is at the much lower field of 20 kV/cm.

The strong noise dependence on the measurement time T_m, once the gap width has been optimized, is also made explicit. Increasing the measurement time from 50 ns to 100 ns would reduce the noise by as much as a factor 2.8.

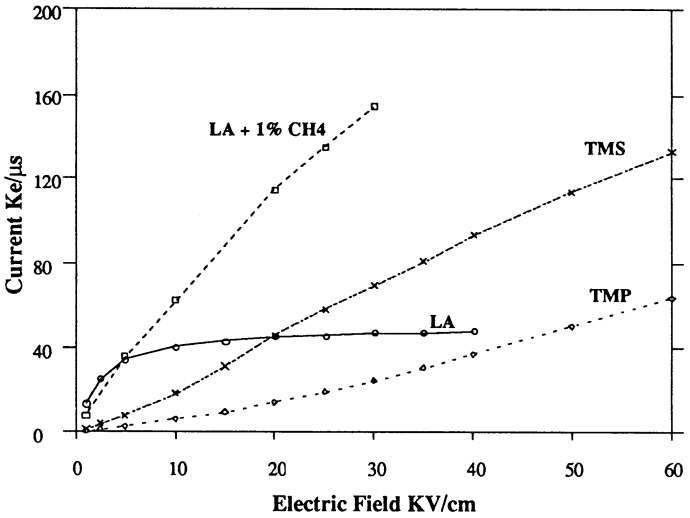

Figure 12. Peak current as a function of electric field.

6.4 Signal/Noise for TMP/TMS compared to liquid argon

For the sake of the comparison let's consider a fast calorimeter with a 50 ns measurement time. The total liquid thickness is fixed at 300 mm. For liquid argon assuming that due to cryogenics problem it is more difficult to build a small gap, this one has been fixed at 2mm. The electric field is set at the standard value of 10 kV/cm. The drift velocity is saturated and the drift time is 400 ns. To keep pile up at an acceptable level we have to use the strong bipolar filter #2 as discussed in section 5. In the case of warm liquid, we will study the noise as a function of the applied electric field. The gap will be varied accordingly to keep the drift time at 100 ns, twice the measurement time. We can then use filter #1. The pile up will be about the same as in the liquid argon case due to the faster drift time. Assuming a 10 x 10 cm2 pad size and collecting results from the previous sections we end up with the results shown in figure 13.

In such devices, M.I.P. can be seen above noise. However the full length of liquid is needed. In the liquid argon case M.I.P. will not be seen in each of the individuals samplings in depth. As the electric field increases, performance of TMP and TMS improves. At 15 kV/cm TMS is as good as liquid argon. TMP has to run at the higher voltage of 37 kV/cm to catch up with liquid argon. The reason for this improvement with electric field is twofold: The peak current increases because the free ion yield increases with electric field and mainly because the drift velocity increases. In

addition, this larger drift velocity allows a larger gap for a fixed drift time reducing the detector capacitance and thus the noise. However practical limitation on the high voltage that can be used makes TMS a much better candidate than TMP if safety issues related to this liquid can be handled.

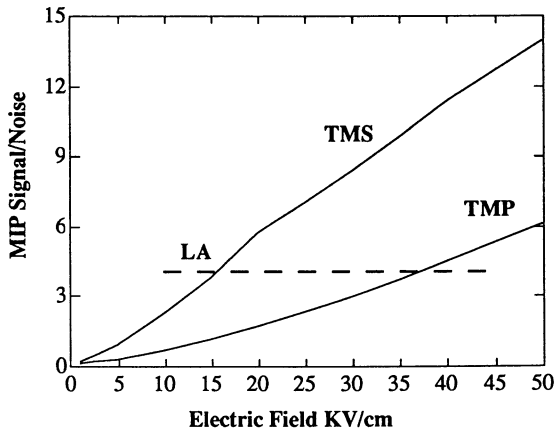

Figure 13. Signal to noise ratio for a minimum ionizing particle as function of the electric field for a measurement time of 50 ns. The pad size is 10cm x 10cm and the liquid depth is 300mm. For TMP/TMS the gap width is varied with high voltage such that the drift time is held at 100ns. Liquid argon is there for comparison; the gap is fixed at 2mm the electric field is 10kV/cm

Let's define the absorber of the calorimeter to translate the noise figures above in unit of energy. Choose 1.2 meters of lead as absorber. This provides for seven collision lengths to absorb hadronic showers. The absorber to detector thickness ratio is 4, which should give compensation i.e same signal response for hadronic electromagnetic showers. A M.I.P. will deposit by ionization 1.6 GeV in the calorimeter but only 3% in the liquid. Electron and hadrons signals are depressed with respect to muon signals. Assuming ratios e/μ=0.6, e/h=1, the M.I.P signal corresponds to the energy deposited by a 2.6 GeV shower. The noise figures then read :

Liquid	gap (mm)	Voltage per gap (kV)	Electronic noise GeV/m2	Pile up noise on transverse energy @10**33 GeV/m2
Liquid Argon	2	2	6.5	.52
TMP@40kV/cm	1.2	4.8	5.8	.56
TMS@20kV/cm	2	4	4.6	.56

These numbers are much larger than we are used to at longer measurement times and reflect the strong time dependence underlined in 6.3. There are probably good enough for the high energy calorimeters will have to measure at SSC.

7. Conclusion

Although liquid ionization calorimeters have been mostly used up to now with slow readout, their signals have a fast rise time. However, it is not easy to get this fast component of the pulse out of the calorimeter. A careful design of the electrodes and of their connections is necessary. A measurement time, i.e. the time between the bunch crossing time and the time when the actual measurement is made, of 50 ns is probably achievable. Pile up contribution to the error in the energy measurement should not be too important for such a short shaping time.

One way to achieve that result is to follow the route pioneered by the Helios collaboration and to use ferrite transformers and preamplifiers buried into the liquid. One other solution might be to use the Electrostatic Transformer approach to keep the detector capacitance low while keeping the number of channels at a reasonable level. This solution allows for the use of transmission lines between the detector and the preamplifiers which can then be located in an accessible area. These cables should be kept short to minimize the added noise. This seems feasible in a room temperature liquid calorimeter.

For fast calorimetry, the signal to noise ratio for room temperature liquids is comparable to or better than the one obtained with liquid argon, at the expense of a slightly higher gap voltage. TMS with its higher drift velocity is very attractive if safety issues can be handled.

In all cases, the electronic noise at the very short shaping times considered in this paper is much larger than what has been obtained with the existing calorimeters using a much longer readout time. This is probably acceptable at SSC where the physics interest is more at the 100 GeV scale.

Acknowledgements

I wish to thank the UA1 collaboration with which I started working on this subject, especially A. Gonidec and D. Schinzel. This work was completed while I was visiting LBL and I want to thank M. Pripstein and W. Wenzel for the opportunity they gave me and for many useful discussions.

References

1- Speed and Noise Limits in Ionization Chamber Calorimeters
V. Radeka and S. Rescia.
Nucl. Inst. and Method A225 (1988) 228-242

V. Radeka.
Proceedings of the 1987 SLAC instrumentation conference

2- Experiment NA34 at CERN

3- Noise and Pile-up in Liquid Sampling Calorimeters
P. Franzini
Proceedings of the 1987 Workshop on Experiments, Detectors and Experimental areas for the Supercollider

4- Fast Hermetic Calorimetry Using Warm Liquids
Proposal for Generic Detector R&D for the SSC/LHC
LBL-09-1987
WALIC collaboration

5- Saturation of ionization signal in TMP and TMS at different angles and electric fields.
B. Aubert et al.
LAPP-EXP/89-08
to be published in NIM

6- Purity in room temperature liquid ionization chambers
S. Ochsenbein, D. Schinzel, A. Gonidec, W.F. Schmidt
Nucl. Inst. and Method A273 (1988) 654-656

Purification de 12000 litres de TMP pour l'expérience UA1 au CERN
A. Gonidec
Journée d'études sur la conduction et le claquage dans les isolants liquides
28-29 Septembre 1989, Toulouse

7- The Physics and Chemistry of Room-Temperature Liquid Filled Ionization Chambers
R. A. Holroyd and D. F. Anderson.
Nucl. Inst. and Method A236 (1985) 294-299

8- Performance of a Uranium/TMP Electromagnetic Calorimeter
UA1 Collaboration, M. Albrow et al.
Nucl. Inst. and Method A236 (1985) 294-299

On the Measurements of Electron and Positive Ion Mobilities in Liquid TMP
A. Gonidec et al.
UA1/TN 87-66

Analysis of the Signal Produced by Cosmics Rays in Liquid TMP
C. Bacci et al.
UA1/TN 86-85

9- Drift velocities of excess electrons in 2,2,4,4-TMP and TMS : a fast technique
H. Faidas et al.
Submitted to Chemical Physics Letters

10- Report of the Large Solenoid Detector Group
Proceedings of the 1987 Workshop on Experiments, Detectors and Experimental areas for the Supercollider

11- Electrostatic Transformers for Large Towers
J. Colas and W.A. Wenzel
Proceedings of the Workshop on Calorimetry fo the Superconducting Super Collider
March 13-17, 1989, Tuscaloosa, Alabama

Liquid Argon Calorimeter for High Energy Heavy Ions*

by Eido SHIBAMURA
Saitama College of Health

Introduction

We can obtain ionization signal and/or scintillation signal in liquid rare gases for incident ionizing radiation. Various liquid argon calorimeters, which use only ionization signal, have been used so far in elementary particle experiments. Some of them gave satisfactory results. Ideally, the magnitude of the ionization signal is proportional to the absorbed energy in the liquid argon under infinite strength of electric field. Actually, the size of the ionization signal is influenced by the velocity and the atomic number of the incident particle under a practical field strength. Recently, we have observed ionization signal I and scintillation signal S in liquid argon simultaneously and obtained a signal linear to absorbed energy for various incident particle from Z=1 to Z=59 under wide range of electric field by making a sum I+aS with a suitable constant a. Instead of observing S by PMT, we can get sum signal in the form of a ionization signal by doping liquid argon with photo-ionizing

* This experiment was performed by the collaboration of Waseda Univ., LBL, and Saitama College of Health.

molecule. Allene (C_3H_4) is a suitable dopant for this purpose. Here, we will present a preliminary report of a experiment of hadron calorimeter filled with liquid argon doped with allene.

Experimental

The main parameters of the calorimeter are shown in Table 1. Liquid argon was directly supplied from a tank-lorry. After purification with molecular sieves 3A cooled at dry ice temperature allene was introduced in calorimeter. The concentration of allene is about 30 ppm.

Electrode system consists of three parts, ΔE, Fe(A), and Fe(B), as shown in Tab. 2 ΔE part, which was located at the front, consists of thin plate of G-10 electrode and liquid argon gap of 3.5 mm. Fe(A) part consists of G-10 electrode and thin(2 mm) iron plates and liquid argon gap of 3.5 mm. Fe(B) part was at the rear, where thick(6 mm) iron plate is used.

The experiment is made at an electric field of 4.5 kV/cm for He(1.7 GeV/amu), Ne(1.0 and 1.7 GeV/amu) and Fe(1.0 and 1.7 GeV/amu) ions at L. B. L. Obtained pulses at read-out channels are summed up in each part. The three sum signals in three part are again summed up, where the fraction (0.634 in ΔE part, 0.348 in Fe(A) part and 0.166 in Fe(B) part) of the energy deposited in liquid argon layer was taken into consideration.

Result and discussion

The observed energy and the resolution is shown in Table 3.

For iron and neon ion the resolution was obtained for spallation events and stop events separately, where the stop events represent ions stopped without changing the initial atomic number. For He ions, the separation was impossible.

The limit of rms energy resolution so far is 40-50 % in hadron calorimeter on the normalization to 1 GeV proton. The present resolution is 30-40 % on the normalization as shown at the bottom in Tab. 3, except for the He ion where separation of stop and spallation event was not made. The present result shows the linear response and good energy resolution of the allene-doped liquid argon chamber not only as a heavy ion calorimeter but also as a high energy hadron calorimeter.

Table 1. Outline of liquid argon hadron calorimeter

diameter	1 m
length	2 m, 6.1 λ_0, 51 r. l.
number of read-out channels	92
liquid argon weight	3 ton
electrode and converter weight	5 ton
vessel weight	2 ton

Table 2. Electrode configuration

	ΔE part	Fe(A) part	Fe(B) part
converter	nothing	Fe(t=2mm)	Fe(t=6mm)
Liq. Ar gap	3.5mm	3.5mm	3.5mm
Total number of cell	9.5	40	110
Number of read-out channels	4	28	60

Table 3

Incident ion	Fe	Fe	Ne	Ne	He
Incident energy (GeV/amu)	1.0	1.7	1.0	1.7	1.7
Total energy E (GeV)	47.2	87.1	18.9	32.9	6.8
Observed energy (GeV)					
Stop events	10.2	19.1	4.08	7.40	
Spallation events	11.0	21.2	4.76	8.06	(1.59)
FWHM Resolution R (%)					
Stop events	2.54	1.93	3.03	5.12	
Spallation events	13.2	9.98	15.8	14.3	(39.3)
$R*E^{1/2}/2.35$ (%)					
Spallation events	38.9	36.6	29.2	34.9	(43.6)

Session 8

CRYSTAL DETECTORS

BaF_2 calorimeters with photosensitive gaseous chambers

G. Charpak[1] P. Miné[2], V. Peskov[1], D. Scigocki[1], J. Valbis[3]

(1) CERN, Geneva, Switzerland
(2) LPNHE, Ecole Polytechnique, Palaiseau, France
(3) Inst. Solid-State Physics, Latvian State University, Riga, USSR

Abstract.

We describe an electromagnetic calorimeter constructed from BaF_2 layers coupled to low pressure MWPC, with TMAE gas as the photosensitive constituent. We review some recently studied organic and organometallic compounds, which are competitive with TMAE. A new family of scintillators are also presented. They exhibit fast scintillation in the UV, like barium fluoride. The possible application to experiments with intense colliders is discussed.

1 – Introduction.

The proposition to couple BaF_2 crystals with a multiwire proportional chamber (MWPC) came from Anderson et al. [1–3], who proposed the name solid state proportional counter (SSPC). In this device the light emitted is detected by a photosensitice vapour such as tetrakis-(dimethylamino)ethylene (TMAE) filling the MWPC.

The properties of BaF_2, which merit its use in high energy intense colliders are: high density, short radiation length, a very fast ultraviolet component [4], and a photon yield independant of temperature [5–6]. Besides, its resistance to radiation damage is the highest of all known scintillators, provided that lead contamination is avoided [7–10]. In the Table 1 we summarize these characteristics, we quote an indicative price, and we compare to NaI(Tl), BGO and CsI(Tl).

A wire chamber is cheap, naturally segmented, and not very sensitive to magnetic fields. We will briefly review the properties of an electromagnetic calorimeter based on this technique. A simpler design, with a parallel plate avalanche chamber (PPAC), working at atmospheric pressure was studied using a small prototype [12–13].

Until recently the BaF_2–TMAE couple was the only possible way to build an SSPC. The discovery [14] of the scintillation of lanthanum fluoride (LaF_3) doped with Nd^{3+}, at 173 nm, was a first step towards finding new scintillators similar to BaF_2. Moreover the mechanism by which BaF_2 emits lights with a fast component is now explained [15], and a new family of inorganic scintillators has been discovered.

We will also examine the possible use of newly investigated organic and organometallic photocathodes [12,16], either in the gas or condensed phase.

Concluding with a discussion of the challenges for electromagnetic calorimetry at high luminosity hadron colliders, we recall the advantages of the SSPC concept, and stress the necessity of a research effort on new photosensitive materials and new fast scintillators.

2 – Principle of SSPC.

At present, the fast component can be detected only by UV sensitive phtomultipliers,or by MWPCs. Photodiode readout is convenient for the slow component at 310 nm [17].

	NaI(Tl)	BGO	BaF_2	CsI(Tl)
Density (g/cm^3)	3.67	7.1	4.88	4.51
X_o (cm)	2.6	1.12	2.05	1.82
dE/dx (MeV/cm)	4.8	9	6.5	6.2
dose max (Gray)	10^3	10^3	10^5	$5x10^3$
vawelength (nm)	410	480	310 220	580 310
time (ns)	250	300	620 0.6	1000 10
price ($/cm^3$)	1.6	17	7	2

Table 1

In an SSPC, the light emitted by the crystal is absorbed in a conversion gap, to give photo-electrons, which are drifted into a MWPC where their signal is amplified. The detection efficiency depends on the photon mean free path, that is on the TMAE vapor pressure. It is important to keep a stable temperature, for exemple 40° C, for a gas depth of 12 mm.

Operating at low pressure [11], gives the advantage of a good time resolution, a high rate capability, and a very low sensitivity to direct ionization. This restricting condition can be avoided if the conversion gap is replaced by an adsorbed layer of photosensitive product, and the MWPC by a PPAC [12-13]. The speed with a PPAC is much higher than with a MWPC, and the amplification is significant only for the signal coming from the photocathode. The drawback of this scenario being a lower gain, which is acceptable for electromagnetic showers in the GeV range.

Sealed devices generally exhibit a deterioration of the gain after a few hours. When the gas volume is constantly renewed by a low pressure bubbling system, a continuous operation is possible [18]. This procedure has the advantage, as in liquid calorimeters, to ensure insensitivity to radiation. Another limiting effect is ageing, decrease of the gain as a function of the integrated charge in the wires. It is presently [19] two orders of magnitude worse than the best standard (1C/cm) for MWPCs.

3 - Fast electromagnetic calorimetry measurement.

Prototype detectors were tested at CERN [18,20] and BNL [21]. The constituents of these aparatus have been described in the quoted references and we will only only briefly recall the measured performances. The CERN device was a 20 radiation length calorimeter made of 14 crystals, exposed to a low energy beam, 108 to 200 MeV, and a medium energy beam 1 to 9 GeV. The BNL device was a single crystal, 5 radiation length, exposed to minimum ionizing particles.

Figure 1 gives the measured energy resolution for different energies. It indicates the contribution coming from leaks, calculated by the EGS electromagnetic shower simulation code, and the contribution from the beam spread. The curve represents an energy dependance $\sigma(E)/E=\sqrt{E}$.

The position of the center of the shower was determined by the center of gravity of the cathode signals. The resolution improved with higher energies and can be represented by $\sigma=3.6/\sqrt{E}$(mm/GeV). Clearly this parameter is strongly dependant of the longitudinal and lateral size of the crystals, and on the number of light detectors per crystal.

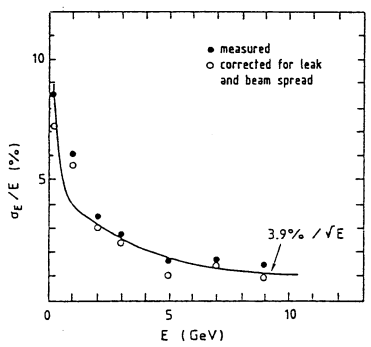

Fig. 1 Energy resolution as a function of the incoming energy.

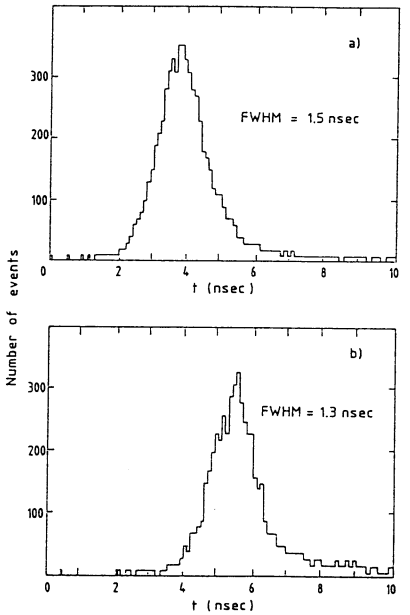

Fig. 2 Time spectra with drift space (a) and without (b).

Figure 2 shows the time resolution. The upper picture corresponds to a measurement where the drift space was neutralized by reversing the voltage, the time resoluiton is improved but the energy resolution is degraded because we keep only the electrons produced in the MWPC. After substraction of the jitter due to the trigger counter we are left with the following standard deviation: (1) σ_1 =400±200 ps, (2) σ_2 =170±130ps.

The gain stability is extremely important for a detector aiming at an energy resolution of the order of a few percent. A qualitative check made with cosmic rays showed that the apparatus was working for several months without cleaning or pumping. With the beam a shorter but more precise determination was made, the gain fluctuated with an amplitude of 2 % and a period of 20 minutes. This effect can be correlated to a variation of the temperature of the tank following the heating cycle.

The high rate capability was estimated by the gain decline as a function or the number of particles per second. The loss was about 25% for $4x10^6$ minimum ionizing particles per second in the calorimeter corresponding to an intensity of 10^{-9} A/mm in the chambers' wires.

4 - New fast inorganic scintillators.

It was found recently [14] that LaF_3 doped with Nd^{3+} has a fast scintillating component at 173 nm with a decay time 6.3 ns. The detection efficiency with a TMAE SSPC is not higher than with BaF_2 and the main advantage of this crystal is its higher density (5.94g/cm^3) and its shorter radiation length.

A significant step forward is due to Jansons et al. [15], who gave an explanation of the fast scintillation and proposed to name it cross-luminescence. Applying their theory, they give a prediction for all cesium

halides and found that the experimental results confirm this expectation. Two other crystals, $KMgF_3$ and $KCaF_3$, exhibit fast scintillation at a wavelength shorter than BaF_2, centered at 170 nm, with a decay time lower than 2 ns. They also made solid solutions of KF + RbF with various concentrations, resulting in a fast cross-luminescence shifting from 250 to 160 nm [22]. The authors of ref. [22] find compatible results.

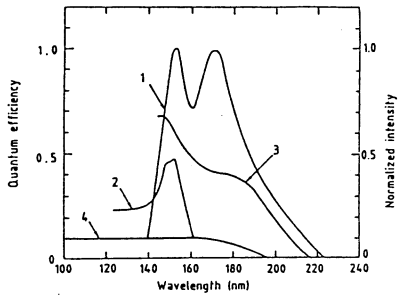

Fig. 3 Emission spectrum of $KMgF_3$ (1) and quantum efficiencies of TEA (2) and TMAE (3) vapours, and of CsI (4) photocathodes as a function of photon wavelength.

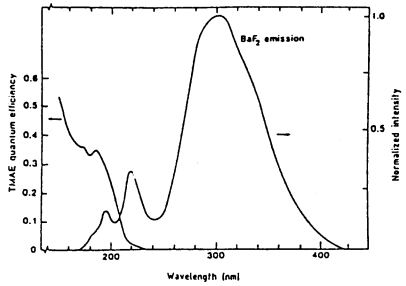

Fig. 4 BaF_2 emission spectrum and TMAE vapour quantum efficiency as a function of wavelength.

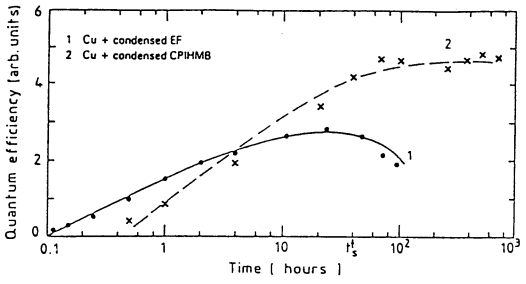

Fig. 5 Quantum efficiency of different organometallic photocathodes as a function of the deposition time.

The advantage of such materials can be seen by comparing the figures 3 and 4, the overlap between the scintillation spectrum and the quantum efficiency is much larger. With $KMgF_3$ it is possible to use TEA as the photosensitive vapour, an efficiency of of 4.5 photo-electrons per MeV was recently measured [24]. The main drawback of these new scintillators is their low density and long radiation length.

5 - New photosensitive materials.

Peskov et al. [16] showed that metal cathodes covered with liquid TMAE or TMPD detect light at wavelengths longer than the vapors do. Even if the efficiency is not very high, this effect can be used to improve the time jitter of the counter, the photoelectrons are generated in a thin layer and not in a depth of a few mm of gas.

Some organometallics were tested to find a new class of photosensitive materials. The highest sensitivities were acheived with ethyl-ferrocene (EF) and cyclopentadienyl-iron-hexamethyl-benzene (CPIHMB) [25]. Figure 5 shows the good stability in time of the adsorbed photocathodes, made simply by flushing the vapor with CH_4 in the chamber. A PPAC using EF photcathode

on a BaF_2 crystal was tested with sources and with a particle beam [12]. A time resolution of 10 ns or better was measured, with a sensitivity better than 1% for wavelenths shorter than 230 nm.

6 - Conclusion.

The challenges for electromagnetic calorimetry at high luminosity hadron colliders are great: time resolution better than 15 ns, good energy resolution, granularity, easy calibration, stability in time, radiation resistance. The SSPC based on BaF_2 and TMAE is well adapted to these requirements. Its density can be increased by sampling with lead sheets. The ageing effect, which is a problem for all gazeous detectors with high gain, deserves more study. Substantial improvements were reported recently and it appears that a detector running with low gas gain may be acceptable [19].

The prediction and discovery of new fast scintillators have not yet produced a direct competitor to BaF_2 for high energy physics. However these scintillators are not unique, and this family has to be explored systematically by investigating such parameters as: radiation resistance, light yields, ease to handle, and of course price. In the field of new photosensitives, ethyl-ferrocene is now a good candidate to replace TMAE.

References.

[1] D. F. Anderson, Phys Lett. 18 (1982) 230.
[2] D. F. Anderson et al., Nucl. Instrum. Methods 217 (1983) 217.
[3] D. F. Anderson et al., Nucl. Instrum. Methods 225 (1984) 8.
[4] M. Laval et al., Nucl. Instrum. Methods 206 (1983) 169.
[5] P. Schotanus et al., Nucl. Instrum. Methods A238 (1985) 564.
[6] M. Suffert and G. Charpak, CERN EP Internal report 86-03 (1986).
[7] S. Majewski and D. Anderson, Nucl. Instrum. Methods A241 (1985) 76.
[8] A. J. Caffrey et al., IEEE Trans. Nucl. Sci. NS-33 (1986) 230.
[9] M. Murashita et al., Nucl. Instrum. Methods A243 (1986) 67.
[10] D. Scigocki, CERN/LAA, private communication.
[11] A. Breskin, Nucl. Instrum. Methods 196 (1982) 11.
[12] V. Peskov et al., Organometallic photocathodes for parallel-plate and wire chambers, Wire Chamber Conference, Vienna, 1989.
[13] V. Peskov, this conference.
[14] P. Schotanus et al., Nucl. Instrum. Methods A272 (1988) 913.
[15] J. L. Jansons et al.,Phys.Stat. Sol. (b) 144 (1987) 835.
[16] V. Peskov et al., Nucl. Instrum. Methods A269 (1988) 149.
[17] E. Lorenz et al., Nucl. Instrum. Methods A249 (1986) 235.
[18] R. Bouclier et al., Nucl. Instrum. Methods A267 (1988) 69.
[19] C. L. Woody , IEEE Trans. Nucl. Sci. NS-35 (1988) 493.
[20] D. F. Anderson et al., Nucl. Instrum. Methods 228 (1984) 33.
[21] C. L. Woody et al., IEEE Trans. Nucl. Sci. NS-33 (1986) 136.
[22] J. L. jansons et al., Solid State Commun. 67 (N0. 2) (1988) 183.
[23] S. Kubota et al., submitted to Nucl. Instrum. Methods.
[24] A. F. Buzulutskov et al., Nucl. Instum. Methods A281 (1989) 99.
[25] D. Astruc et al. , Proc. Int. Workshop on Liquid-State Electronics, Berlin, 1988 (Hahn-Meitner-Institut).

NEW DEVELOPMENTS IN CALORIMETRY BASED ON VUV SCINTILLATORS COUPLED TO PHOTOSENSITIVE GASEOUS DETECTORS

G. Charpak, D. Lamb, V. Peskov and D. Scigocki
CERN, Geneva, Switzerland
and
J. Valbis
Inst. Solid-State Physics, Latvian State University, Riga, USSR

(Presented by V. Peskov)

1. INTRODUCTION

It is commonly acknowledged that the main requirements for the calorimetry to be used at future colliders such as the Large Hadron Collider (LHC), the Superconducting Super Collider (SSC), or the Eloisatron (ELN, 200 TeV), are high speed (~ 15 ns bunch crossing), high radiation resistance (up to 0.1 MGy), a very good energy resolution, and the best possible hermeticity. There are several projects that claim to have found ways of meeting these demands [1]. One of the most promising is based on the use of VUV scintillators in liquid phase with noble gases [2], or of solid, dense, inorganic scintillators [3], for example BaF_2 [4, 5]. In the case of VUV scintillators, liquid or solid photocathodes [6] combined with gaseous detectors can be used for the readout [2, 3, 5]. One of the main advantages of this type of combination is that very high speed and time resolution can be achieved because there is virtually no time jitter [3]. In this paper we present our latest results concerning photocathodes and VUV scintillators used in a solid scintillator proportional counter (SSPC) made of inorganic scintillators coupled to photosensitive gaseous detectors.

2. PHOTOCATHODES FOR AN SSPC

During the last two years we have investigated different photocathodes [3, 6–9] for gaseous detectors. Some of them, such as solid tetrakis(dimethylamine)ethylene (TMAE) + neopentane, have high efficiency in the wavelength region below 200 nm (more than 5%) [6]. Unfortunately, most of these organic photocathodes are based on TMAE vapour, which interacts strongly with air and is very corrosive for many materials, and which also has bad ageing effects when used as a gas in wire chambers [10]. Thus a complicated technology is required in order for these substances to be deposited as photocathodes in SSPCs, because it is necessary to work under very clean conditions and to be able to cool the surface where the photocathode will be condensed in liquid or solid phases. For applications in calorimetry, where huge detectors will be built, it may be of interest to use a simpler technology; hence these requirements restrict the use of these organic photocathodes.

For these reasons, during the last year we concentrated our investigations on new photosensitive elements which do not interact with air and which can be used at room temperature, using a simple technology to deposit them on surfaces as photocathodes. Good candidates are triethylamine (TEA) [11] and some organometallic compounds [7], for example diethylferrocene and ethylferrocene (EF) [6, 9]. The experimental set-up used to study these photocathodes is described in Ref. [6]. We used a monochromator system to measure the quantum efficiency of these substances, as well as a small

prototype SSPC made with BaF_2 crystals coupled to a wire chamber to investigate these photocathodes in a real experimental situation. The technique for obtaining these photocathodes is simple. Vapours of TEA, diethylferrocene, or EF are introduced into the detector at room temperature. An adsorbed photosensitive layer is thus formed everywhere in the detector and can be used as a photocathode. The use of a TEA adsorbed layer as a photocathode was studied, and its quantum efficiency for different TEA vapour pressures is shown in Fig. 1. The TEA photocathode is sensitive to the fast emission of BaF_2, but has a poor quantum efficiency. We have obtained better results (between 5 and 10 times higher) with organometallic photocathodes—especially with EF, which was finally chosen for use in further experiments. In the case of an adsorbed layer, we have measured a quantum efficiency of about 1% at 193 mm, but this depends slightly on the materials used as the support for the EF photocathode (see Fig. 2). The same efficiency is obtained when the EF adsorbed layer is formed on a BaF_2 crystal covered by a mesh and working as a semitransparent photocathode. This means that this device can be used as the photosensitive element in an SSPC. The efficiency obtained is smaller compared with the one using TMAE vapour in the traditional SSPC approach. However, with absorbed layers instead of vapours as the photosensitive element in SSPCs, it is possible to replace the low-pressure multiwire proportional chamber (MWPC) with a parallel-plate avalanche chamber (PPAC) without having an intermediate conversion gap [3]. This geometry makes it possible to build very fast detectors, working at one atmosphere and with less sensitivity to ageing effects than wire chambers since the charge density in the avalanches is lower. A prototype made with a BaF_2 crystal coupled to a PPAC with an EF adsorbed layer as the photocathode was tested in a CERN beam [9]. An energy resolution of about 14% at 1 GeV was measured. It was found to be three times worse than the one with the low-pressure MWPC and TMAE vapour. The poor efficiency of the EF adsorbed layer is a result of

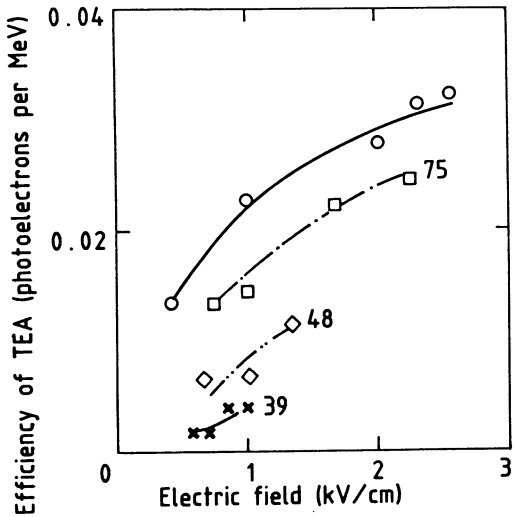

Fig. 1 Quantum efficiency in photoelectrons per MeV deposited in the BaF_2 crystal as a function of the electric field applied on the photocathode (in kV/cm), for TEA adsorbed layers at different TEA vapour pressures (75 Torr, 48 Torr, 39 Torr) and for a TEA condensed layer deposited on the BaF_2 surface.

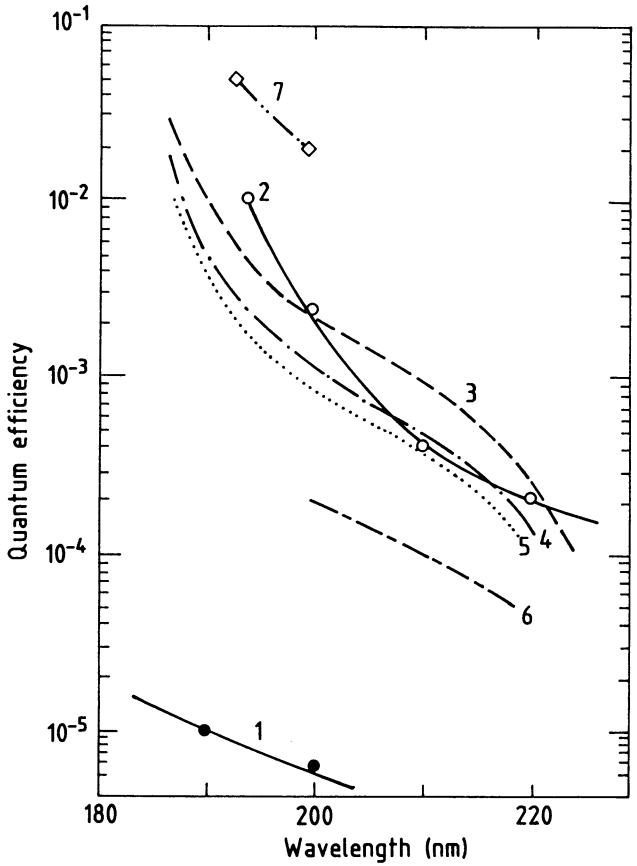

Fig. 2 Quantum efficiency of photocathodes as a function of the photon wavelength λ:
(1) Clean copper cathode.
(2) An EF adsorbed layer deposited on a copper cathode. The EF was produced in the USSR.
An EF adsorbed layer (synthetized at the University of Geneva):
(3) deposited on a copper cathode;
(4) deposited on an indium cathode;
(5) deposited on an aluminium cathode;
(6) when the metallic cathodes (Cu, In, and Al) were kept at 80 °C.
(7) A 1 mm thick EF liquid layer, synthetized at the University of Geneva.

its thickness. Only a few per cent of the BaF_2 light emission is absorbed in the layer. Figure 3 shows the increase of the efficiency with the EF thickness. In the case of a condensed layer, the efficiency at 193 nm is 7% [3]. We are now preparing a beam test with a prototype of an SSPC calorimeter comprising BaF_2 crystals combined with PPACs and a condensed layer of EF. We expect an

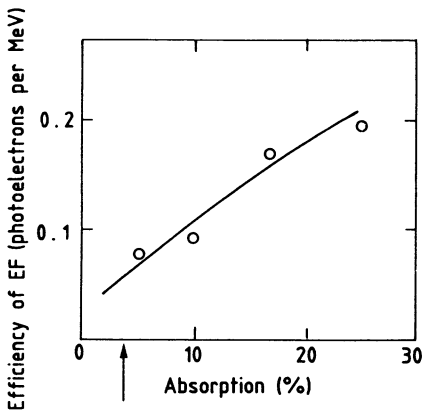

Fig. 3 EF layer quantum efficiency in photoelectrons per MeV deposited in the BaF_2 crystal as a function of the absorption light at 193 nm in the EF semitransparent photocathode formed on the BaF_2 crystal. The arrow indicates the EF layer conditions of the beam test.

improvement of 2 or 3 in the energy resolution, compared with the resolution obtained with an EF adsorbed layer, which should be close to the one of an SSPC with TMAE gas.

As the next step, we plan also to build sealed detectors made with PPACs and with EF photocathodes deposited on the BaF_2 crystal used as the window, or on a quartz window to separate the gaseous detector from the crystal, as with photomultipliers (PM). This design should greatly simplify the construction of calorimeters, where each crystal is read out by its independently sealed gaseous detector, as in geometries with PMs or photodiodes. We have already tested a sealed single-wire counter filled with EF vapour. Continuous tests made at 1 kHz during two years have proved the good stability of this type of detector. However, the stability of sealed gaseous detectors under high radiation levels remains to be investigated.

3. NEW SCINTILLATORS FOR AN SSPC

The efficiency of all the photocathodes we have studied has strongly increased in the wavelength region below 200 nm. This means that SSPCs using these photocathodes will be much more efficient with scintillators that could emit in this region and thus achieve better energy resolution.

However, until recently BaF_2 was the only known scintillator to possess adequate properties for SSPCs: a high density (4.9 g/cm^3); a short radiation length (2.05 cm); a very fast ultraviolet scintillation component with a decay time of 600 ps [12]; a photon yield that is independent of temperature [13, 14]; and a resistance to damage caused by radiation up to 10^5 Gy [15, 16]. The discovery of a scintillation that peaks at 173 nm and has a decay time of 6.3 ns, in lanthanum fluoride (LaF_3) crystals doped with Nd^{3+}, allows the use of LaF_3 in an SSPC filled with TMAE vapour [17]. The main advantages of LaF_3 over BaF_2 are its higher density (5.94 g/cm^3) and its shorter radiation length (X_0 = 1.7 cm), but the light yield is small (because it is difficult to obtain crystals with a good transparency in the wavelength emission region), and the detection efficiency is not higher than that obtained with the BaF_2 device.

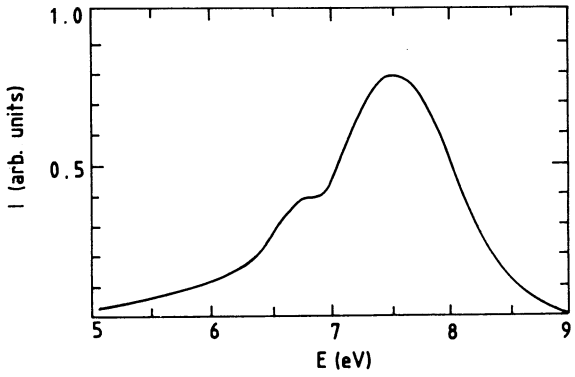

Fig. 4 Emission spectrum of $KLuF_4$ as a function of photon energy.

On the other hand, the mechanism by which BaF_2 emits light with a fast component was not understood until recently, when the studies made by Valbis and his group [18] enabled them to explain this mechanism, and why BaF_2 has such a unique ensemble of properties as a scintillator. Based on this research, a new family of inorganic scintillators was discovered [18, 19]. Their properties are similar to those of BaF_2 but their maximum light emission is in a wavelength region between 140 nm and 200 nm (see Fig. 4), where the known photosensitive vapours and photocathodes achieve high efficiencies. In these crystals the energy separation between the valence band—involving mainly the halogen electronic states—and the upper cation core band is smaller than the band gap. After excitation, which causes holes to appear in the core band, radiative electronic transitions from the valence band to the core band take place, giving rise to a specific emission which is called cross-luminescence (CRL). This mechanism explains the fast component of the BaF_2 scintillation. The CRL was measured in CsCl, CsBr, RbF, and RbCl [18], as well as in KF [19]. It is possible to add a third component to these simple crystal bistructures to obtain crystals of higher densities, with the same light emission. The first crystals of this type were $KCaF_3$ and $KMgF_3$ [19]. An SSPC with a $KMgF_3$ crystal coupled to a wire chamber filled with TEA vapour achieved half the efficiency obtained with BaF_2 and TMAE vapour, i.e. four photoelectrons per MeV [20].

A new concept of an SSPC was developed. It consists of scintillators coupled to PPACs, working at room temperature, with a gas mixture at atmospheric pressure and with an adsorbed, liquid, or solid layer as the photocathode [9]. This type of detector permits us to retain most of the properties of the traditional SSPC (i.e. a low-pressure MWPC filled with TMAE vapour and working at high temperature), and at the same time to eliminate its main disadvantages; but as explained above, the efficiency is smaller with BaF_2 as the scintillator. Then a prototype made of a $KMgF_3$ crystal coupled to a PPAC filled with TEA was tested in Serpukhov, and an efficiency of four photoelectrons per MeV was measured [21]. But if the new scintillators, such as $KMgF_3$, have scintillation properties equivalent to those of BaF_2 and a similar high resistance to radiation, they suffer from lower density, 3.1 g/cm^3, and from longer radiation lengths, X_0 = 7–8 cm. One of us (J.V.) and his group, within the framework of the LAA project, are now working on new crystals based on lutetium [22] (see Fig. 4) or yttrium, which have higher density and shorter radiation length— ~ 5 g/cm^3 and ~ 2 cm, respectively, for $KLuF_4$. The first samples that were obtained are very small (a few millimetres) and have an irregular shape, which makes them very difficult to

combine with a PPAC. But it seems possible to measure the intensity of the light emission and compare it with that of BaF_2 fast emission, using photomultipliers.

The above tests are being prepared in our group, and independently by Buzulutskov et al. at Serpukhov [23]. But the main limitation comes from the fact that these new dense crystals probably cannot be obtained in the form of real scintillators, because their thermochemical properties do not allow the use of large autoclaves similar to those used in producing large SiO_2 crystals for example, and they cannot be obtained from the melt by other methods. However, other techniques are now being used to develop new crystals that are optically perfect, of a reasonable size, and have good properties as scintillators [23].

Acknowledgements

The authors would like to tender their appreciation to I. Crotty for his technical assistance and his advice.

This work was carried out within the framework of the LAA project.

REFERENCES

[1] See the proceedings of this conference.
[2] T. Ypsilantis et al., this conference.
[3] G. Charpak et al., preprint CERN-EP/89-66 (1989), presented at the Symposium on Particle Identification at High-Luminosity Hadron Colliders, FNAL, Batavia, 1989.
[4] R. Bouclier et al., Nucl. Instrum. Methods **A267** (1988) 69.
[5] P. Miné, this conference.
[6] V. Peskov et al., Nucl. Instrum. Methods **A269** (1988) 149.
[7] D. Astruc et al., Proc. Int. Workshop on Liquid-State Electronics, Berlin, 1988 (Hahn-Meitner-Institut, Berlin, 1988), p. 109.
[8] G. Charpak et al., ibid., p. 85.
[9] V. Peskov et al., Organometallic photocathodes for parallel-plate and wire chambers, presented at the Wire Chamber Conference, Vienna, 1989.
[10] C.L. Woody, IEEE Trans. Nucl. Sci. **NS-35** (1988) 493.
[11] R.A. Holroyd, paper 6408, submitted to the 23rd Int. Conf. on High-Energy Physics, Berkeley, 1986.
[12] M. Laval et al., Nucl. Instrum. Methods **206** (1983) 169.
[13] P. Schotanus et al., Nucl. Instrum. Methods **A238** (1985) 564.
[14] M. Suffert and G. Charpak, CERN EP Internal Report 86-03 (1986).
[15] S. Majewski and D. Anderson, Nucl. Instrum. Methods **A241** (1985) 76.
[16] A.J. Caffrey et al., IEEE Trans. Nucl. Sci. **NS-33** (1986) 230.
[17] P. Schotanus, C.W. Van Eijk and R.W. Hollander, Nucl. Instrum. Methods **A272** (1988) 913.
[18] J.L. Jansons et al., Phys. Status Solidi b **144** (1987) 835.
[19] J.L. Jansons et al., Solid State Commun. **67** (2) (1988) 183.
[20] A.F. Buzulutskov, L.K. Turchanovitch and V.G. Vasil'chenko, Nucl. Instrum. Methods **A281** (1989) 99.
[21] A.F. Buzulutskov, L.K. Turchanovitch and V.G. Vasil'chenko, Submitted to Nucl. Instrum. Methods.
[22] A. Zichichi et al., Report on the LAA project (vol. 6), presented at the Third LAA Open Meeting, CERN, Geneva, 1989.
[23] J. Valbis, Private communication.

Measurements of CsI(pure) Performance

C. M. Rozsa, R. Schreiner, N. Johnson, G. Mataraza,
Bicron Corporation, Newbury Ohio

Pure CsI is an intrinsic scintillator that has a fast component with a 10 nsec decay constant emitting at 310 nm. It is a candidate material for a large calorimeter for the SSC and LHC. In principle, there is capacity to produce the 40 m^3 of CsI required for one calorimeter in about two years.

A 50 cm diameter by 40 cm tall ingot of CsI grown by Stockbarger process was sampled and analyzed. The first grown part of the ingot (bottom) is typically the purest material due to segregation and rejection of contaminants. Measurements of the fast component, where charge is integrated for 100 nsec, show a decrease in photo-electron (pe) yield with height in the ingot. The total pe yield measured in 5 μsec tends to increase with height. The figure of merit defined as the ratio of fast-to-total decreases not only because the fast component is decreasing but also because the total is increasing. Fig. 1 shows typical results for the fast, total and fast-to-total ratio for a series of 2.5 cm diameter by 2.5 cm tall samples cut at different vertical positions in the ingot.

^{241}Am excited emission spectra from 200 nm to 900 nm of the samples from 60 keV excitation show the 310 nm fast component at all positions. The increase in concentration of contaminants with height is evident from the additional structure in these spectra from 400 nm to 700 nm. The 310 nm peak region decreases in overall yield but does not show any obvious shape changes.

Analysis of single photon emission spectra over a 200 nsec time interval verified the 10 nsec and 36 nsec components (Ref.1). These measurements showed increased yield for longer lifetime components near 200 nsec, but a longer time scale is required to define it.

The results of these and other measurements made on the ingot samples are summarized in the table. Results are consistent with the slow component increasing with height of the ingot and the fast component decreasing. The particular contaminants have not been identified.

Table: Characteristics of Pure CsI

Wavelength of emission of fast component	310 nm
Maximum photoelectron yield in R2256 PMT for two geometries:	
2.5 cm dia. X 2.5 cm	400 e
7 cm X 7 cm X 30 cm	125 e
Fast decay constant components:	10, 36 nsec
Pulse height resolution (FWHM) for 2.5 cm	
662 keV	19%
1115 keV	15%
Coincidence resolving time for 511 keV from ^{22}Na with	
200 keV discrimination	677 psec

Figure 1. Fast and total photo-electron yield, and fast-to-total ratio for a series of 2.5 cm dia. x 2.5 cm high samples cut from different vertical levels in the ingot

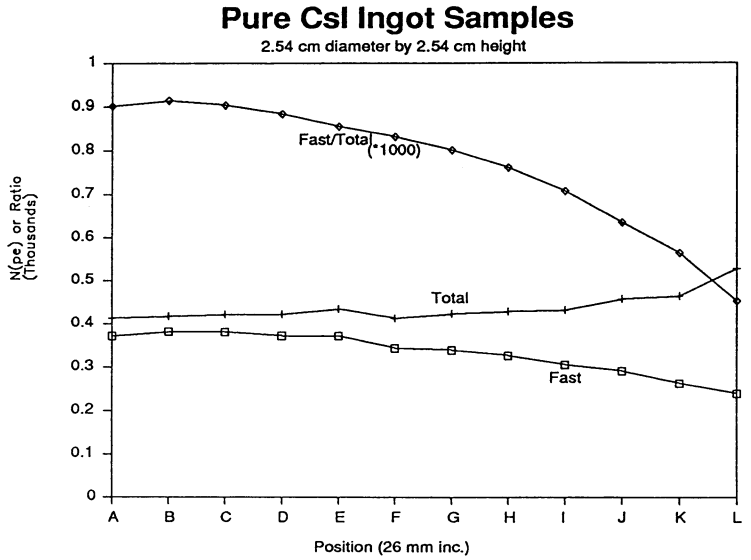

Reference 1. A NEW SCINTILLATION MATERIAL: PURE CsI WITH 10 ns DECAY TIME; S. Kubota, et al; *Nuclear Instruments and Methods in Physics Research* A268 (1988) 275-277

RADIATION DAMAGE OF CsI(Tl) CRYSTALS

D. Renker
Paul-Scherrer-Institute
Switzerland

1 Introduction

During the last years CsI(Tl) became one of the favorite materials in the construction of big electromagnetic calorimeters with high energy resolution (CLEO II, Crystal Barrel e.c.). The advantages of CsI(Tl) are obvious: high light yield and relative low cost (both comparable with NaI(Tl)), shortest radiation length of common scintillators besides BGO, weak hygroscopicity, very good mechanical and thermal stability and an emission spectrum matching to photodiode readout. But CsI(Tl) is reputed to be very sensitive to radiation and previous measurements showed a significant reduction of the light output already at a dose level of 100 rad [1-5]. This is demonstrated in Fig.1, where all published data are summarised.

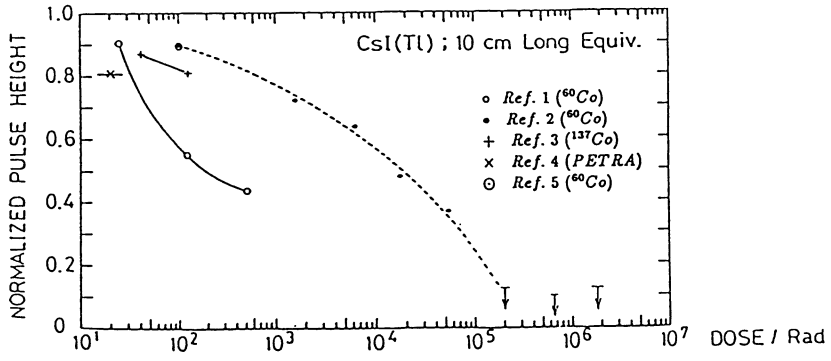

Figure 1: Normalized pulse height as function of the exposure to γ sources. Data points from ref. 1-5

Up to now no correlations have been established between radiation damage and specific crystal impurities. Since they could be very important for the quality control at one hand and at the other hand for a reduction in the demands to the manufacturers and by this the prices, a further study of radiation damage was started at the Paul-Scherrer-Institute.

2 Measurement of radiation damage

Small cubic CsI(Tl) crystals with a volume of 1 ccm from all manufacturers worldwide were irradiated with γ sources. Before, during and after the irradiation the absolute light output was measured, together with the transmission of light in the range between 250 and 700 nm and the spectrum of fluorescence when the crystals were excited with UV-light of 250 nm. After the last exposure the crystals were analysed chemically.

At the beginning the investigations were done in the usual way [1-3,5]: the crystals were irradiated at a special facility with a strong (74 Tera-Bequerel) ^{137}Cs source and the measurements were done in a laboratory. This caused the problem of mounting the crystals in a reproduceable way to the measureing devices and by this introduced large errors.

Five of six crystals were not effected by the radiation even at doses as high as 50 000 rad. There was only one crystal which showed a linear decrease of the light output with the exposure. The decrease was 8 % at 500 rad. At higher doses a saturation effect occured. This crystal became slightly reddish and less transparent to short wavelength. A similar behaviour was reported earlier [1-5]. The radiation damage did not recover spontaneously and a heat treatment only partly cured it. The chemical analyses indicate higher impurities (Rb, K, Na, Ba) compared to the other crystals.

Radiation damage manifests itself by an increased selfabsorption of the szintillation light due to the formation of colour centers. Thus the effect in the 1 ccm crystals used in this study is small compared to the errors of the measurement. Since high doses are not necessary and the value of dose per time is irrelevant the method was changed: the crystals remained connected optically to a photodiode and were irradiated with a moveable ^{60}Co source. This gave an inhomogeneous radiation field, but avoided the problem of reproduceability. Fig. 2 shows a sketch of the setup.

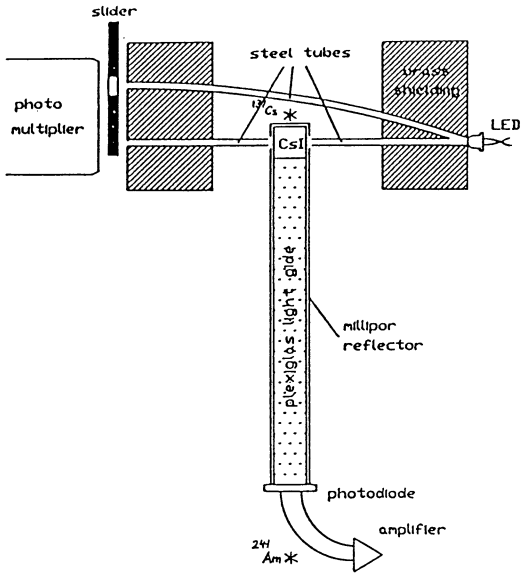

Figure 2: Experimental setup. See text

A light guide between the crystal and the photodiode, made of 10 cm long plexiglas bar, protected the photodiode from the radiation of a strong (15 mCi) ^{60}Co source which could be placed from top close to the crystal. The light output was measured with a permanently mounted ^{137}Cs source. To monitor the stability of the amplifier chain a ^{241}Am source was installed near the photodiode and the conversion of the 60 keV line in the silicon was recorded. The spectrum of transmitted light was measured before and after the irradiation, while during the exposure the transmission was determined solely for one wavelength with a light emitting diode by comparison of the direct light to that going through the crystal. A slider allowed to select one of the two light guiding tubes remotely. This gave an absolute normalisation of the transmission spectra at the wavelength of the LED, which was 635 nm, that is about the wavelength of the scintillation light. The whole assembly was mounted inside a housing made of 1 ton of lead bricks.

3 Results

Again no radiation damage was observed with most of the crystals. Two of them even showed a slight increase (2-3 %) of the light output after an exposure to 100 rad. Fig. 3 demonstrates the stability of one of the crystals.

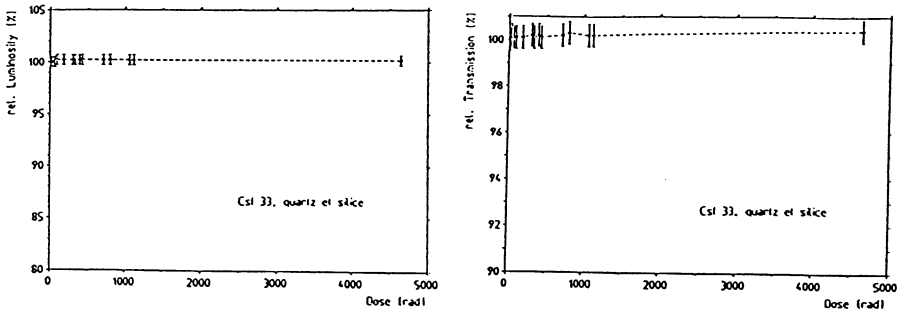

Figure 3: Relative light yield and transmission for green light (635 nm) as function of the exposure to a ^{60}Co source for one of the crystals.

Only 4 out of 28 samples showed a reduction of the light output between 3% and 20% after a dose of 500 rad. The most interesting one was a crystal cut from top of an ingot since a piece from the bottom of the same ingot showed only a small effect (fig 4 and 5). This boule was grown with the vertical Bridgman method. In this procedure the thallium and also the impurities are concentrated more on top of the boules rather than at their bottom. In this case the Tl-concentration on top was 980 ppm, while the bottom part only had 260 ppm. The light output of the top sample was merely 5 % higher than that of the bottom, reflecting the wellknown fact, that it is almost independant of the thallium concentration over a wide range (fig.6). This could indicates that a surplus of thallium causes the sensitivity to radiation. The conclusion unfortunately is not stringent since the chemical analyses showed a higher concentration of impurities (Fe, Rb and Ba) in the top sample.

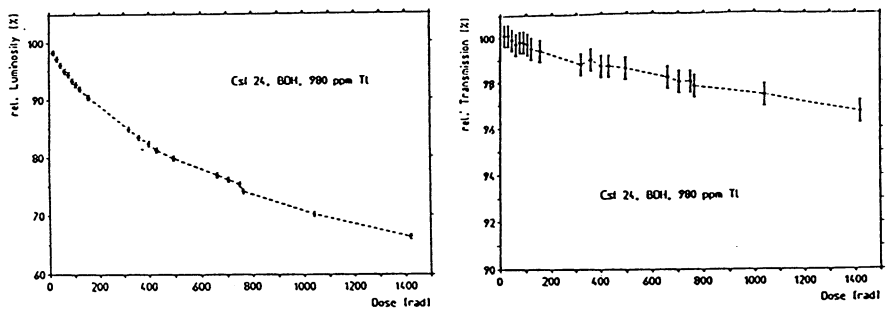

Figure 4: Relative light yield and transmission for green light (635 nm) as function of the exposure to a ^{60}Co source for crystal 24 cutted from top of a boule.

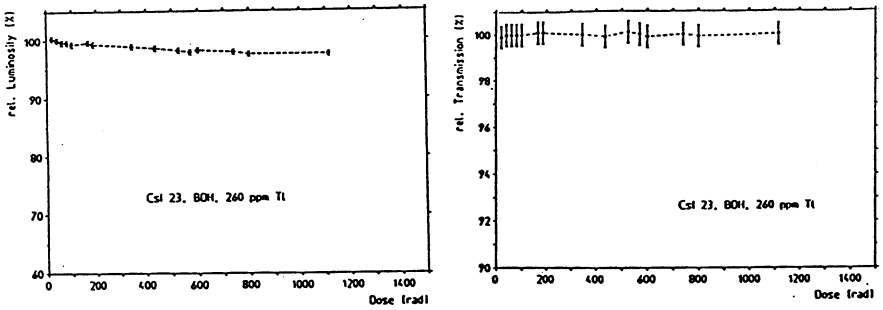

Figure 5: Relative light yield and transmission for green light (635 nm) as function of the exposure to a ^{60}Co source for crystal 23 cutted from bottom of the same boule.

To clear up the situation six crystals were grown at the Max-Planck-Institute in Munich. The raw material was the same for all (Chemetall, highest purity) but the amount of Tl-iodine mixed to it was varied, giving concentrations between 0.01 % and 0.6 %.

The light yield ranged from 28000 to 48000 photons/MeV for the crystal with lowest to that with the highest Tl-concentration (fig. 6), nicely reproducing the measurement of ref. 7 .

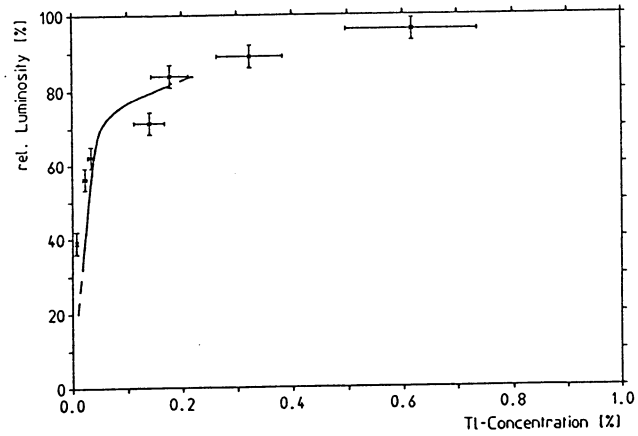

Figure 6: Relative light output as function of the Tl-concentration. The solid line is taken from ref. 7.

All crystals showed a relative strong afterglow, propable because they were cooled too fast after the growing, strongest those with low concentrations, but none of them was effected by the radiation.

4 Conclusion

CsI(Tl) gives high light output over a wide range (more than one order of magnitude) of Tl-concentrations. The radiation hardness is not effected by the doping, but very serious by impurities. High purity crystals are insensitive to radiation. Up to now it cannot be said, which elements or radicals cause the problems, and this study will go on.

From the fact, that most of the manufacturers provided us with radiation hard test crystals it cannot be concluded, that crystals from a mass

production will be as good.

As a rule of thumb one third of the price for CsI(Tl) crystals is the cost for the raw material and high purity CsI powder is only 50 % more expensive than the usual. An acceptable increase of the total price by 10 %, still low compared to other inorganic szintillators, should result in crystals with good radiation hardness.

5 Acknowlegments

We thank Eckart Lorenz from the Max-Planck-Insitute in Munich for many fruitfull discussions and for his help to the growing of crystals. Rolf Keil from PSI we thank for the promt chemical analysis.

References :

[1] G.J. Bobbink, A. Engler, R.W. Kraemer, J. Nash and R.B. Sutton
Nucl. Instr. Meth. 227 (1984) 470
[2] M. Kobayashi and S. Sakuragi,
Nucl. Instr. Meth. A 254 (1987) 275
[3] Ch. Bieler, D. Burkart, J. Marks, M. Riebesell, H. Spitzer,
K. Wittenburg and G.G. Winter
Nucl. Instr. Meth. A 234 (1985) 435
[4] S. Schloegl, H. Spitzer and K. Wittenburg,
Nucl. Instr. Meth. A 242 (1985) 89
[5] CLEO Collaboration: CLEO II - Updated Proposal CLNS 85/634, 1985
[6] D.E. Groom for the Task Force on Radiation Levels in the
SSC Interaction Regions, Nucl. Instr. Meth. A279 (1989) 1
[7] B.C. Grabmaier, IEEE Trans. Nucl. Sc.,
NS-31, No 1 (1984) 372

Applications of drift photodiodes in future experiments

G. Hall

Blackett Laboratory, Imperial College, London SW7 2BZ, U.K

Abstract

Recent developments of low capacitance photodiodes[1] are discussed, with emphasis on future applications in high luminosity collider experiments.

Introduction

In recent years silicon photodiodes have become essential devices in particle physics; several large experiments currently use them for scintillating crystal readout. Their pros and cons are now well known - the advantages include low cost, robustness, immunity to magnetic fields, a high quantum efficiency over a wide spectral range and, because of the unity gain, no sensitivity to bias voltage variations. However they require a low noise amplifier for read out, which to date has been a relatively expensive item, and to achieve a satisfactory signal to noise ratio a pulse shaping time of a few μsec is required. This comes about [1] because the electronic noise depends mainly on three parameters: the total input capacitance (C_{in}) , diode dark current (I_{dark}) and amplifier time constant (τ). This can be expressed by the Equivalent Noise Charge (ENC) which has the dependence

$$ENC^2 \sim a\,C_{in}^2/\tau + b\,I_{dark}\tau + c$$

Thus, for a diode with a large capacitance, a long time constant is required to reduce the contribution from the first term which originates in thermal noise in the first transistor of the preamplifier. Typically in high energy physics applications ENC values of ~400 electrons can be achieved with 1cm^2 photodiodes of 80pF capacitance and very low leakage current, ~1nA.

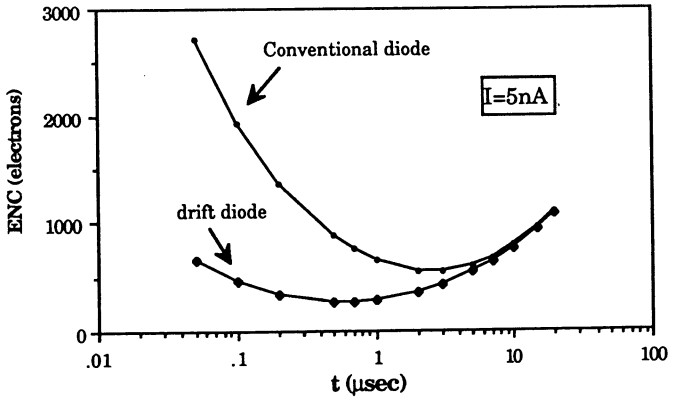

Fig.1. Comparison of the likely performance of a conventional photodiode, C~80pF, read out by a high quality JFET preamplifier and a drift photodiode, C~4pF, read out by matched CMOS electronics. The pulse shaping is assumed to be a CR-RC filter.

[1] *The work described here has been carried out by a collaboration between Imperial College, the Senter for Industriforskning, Postboks 124 Blindern, 0314 Oslo 3, Norway and AME A/S, Horten, Norway [5].*

It is hard to see how long shaping times could be tolerated in an SSC or LHC environment, even in a heavily segmented system with low occupancy. A reduction in time constant leads to an increase in noise and, eventually, loss of peak signal since the preamplifier rise time is ultimately limited by the input capacitance. Fig. 1 shows what might be achieved with a conventional diode and high quality amplifier.

Thus, although silicon is often cited as an intrinsically fast detection medium, it is usually difficult to take full advantage of its speed because of signal processing limitations. A possible way is to exploit alternative detector designs which trade off some of the detector speed against capacitance to reduce signal processing times.

The silicon drift diode

A natural way to achieve this is based on the idea of the silicon drift detector [2] whose principles are explained more fully elsewhere [3]. Briefly, a detector is constructed by implanting p-type electrodes into both surfaces of an n-type silicon wafer. The devices are fully depleted and a field is set up inside the detector which transports electrons liberated by ionisation to a readout electrode some distance away. These devices were originally proposed and demonstrated as position sensitive detectors and drift times of many μsec have been observed. However, perhaps the most interesting property of such detectors is their low intrinsic capacitance, independent of area, since the device capacitance is essentially defined by the geometry of the read out electrode alone.

A photodiode based on the same principle can be constructed by a modification to the design of a conventional diode. A uniform p-type implant forms the photosensitive surface in the usual way; the surface that is implanted to make the ohmic contact is instead subdivided into several cells as shown in fig 2. Each cell comprises a central n-type anode surrounded by a rectangular array of p-type cathodes. In our designs the cells are all connected together by the outermost cathode so that biasing becomes quite simple. A sufficiently large reverse bias is applied to the outermost cathode to fully deplete the detector. The anodes are connected to ground at the preamplifier and intermediate cathodes and the photosensitive surface float to their operating voltages. Electrons drift within each cell, in a direction orthogonal to the electrodes, to the anode.

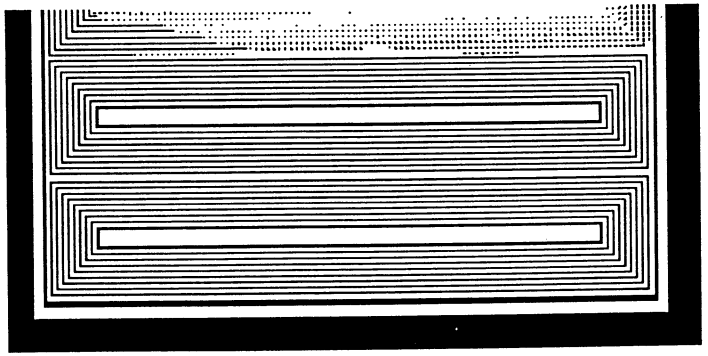

Fig.2 A section of one surface of a drift photodiode, showing two cells of the device. The photosensitive surface is opposite this one. Each of the five cells is 2mm by 10mm laid out so that a central anode is surrounded by field shaping cathodes to provide the drift field. The total active area is 1cm^2

The principle of the detector was first demonstrated in 1985 [4] and, indeed, many drift detector designs have been demonstrated by a collaboration between Kemmer, MPI (Munich) and others. Other manufacturers who have attempted to make drift detectors have rarely been successful. In

our own case several attempts have produced working detectors with readily observed drift properties but with leakage currents much higher than would normally be considered useful. This originally surprised us since the process being used to fabricate the detectors is a well established one which produces very low leakage microstrips and large area diodes, recently as low as 50pA/100μm/cm^2.

This year, after some research on the gettering processes responsible for reducing leakage currents in diode detectors, we succeeded in producing very high quality drift photodiodes [5]. Devices with leakage currents as low as ~2nA, at the operating voltage of ~90V, have been tested and the yield of the very best detectors is promising enough to believe that further optimisation can be achieved. The total capacitance for the 1 cm^2 area is ~4pF. Some results obtained are shown in fig. 3. The roughly parabolic time distance relationship is a characteristic of this design; the maximum drift time can be altered by material resistivity as well as design.

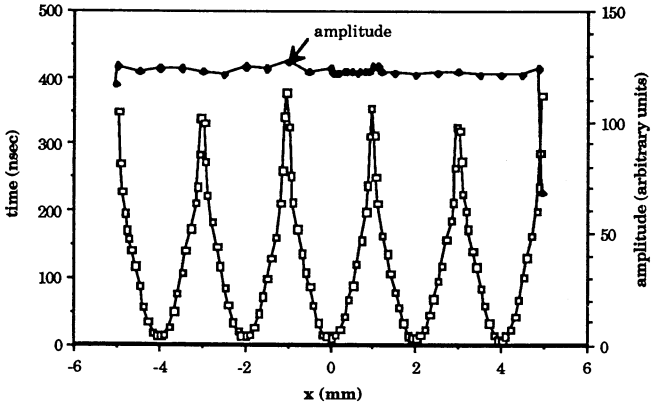

Fig.3. Variation of the drift time and amplitude with position of one of the drift photodiodes described. The detector was scanned with a 50μm diameter light spot at 850nm wavelength in a direction orthogonal to the anodes.

Immediate requirements

To demonstrate the full potential of drift photodiodes some further work is needed. A reduction in maximum charge collection time by reduction of cell width seems rather easy to achieve and optimisation for specific areas could be undertaken. More important are longer term studies of stability and radiation hardness and optimisation of the process to improve production yields. So far the detectors tested have shown pleasing behaviour since they appear to be very stable with no special attention paid to humidity, temperature,etc. More long term observations are certainly required. Radiation damage effects can be predicted as far as bulk leakage current changes; more subtle effects affecting charge collection as a consequence of both bulk and surface damage must be examined. Because of the simple design and the absence of detailed position measurements drift photodiodes are expected to be more radiation tolerant than complex drift devices.

Future developments

The results shown in fig. 1 could be obtained with a good quality preamplifier using a monolithic JFET as the input device. For large scale future applications these amplifiers are not likely to be suitable unless integrated devices can be produced. For photodiode read out the JFET is usually operated with a drain current of at least several mA to produce the high transconductance needed for low noise and the preamplifier is usually produced in hybrid (surface mount) technology. In contrast,a drift diode, with a capacitance of, say, 4pF could be easily matched to an MOS transistor produced on a CMOS chip. This is a major advantage for large scale applications - yet the system performance should be better than currently possible in several ways. Fig. 1 compares the performance that might be achieved with a CMOS circuit [6] and a drift diode assuming a transistor drain current of only 100μA. A very low power system could be implemented on a large scale. Jarron [7] has pointed out that lower detector capacitance also enables one to trade power consumption at the front end, signal processing time, segmentation and noise to achieve the required system performance. It is clearly possible to consider instrumenting individual cells using integrated circuit technology; this could lead to additional possibilities such as the local rejection of anomalously large signals caused by the passage of a charged particle through the diode.

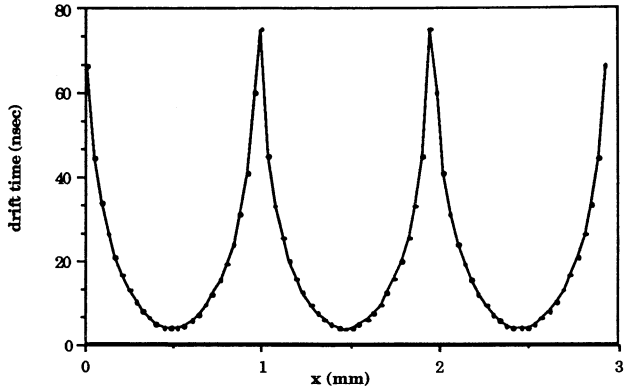

Fig.4. A simulation of three 1mm wide cells of a drift photodiode assuming similar properties to actual photodiodes tested. The reduction in the cell width leads to a significant reduction in collection times.

A shaping time constant of 0.2μs might well be acceptable for most calorimeter type applications at SSC, given likely occupancies, provided the time development of signals at the amplifier outputs are recorded. However it is still desirable to minimise charge collection times. This can certainly be done by optimising the cell design; fig. 4 shows what is expected for a cell width of 1mm compared to the 2mm used so far. A current pulse from uniform illumination of the surface will have the usual fast rise but an extended tail compared to a conventional diode. There are likely to be other geometries which can made just as simply for specific requirements.

The original motivation for the development of drift photodiodes was for scintillation light detection with improved resolution. This is expected to be of even greater importance in future with the use of faster scintillators. Some important materials, such as barium fluoride, have relatively low light output [8] and they also radiate at short wavelengths where conventional diodes are insensitive because of surface coatings. However previous work by one of us [9] has shown that high quantum efficiency at wavelengths as short as 200nm can be obtained with optimised processing; preliminary measurements indicate that our drift diodes show similar behaviour. It is not clear whether the spectral response can be extended further to the region of interest for liquid xenon scintillation; wavelength shifter coatings may be required.

Further improvements in charge collection speed can be obtained by cooling detectors and this can have a marked effect on leakage currents too. Electron mobilities are known to increase as $T^{-2.42}$ and leakage currents decrease as exp(-E/kT), with E≈0.5eV in the case of ideal, bulk-dominated currents. Fig. 5 shows some recent examples of our detector behaviour. Operation at liquid xenon temperature should lead to a further gain in speed of a factor ~3. We plan to verify this expecta-

tion using some of the present devices in the near future.

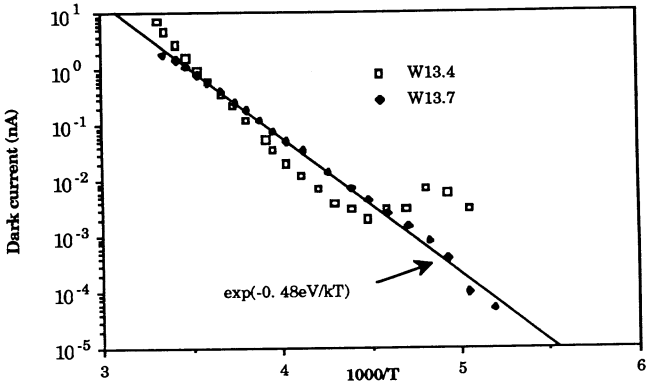

Fig. 5. Recent results for two photodiodes showing the reduction in leakage current with temperature. The line is a fit to the form shown for the diode W13.7.

Price is likely ultimately to be a major concern but at present it is too soon to estimate the economies of scale likely to be applicable in future. Any simplification of the design will certainly lead to eventual cost reduction. One might hope that simple drift devices like those described here could be produced for little more than conventional diodes. In addition one should not forget that the cost of the amplifier usually represents a major contribution to the total system; a device using a VLSI amplifier can contribute a major saving, as well as simplifying construction.

Conclusions

Low leakage current drift detectors have been produced for the first time in a commercial process. They offer the possibility of high rate readout of scintillators with better noise performance than obtained with conventional photodiodes and with the additional advantage of a low power large system when matched to integrated electronics. Further optimisation is required to improve yields and study the long term behaviour of the detectors but many promising applications can be foreseen. Although the technology is already fairly advanced to realise them on the scale of an LHC/SSC detector will require a sustained R&D effort. Such an effort would seem well justified given the potential.

References

1. V. Radeka. Ann. Rev. Nucl. Part. Sci. 38 (1988) 217.
2. E. Gatti & P. Rehak. Nucl. Instr. Meths. 225 (1984) 608.
3. G. Hall. Nucl. Instr. Meths. A273 (1988) 559.
4. J. Kemmer et al. Nucl. Instr. Meths. A253 (1987) 378.
5. B. Avset, J. Ellison, L. Evensen, G. Hall, T-E. Hansen, S. Roe, R. Wheadon. IC/HEP/89/5, March 1989. To be published in Nucl. Instr. Meths.
6. These estimates are my extrapolation of the performance of an amplifier under design at Rutherford Appleton Lab and Imperial College.
7. P. Jarron. These proceedings.
8. I. Holl, E. Lorenz, G. Mageras. IEEE Trans. Nucl. Sci. 35 (1988) 105.
9. T-E. Hansen. Nucl. Instr. Meths. A235 (1985) 249.

LARGE SCALE PRODUCTION OF SCINTILLATOR CRYSTALS

BDH Ltd.
K. Matthews

BDH

MERCK CRYSTAL GROUP

Production Sites:

KORTH	Keil, West Germany
BDH	Poole, U.K.
OPTOVAC	N. Brookfield, MA, U.S.A.

BDH

KORTH CAPACITY - BaF_2

10 Furnaces

Maximum Diameter 210mm

Maximum Length 280mm

Maximum Weight Crystal ~ 23Kgm

Growth Cycle 3 / 4 weeks

Therefore Maximum Capacity ~ 3 tonnes / p.a.

BDH

MERCK GROUP - BaF_2 PROJECTS

Project		Number	Kgm
CRN Strasbourg	100mm Ø x 140mm Hexagons	100	~ 450Kgm
UNIV Padua	85mm Ø x 120mm Hexagons	60	~ 190Kgm
UNIV Bonn	45mm Ø x 85mm Cylinders	8	~ 4Kgm
INFN Milan	145mm Ø x 175mm Complex	8	~ 100Kgm
Nuclear Res Karlsruhe	145mm Ø x 150mm Complex	46	~ 320Kgm
GSI Darmstadt	65mm Ø x 200mm Hexagons	60	~ 160Kgm
LETI PET Scanner	45 x 18 x 5mm	4500	~ 125Kgm
TAPS Collaboration	68mm Ø x 250mm Cylinders / Hexagons	320	1100Kgm
Range of Projects ~ $7 / cc			~ 2500Kgm

BDH

BDH CAPACITY - CsI

220 Furnaces

Maximum Diameter 98mm

Maximum Length 330mm

Maximum Weight Crystal ~ 11.5Kgm

Growth Cycle 3 / 4 weeks

Therefore Maximum Capacity ~ 30 tonnes / p.a.

BDH

CRYSTAL GROWING FURNACE

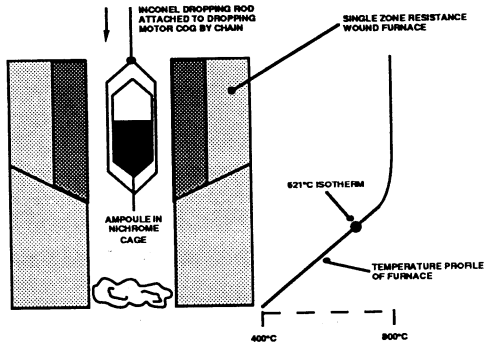

BDH

MERCK GROUP - CsI PROJECTS

CORNELL CLEO 2	50 x 50 x 300mm	50 80	1984 1985	170Kgm 270Kgm
GRENOBLE / UNIV LYON	104mm Ø x 30mm Hexagons + Trapezoids	130	1985	125Kgm
CORNELL CLEO 2	Tapered trapezoids 800 to 1000cc various	3696	1985 to 1988	15.6 tonnes
U Karlsrake CERN Crystal Barrel	Tapered trapezoids ~ 600cc various	1380	1988 to 1989	3.7 tonnes
KEK Japan (Pure CsI)	70 x 70 x 300mm	450	1989	3.0 tonnes

Budget Price $1.6 to $2

BDH

MELT PURGING & FILTRATION APPARATUS

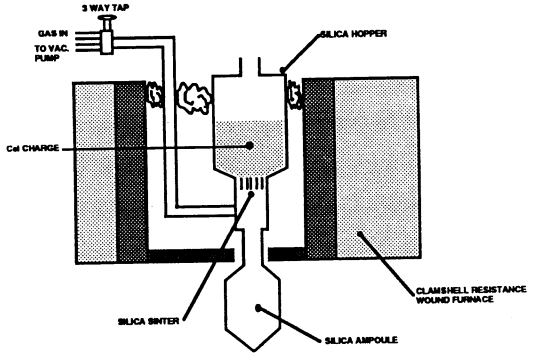

BDH

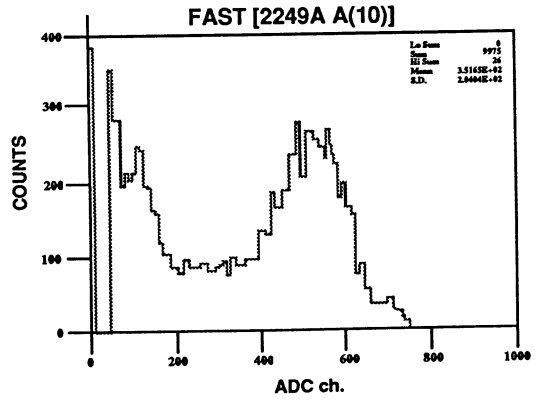

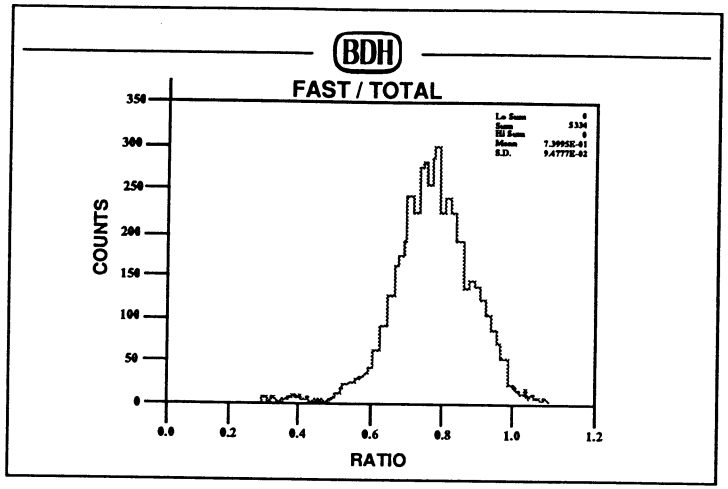

BDH

OTHER MATERIALS

Sodium Fluoride	BDH
Zinc Tungstate	BDH
Cerium Fluoride	OPTOVAC
Lead Fluoride	OPTOVAC

CRYSTAL CALORIMETERS FOR FUTURE HIGH LUMINOSITY HADRON COLLIDERS

E. LORENZ

MAX-PLANCK-INSITUTE FOR PHYSICS AND ASTROPHYSICS

FOEHRINGER RING 6, D8000 MUNICH 40, FRG

Abstract: Prospects and limitations for the use of high resolution electromagnetic scintillation calorimeters for future high luminosity colliders like LHC or SSC are discussed. This report summarizes mainly the ideas and presentations as contributed to this conference. The main outcome of the discussions was that scintillation crystal calorimeters are only useful for central general purpose detectors with a rather large radius of the inner cavity. The large radius is dictated by good two track separation, resolution time and reduced radiation loads.

1. Introduction.

In the quest for understanding the fundamental laws of interactions the high energy physics community is pushing the range of research well beyond the Z^0 mass scale. New high energy hadron colliders are on the drawing boards or their construction might start soon(LHC, SSC and UNK). In hadron colliders the interesting physics will only be a minute fraction ($<< 10^{-8}$) of the total cross section thus pushing the required luminosity to extremly high values. The expected interaction rate will be around 10^8/sec at the SSC and up to 2.5×10^9/sec at the LHC, respectively. This poses a challenge to build detectors that can survive the high radiation levels, being dominated by the interactions themselves, and are able to filter out the reactions one is looking for.

In the past the decisive reason for many discoveries was the superior resolution of detectors. On the other hand the tools for tagging this physics were very often the measurements of leptons -e, μ- and to some extend γ's. Possible lead reactions are:

$H \rightarrow \gamma\gamma$, $H \rightarrow Z^0Z^0 \rightarrow e^+e^-e^+e^-$, $e^+e^-\mu^+\mu^-$, 4μ

or $B \rightarrow J/\psi\, K \rightarrow e^+e^-\, K$ or $B \rightarrow K\gamma$

High resolution will be crucial to discover and to study in detail reactions like the ones mentioned above.

In this paper the possibilities for the construction of a high resolution electromagnetic calorimeter for detectors at the LHC, SSC or UNK will be discussed. The conclusions drawn here are mainly the result of contributions to this conference and from the discussions of the working sessions.

Presently the highest resolution for energy measurements of electrons and γ's can be achieved with fully active scintillation calorimeters based on high Z crystals. Their energy domain will be in the region between, say 1 to about 200 GeV. At around 200 GeV their advantages against sampling type calorimeters will diminish. The upper limit is not so much set by material parameters but more by the lack of past precision studies, difficulties of calibration and understanding of small systematics at a level of 0.1-0.2%.

Inherent to any high precision measurement is that only one particle should be present in space and time in the volume of the relevant calorimeter section. An immediate consequence for high multiplicity reactions is the subdivision of the calorimeter into a large number of cells with independent readout. The characteristic area for measurements for <1% error is (5 Moliere radii)^2. The characteristic time is the occupancy of ≤ 0.1 particle/(5 MR)$^2\tau$; τ being the readout integration time or the scintillation decay time. Proven materials have a MR of 2-5 cm and a τ ranging between a few nsec and μsec. In order to satisfy both conditions one has to install the calorimeter at a sizeable distance from the interaction point. Both the flux per characteristic area and time scale with about $1/r^2$. Fig 1 shows the expected flux as a function of the radial distance from the interaction point for both the SSC and LHC, from ref [1]. Also the corresponding integrated radiation levels/year for 'thin' detectors are given. Inside calorimeters the

local radiation level will rise due to the showering process. In fig.1 also the limits of tolerable radiation dose/year are given for two materials. At present all possible materials have some deficiencies.

The planned detectors for LHC, SSC, UNK will be large and complex and have a long construction time. The detector structure will be onion shell like with one detector element encapsulating another one. Large detectors have their own rules. As detectors become larger and more expensive they have to be more conservative. The design parameters have to be frozen rather early thus leaving very little room for incorporating ongoing developments. High reliability becomes more important as access and repair inside a large 4π detector becomes nearly impossible.

In the following chapters we will present a model detector as basis for discussions. Then we will discuss in detail the resolution limits. In the material chapter we analyze mainly the prospects for using well proven material. In the following chapter readout options and problems are discussed. The next chapters deal with calibration, reliability, prices and possible time scales. Finally some areas for urgent research are listed.

2. A model detector as a basis for discussion.

In order to facilitate the discussions a model em calorimeter for a general purpose detector is used. Fig 2 shows a quadrant of the inner section.

A barrel shaped em calorimeter surrounds some type of tracking detector around the interaction point. The em calorimeter itself is encapsulated by a hadron calorimeter of typical 6-8 hadronic absorption lengths depth. The calorimeters are mounted inside a solenoid. The em calorimeter consists of crystal slabs pointing towards the interaction region. We assume inner cavity dimensions of 2 m radius and 6 m length with rather large holes along the beam direction (space angle coverage of 95% of 4π). For good e/h separation a subdivision in depth at around 4 and 15 rl is assumed. The total

depth will be between 24-27 rl. For cost reasons one might consider to shorten the calorimeter and to use the hadron calorimeter as a backup tail catcher. Unfortunately the resolution of current hadron calorimeters is not good enough for this purpose.

A possible readout could consist of small wave length shifter plates coupled to a multiplexed photodiode readout system. The intrinsic cell size would be rather small with typically 2.5x2.5 to 3.5x3.5 cm^2 cross sections. The crystals are hold in place by a pigeon hole carbon fiber matrix with walls progressing in thickness and strength towards the rear.

As the total no of individual elements range between 100 000(simplest version with no depth subdivision) to 600 000 one cannot install mayor parts of the readout electronics outside the detector for easy access. The electronics has to be mounted inside the calorimeter. From the radiation levels inside the em section (see fig 1) it follows that the readout electronics and sensors should be located either at the front surface or at a depth of at least 15 rl . The total weight of such a calorimeter will be in the range of 200 tons.

As can be seen from fig 1 the flux and radiation levels in the very forward direction will be extremely high, well above our best known material in radiation hardness- BaF_2. The only solution for high resolution calorimetry in the forward direction might be to place calorimeters far upstream of the interaction point and conserve the large radial distance from the beam line. At present no solution is found for the very forward direction due to price, radiation hardness and insufficient time resolution. From now on we will consider only 'central' calorimeters.

Before analyzing possible materials we will discuss the resolution in some detail.

3. Resolution

In general the analytical form of the dependence of the resolution as a function of incident particle energy is given by:

$$(d\sigma/dE)^2 = (A_1/\sqrt{E})^2 + C^2 \qquad (1)$$

In the past this was sufficient for sampling calorimeters with $A/\sqrt{E} >> C$ while for the envisioned high resolution calorimeters to be operated in a large energy range a more refined equation has to be used.

$$(d\sigma/dE)^2 = (A_0/E)^2 + (A_1/\sqrt{E})^2 + C^2 \qquad (2)$$

the first term describes the contribution from the various 'noise' terms:

$A_0 = \sigma_{rn} + \sigma_{pu} + \sigma_{n\,bg} + \sigma_{ag} + \sigma_{ir} + \sigma_{hd}$

with

σ_{rn} = readout noise summed in quadrature over the cells of $(5MR)^2$area

σ_{pu} = contribution of coherent pickup noise

$\sigma_{n\,bg}$ = noise induced by low energy neutrons

σ_{ag} = noise generated by afterglow

σ_{ir} = noise from induced radioactivity

σ_{hs} = noise from the so-called hadronic spray

particularly bothersome can be the so-called hadronic spray caused by secondary particles originating from the same reaction and interacting somewhere else in the detector. The hadronic spray scales with about $1/r^2$, e.g. it will be more of a problem for compact designs including the very forward and backward high energy particle flux and beam halo. The A_0 term can become quite big for scintillators of low light yield or short readout integration time. Nevertheless the A_0 term is only relevant for energies below 1 GeV.

The second term, $A_1/\sqrt{E}$, takes the statistical fluctuations of the

photoelectrons into account. One expects $A_1/\sqrt{E} \approx 1/\sqrt{n}$; n = number of photoelectrons. For the very best scintillators the high light yield should give values for A_1 well below 1%. Detailed studies have shown that the $A_1/\sqrt{E}$ term is about a factor 2-3 worse than $1/\sqrt{n}$. This so-called scintillation broadening is caused by local effects, for example variation in activator concentration. For a model with a 5% sigma of the scintillation light yield variation per cc it could be shown by Monte Carlo studies that the resolution will improve with about $1/\sqrt[4]{E}$. We expect A_1 to be around around 1-3%x$\sqrt{GeV}$ for common materials (BGO-fast component of BaF_2).

The third term C is very important because it will dominate the resolution at energies above about 10-20 GeV. A closer inspection of this term shows that this term is rather complex and is actually slowly varying with energy.

$$C^2 = \sigma^2_{leak} + \sigma^2_{dm} + \sigma^2_{ical} + \sigma^2_{nlin} + \sigma^2_{nc} + \ldots\ldots \qquad (3)$$

σ^2_{leak} = fluctuation of the front-, rear- and side leakage out of the fiducial calorimeter volume. The front leakage is very small and can be neglected in general. The rear leakage is caused by insufficient depth of the calorimeter. Rear leakage fluctuations will slowly increase with energy. Side leakage depends on the transverse cut applied to the data.

σ^2_{dm} = fluctuation of energy deposited in dead material between crystals, like mounting or incorporated readout. As a rule of thumb the fluctuations are about 1/3 of the energy deposited. This term will very slowly drop with energy.

σ^2_{ical} = cell to cell intercalibration error. For very small cells this error will go down with increased energy. For large cells (few rl^2 cross section) this error is nearly independent of energy.

σ^2_{nlin} = effects from nonlinearity in light yield due to doping profiles or variations in light transmission. Use of intrinsic scintillators

with low concentration of impurities or better production methods should make the first contribution small. The second contribution is more user dependent. Temperature gradient effects for scintillators with temperature dependent light yield would contribute also to this term. It should be possible with modern instrumentation to trim light collection variations to very low values. These methods have not yet been fully explored in the past. In general the so-called nonlinear effects will go down slowly with increased energy as the shower spreads more and more over the cells.

σ^2_{nc} = contribution from the so-called nuclear counter effect. Particles from the shower process sometimes pass the optical sensor which is normally highly sensitive to charged particles (Cerenkov light in photomultiplier windows, particles passing the depletion layer of photodiodes or the sensitive volume of photosensitive gaseous detectors). There is no general rule about its dependence on incident energy; depending on the device, its location and sensitivity ratio the effect can go down or increase with energy.

In principle all these contributions can be made small and controllable. With extensive Monte Carlo simulations with EGS one has a good handle to understand them and concentrate the efforts accordingly. The leakage term and the intercalibration term are the most difficult ones to control. The former contribution can only be corrected by the very costly enlargement of the depth. The problematics of the latter are addressed in a separate section.

To highlight the some of the contributions to the so-called constant term we show in fig 3 the results of Monte Carlo simulations from an old detector proposal[2].

Presently the best value of resolution at E>>5 GeV has been obtained by the L3 collaboration with a BGO calorimeter [3]; see fig 4. At around 50 GeV -where their resolution is dominated by C- a value of 0.5% has been measured. This error is dominated by the leakage term. The calorimeter is 21 rl deep. With our modern tools at hand and a large data bench for all parameters of individual cells one can expect a short term C value of 0.1%

and 0.2 for long term stability (24-27 rl deep calorimeter, corresponding energy range), provided that the calibration will be adequate and that radiation damage is small.

4. Radiation damage

The radiation levels around the interaction regions will be excessive, only experienced up to now close to beam dumps. Due to current believe, the radiation levels originate from the interactions themselves and not from beam-gas interactions or beam halo. Also the background from low energy neutrons will be enormous. We refer for details to the contribution from D. Groom to this conference[1]. The high radiation loads will result in damage of the detector elements. As a consequence the resolution will be affected. One has to consider radiation damage for all incorporated elements: the crystals, the wrapping material (optical parameters), intermediate light transporting elements or optical joints, the photosensors and the readout electronics buried inside the calorimeter. From fig. 1 it is obvious that the most trivial solution against radiation damage is to increase the radius up to the limit given by available funds (for physics reasons this is not always obvious like increasing π,k-μ decay volume).

The condition of large two track separation for high resolution requires that the calorimeter has to be installed at a radial distance from the interaction point where the radiation level is nearly acceptable even for radiation resistant BGO.

Radiation damage in crystals is firstly manifesting itself in reduced transmission due to the formation of color centers, while damage of the intrinsic scintillation process has not been observed for common scintillators up to levels of 10^9 rads (no tests at higher levels have been published up to now). The origin for reduced transmission are impurity atoms embedded in the crystal lattice and acting as trapping centers. Presently

procedures for scintillator crystal growth control the levels of impurities to the order of ppm with rather large fluctuations. It is this fluctuation- coming both from meltstock production and from segregation effects during crystal growth- which makes radiation damage studies so inconsistent. The reduction of impurities down to the ppb level would be very costly; also the dangerous impurities are often not known. We have only indications that some heavy metals like Pb in BaF_2 or Fe in BGO are particularly bad. Ongoing studies are leading to a better understanding of the damage process and to possible ways to cure it. The direction of research is not so much to improve the purification but to find ways to deexcite the trapping centers either by heat, light or addition of other impurities which have energy levels close to the trapping atom such that the trapped electrons can be transferred and subsequently the electron can decay to the valence band via emission of light. For example the Shanghai Institute of Ceramics was able to harden Fe containing BGO by adding the rare earth element Eu in ppm quantities [3]. Because the electron transfer takes some time a small afterglow in the far red spectrum can be observed. More research in the field of radiation hardening is crucial.

Another indirect cure of the radiation hardening consists in using smaller crystal volumes with shorter light paths. The 'visibility' of radiation damage scales in first order with the square of the cell length.

One tends to look only to the radiation damage of crystals. An equally important area of studies is the radiation resistance of the light sensors and the electronics. For example standard CMOS memories start to show damage already in the krad region where better crystals are still perfect to use.

For detailed information of radiation resistance of possible crystals we refer to the next chapter.

5.Crystal materials

Possible candidates for scintillators must fulfill the following criteria:

i) short radiation length

ii) sufficient scintillation light (>500 photons/MeV)

iii) radiation hardness to withstand the radiation levels of the LHC/SSC

iv) short scintillation decay time

Other parameters like mechanical, chemical, and thermal stability, long hadronic absorption length with respect to the radiation length(rl) etc. have also to be considered but are less decisive. As already pointed out in the introduction one has to be rather conservative for large detectors. A detailed data bench for all material parameters is needed, which can only be assembled over years. Also it must be guaranteed that industrial production is well under control and has reached a sizeable volume. In the past it took about 6-10 years of research and production for establishing a new material. Therefore is was concluded that only materials in widespread use should be considered for the first round of detectors for the LHC/SSC.

Our presently best material for high resolution calorimetry-CsI(Tl)- cannot be used because its long decay time and weak radiation resistance.

We have 3 possible candidates for a calorimeter as outlined in section 2 at hand: BaF_2, pure CsI and BGO. The following table lists the most relevant parameters:

	BaF_2	CsI	BGO	
radiation length	2.05	1.86	1.13	cm
hadr. absorption length	21.4	36.4	23	cm
Moliere radius(MR)	4.3	3.8	2.7	cm
$<\lambda_{scint}>$	220*	300*	440	nm
decay time	0.6*	10; 30a*	300;60	nsec
light yield	1000-2000	1000-2000	8000	phots/MeV
large volume price	8**	1.6	10**	$/cc

---

*) = fast component only

**)= extrapolated to large volume production with big uncertainties

BaF_2 has by far the shortest scintillation time [4] and highest radiation resistance; it can withstand integrated radiation levels of the order of 10^8 rads[5]. But it should be mentioned that radiation damage studies have been concentrated on the slow component and only relatively short samples(< 10 rl length) have been tested. A detailed study of radiation damage for the fast component is missing. The rl and the Moliere radius are the worst of the 3 materials. The unfavorable ratio of hadronic absorption length/radiation length makes e/hadron separation more difficult and increases also background from nearby interacting particles. Also its mechanical properties are not ideal. The crystals cleave easily, making the construction of a 200 ton calorimeter difficult. The surface has to be very clean in order to collect the fast component in long crystals. This cleanness has to be conserved over many years. On the other hand its temperature stability is a big advantage over CsI and BGO which would both need temperature stabilization or tracking at a level of 0.1^0C. Some parameters, like the detailed spectrum and light yield of the fast component are still under study, see report by P. Mine at this conference[6].

Recently fast scintillation has been discovered in pure CsI [7]. Decay constants of 10 and 23 nsec are well matched to the rates at the LHC/SSC. The material is by far the most attractive due to its superior mechanical properties and its low price. Still some fundamental research has to be done, see also the conference contribution from C. Rosza[8]. The main uncertainty is the unknown radiation resistance. CsI(Tl) is radiation 'soft', and its

damage does not cure with time. Not very much is known about the mechanism and the impurities. At this conference D. Renker reported about new studies with CsI(Tl) crystals grown from high purity meltstock [11]. Although the measurements were not yet completed, the crystals showed at least a factor 10 better resistance when compared to data from previous publications. In general radiation resistance is linked to impurities. Therefor we expect that high purity undoped CsI has also a high radiation resistance. New results are expected soon.

BGO is the most favorable material with respect to short rl and Moliere radius. In principle one could build a BGO calorimeter with about 5x smaller volume of crystals compared to BaF_2 if the basis of selection would be the 2 track separation. The scintillation time of 300 nsec is long but the light yield is large enough to allow one to clip the signal to 20-50 nesc. The main disadvantage is its weak radiation resistance. Normal production quality cannot be used. Recently it was possible to develop radiation hard BGO [3] which would even without further improvements be acceptable for the barrel calorimeter.

If our present understanding for radiation damage in scintillators is correct then there is good hope to improve the radiation hardness of all 3 candidates. Intense research and further theoretical work is absolutely necessary. Also some method is necessary to predict radiation hardness at the production level in order to guarantee radiation hardness for a large production.

A calorimeter for the model detector would need in the order of 20 cbm BGO or 40-50 cbm CsI or BaF_2. This is about a factor 5-15 bigger than existing calorimeters like in the L3 or CLEO II detector. Therefor one should not expect serious production problems given sufficient preparation time of 1-2 years. According to industry the price for BGO and BaF_2 is dominated by

the production process while for CsI the raw material price is substantial. It should be pointed out that industry has not yet mastered the production of long BaF_2 crystals while particularly CsI can be grown into very large ingots. According to industry information no shortage of high purity raw material is expected.

The research on new materials should be intensified if the start of LHC/SSC is substantially delayed. Directions of research should be for materials with short radiation length and short decay time. P. Mine [6] and V. Peskov [10] reported about new materials that fulfill these criteria. Details can be found in the proceedings of this conference.

6. The readout

The scintillation light has to be converted into electrical signals for processing and recording onto some type of storage medium. The general requirements for the light sensors are:

- i spectrally matched to the scintillator
- ii high quantum efficiency
- iii efficient coupling to the crystals
- iv insensitive to magnetic fields
- v large dynamic range and good linearity
- vi low intrinsic noise
- vii readout speed matched to particle flux
- viii low drift and long system life times (>10^5years/cell)
- ix prices in the order of 10-30$/cell
- x low operation costs
- xi compact
- xii simple to operate
- xiii sufficient radiation hardness

The light yield of useful crystals is generally low, in the range of a few 100 to 2000 photons/Mev deposited energy. Even with the relatively modest size of crystal slabs only a small fraction of this light is collected at the sensor plane, which has to be either the front or the rear surface of the slabs because of hermeticity of the calorimeter. Therefore only light sensors with high quantum yield and very low intrinsic noise are acceptable. We have presently three types of optical sensors at hand:

- i vacuum photocells without or with some built-in gain like phototriodes, photopentodes or photomultipliers(PM's)
- ii low noise PIN photodiodes(PD's) or drift photodiodes(DPD's)
- iii light sensitive gaseous detectors with internal amplification like light sensitive proportional chambers or streamer chambers

None of the presently available sensors fulfills all the above listed requirements. Vacuum photodevices like PM's are sensitive to magnetic fields, bulky, intrinsically not stable and relatively expensive. Their main advantage is the high speed, easy coupling to crystals, low operation cost and proven mass production technique.

By far the most promising sensors are silicon photodiodes. They fulfill most of the requirements except iii), vi) and in case of UV emitting crystals ix) when used with a plastic coating. The main limitation comes from noise which is in first order proportional to the diode area. PD's are inherently fast; only for noise reduction one has to use special preamplifiers and shaping amplifiers with the caveat of reducing substantially the readout speed and in turn the time resolution. If one relaxes the energy resolution at the very low end of the energy range, say below 10-20 MeV, the PD readout can be made much faster. A time separation of two events in the order of 20 - 200 nsec should be possible with state of the art electronics provided that

the scintillator decay time is not too long. There is a rather simple solution to overcome the area mismatch of PD's and crystal end faces and also the spectral mismatch by coupling small diodes to so-called fluorescent flux concentrators (FFC's) . These are wavelength shifter plates acting both as efficient light collectors and flux concentrators onto small area PD's or DPD's and converting short wave scintillation light to a wavelength where the diodes are highly sensitive. This technique has been tested recently with a Bariumfluorid calorimeter[12] and is used for example in the crystal barrel calorimeter. One can obtain the necessary system lifetime of $>10^5$ years/cell by coupling to one FFC many diodes and reading them out in parallel. This concept also reduce very much the background from charged particles passing occasionally the depletion layer of a diode. (This is one of the reasons why in the proposed model calorimeter the readout should not be placed at the depth of the shower maximum). For example the parallel readout with 4 diodes will be used in the CLEO II electromagnetic calorimeter[15].

In case a readout with ≥100 nsec integration time can be tolerated photodiodes on the basis of the drift concept (DPD) are a promising alternative to ordinary PD's. In DPD's one trades in speed for low noise by drifting electrons to a small area pickup anode. With the appropriate geometry one might both collect electrons within 200 nsec and obtain a noise reduction of about a factor 5-10 compared to standard PD's. For details of a practical device see the contribution to this conference by G. Hall[13].

Recently large area avalanche PD's became available commercially. Due to their internal amplification a reduction in noise and improved immunity against electromagnetic interference is expected. Still a suitable gain stabilization system has to be found. Recent progress on avalanche PD's has been reported during this conference by A. Lightstone [14].

In the past few years significant progress has been made to build light

sensitive gaseous detectors with internal gain [6,10, further references there]. These detectors are only sensitive to UV light below 250 nm. This limits their potential use only to the fast component of Bariumfluoride and to some recently discovered scintillators as mentioned in a previous section. The insensitivity to the long wavelength UV and the visible part of the spectrum has the advantage to suppress the slow decay component which is present in all inorganic scintillators. One can obtain similar performances for the PD readout by choosing the appropriate dye for the FFC's. The main disadvantage of gaseous photodetectors will be their low tolerances on radiation damage, additional gain calibration and the difficulty to design a practical system built into a layered 4π calorimeter. It will be difficult to incorporate redundancy in cases of chamber breakdowns. The calorimeter will be completely inaccessible after the assembly. Large area chambers will increase the complexity of the mounting of the individual cells and in turn add a lot of inactive material inside the calorimeter. It will take still some years of R&D for practical solutions.

Finally we would like to mention a possible solution for very fast timing information in case of bunch crossing rates in the order of 10 nsec. Recently we have tested a device consisting of a 1 mm scintillating fiber coupled to a small area avalanche photodiode [14,16]. This PD is operated in the so-called Geiger mode with an excess gain of 10^8, e.g being sensitive to a single photon. Such a device has a time resolution of <1 nsec. With an active quenching circuit it can be made sensitive only during bunch crossing time. The device is extremely compact and can be attached to each cell. The large gain minimizes additional electronics. By selecting a dye sensitive to the fast component only (BaF_2, pure CsI) one can reduce false triggers from the normal slow component.

7. Calibrations

High resolution of a multicell calorimeter depends crucially on the knowledge of the conversion factors of the deposited energy into an electrical signal and the tracking of these factors over the operation time of the experiments. Calibrations have to be precise to <0.2% if one wants to operate the calorimeter within the limit of the intrinsic material resolution.

Somewhat arbitraryly the problem can be split into short term fluctuations, say on a daily scale and into long-term drifts over a time scale of years. Sources of short-term fluctuations are usually temperature effects of scintillation light yield, conversion factors of the light sensors and electronics and for example the variable transmission of BGO under the influence of radiation. Long-term drifts are usually caused by nonrecoverable radiation damage of crystals, ageing of the light sensors and electronics components. It is not possible to transport the calorimeter to a test beam and to perform the calibration. Relative calibrations can be performed with light pulsers illuminating either directly the light sensors or passing the light at first through the scintillator and exciting the WLS. Although light pulser calibrations are very convenient, they do not exactly calibrate the correct calorimeter performance because of the light flash is not generated over the entire crystal volume according to the showering process and does not have the same spectral distribution. The calibration of a PM like readout is more complicated compared to the PD readout because the former devices have an internal amplification with drifting gain. In the case of PD readout precision charge pulses can be injected into the preamp inputs for calibration of the entire electronics readout chain. Obviously the light pulser system itself has to be calibrated and monitored for drift, too. The real difficult task is the absolute calibration, which has to cover the full range of expected energy. Calibrations with radioactive sources in the 1-3 MeV region are of such a low energy that they cannot be distinguished

from noise. Even if this would be possible then the long extrapolation to the multi GeV region would be unreliable. Recently it has been proposed by Zhu[17] to use a small RFQ accelerator to excite a small target located in the center of the detector and in this way to generate bursts of gammas in the 10-20 Mev. The main disadvantage of this very promising method is, that it can only calibrate the inner section of a layered calorimeter. Normal hadronic interactions produce an abundance of charged particles. About 1/4 of these mostly minimum ionizing particles will pass the calorimeter without interacting and will deposit about 250 MeV energy uniformly over the cell length. Due to the Landau smearing one will not observe a sharp line, but due to the large statistics a precision of 0.2% should be obtainable within a few hours. As usual the software overhead for a calibration of 100-600k cell system will be quite big.

Unfortunately no acceptable solution for absolute calibration at the upper end of the energy range has been found. Electrons from converted gammas might be used for a (poor) calibration in case of a high resolution tracking device inside the calorimeter. Even for a 1% radiation length beam pipe one expects a flux of the order of 10-100 electrons(positrons)/cm^2 sec, mostly in the energy range from 1-10 GeV. Z^0-> e+e- or Y->e+e- decays might serve as calibration sources.

Finding an 'in situ' absolute calibration in the high energy range is one of the major research items for the next years.

On a more general basis it can be concluded that crystals and readout elements of intrinsically high stability should preferentially be used even if their performance is somewhat inferior compared to the best available materials.

8. Reliability

As already mentioned reliability has a direct impact on the resolution. In

calorimeters one cannot build in redundancies like in multiwire tracking chambers. Multiple track measurements guarantee that failures of single wires will not affect the measurements very much. In calorimeters a dead cell is not only a 'black spot' , but it will also reduce the performance of the surrounding area due to the lateral shower spread. Defect cells will reduce the resolution of at least 10 times their own area. The complexity of large 4π detectors will not allow easy access to most of the components for repair. The conditions will be particularly stringent for the calorimeter because the dead material for mounting the crystal has to be minimized and no device for easy extraction can be planned, e. g. except for a few spots the calorimeter will be very likely inaccessible for the entire life of the detector. The frontend electronics will be buried inside the calorimeter. Therefore the components have to have an extreme high reliability going beyond todays performance of electronic circuits. The only solution for increasing reliability is the use of multiple parallel circuits. Obviously this has an impact on the price. Also the most advanced devices cannot be used because they lack long testing. In summary the question of reliability has to be taken into account in the very early phase of the design.

9. Possible timetable

High resolution detectors of large volume and complexity need long construction times. A calorimeter as outlined in section 3 would take at least 8 years to be build while a time of 10 years is more likely.

Based on past experience a possible time scenario could be:

3-4 years of R&D

1-2 years of finalizing the overall detector design

3-4 years of production and assembly

1-2 years of tests and run-in

with partial overlap in time. In case specifications are relaxed and funds

are not constraining the production a shorter overall time is possible.

We would like to iterate that at the moment of finalizing the overall design of the detector there is very little room for modifications.

10. Comment on prices

Prices were not a primary subject of the discussions. Also it is very difficult to make projections. Large volume production, new improved production methods or more stringent requirements for radiation resistance. can alter the priceses over a large range. Nevertheless some comments can be made:

i) The overall calorimeter price will not be dominated by the crystal price. Very likely the crystal price will be <50% and in case all labor is included < 30% of the total investment. For example the complex readout, calibration tools, high strength lightweight mounting and high reliability will drive the costs up. On the other hand the crystal price will be the most transparent one.

ii) When comparing different calorimeters also the cost impact on the surrounding elements has to be taken into account.

iii) The initial price will be high while the operation costs for an 'all solid' calorimeter will be low.

The overall cost of a calorimeter like the model under discussion will be clearly well above 100 MSFR.

11. Areas of urgent research

The discussions during this conference have revealed areas where intense research is needed in order to provide solutions for high resolution calorimetry for the first generation of detectors at the SSC or LHC.

The most important issue is the improvement of the radiation hardness of

the most likely candidates : BaF_2, pure CsI and BGO. This research cannot be done by industry alone because it is not obvious that the invested money will guarantee an order. Close collaboration with potential users and sufficient financial support is needed.

Secondly the R&D for photosensors should be intensified. Most promising devices are the drift photodiodes and high stability large area avalanche photodiodes. In both cases we are very likely close to devices which can be produced in large quantity on industrial bases. Also a modernization of the classical photomultiplier which might see a revival in the high rate environment should be undertaken. Current PM's are based on ideas from 30 years ago. PM's should be made much more compact (2cm high?), insensitive to magnetic fields and with higher stability by using less stages and incorporation of fast semiconductor amplifiers.

The third area of immediate intense R&D is the design of the readout electronics. These circuits have to be custom designs both for the analog and digital part. Most of the front-end electronics will be buried inside the calorimeter and inaccessible for the entire lifetime of the detector. Due to the required very high reliability, low power consumption and immunity against EMI and radiation damage, designs have to undergo many long term tests.

It was felt that R&D funds of about 2-5 % of the final calorimeter price would be a reasonable amount.

12.Conclusions

From the discussions and informations at this workshop it was concluded:

i) a high resolution calorimeter is only useful for designs with an inner cavity radius substancially larger than 1 m due to the large 2 track separation for good resolution. The >1 m radius condition eases the radiation damage problems and readout/scintillation decay time requirements, at least at the level of the SSC interaction rate.

ii) 'proven' materials like BaF_2, pure CsI and to some extend radiation hardened BGO can be used.

iii) The resolution will be dominated by the so-called constant term in eq (3). A perfect control of the many contributing factors is mandatory.

iv) The price will be very high, but not only due to the crystal prices. The price will be >100 MSFR but still in acceptable levels when compared with the accelerator prices for LHC/SSC.

v) the main uncertainties in the operation will be the radiation resistance and the calibration

vi) The construction time is about 10 years

In essence it was felt that a large crystal calorimeter can be built. Precision instruments were never easy to build and were never cheap, but the exploitation of 'new physics' with such instruments proved to be very rewarding in the past.

13. Acknowledgements

Many ideas and conclusion have been worked out in the working session of this conference. Herewith I would like to thank V. Baier, G. Hall, P. Lecoq, P. Mine,V. Peskov, D. Renker, V. Sidorov. Also I would like to thank the colleagues from industry, S.O. Flyckt, A. Lightstone, K. Matthews and C. Rosza for their contributions and their help to clarify questions about the industrial production of crystals and light sensors.

The field of research for scintillating crystals is very active. Due to the short time for the preparation of this report it was not possible to list all the relevant references.

14. References

[1] D. Groom.: Radiation levels in SSC detectors. Contribution to this conference

[2] C. Bebek et al.:A design for an upsilon state detector(UPSTATE) for the north area of CESR, Cornell(1983)

[3] P. Lecoq: Operation experience of a large crystal calorimeter for L3 Contribution to this conference.

[4] M. Lavel et al.: Nuc. Inst. Meth. A 206(1983)169

[5] S. Majewski et al.: Nuc. Inst. Meth. A260(1987)373, further references there.

[6] P. Mine: BaF_2 calorimeters with photosensitive gaseous chambers. Contribution to this conference.

[7] S. Kubota et al.: Nuc Inst. Meth. A268(1988)275

[8] C. Rosza: Recent progress on pure CsI performance. Contribution to this conference.

[9] D. Renker: Radiation damage studies of CsI(Tl). Contribution to this conference.

[10] V. Peskov: New photocathodes and new scintillators. Contribution to this conference.

[11] J. Giehl et al.: Nuc. Inst. Meth. A263(1988) 392

[12] G. Hall: Current status of silicon photodiodes based on electron drift. Contribution to this conference.

[13] A.Lightstone: Capabilities of avalanche photodiodes. Contribution to this conference.

[14] The CLEO II detector, CLEO II Updated Proposal 85/634(1985)

[15] E. Lorenz: A new detection method for scintillation and Cerenkov light. Topical seminar on heavy flavor, San Miniato 25.-29.5. 1987.

[16] R.Y. Zhu: A high resolution BaF_2 crystal array. CALT-68-1566

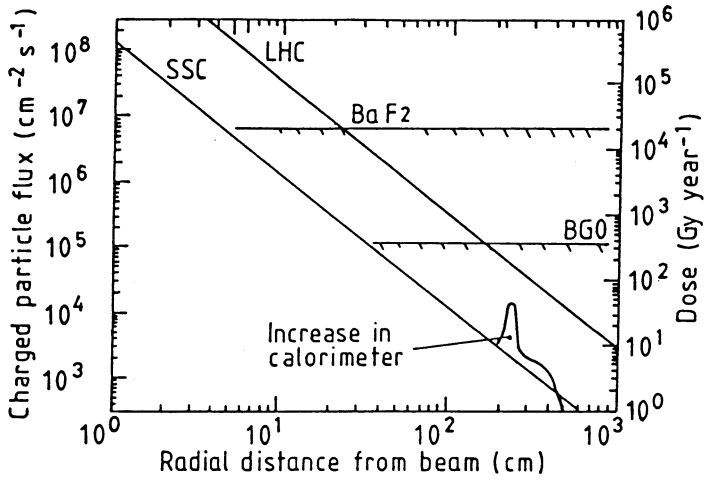

Fig 1: Flux of secondary particles and integrated radiation levels as a function of the radial distance from the interaction point for the SSC and for the high luminosity version LHC.

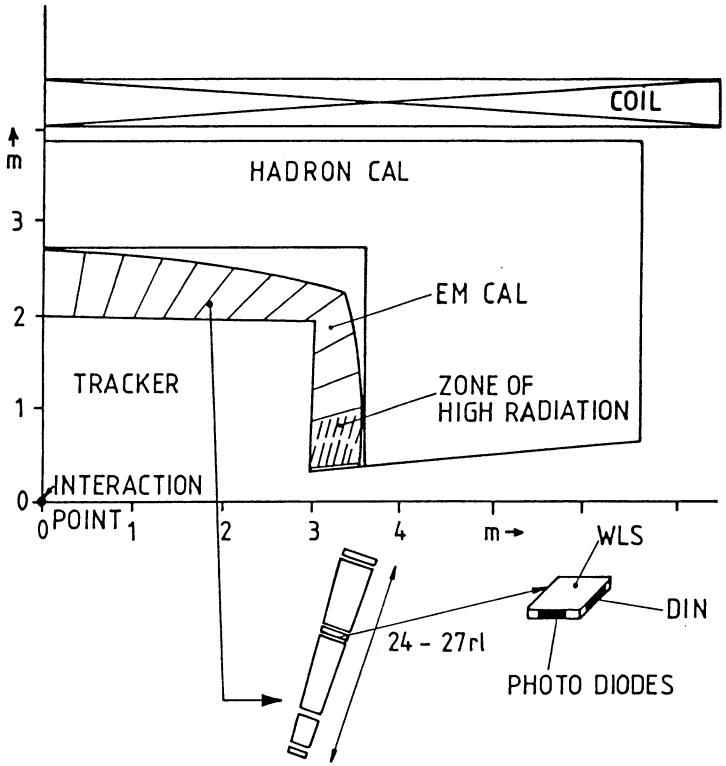

Fig 2: Model of a general purpose detector as a basis for discussion. Only a quadrant of the inner section is shown.

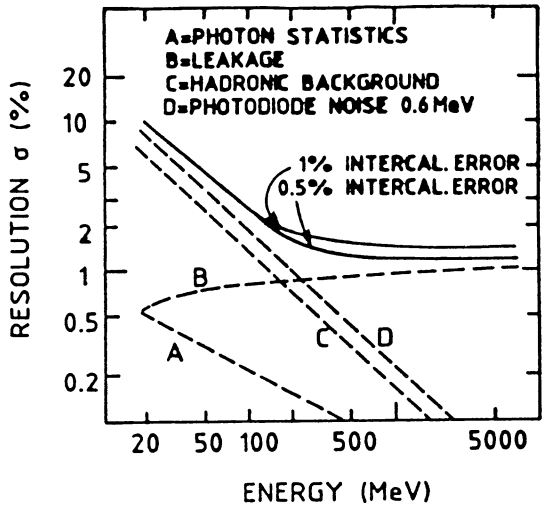

Fig 3: Monte Carlo simulation of different contributions to the resolution for a 18 rl fine grain BGO calorimeter. From the 'Upstate' proposal [2].

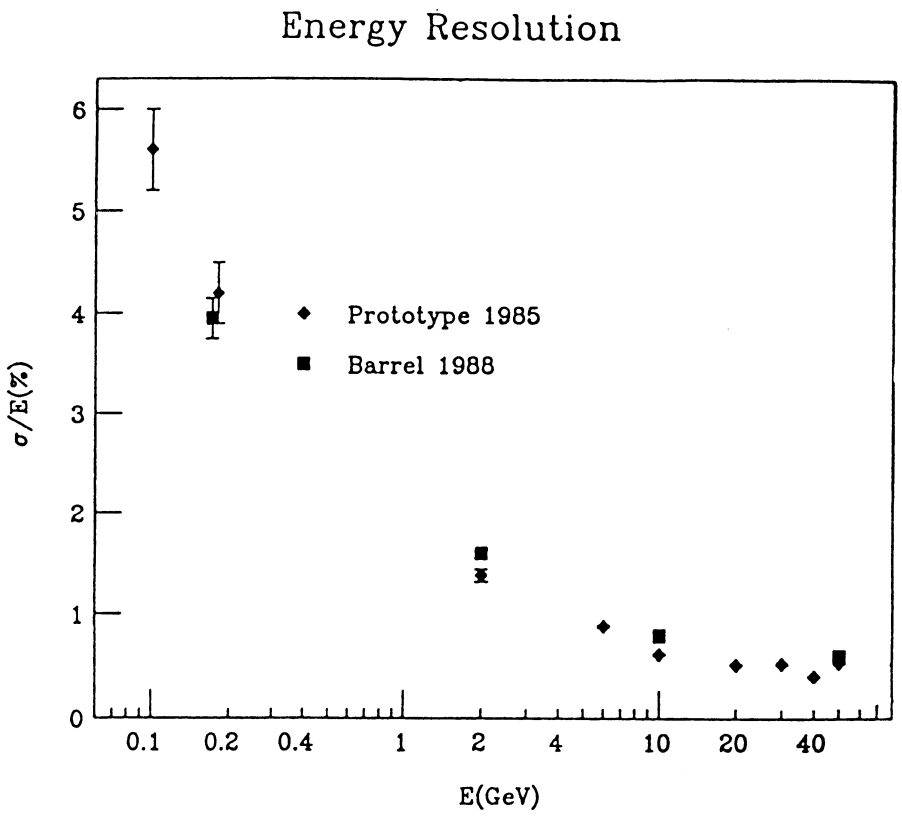

Fig 4: Energy resolution of the L3 BGO calorimeter. Contribution to this conference, P. Lecoq [3]

Session 9

PARTICLE IDENTIFICATION USING TRANSITION RADIATION DETECTORS AND RING IMAGING CHERENKOV COUNTERS

THE TRANSITION RADIATION DETECTOR FOR HIGH-LORENTZ-FACTOR PARTICLE IDENTIFICATION AT HIGH-LUMINOSITY HADRON COLLIDERS

Boris Dolgoshein,
Moscow Physics Engineering Institute, USSR
Convener of the Particle Identification Group (P9)

1. INTRODUCTION

Experimentation at future colliders (SSC, LHC, UNK) is meant to open up a new domain of phenomena at the energy scale of 1 TeV. At this energy scale, the relevant particles are quarks, fragmenting into jets and leptons. The energies of these final-state particles lie in the region of tens to hundreds of GeV, and the Lorentz factors, $\gamma = E/mc^2$, are in the region of 10^2–10^3 (for hadrons and muons) and $\sim 10^5$ (for electrons).

It is a well-established fact that much of the interesting physics to be studied in this energy region is mostly accessible through the study of leptonic channels (e, μ, ν). These may be direct decay products, as in the case of a massive $Z' \to \ell^+\ell^-$, or they may arise from the decay of W or Z bosons (or from heavy quarks produced in the primary decay. Efficient lepton identification over a large solid angle (outside and inside jets) will be essential for these multileptonic decays.

2. MAIN FEATURES OF TRANSITION RADIATION AND THE ROLE OF THE TR DETECTOR

The observation of transition radiation (TR) can provide valuable *non-destructive* information for particle identification, which is both complementary and supplementary to calorimetric measurements. Transition-radiation photons are emitted when a charged particle crosses an interface between two media having different dielectric constants [1, 2]. Table 1 presents the main properties

Table 1
The main properties of TR

	Transition radiation	Cherenkov radiation
Total energy (or No. of photons)	$\propto \gamma = E/mc^2$	$f(\beta)$
$E_{photons}$	$E_{max} \simeq \omega_{pl}\gamma$ (plasma frequency $\omega_{pl} \simeq 20$ eV) $E_{eff} \simeq 3$–30 keV	Optical
$N_{photons}$	$\propto \alpha = 1/137$ per interface $\simeq 0.2$ photon per centimetre	$\sim 10^2$ photons per centimetre
Radiation angle	$\theta > 1/\gamma$	arccos 1/n

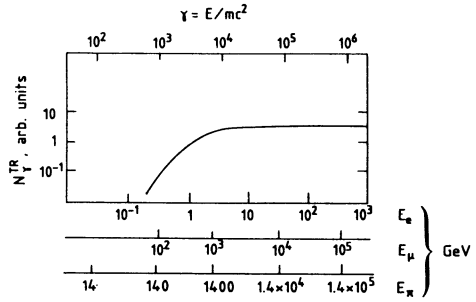

Fig. 1 The $\gamma = E/mc^2$ dependence of the TR X-ray yield.

of TR [3], in comparison with Cherenkov radiation. It is necessary to emphasize the two most important features:

i) The number of TR photons per centimetre is extremely small (0.1–0.2); therefore, for the performance of the transition radiation detector (TRD) system to be adequate, the thickness of the detector package must be at least 50 cm [3];

ii) the TR yield dependence on $\gamma = E/mc^2$ has a threshold behaviour (see Fig. 1). This means that a TRD in the TeV energy domain has to be a good identifier of high-γ ($\gtrsim 10^3$) particle tracks—that is, a high-energy electron, muon, and hadron tracker. It can be seen from Fig. 1 that most of the hadrons inside a jet (E_{jet} = 500 GeV, $\bar{E}_h \cong 4$ GeV) are in the γ region well under the TR threshold.

Figure 2 displays two events from the HELIOS-1 experiment (pBe collisions, 450 GeV) as an example of TRD operation when the density of secondaries is high. With about 12 charged secondary

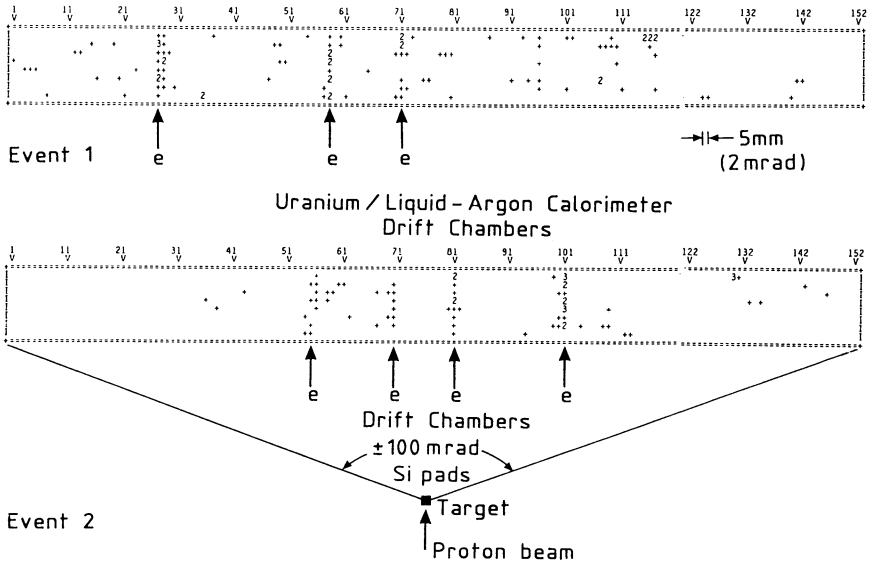

Fig. 2 The display of two events in the HELIOS TRD. The dead space in the TRD is ±13 mrad around the beam. There are eight (radiator + drift chamber) sets. Each radiator consists of 200 polypropylene foils of 20 μm thickness, 200 μm apart.

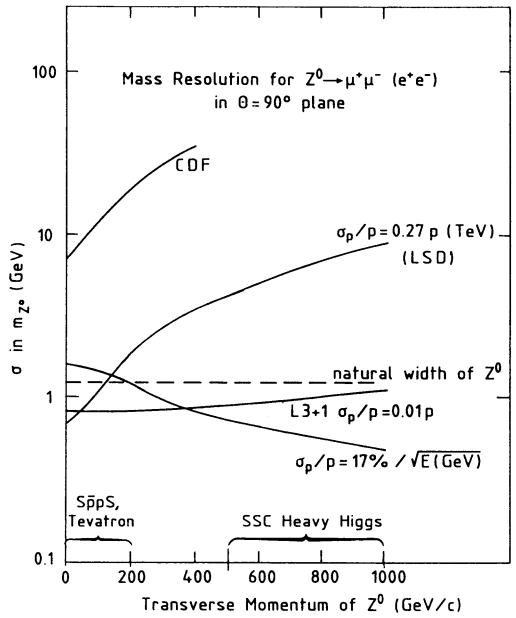

Fig. 3 The mass resolution for $Z^0 \to \ell^+\ell^-$ in the $\theta = 90°$ plane as a function of Z^0 transverse momentum for the different momentum resolutions of the leptons.

particles, we 'see' only tracks of electrons, which look like chains of numbers (numbers of clusters) in each of the eight proportional chambers (PCs) of the TRD [3]. There is also the 'grey background' originating from relatively low $\gamma = E/mc^2$ ($E \simeq$ few GeV) secondary hadrons.

The main task of a TRD at a high-energy collider is *electron* identification; the detection of the decay products e^+e^- and $e\mu$ (and not only $\mu^+\mu^-$) became acceptable with adequate momentum (energy, mass) resolution (see Fig. 3).

The space available for a TRD is limited, and it may be placed as near as 20–100 cm to the beam line. It will always be followed by an electromagnetic calorimeter, which provides an important part of the electron identification. Using information about the longitudinal as well as the transversal development of the shower, it is possible to achieve a hadron rejection of > 100 at an electron registration efficiency of 90–95% without momentum measurements in the magnetic field, or a rejection of $\sim 10^3$ with such measurements.

There are two different motivations for the use of TRDs in high-energy colliders [4]:

i) The identification of *isolated* electrons. This is the case for the decay of heavy objects such as Higgs, new quarks, SUSY particles, new intermediate bosons W′ and Z′, and other high-mass particle decays.

ii) The identification of *non-isolated* electrons inside jets. This can be important in the case of decays of heavy particles with b-quarks in the final state, for example
- charged-Higgs decay [5]:

$$pp \to W^{\mp}H^{\pm} \to tb \to \text{electron(s)}$$

- heavy t-quark production by W–gluon fusion [6], and also for a better understanding of background processes.

There are two questions about what has been mentioned above: 'isolated' and 'non-isolated' electron identification. These questions are:

i) What degree of electron identification (hadron rejection) do we need?

ii) What is the main source of false electrons?

The answer to the second question is given by using the experience of the TRD performance in the UA2 experiment [7], in the HELIOS-1 experiment (see below), and by the Monte Carlo study for the SSC environment [4]. It is: that the main source of false electron background is the overlap of γ conversions from hadron decays (π^0, η^0 ...) with charged-hadron tracks (within the spatial resolution of the calorimeter or preshower counter). For example, such an overlap is about 8% for the HELIOS-1 experiment within ± 5 mm (pBe, 450 GeV).

The answer to the first question can be obtained from Fig. 4 [4]. This figure shows the rates for different processes:

- the signal $H \to WW \to e$ + jet(s);
- the background of real electrons [$pp \to W$ + jet(s); $t\bar{t} \to WW \to e$ + jet(s); $b\bar{b} + c\bar{c} \to e$ + jet(s)];
- the background of false electrons: the overlaps between γ conversions and charged-hadron tracks for
  - QCD jets and
  - direct γ production (QCD, Compton)

  within particle-shower spatial matching: $\pm 2\sigma = \pm 2$ mm. These processes have the same final-state particle content as the signal ($E_e > 25$ GeV, $E_{jet} > 100$ GeV).

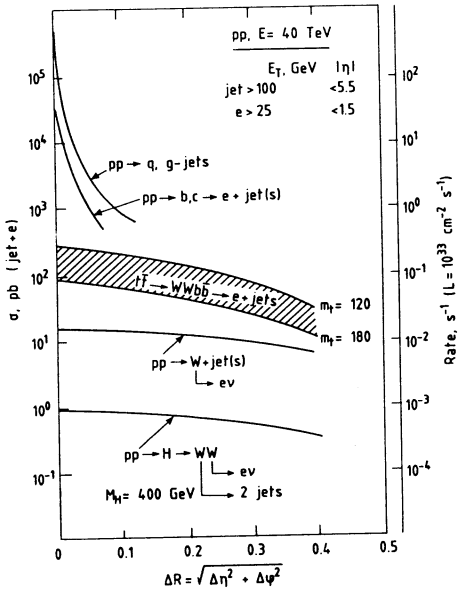

Fig. 4 Cross-sections for different processes for real and false electrons as a function of an isolation cut ΔR. The false electrons originate from the spatial overlap of γ's with hadrons, assuming a spatial accuracy of $\sigma = 1$ mm and using a 2σ cut.

Examining the curves for these two backgrounds, we can see that their relative importance depends on the range of the 'isolation cone' ΔR that is chosen. A cut $\Delta R \geqslant 0.15$ loses ~ 30% of the signal. Whether this cut brings the QCD jet background below the direct photon production depends on (unknown) fragmentation functions. We can see that a rejection of 'isolated' false electrons ($\Delta R \approx 0.15$) about 10^{-2}–10^{-3} is needed, but recognizing that the kinematical cuts needed to suppress physical (real electron) backgrounds may also suppress false electrons.

For electrons inside the jets ($\Delta R = 0$), the reduction of false electron background to below the level of real electrons from (b + c) decays requires a hadron rejection of $\leqslant 10^{-2}$. For both cases ($\Delta R = 0.15$ and $\Delta R = 0$), the calorimeter offers little further rejection of this type of false electron (overlaps γ + hadron).

We can conclude that hadron rejection by the TRD at the level of 10^{-2}–10^{-3} (following calorimetric selection of electron candidates) will be required for high-energy collider physics. The hadrons to be rejected are predominantly low-energy ones. In effect, the TRD replaces one function of a high central magnetic field.

Another important goal of the TRD is to tag the high-energy muons ($\geqslant$ 100 GeV) inside jets among the relatively low momentum hadrons (typically about a few GeV) so as to link up with the muon tracks from the muon spectrometer. The achievable hadron rejection factor for 90% muon acceptance is shown in Fig. 5 [4] as a function of the muon energy for several values of the polar angle.

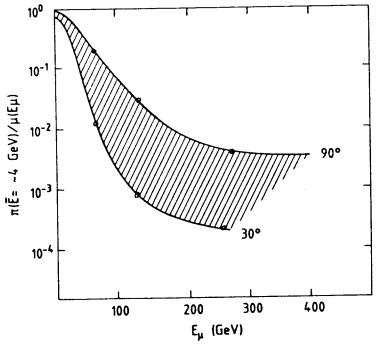

Fig. 5 Rejection of typical pions as a function of muon energy for criteria that give 90% muon acceptance, demonstrating the powerful 'muon-tagging' capability of the proposed TR tracker.

3. TRD PERFORMANCE AND REJECTION POWER AT A HIGH-LUMINOSITY MULTI-TeV COLLIDER

In the foregoing, it has been mentioned that the rejection power required against hadrons is about $R \simeq 10^{-2}$–10^{-3} for isolated as well as non-isolated particles. A number of TRDs have been proposed [8–16] and used in accelerator experiments [3, 7, 17]. The hadron rejection capability for these TRDs is shown in Fig. 6 as a function of the length of the detector [3]. We can see that in the case of *isolated* particles, the value $R \simeq 10^{-2}$–10^{-3} can be achieved for a TRD length $\ell_{TRD} \geqslant 50$ cm. However, this is not the case for non-isolated particles. Figure 7 (HELIOS-1 experiment) shows the comparison of the rejection powers for isolated particles (π/e, test beam 5 GeV, and calibration beam 45 GeV) and real pBe, 450 GeV interactions ('non-isolated' particles, charged-particle

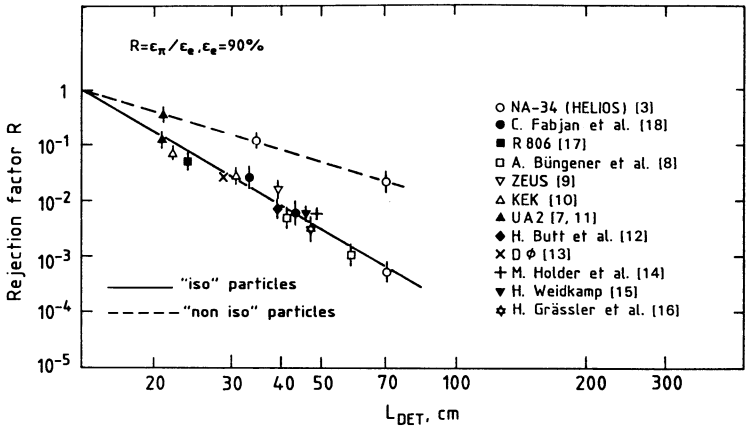

Fig. 6 Capabilities of various TRDs for discriminating π/e.

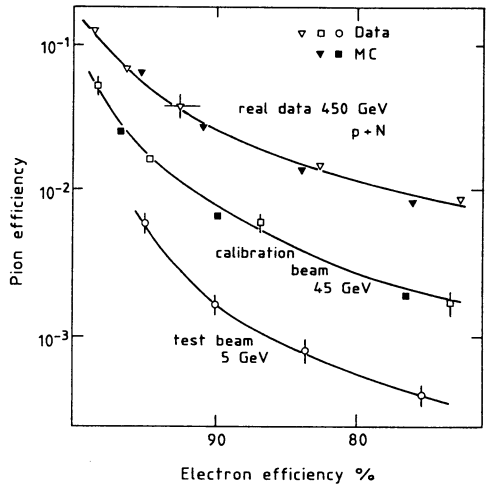

Fig. 7 Rejection power of the HELIOS TRD under different conditions.

multiplicity of about 12). For isolated particles, the rejection power changes from $\sim 2 \times 10^{-3}$ (5 GeV) to $\sim 10^{-2}$ (45 GeV) owing to the relativistic rise in the pion ionization losses; in the case of the 450 GeV 'proton jet', the rejection power deteriorates.

The first example of TRDs being used as track detectors (TR tracker, Fig. 2) is in the HELIOS-1 experiment. A HELIOS TRD consists of eight sets of radiator + PC, with anode and cathode strip readout for each of the eight chambers, and uses the cluster-counting method [18] for the identification of electrons. The anode and cathode pitches are different for each chamber because the corresponding eight anode and cathode strips cover different sectors with respect to the small (50 μm) target. For the electron trigger, the electron correlation logic allows one to use the

information about correlations in space between energy deposition in the electromagnetic part (tower) of the calorimeter, the anode and cathode strip sectors of the TRD, and the corresponding pad of the silicon detector just behind the target. The silicon pads allow rejection of the electron-positron pairs that are due to γ conversions and Dalitz decays of π^0's and η's. The total length of the TRD is 70 cm and the fiducial volume is 70 cm in diameter. Each of the eight radiators consists of 200 polypropylene foils, 20 μm thick. Each of the eight PCs consists of an anode space (2 × 4 mm) containing 156 anode wires (pitch from 2.3 to 2.8 mm, and a drift space (10 mm) containing 62 cathode strips. The two-dimensional analysis shown in Fig. 8 has been used for π/e rejection. This method selects the event on the scatter plot (anode hits versus cathode hits; a hit is an ionization cluster with energy more than 5 keV); for $N > N^{\text{threshold}}_{\text{anodes (cathodes)}}$, there is a corresponding 90% electron efficiency (Fig. 8a). It also gives the pion contamination ϵ_π (Fig. 8b), and is used for fast triggering. In the case of the '450 GeV proton jet' (Fig. 8c), the scatter plot for pions is dramatically changed owing to the presence of extra particles, which lie in the 'anode-cathode point of intersection' (upper right-hand part of Fig. 8c); these particles produce a lot of uncorrelated hits and increase the number of false electrons. This is the main reason why the hadron rejection power

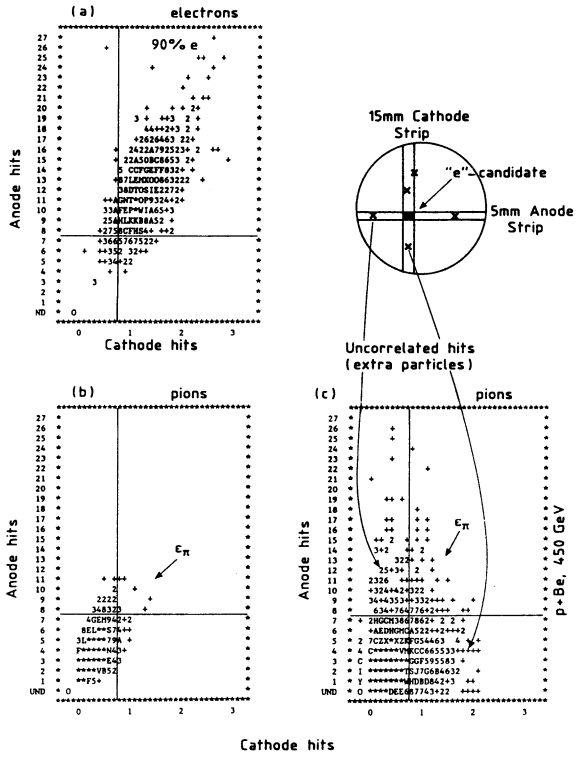

Fig. 8 Scatter plots (anode hits versus cathode hits) for isolated electrons (a), isolated pions (b), and pions inside the 'proton jet' (c). The straight lines correspond to a 90% electron efficiency (upper right-hand section).

deteriorates for non-isolated particles. In fact, it is a case of misidentification, not only for a single pion but also for 2π, 3π, $\pi + \gamma$ conversion, heavily ionizing particles, and so on, which are positioned inside the same anode (cathode) strip as the electron candidate. The analysis of the HELIOS TRD operation shows about 40% of 'pure' pions among the 'electron candidates' for the '450 GeV proton jet', and ~ 60% many-particle overlaps (extra particles). The estimation of these extra particles, from the HELIOS and the UA2 [7] TRDs, is as follows:

	HELIOS (%)	UA2 (%)
Many pions	~ 30	~ 50
Electron(s)	~ 20	
γ conversion(s) in the radiator	~ 30	~ 50

As a result, the rejection power of TRDs for high-multiplicity events becomes worse (see Fig. 6). Nevertheless, the rejection power of the HELIOS TRD for the '450 GeV proton jet' case is 2.5×10^{-2}, which allows a clean enough sample of inside-'jet' electrons (Fig. 9) to be obtained.

There are at least two ways of achieving a better TRD rejection power under conditions of high multiplicity:

i) by avoiding extra particles with the aid of the pixel (tower) structure of the TRD—a difficult and quite expensive method;

ii) by controlling the extra particles by means of the measurements of dE/dx and TR X-rays from the same anode wire.

The second way has been used in the proposal for the TR tracker [4] based on the azimuthally oriented 'straw design' (Fig. 10). For a straw diameter of 4 mm, the total drift time of the electrons is less than 40 ns; under these conditions the reduction of piled-up events and straw occupancy for the SSC ($L = 10^{33}$ cm^{-2} s^{-1}) looks very promising (Fig. 11). Figure 12 shows the expected electron identification (carried out by the MC) for this TR tracker [4] for one of the analysis options (triple-threshold analysis). One chooses three different threshold levels for the detection of ionization clusters in each straw. The first threshold level (TH1 at 0.2 keV) gives about 80% efficiency for relativistic particles. The second threshold level (TH2 at 1.0 keV) is located between one- and two-particle energy cluster distributions, and has ~ 50% efficiency for minimium-ionizing particles and ~ 90% for conversions. The third threshold level (TH3 at 4.5 keV) corresponds to ~ 80% efficiency for TR X-rays. The abscissa of each scatter plot in Fig. 12 indicates, for a given particle,

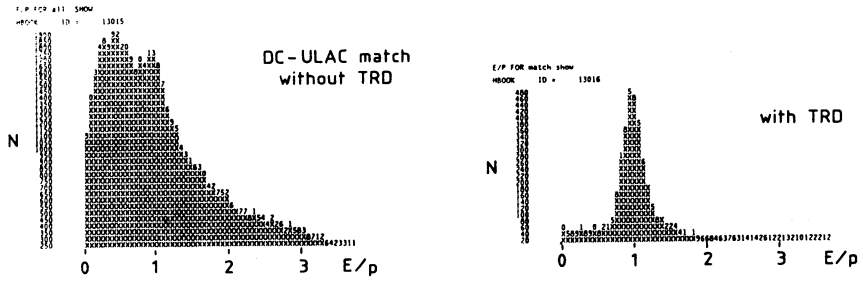

Fig. 9 The cleaning of the electron candidate sample by the HELIOS TRD inside the '450 GeV proton jet'.

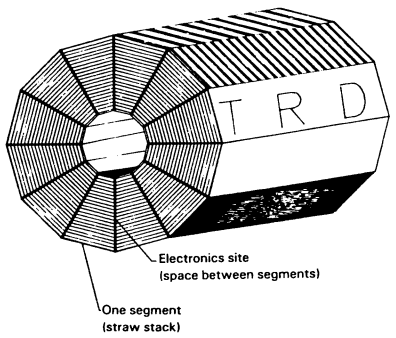

Fig. 10 Possible construction of a TRD, based on azimuthally oriented straw tubes. The electronics are placed in cracks between the segments.

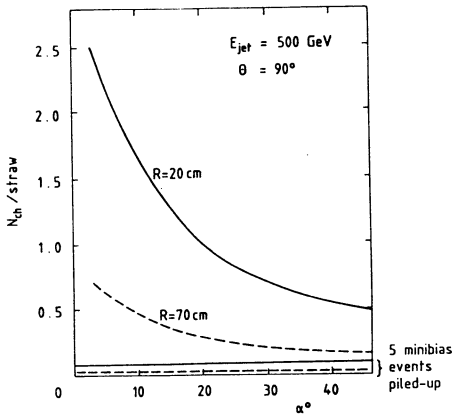

Fig. 11 Occupancy of straws by charged particles as a function of the angular separation from the jet axis. The occupancy due to TR clusters is approximately an order of magnitude less.

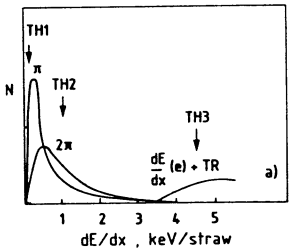

Fig. 12 a) Energy deposition in a single straw by one and two pions and by TR X-rays. b–f) Acceptance of electrons and rejection of different sources of background.

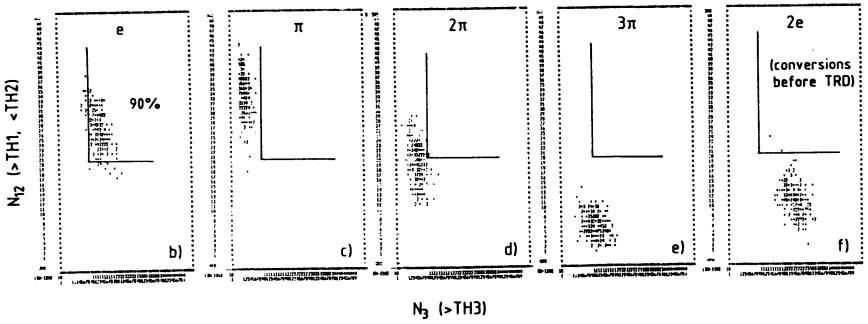

the number of straws where the energy deposition is above TH3; the ordinate shows the number of straws with energy deposition between TH1 and TH2. This triple-threshold method permits efficient discrimination not only between electrons and π, 2π, 3π, and γ conversions before the TRD (Fig. 12), but also between electrons and γ conversions inside the transition radiator (Fig. 14 of Ref. [4]).

4. CONCLUSIONS

The multi-TeV collider high-p_T experiments require not only the conventional calorimetry but also the additional electron discrimination against hadrons. The majority of the false electrons come from the overlap between γ's and charged-hadron tracks. Good hadron rejection ($< 10^{-2}$) can be achieved by the TRD for isolated (outside jet) and non-isolated (inside or near-jet) electrons.

The experience gained with a TRD in a high-multiplicity environment (HELIOS, UA2) makes it possible to establish the reasons for the deterioration of the TRD rejection power under such conditions.

The TRD based on azimuthally oriented straw tubes looks very promising in a high-rate transition radiation tracker (TRT), and it has good compatibility with the high-luminosity environment of the hadron collider. The simultaneous measurements of TR X-rays and dE/dx energy deposition allow a hadron rejection of $< 10^{-2}$ to be achieved, and provide additional possibilities for tracking and triggering.

In fact, such a TRT is a high $\gamma = E/mc^2$ tracker for
- electrons
- muons
- hadrons (leading hadrons inside jets),

at $E/mc^2 \geq (1\text{–}2) \times 10^3$.

Acknowledgements

As convener of the Particle ID Group, I would like to thank all the physicists who participated in this meeting. I am very grateful to C. Fabjan, D. Froidevaux and W. Willis for very useful discussions.

REFERENCES

[1] V.L. Ginzburg and I.M. Frank, Zh. Eksper. Teor. Fiz. **16** (1946) 15.
[2] G.M. Garibyan, Sov. Phys.-JETP **10** (1960) 372.
[3] B. Dolgoshein, Nucl. Instrum. Methods **252** (1986) 137.
[4] S. Ahlen et al., Proposal to develop an integrated high-rate TRD and tracking chamber for the SSC, contribution to this ECFA meeting.
[5] D.A. Dicus et al., $W^{\pm}H^{\mp}$ production at hadron colliders, Univ. Wisconsin preprint MAD/PH/468 (1989).
[6] C.P. Yuan, New method to detect a heavy top quark, Argonne preprint ANL-HEP-PR-89-44 (1989).
[7] J.P. Repellin et al., Comments on the TR detector in UA2, presented at this ECFA meeting.
[8] A. Büngener et al., Nucl. Instrum Methods **214** (1983) 261.
[9] R.D. Appuhn et al., Nucl. Instrum. Methods **263** (1988) 309.
[10] Y. Watase et al., Nucl. Instrum. Methods, **248** (1986) 379; KEK preprint 87-29 (1987).
[11] R. Ansari et al., Nucl. Instrum. Methods **263** (1988) 51.
[12] H.J. Butt et al., Nucl. Instrum. Methods **252** (1986) 483.
[13] J.F. Detoeuf et al., Nucl. Instrum. Methods **265** (1988) 157.
Ph. Mangeot, Contribution to this ECFA meeting.
[14] M. Holder et al., Nucl. Instrum. Methods **263** (1988) 51.
[15] H. Weidkamp, Diplomarbeit, Rhein.-Westf. Tech. Hochschule Aachen (1984).
[16] H. Grässler et al., to appear in Proc. Vienna Wire Chamber Conference, 1989.
[17] J. Cobb et al., Nucl. Instrum. Methods **140** (1977) 413.
[18] C.W. Fabjan et al., Nucl. Instrum. Methods **185** (1981) 119.

PARTICLE IDENTIFICATION AT HADRON COLLIDERS

Thomas Ypsilantis, Collège De France, Paris

1.PARTICLE IDENTIFICATION LIMITS

1.1 INTRODUCTION

The particle identification (ID) capability of a Ring-Imaging CHerenkov (RICH) detector may be obtained from the basic Cherenkov relation $n\beta\cos\theta=1$ which may be rewritten as

$$U=\sin^2\theta=[(\gamma/\gamma_t)^2-1]/(\gamma\beta)^2=\gamma_t^{-2}-(m/pn)^2 \qquad (1)$$

where γ is the Lorentz factor of the radiating particle, p its momentum, m its mass, n the refractive index and $\gamma_t=n/(n^2-1)^{1/2}$ the γ threshold of the radiator. The number of standard deviations n_σ for discriminating mass m_2 from m_1 is then

$$n_\sigma=(U_2-U_1)\sqrt{N}/\sigma_U=[(m_2^2-m_1^2)/p^2n^2]\sqrt{N}/\sigma_U \qquad (2)$$

where σ_U is the r.m.s. error in the measure of U and N is the number of photoelectrons of the ring image. The number of photons dN_{ph} per unit energy interval dE for a radiator of length L is given by the Franck-Tamm relation

$$dN_{ph}/dE=(137hc)L\sin^2\theta \qquad (3)$$

which may be integrated over ΔE the energy bandwidth of the detector, to give (for an approximately constant Cherenkov angle)

$$N=N_0L\sin^2\theta \qquad (4)$$

with the detector response parameter

$$N_0=(137hc)\int QTRdE=(370eV^{-1}cm^{-1})\Delta E\,\varepsilon \qquad (5)$$

where ε is the energy average of the detector efficiencies (Q=quantum, T=transmission, R=reflection). Inserting Eq.4 into Eq.2 and noting that $\sigma_U=(2\sin\theta\cos\theta)\sigma_\theta=(2\sin\theta/n\beta)\sigma_\theta$, we obtain

$$p=[(m_2^2-m_1^2)/2n_\sigma k_c]^{1/2} \qquad (6)$$

the momentum for particle ID, where the characteristic RICH detector constant is

$$k_c=n\sigma_\theta/\beta(N_0L)^{1/2} \qquad (7)$$

and σ_θ is the total angular error per detected photon.

To get optimal particle ID, the requirement is that k_c be minimum, and since N_0 and σ_θ are proportional to ΔE (see Eq.'s 5,10,11 and 13) then Eq.7 shows that k_c is proportional to $\sqrt{\Delta E}$. This implies that the detector should have minimal bandwidth but with sufficient photoelectrons N for pattern recognition. Increasing N by increasing the detector bandwidth ΔE is counterproductive and should be avoided. Radiators with the lowest chromatic dispersion should be used unless space point measurement errors dominate σ_θ.

The momentum resolution σ_p of a RICH detector is, after the particle mass has been identified, given by the relation

$$\sigma_p=k_cp^3/m^2 \qquad (8)$$

which for heavy particles (K,P) may be more precise than the magnetic deflection measurement. The two determinations are, in any case, independant and should be considered together.

1.2 IRREDUCIBLE ERRORS

The geometry of a RICH gas radiator is shown in Fig.1. The measurements necessary to define the Cherenkov angle θ are the photon detection point (x,y,z), the photon emission point (x_e,z_e) and the particle direction (θ_p,φ_p). The photon emission point along the particle path in the gas radiator is z_e , whilst the particle impact parameter relative to the mirror center of curvature is x_e. Six of these variables $(x,y,z,x_e,\theta_p,\varphi_p)$ can, in principle, be infinitely well measured. The photon emission point however has an irreducible error

$$\sigma_{z_e}=L/\sqrt{12} \qquad (9)$$

which cannot be improved without reducing the radiator length. Similarly, the photon energy error is

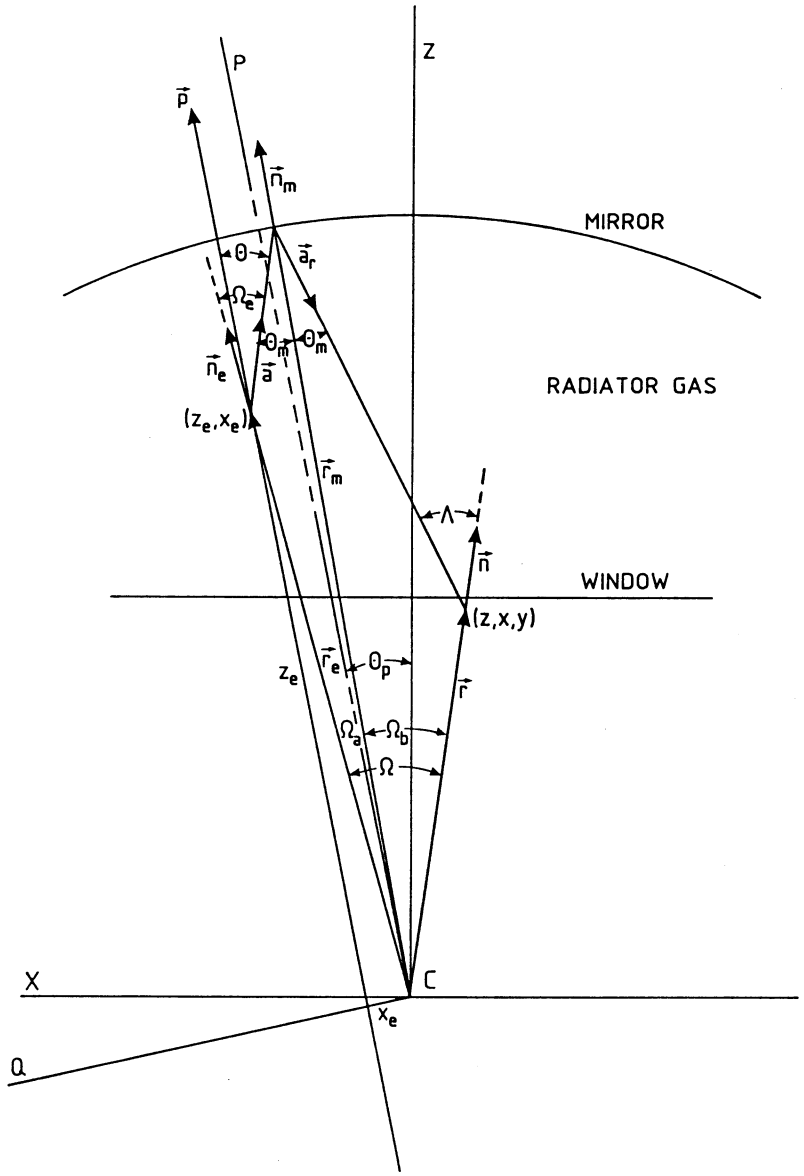

Fig.1. Geometry of Gas Radiator with Mirror.Photon Emission from the point $(z_e,x_e,0)$ of the PQR coordinate system. Photon Detection at the point (z,x,y) of the ZXY system.

$$\sigma_E = \Delta E/\sqrt{12} \quad \text{for a square response} \tag{10}$$

$$\sigma_E = \Delta E/\sqrt{24} \quad \text{for a triangular response} \tag{11}$$

always for a base width ΔE. This error cannot be reduced without decreasing the detector bandwidth ΔE. The corresponding errors in the Cherenkov angle θ are

$$\sigma_\theta(z_e) = (\partial\theta/\partial z_e)\sigma_{z_e} \tag{12}$$

and

$$\sigma_\theta(E) = (\partial\theta/\partial n)(dn/dE)\sigma_E \tag{13}$$

These two errors are therefore irreducible and determine the limits of resolution. The chromatic contribution to the total angular error σ_θ is considered in the next section while the emission point and measurement errors will be considered in section 1.4

1.3 CHROMATIC ERRORS

The first factor of Eq.13 is given, for a mirror focused image (see Fig.1), by the derivative of the Cherenkov relation $n\beta\cos\theta=1$, hence

$$\partial\theta/\partial n = 1/(n*\tan\theta) = (\gamma_t - 1/\gamma_t)/[1-(\gamma_t/\gamma)^2]^{1/2} \tag{14}$$

For a proximity focused image Eq.14 is multiplied by an additional factor $(n\beta)^2/(1-\tan\theta_p\tan\theta\cos\varphi)$ owing to refraction of the Cherenkov cone as it exits from the radiator medium [1]. The chromatic error $\sigma_\theta(E)$ depends, in this case, on the azimuthal angle φ.

The second factor dn/dE is the dispersion of the radiator medium which may be evaluated from the Lorentz-Lorenz equation

$$(n^2-1)/(n^2+2) = cf(E) \tag{15}$$

with the density dependant constant $c=(4\pi/3)a_0N_A\rho/M=.3738cm^3\ \rho/M$, a_0 is the Bohr radius, N_A is Avogadro's number, ρ/M the molar density of the radiator medium=P/RT for an ideal gas (P is the pressure, R the gas constant, and T the temperature). The energy dependence of the molar refractivity f(E) is usually fit to a Sellmeir two-pole form,

$$f(E) = F_1/(E_1^2-E^2) + F_2/(E_2^2-E^2) \tag{16}$$

The derivative of Eq.15 gives directly the dispersion

$$dn/dE=[(n^2+2)^2 c\,df/dE]/6n \qquad (17)$$

with n from Eq.15, c from the density, and

$$df/dE=2E[F_1/(E_1{}^2-E^2)^2+F_2/(E_2{}^2-E^2)^2] \qquad (18)$$

the derivative of Eq.16.

The indices of some common gases (He,Ne,Ar,Kr,Xe,H_2,N_2,O_2) have been measured [2] in the visible and UV and fit to Eq.16 to obtain the Sellmeir coefficients (E_1,E_2,F_1,F_2) listed in Table 1.

We have measured the refractive indices of some liquid fluorinated alkanes (CF_4,C_2F_6,C_4F_{10},C_5F_{12},C_6F_{14}) [3]. The results are shown in Fig.2 for the cryogenic liquids (CF_4 and C_2F_6) and room temperature liquids (C_5F_{12} and C_6F_{14}) over the measurement interval 5 to 7eV (248 to 177nm). It can be seen that the refractive indices are very low (1.22 to 1.275) and that the dispersion is small. Because of the limited range of the data a linear fit of the form

$$n=a+bE \qquad (19)$$

sufficed. The fits are shown as the full lines in Fig.2 and the fit coefficients are tabulated in Table 2 along with the liquid density ρ and the molecular weight M. From the fit n(E), the molar refractivity f(E) may be calculated from Eq.15 and df/dE from Eq.17 since dn/dE=b for the fit of Eq.19.

The dispersion dn/dE for the gaseous state may then be evaluated through Eqs.15 and 17 given f(E) and df/dE (as determined above) and c=.3738cm^{3}P/RT, for the gas in question.

Solid transparent materials are also of interest as windows and as Cherenkov radiators for low momentum particles. The Sellmeir coefficients of Eq.16 are listed in Table 3 for CaF_2, NaF and fused quartz. The first two are single crystals with good transmission to about 10eV, whereas fused quartz is amorphous (hence cheaper), with transmission to about 8eV. For CaF_2 and fused quartz the fit was to $f(E)=n^2-1$ whilst for NaF [4] the fit was to $f(E)=(n^2-1)/(n^2+2)$. Here, the constant c has been absorbed into f(E), since the density of these solids is constant.

With the data of Tables 1 and 2 and Eqs. 15 to 19 the chromatic errors $\sigma_\theta(E)$ have been calculated for a TMAE based detector (isobutane +methane amplifying gas; triangular response between 6.1 to7.1eV) coupled to various gas radiators (1bar,40°C).In Table 4 are listed the

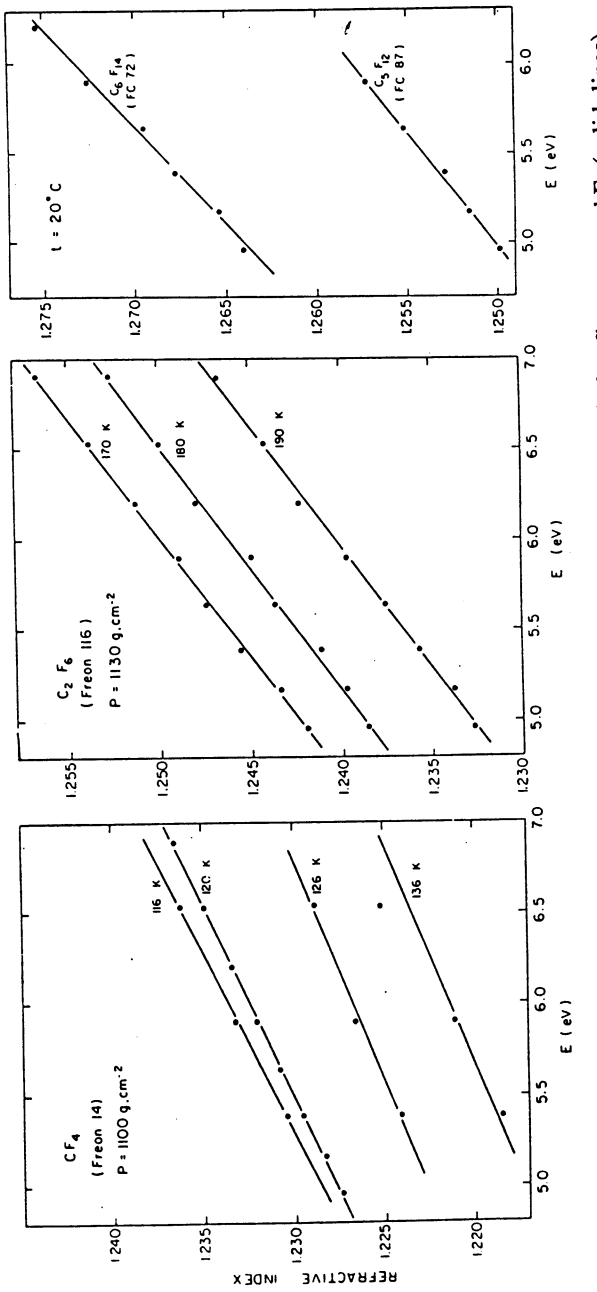

Fig.2. Measured refractive indices (points) of some fluorinated alkanes and the fits to n=a+bE (solid lines).

radiator gas, γ_t, $\sigma_\theta(E)$ and $\sigma_\theta(E)/\theta$ for $\beta=1$ particles ($\gamma=\infty$ in Eq.14). The last quantity is the fractional error in the Cherenkov angle, which is constant with changes in density. Also listed in Table 4 is the radiator lengths L that are needed to get N=9 for a detector with a specific response $N_0=65cm^{-1}$(corresponding to $\varepsilon=.175$ e.g. TR=.7 and Q=.5 at the maximum of the triangular response). The RICH constant k_c (Eq.7), due to the chromatic error only, and for the listed length L, is also given with the momentum $p_{K\pi}(3\sigma)$ to obtain $n_\sigma=3$ (Eq.6). The particle ID momentum limits are plotted in Fig.3. The obvious inferences from Table 4 are:

1) that whilst He and Ne give excellent upper limits for Kπ ID (880 and 620GeV/c), they must be exceedingly long (21 and 11m respectively), hence they are practical for limited solid-angle spectrometers only;

2) that Ar, Kr, Xe and N_2 are not very good radiators relative to the fluorinated alkanes;

3) that CF_4 is the best medium (equal to high density He or Ne) and C_5F_{12} has the lowest threshold. A combined CF_4(1.4m) + C_5F_{12}(0.4m) radiator with a quartz separator plate and a single mirror and detector could attain Kπ ID from 2.4 to 240GeV/c.

A proximity focused RICH comprised of 1cm of liquid C_6F_{14} with a 20cm lever arm can cover the low momentum region between 0.17 and 6GeV/c thus allowing complete particle ID up to 240GeV/c in 2m total distance.

1.4 EMISSION AND MEASUREMENT POINT ERRORS

As an example, a RICH comprised of two radiator gases (1.4m of CF_4 and 0.4m of C_5F_{12} seperated by a transparent quartz plate) with a reflective mirror (r=3.6m) viewed by a single detector near the focal surface (r=1.8m) would have a φ averaged emission point error less than half of the chromatic error of 60 (or 166)μrad if the detection point is within 8 (or 35)mm of the focal surface for radiators CF_4 (or C_5F_{12}) respectively. A detector designed for the CF_4 radiator more than suffices for the C_5F_{12} radiator.

The total measurement error $\sigma_\theta(m)$ is the error sum, in quadrature, from the measurements of the photon emission point (z_e, x_e) and detection point (z,x,y) [5]. It is shown in Fig.4 (for the CF_4 radiator example) for θ_p=0, 0.2, 0.3, and for x_e between 0 and 80mm at detection radius of r=1800mm. Very similar curves are found at

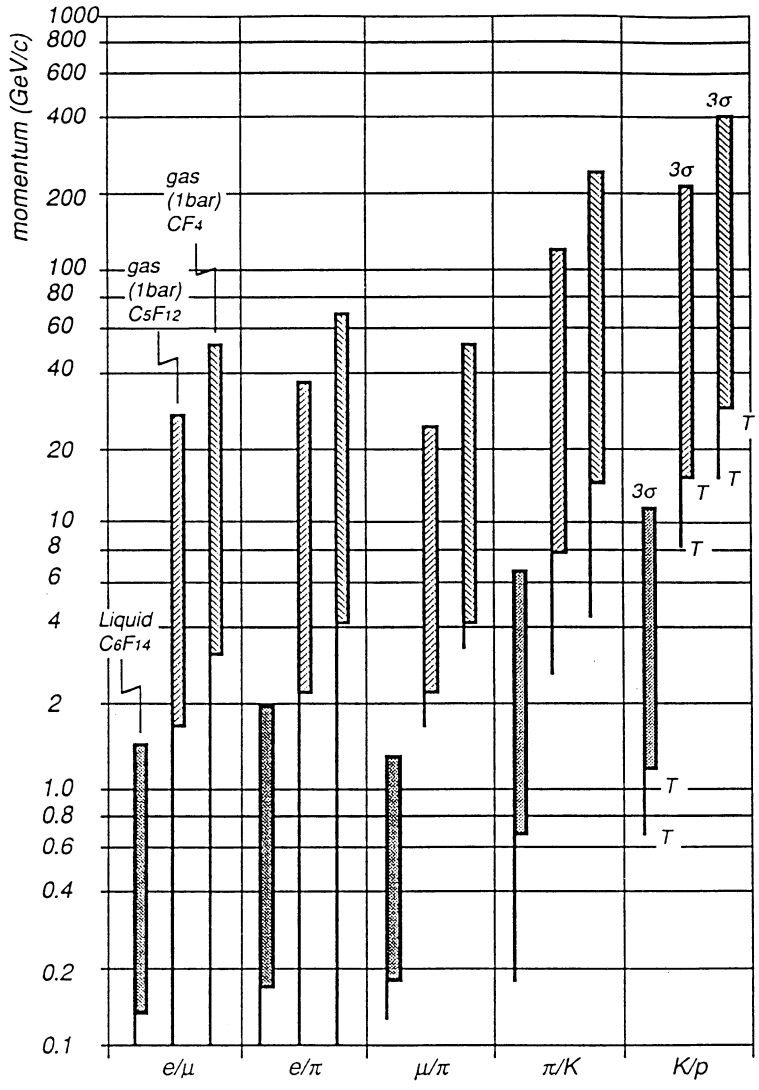

Fig.3. Particle ID limits for three radiators: 1cm liquid C_6F_{14} with proximity focusing and 0.2m lever arm; 40cm of C_5F_{12} gas with mirror focusing (f=1.8m); 140 cm of CF_4 gas with mirror focusing (f=1.8m). The thin lines show the region where particle ID is by threshold (T) and the thicker lines the region where particle ID is by the size of the ring image. The top limit corresponds to $n_\sigma=3$.

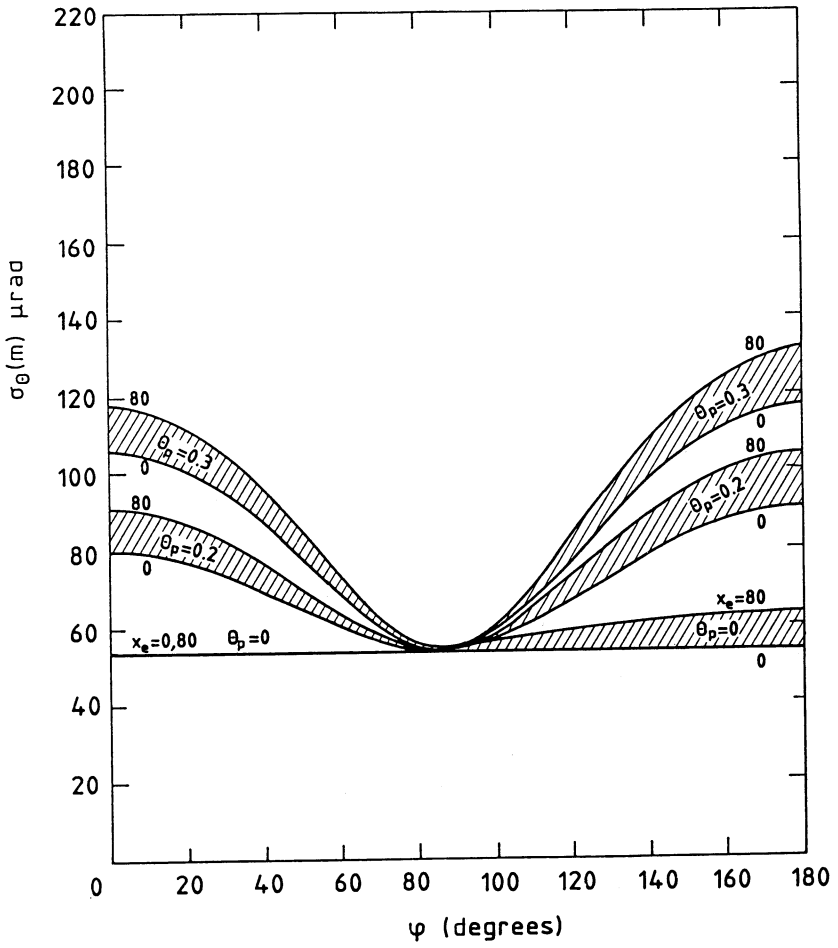

Fig.4. Total non-chromatic error $\sigma_\theta(m)$ due to measurement errors of the photon emission point (z_e,x_e) and detection point (z,x,y) versus azimuthal Cherenkov angle φ for r=1800mm, θ_p between 0 and .3 and x_e between 0 and 80mm. The measurement errors are given in the text. Other fixed parameters are r_m=3600mm, z_{eb}=2200mm, $z_{et}=(r_m^2-x_e^2)^{1/2}$ with a CF4 gas radiator (1 bar, 40°C, γ_t=31).

r=1792mm and r=1808mm. In calculating these curves, measurement errors of $\sigma_{z_e}=1400/\sqrt{12}=404$mm, $\sigma_{x_e}=.29$mm, $\sigma_z=.6$mm, $\sigma_x=\sigma_y=1\text{mm}*cg/\sqrt{12}$ have been assumed (cg=1/3 for digital center of gravity). This error is evidently φ dependant, as is the total error σ_θ, which is the sum, in quadrature, of $\sigma_\theta(m)$ and the chromatic error $\sigma_\theta(E)=60\mu$rad. The total error is minimum (86μrad) near $\varphi=90°$ and maximum (110μrad) at $\varphi=0°,180°$. The reconstructed Cherenkov angle should be weighted by $1/\sigma_\theta^2$ to obtain the best resolution and the sharpest peaks for pattern recognition (identification of the photoelectrons belonging to a given ring image). The degradation of the total error from the chromatic limit of 60μrad to a φ averaged value of 95μrad entails a 58% increase of the Cherenkov constant k_c (Table 4) and a 26% decrease of the Kπ momentum separation limit (n_σ=3) to 194Gev/c.

2. FAST DETECTORS AND ELECTRONICS

2.1 FAST PHOTODETECTORS

A program of development of fast photodetectors (σ_t<10ns) with pad readout is in progress [6]. In order to get photodetectors with fast response the photon absorption length l_{ph} must be less than 0.5mm so that the variance of the electron drift time to the amplifying wire be less than 10ns. For a detector with a predominantly methane gas filling the electron drift velocity v_D is about 50μm/ns hence $\sigma_t=l_{ph}/v_D=10$ns. The vapor pressure of the photosensitive molecules Tri Ethyl Amine (TEA) and Tri Methyl Amine (TMA) are sufficient at 20°C to satisfy this condition but Tetrakis Methyl Amino Ethylene (TMAE) does so only at 95°C. Identification, synthesis and characterization of new photosensitive molecules for RICH detectors seems necessary and a collaboration to pursue this goal has been started with Professor Alan Katritzky,a chemist at the University of Florida.

Photocathodes have been made of thin solid or liquid films of TMAE [7]. These cathodes are also fast since the electron drift velocity is 1μm/ns at 1KV/cm hence a 5μm thick film with $l_{ph}=1\mu$m has a time variance σ_t=1ns.

In either case (solid or gas phase photocathode) gas phase wire amplification with pad read is envisaged as shown in Fig.5. We have measured the pad response in a methane with 50 torr TEA filled chamber (entry window to wire =2.5mm, wire to pad=0.4 or 0.5 mm, wire spacing= 1.27mm, pad size 5 by 7mm) and observed the fast response and shown that high pad efficiency (>95%) is easily attained [6].

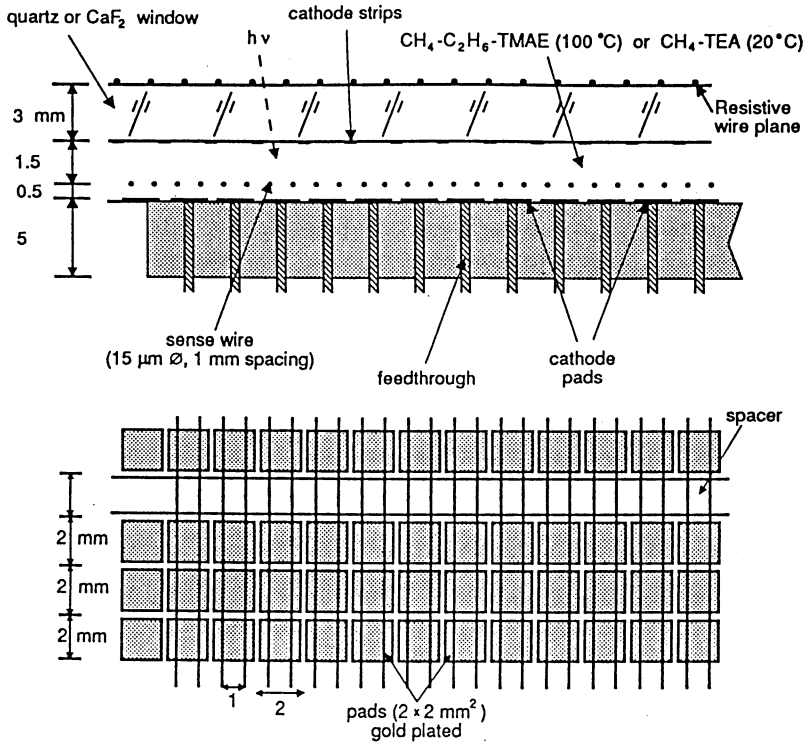

Fig.5. An example of a photosensitive pad detector operating with a photoionizing gas. It can also operate with a reflective solid photocathode deposited on the pads.

With regard to TMAE photocathodes we have already established [7] that they have significant quantum eficiency. A new setup has been designed and tested with thin liquid TMAE films (by gas flow and cryopumping), thin CsI films (by vacuum deposition) and mixed CsI(TMAE) films made by TMAE gas absorption on prepared CsI films [8]. The results indicate extremely high quantum efficiencies i.e. 60% at 170nm for a reflective cathode geometry. Such a geometry is compatible with the chosen pad geometry. Operation of pad detector with a reflective CsI(TMAE) cathode would require a quenching gas, such as isobutane. It absorbs the C* photon feedback lines at 156 and 166nm but is transparent to the line at 193nm. It is believed that this quenching will suffice to allow stable detector operation with sufficient gain for single electron detection on the pad. The use of solid cathodes for RICH opens the possibility of windowless detectors with the concommitant gain in photon transmission as well as simplicity and reduced cost.

2.2 VLSI PAD ELECTONICS

The critical feature of this type of detector is the quantity of readout electronics which will be between 1/4 and 1Million channels/m^2 .The readout electronics has been designed and prototype circuits have been fabricated. The participants in this development include physicists and engineers at RAL, College de France, CRN Strasbourg, Paul Scherrer Institute and LAA project at CERN. The electronics chain consists of an analogue bipolar chip with 8 channels of a low noise (<1000e) transimpedance input preamplifier, amplifier and discriminator. This is followed by a digital CMOS chip with 16 inputs which reads only the hit pads. It contains a FIFO buffer for separate read and write operations, facility for on chip encoding, data compression and output bus arbitration. The readout time for 10^5 pads is expected to be less than 10μs. First circuits are to be produced by late 1989 and 40K channels (first production run) will become available by summer 1990. This will suffice to equip a prototype 200mm by 200mm detector with 1mm^2 pads. The price per channel is expected to be about 2 swiss francs excluding development costs.

3 PHYSICS REQUIRING PARTICLE IDENTIFICATION

Exclusive particle decay modes must be identified in order to measure the invariant mass of the particle. A much increased efficiency in identification of heavy flavor states, such as D and B mesons, can be realized with secondary vertex detection coupled with complete particle identification. A large RICH detector has been built for DELPHI-LEP at CERN [9], and proposed for the B Meson Factory at PSI [10], the SPPS collider at CERN [11] and the TEVATRON at FERMILAB [12]. It has been

shown that identification of K mesons is an excellent tag of the accompanying B flavour [11]. Such tagging is necessary in B mixing studies. Experiments at the SPS and TEVATRON Colliders will show if B physics at hadron colliders can compete with electron-positron colliders. If so, such experiments will also be important at LHC, SSC and ELOISATRON because the gluon fusion cross section for B pair production becomes even larger (about 1% of the total cross section) at these energies.

REFERENCES

[1] R.Arnold Nucl. Instr. and Methods A270 (1988) 289. See Appendix A.

[2] P.W.Langhoff and M.Karplus. Jour. Opt. Soc. Amer. 59 (1969) 863

[3] J. Seguinot and T.Ypsilantis. Refractive index measurements of fluorinated alkane liquids at photon energies between 5 and 7 eV, in preparation.

[4] M.Hempstead, J.Chaveau, G.Comby, J.Seguinot and T.Ypsilantis. Far-UV refractive index measurements of monocrystalline sodium fluoride, in preparation.

[5] T.Ypsilantis. CERN EP/89-150. Invited talk at the Symposium on Particle Identification at Hadron Colliders, Fermilab, Batavia,Illinois, 5-7 April,1989, In press.

[6] R.Arnold, Y Giomataris, J.L.Guyonnet, J.Seguinot and T.Ypsilantis. Response of a UV Sensitive Pad Chamber as a Ring Imaging Cherenkov Detector. In preparation.

[7] V.Peskov, G. Charpak, P.Mine, F. Sauli, D. Scigocki, J.Seguinot, W.F.Schmidt and T.Ypsilantis. Nucl. Instrum. Methods A269 (1988) 149.

[8] J.Seguinot, G.Charpak, V.Peskov and T.Ypsilantis. Solid and liquid UV photocathodes, in preparation.

[9] Delphi technical proposal, CERN-LEPC/P2, 5 May 1983.

[10] Proposal for an electron-positron collider for heavy flavour physics and synchrotron radiation, Paul Scherrer Institute, Villigen, Switzerland, PR-88-09, July 1988.

[11] Study of beauty physics at the SPS-collider with real time use of silicon microvertex information, P.Schlein et. al. CERN-SPSC/88-33/P238.

[12] Letter of Intent for a Bottom Collider Detector BCD. N.Lockyer et.al. Fermilab 1988.

TABLE 1
Sellmeir Fits to Molar Refractivity $f(E)=[F_1/(E_1^2-E^2)+F_2/(E_2^2-E^2)]$

MOLECULE	E_1(eV)	E_2(eV)	F_1(eV^2)	F_2(eV^2)
He	23.389	40.412	451.53	788.71
Ne	17.419	45.501	278.09	3625.9
Ar	13.084	24.217	791.68	3794.0
Kr	11.500	19.790	851.67	4034.7
Xe	8.885	25.358	813.16	10961.
H_2	12.884	20.250	638.90	653.34
N_2	13.414	23.215	921.28	3569.6
O_2	13.936	16.872	1505.6	810.94

TABLE 2
Liquid Refractive Index n=a+bE

MOLECULE	a	b(eV)	ρ(g/cm^3)	M(g/mole)	B.P.(K)
CF4	1.2039	.00475	1.603	88	146
C2F6	1.1956	.00746	1.608	138	195
C4F10	1.2037	.01025	1.594	238	265
C5F12	1.2109	.00785	1.63	288	303
C6F14	1.2177	.00928	1.68	338	329

TABLE 3
Sellmeir Fits to Refractivity $f(E)=[F_1/(E_1^2-E^2)+F_2/(E_2^2-E^2)]$

SOLID	f(E)	E_1(eV)	E_2(eV)	F_1(eV^2)	F_2(eV^2)
CaF_2	n^2-1	12.350	24.667	71.855	345.36
Fused Quartz	n^2-1	10.666	18.125	46.411	228.71
NaF	(n2-1)/(n2+2)	10.435	18.275	2.5764	57.788

TABLE 4
Chromatic Errors for Gas Radiators (1 bar,40°C) and a TMAE Detector (6.1 to 7.1eV triangular response, N=65 cm^{-1}, N=9 photoelectrons)

GAS	γ_t	(μrad) $\sigma_\theta(E)$	$\sigma_\theta(E)/\theta$	(m) L	k_c*10^8	(GeV/c) $p_{K\pi}(n_\sigma=3)$
He	124	18	.00224	21.3	4.84	877
Ne	90	26	.00236	11.2	9.60	622
Ar	42	151	.00627	2.4	120.0	176
Kr	33	274	.00900	1.5	277.0	116
Xe	24	941	.02220	0.8	1307.0	53
N_2	41	153	.00618	2.3	124.0	173
CF_4	32	60	.00194	1.4	62.5	244
C_2F_6	25	115	.00291	0.87	153.0	156
C_5F_{12}	17	166	.00284	0.40	325.0	107

Session 10

READOUT ELECTRONICS, VLSI, AND OPTICAL READOUT

A SWITCHED CAPACITOR ANALOGUE STORAGE LINE

A.Olsen and H.vd.Lippe [Center for Industrial Research, Oslo]
P.Jarron, F.Anghinolfi and E.Heijne [CERN]

INTRODUCTION

As a project in the LAA program, Pierre Jarron, Francis Anghinolfi and Erik Heijne at CERN proposed a fast analog storage and delay line for application in front end electronics systems with high rate capability, since future super colliders need temporary analog storage before data filtering by first level trigger. The proposal included data selection by the first level trigger and conversion of the random bursts of valid samples to a stream of analog data at regular speed. In order to get an idea of the possible speed, resolution and linearity, a preliminary experimental 8 elements storage line was designed. Based on the experience with that circuit, a prototype was designed with 64 analog storage elements in the delay line, 8 analog storage elements in the output buffer, pedestal tracking facility and event identification. Both circuits are designed for Mietec's 3 µm CMOS process.

EXPERIMENTAL CIRCUIT

The principal idea shown in fig.1 was investigated with the preliminary test circuit. The integrated charge is kept on the capacitor during storage and readout and not transferred to another capacitor. By switching the capacitor back in the feedback loop in the readout sequence to a separate amplifer, simultaneous write and read is possible.

OTA: The amplifier is a general 1mW folded cascode OTA. Measured frequency respons for the OTA gives the unity gain 40 MHz. The nonlinearity in the range +/- 1.5V, is less than 0.2%.

Linearity: Output voltage as function of input charge is shown in fig.2. The nonlinearity is measured to be 0.9%, which is less than the inaccuracy of the measurement (1.3%).

Gain variation: The gain variation in fig.3 expresses the variation of the capacitor value. The figure shows the relation between 8 elements on a typical sample of the circuit. The standard deviation is 5.3%. There is evidence to claim that a systematic shift is present between the first 4 and the last 4 elements. This can be explained by a corresponding grouping in the layout. For capacitors within the same group, the standard deviation is around 3 %.

Offset variation: The offset is measured at zero input current (fig.4). The offset variation is due to charge injection and crosstalk from the control signals where there is mismatch between switches, and differences in distance between the paths of the control signals.

Speed: The settling time of the output signal is 150 ns and limited by the amplifier speed. So, the highest sampling rate is around 7 MHz.

Noise: The spectrum in fig.5 is recorded by repeated write/read on one capacitor. The FWHM (close to the RMS value), is 1.1 mV which corresponds to signal to noise ratio of 58 dB.

PROTOTYPE. FUNCTIONAL DESCRIPTION

Figure 6 shows the functional diagram of the SAPE. It consists of two units. A "delay unit" and a "derandomizer unit" (FIFO buffer). The shift registers act as pointers to the capacitors: one bit is circulating and the distance between them can be initialized to the desired delay. The function of the derandomizer unit is to convert the readout speed to the mean rate of valid samples. This is done by storing the trigged sample in the analog storage block with a speed of ten times the readout speed. The address of the capacitor in which the sample was stored on in the delay unit, is stored in the digital storage block together with the corresponding trigger number. Since the read and write speed differ, the read/write inhibit logic is necessary to prevent any of the pointers in the derandomizer to overtake the other. This is done by stopping the clock to the "R SHIFT REG" and "W SHIFT REG". The "10 BIT COUNTER" holds track of the trigger number of the triggered samples written to the derandomizer. The trigger burst can not be longer than 7 samples without generating overflow. The samples triggered after the overflow occurs, will be rejected, but when one sample is read out, a new sample can be written into the derandomizer. So at a constant high ("1") trigger, each 10th sample will be written into the derandomizer, and the trigger numbers will not be continous.

OTA: The improved amplifier is designed for 3ns rise-time, or unity gain of 117 MHz. The power dissipation is limited to 4.5 mW.

In the simulation, the sampling (clock) rate is found to be limited by the critical path in the digital logic to 20 MHz.

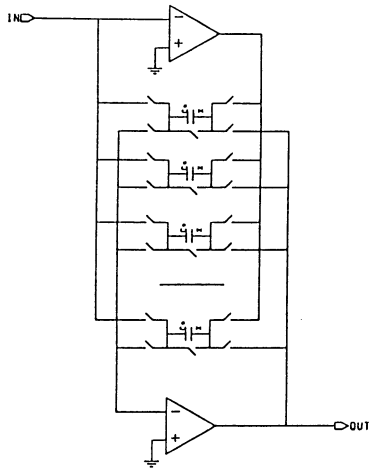

Fig.1: Principle of analogue storage

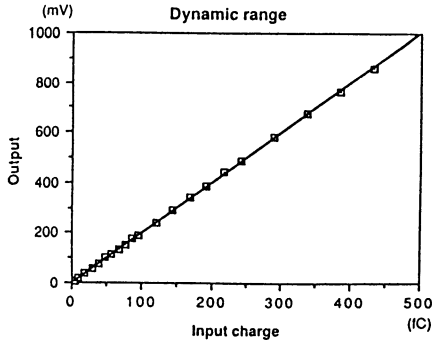

Fig.2: Linearity, experimental circuit

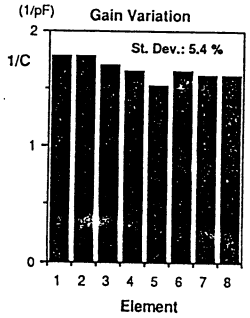

Fig.3: Capacitor variation

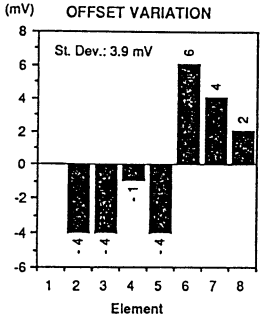

Fig.4: Pedestal shifts

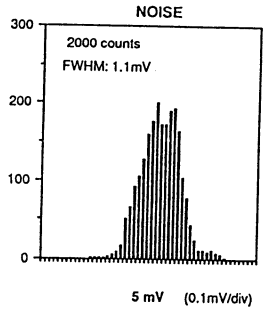

Fig.5: Variation, one elem

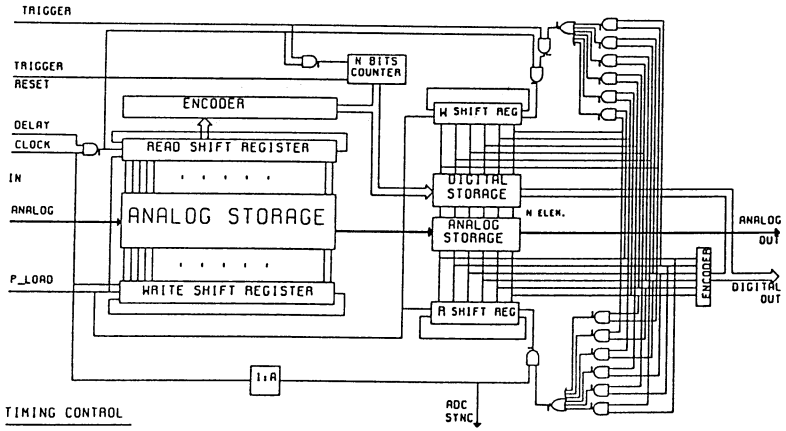

Fig.6: Principle of the prototype

Radiation Hardening of VLSI-Electronics

F.Wulf, D. Bräunig, A. Boden
Hahn-Meitner-Institut Berlin GmbH
Glienicker Str. 100, D-1000 Berlin 39, West Germany

Introduction

Future detector applications require radiation hardened CMOS devices to operate at a total dose level up to 100 Mrad(Si), which is beyond the capabilities of today's rad-hard components (see Fig. 15, [1]). Special design and processing techniques accomplished guaranteed radiation hard devices from 0.1 to 1 Mrad(Si). In some cases, the digital devices show no functional failure up to 10 Mrad(Si). For 1 Mrad(Si) hard devices the CMOS-SOS or CMOS-SOI technology is favoured. Transistors from this technology exhibit higher noise figures than standard CMOS transistors, due to the second interface.

Hardening Aspects

The optimization of bulk CMOS devices by reducing the oxide thickness, the oxidation and annealing temperature for the gate oxide growth, results in the production of rad-hard devices up to 100 krad(Si) [2]. Above this level, additional design change is necessary.

The field oxide undergoes the same effects (trapping of positive oxide charges and generation of interface states) as the gate oxide. This causes an inversion layer between the p-well and the substrate of a CMOS inverter (Fig. 1). The introduction of a P^+ guardband prevents this parasitic channel (Fig. 2a). Additional processing techniques are implemented to harden the gate and field oxides [5]. A second hardening technique has been developed by the Harris Semiconductor [3]. It provides the same hardness levels and the same post-radiation leakage current behavior as the guardband process (Fig. 2b). The advantage of this technique is the higher packing density and the fact that standard CMOS masks can be used.

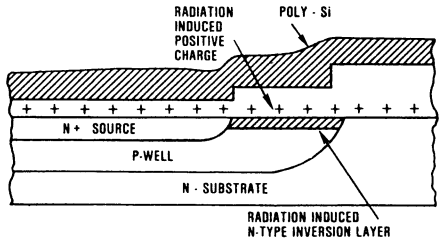

Figure 1. Inversion layer in a p-well of an NPN structure [3].

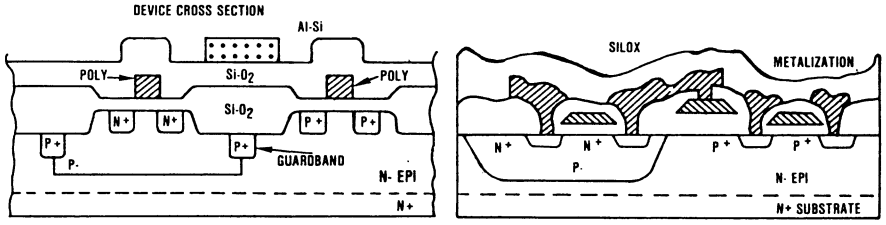

a) b)

Figure 2. a) P^+ guardband techniques of a bulk CMOS inverter [4].
b) Harris Semiconductor field oxide controlled CMOS inverter [3].

A third technology is the Silicon Isolated by Implanted Oxygen process (SIMOX) (Fig. 3), which has nearly the same advantages as the Silicon on Sapphire (SOS) techniques without the problems associated with sapphire and then growing silicon on top of it. The SIMOX (SOI) and SOS technologies are designed to prevent latch-up and transient effects, but are also optimized to high total dose levels (1-10 Mrad(Si)).

Sidewall effects increase the leakage current of bulk CMOS transistors. An additional p^+ implantation prevents the n-channel transistor from this source of undesigned current (Fig. 4). Edge and interface effects also reduce the radiation levels from SOI, SOS technologies. Edgeless SOI transistors exhibit better performance [6].

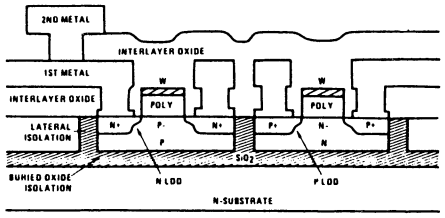

Figure 3. Structure of a Silicon Isolated by Implanted Oxygen (SIMOS) technique [3].

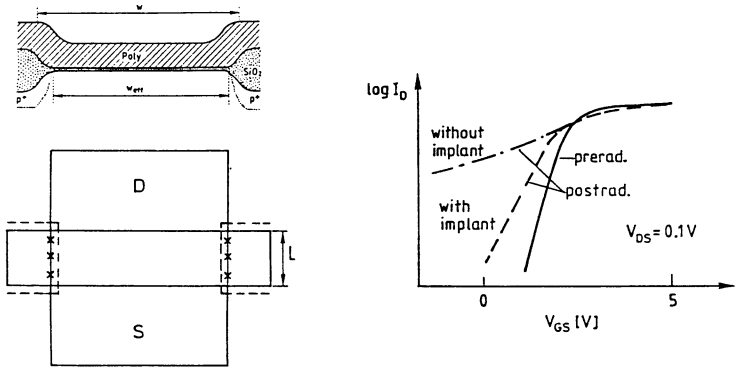

Figure 4. Edge effects on bulk CMOS n-channel transistors.
a) Structure of the channel width.
b) I_D-V_{gs} curve with and without channel stop implant.

Consequences

There are some manufacturers (see Fig. 15, [1]) which produce rad-hard devices according to MIL-STD-M3851 (table 1). These devices are very expensive, the delivery time is long and there are some limitations about the export licence for devices coming from the US. In the US there are a lot of activities for the standardization of radiation tests (e.g. JEDEC Committee IC-13.4 1986; Space Parts Working Group; ASTM neutron, gamma, x-rays, SEE tests; Defence Nuclear Agency).

DESIGNATOR	TOTAL DOSE RAD(SI)	NEUTRON FLUENCE LEVEL n/cm^2
/	NO RHA	NO RHA
M	3000	2×10^{12}
D	10^4	2×10^{12}
R	10^5	10^{12}
H	10^6	10^{12}

Table 1. MIL-STD-3851 of radiation hardness assurance designators.

For Europe and particularly for CERN a radiation hardness assurance program (RHAP) should be established which defines the test procedures and also an approved part list (APL). A cooperation between the US and European activities would be desirable.

References

1 F. Wulf, D. Bräunig, A. Boden
Electronic Components in a High-Dose Environment
Proceedings this issue

2 RCA Solid State
High Realiability Integrated Circuits
1982

3 Harris Corporation
Rad-Hard/HI-Rel CICD Data Book
1987

4 J.E. Schroeder, R.L.Lichtel and B.L. Gingerich
An Advanced, Radiation Hardened Bulk CMOS/LSI Technology
IEEE Trans. on Nucl. Sci., Vol. NS-28, No. 6, Dec. 1981, pp 4033-4037

5 T.J. Sander
CMOS Hardness Assurance Through Process Controls and Optimized Design Procedures
IEEE Trans. on Nucl. Sci., Vol. NS-24, No. 6, Dec. 1977, pp 2051-2055

6 S-S. Tsao, D.M. Fleetwood, H.T. Weaver, L. Pfeiffer and G.K. Celler
Radiation-Tolerant, Sidewall-Hardened SOI/MOS Transistors
IEEE Trans. on Nucl. Sci., Vol. NS-34, No. 6, Dec. 1987, pp 1686-1691

Session 11

DATA ACQUISITION AND SYSTEMS ASPECTS, INCLUDING TRIGGERING

ISSUES FOR TRIGGER PROCESSING AT HIGH LUMINOSITY COLLIDERS

A. J. Lankford

Stanford Linear Accelerator Center
Stanford University, Stanford, California 94309

Abstract

A number of issues for the design of trigger processors at future high-luminosity, high-energy colliders such as the Superconducting Super Collider and the Large Hadron Collider are discussed.

Introduction

Trigger processing is perhaps the most exciting technical challenge at future colliders. It is crucial for extracting the physics signals which we seek to study from extremely high rates of complex background events. In fact, unprecedented interaction rates will require the full power of offline physics analysis techniques to be available in the trigger for event filtering. Consequently, the trigger interacts broadly with both physics goals and detector design.

This workshop contribution identifies some of the issues important to trigger design. It is far from being a comprehensive study. Hopefully it is a provocative introduction to some of the physics requirements and to the range of technical solutions.

Overview of the Trigger

The trigger selects event candidates in a series of stages, or levels, which are progressively more complex and more time-consuming. Each level, by reducing the rate of event candidates, affords the subsequent level more processing time. Although other numbers of levels are possible, this overview will discuss a model trigger with three levels for triggering for high-P_T physics.

At future colliders, even the first stage of trigger decision cannot be made during the interval between bunch crossings. Consequently, every detector signal from every bunch crossing must be buffered until the level 1 trigger decision is complete, and the level 1 trigger must complete a trigger decision each 16 nsec in order to keep pace with the rate of bunch crossings. The level 1 processing time must be minimized in order to reduce the number of bunch crossings for which data will be buffered. Decision times of about 1 μsec are generally discussed in light of the propagation times to and from the trigger on a large detector (about 1/2 μsec) and the need to form some global event quantities such as missing E_T. A fully pipelined hardware processor which exploits extensive parallelism in order to reduce latency will address these requirements. Its pipelined architecture suggests that this processor will have a fixed decision time, which is also convenient for the architecture of the signal buffers. A subset of all detector signals will be provided to the level 1 processor on data paths which are separate from the paths used for data acquisition. The level 1 trigger will provide rejections of between 10^3 and 10^4.

Between 10^4 and 10^5 event candidates per second remain at the input to the level 2 trigger, affording it 10–100 μsec on average per decision. Thus, its processing must be prompt; however, the additional decision time available allows iterative processing, such as sequential processing of track candidates. Additional time also allows event candidates to be directed to independent processors for processing in parallel. In this way, the level 2 trigger can exploit "event parallelism" in the processor farm sense, as well as "parallelism within an event" as used by level 1. With or without the use of event parallelism, microprocessors embedded within the level 2 architecture may play a significant role in the level 2 trigger selection. The level 2 processor will still operate only on a subset of all detector data transported on a separate data path, including the data used by level 1 and the output of level 1.

The iterative nature of level 2 suggests that its decision time will be variable, in the range of tens of microseconds; however, for the convenience of the architecture of the front-end signal buffering, the level 2 trigger processor will preserve the order of event candidates, performing resequencing if trigger decisions complete out of order. Rejections of about 10^2 are expected for level 2.

The rate of event candidates into the level 3 trigger is then between 10^2 and 10^3, a rate which is sufficiently low to allow transport of data from all parts of the detector and to accommodate a farm of microprocessors as the level 3 trigger processor. In fact, rates into level 3 higher than 10^4 may be feasible. The full event, with the full detector resolution, consequently is available, as are the power and flexibility of general-purpose, high-level language programmable CPU's. Rejections of between 10 and 10^2 are expected from level 3, resulting in a final rate of event candidates of a few 10's per second.

Physics Goals

Triggers at future colliders must be designed to identify, count, and measure the quanta which characterize the physics at high energies: jets, muons, electrons, photons, and weakly interacting particles, such as neutrinos, which leave missing E_T. The trigger must also be able to combine requirements on these quanta and on event topology in order to select event candidates. Although triggering on the physics at the highest mass scales will not be difficult, a number of reasons for triggering on physics at lower energies also exist. These reasons include the goal of linking the physics at the highest energies to the physics at present colliders, the goal of studying a relatively low mass (150 GeV) top quark, and the need for adequate calibration events such as W's and Z's. Preliminary studies suggest that the physics goals can be met by prompt triggers which also provide the desired reduction in trigger rates. For instance, for inclusive triggers, thresholds may be set at approximately 40 GeV for inclusive electrons and muons, 1 TeV for single jets, and 175 GeV for missing E_T.

Single Electron Trigger: An Example of a Prompt Trigger

A prompt inclusive electron trigger studied by Sakai of KEK illustrates the nature of selection criteria which might be used and the rate reduction possible. He used a simple calorimetric model with fast shower simulation of QCD events by ISAJET. By requiring a calorimeter tower of size $\Delta\phi \times \Delta\eta = 0.2 \times 0.15$ with electromagnetic energy deposit greater than 20 GeV but with the energy in the hadronic section less than 20% of the energy in the electromagnetic section, he achieved a rejection of greater than 10^4. By also requiring a stiff

track ($P_T > 5$ GeV) pointing towards the trigger cell in ϕ (i.e., with no z requirement) and requiring that the trigger cell be isolated (i.e., the energy in nearest neighbor cells is less than 20% than in the trigger cell), the rejection is greater than 10^6 for all energies greater than about 12 GeV.

Although this study deals only with a simplified model of a calorimeter, it suggests strongly that rejections of greater than 10^5 can be achieved by prompt triggers for isolated electrons with P_T greater than 40 GeV.

Inputs to Prompt Triggers

Only a modest fraction of all detector signals is required for prompt triggers. Electron triggers require electromagnetic calorimeter towers of about $\Delta\phi \times \Delta\eta = 0.2 \times 0.2$ over about five units of rapidity, hadronic towers over the same region, and track segments from chambers immediately in front of the calorimeter. By requiring track segments at the outer radius of the tracking volume which point towards the interaction vertex, only stiff tracks (with $P_T > 5$–10 GeV) will be matched to electron candidates in the calorimeter.

Muon triggers will require track segments from the muon chambers, signals from muon system scintillators (if they exist), and track segments from the outer tracking volume. Signals from the hadronic compartment of the calorimeter may also be used.

Jet triggers, and ΣE_T and missing E_T triggers, will require only calorimeter towers which sum the electromagnetic and hadronic portions.

Some General Technical Design Considerations

The bandwidth required to transport data to prompt trigger processors for 60 MHz bunch crossings is quite high, even for subsets of the detector data. For instance, 5000 calorimeter sums of two bytes each require a bandwidth of 600 Gbytes per second .

Most trigger quantities are topologically localized on the detector. For instance, the detector signals which characterize an electron originate in a small region of solid angle. Consequently, much trigger processing could be done locally, which would ease the data bandwidth problem.

Power dissipation of trigger processors, and of drivers which transmit data to the trigger, may limit the amount of trigger processing on various parts of the detector, or it may limit the amount of data which is available to the trigger. For instance, transmission of all hit wire information from a central drift chamber to a remote trigger processor may be problematic, as may be local processing of all hit wires into track segments.

The trigger latency, even for deadtimeless triggers, is important in that it affects the design of front-end electronics. In the simplest solutions, it affects the amount of buffering, and possibly the architecture of the buffers, in the front-end. In some solutions, such as "smart" pixels, the effect on occupancies, ambiguities, and resets is profound. The level 1 latency is at least half a microsecond, which is the propagation time of signals to and from a central trigger processor.

Detector response times and propagation delays within the detector are often longer than the time between crossings. Consequently, signal collection for the trigger, as well as strobes back to the detector, must be time synchronized. Delays will need to be adjusted for groups of channels. Empty beam buckets may help select these delays.

When designing a fast trigger, the designer often has a choice between exploiting event parallelism or parallelism within an event. Event parallelism is exploited by processors working in parallel on separate events, as in a microcomputer farm; whereas, parallelism within an event is exploited by parallel processors working on separate portions, such as different regions of solid angle, of the same event.

The questions of: "How selective should the trigger be?" and "How many events should be written to tape?" are closely related to physics goals. However, there exist tradeoffs between recorded event size and number of events recorded, as well as in applying processing power to reducing one or the other. Both reductions are forms of data filtering.

Event Pileup

Event pileup affects detectors with fast response times, as well as slow detectors, because of multiple interactions per crossing. For an average of 1.6 interactions per crossing, the probability of having more than one interaction is 48%. Given that there was at least one interaction, the probability of having more than one interaction in the same crossing is 60%. Of course, the effect of pileup is smallest for detectors with single crossing response times.

Each detector entity which provides a trigger, e.g., each calorimetric trigger tower, must identify the bunch crossing being triggered upon. Positive crossing identification is possible even for detector components which do not have single crossing response times. For instance, the time of arrival of liquid ionization calorimeter signals can be derived from the zero-crossing of their predictable pulse shape. Time resolution in the 1–2 nsec range should be achievable for 10 GeV electrons and 50–100 GeV jets in liquid argon calorimeters. In drift chambers, correlations in drift times between nearby, offset layers allow untangling of the drift time from the time origin of the ionization.

Event overlap arising from multiple interactions during the resolving time of the detector does not seriously confuse physics. This fact is because the probability of two rare events overlapping to fake a more rare event is small. In addition, the probability of an ordinary event overlapping a rare event to fake a more rare event is less likely than an extra hard gluon radiation within the rare event.

Event overlap does not significantly increase trigger rates for hard processes because it is unlikely to combine hard scatterings from multiple events. Increasing the number of interactions within the resolving time of the detector increases the trigger rate by the same factor; however, it does not change the ratio of accepted to rejected interactions. Isolation cuts, on the other hand, may be compromised by the addition of soft particles within the isolation cone.

ΣE_T is not a good event selection variable because it does not select only hard scattering. Consequently, event pileup significantly increases rates for ΣE_T triggers. Missing E_T, however, is not seriously affected by event pileup because overlapped events do not have large E_T, and hence do not have large missing E_T.

Calorimeter Triggers

Calorimeter triggers require minimal pattern recognition and are naturally implemented in prompt triggers. In fact, the full granularity of the calorimeter, which is driven by detailed e/π separation and by mass resolution for decays of W's into jets, is not needed by the prompt trigger. Consequently, the first step in forming a prompt calorimeter trigger is

and 0.2× 0.2. The input signals to the tower sum will be analog, with digitization occurring subsequently; however, particular care must be paid to maintain uniform calibration and timing in order to preserve resolution.

The level 1 trigger can be implemented as a pipelined digital processor, of which the Zeus and D0 level 1 triggers are examples. Digital processing affords well-defined synchronization to a system clock and facilitates, via memory look-up techniques, application of thresholds, weights, and calibration. It will be important, however, to determine the dynamic range which must be maintained during digitization and digital processing.

A variety of prompt jet algorithms are now in use. These include energy clustering about a seed tower as done by CDF, energy summing in overlapped fixed cones as done by UA1, energy clustering in detector subregions with special treatment of edge effects as done by Zeus, and identifying a seed tower only as done by D0.

In order to avoid a separate trigger bias, the trigger should achieve the required level of rejection using the same jet algorithm, or a subset of it, as is used offline for physics analysis. For ease of theoretical interpretation, most experiments now seem to prefer a jet algorithm which defines a jet as energy flow within a fixed cone about a jet axis. The cone size, however, varies with the physics being studied.

What is the ideal prompt calorimeter trigger? Perhaps it would be provided by a massively parallel architecture in which a single, simple processor corresponding to each tower investigates the hypothesis that its tower is the center of an energy cluster (for several fixed apertures), with all towers being processed in parallel, and perhaps even employing the full granularity. A second level of logic could arbitrate overlapping clusters. This trigger implements an offline algorithm with the full resolution of the offline analysis. On the other hand, a much less ambitious solution may also provide the required level of rejection without introducing trigger biases.

Any future prompt calorimeter trigger will more fully exploit the segmentation, calibration, and resolution of the calorimeter than in the past. In fact, few selection criteria may remain for use by the higher level trigger. Higher-level triggers may be limited to refinement of electron identification and further selection and combination of criteria which are formed by the prompt logic.

Tracking Triggers

Tracking of charged particles by the trigger is instrumental to selection of electron and muon candidates. For electrons, the presence of a stiff charged track directed towards an electromagnetic shower reduces photon and π^0 backgrounds. In addition, tracking can link information from transition radiation detectors to showers and can provide an E/p check to help reject chance overlap of a charged track with a shower produced by a photon. Identification of track segments, rather than full track reconstruction and momentum measurement, may be sufficient for any of these tasks.

For high-P_T muons at large angles, sufficient rejection will be provided by simply demanding the presence of a penetrating track segment in the muon system which points back to the interaction vertex, where a cut on the angle of the segment in the bend plane provides a P_T cut. At smaller angles, below about 15 degrees, a sharper P_T cut, in the range of 10–15 GeV will be needed. This requires use of drift time information and track reconstruction even at Level 1.

Beauty physics places a premium on track finding by prompt triggers since the transverse momenta of particles from B decay are not sufficiently large for calorimeter triggers. On the other hand, relatively stiff tracks, in the few GeV range, do arise from the B mass and P_T. A prompt trigger which selects events with at least one track with $P_T > 3$ GeV or at least two tracks with $P_T > 2$ GeV may provide an enhancement in B events of about a factor 50. For this purpose, it may be possible to define a track as a segment at the outer radius of the tracking system whose P_T is measured by linking the segment to the interaction vertex.

Novel techniques for recognizing or measuring charged tracks in prompt triggers include the use of associative memory and of data-driven pipelined processors. Associative memories, including custom VLSI applications for high energy physics, implement template matching techniques which can greatly increase the number of patterns searched as compared to simple memory look-up techniques. The CDF level 2 track finder is an example of a pattern matching segment finder which uses similar techniques to identify tracks with $P_T > 3$ GeV. Data-driven pipelined processors, as implemented for Fermilab E690, can implement track finding and fitting which exploit combinations of parallel processing and processing pipelines to create a machine which is economical in its use of hardware and nearly fully efficient in its use of processing. This architecture could also exploit modern ASIC implementations of many hardware functions, or for that matter could allow embedding of programmable processors for certain tasks.

Higher-Level Triggers

Higher-level triggers will require considerable processing power in order to apply sophisticated event selection criteria to the high input rate of event candidates. Considerable flexibility will be required of the trigger processors in order to allow changes in the event selection criteria as physics experience is gained and as physics goals evolve. This flexible processing power will be provided by large "farms" of powerful commercial microcomputers. For example, between 1000 and 5000 future processors might provide an aggregate CPU power of between 10^5 and 10^6 VAX equivalents, or about 10–100 "VAX-seconds" per event candidate. The processors might be implemented with four RISC processors per board using FUTUREBUS+ with data input via a high-speed external bus. Each processor crate might also include a boot node and a shared mass storage device.

Industry has taken an interest in massive parallel computing on a similar scale. More than one firm now discuss 10^3 to 10^4 parallel nodes for scientific computing using loosely-coupled RISC processors and message passing. Perhaps the future will offer a commercial solution for the higher level trigger.

Such a massive application of processors, however, will demand significant development of software system tools. For instance, the operating system must allow management of data flow and of processing, continuous operation during configuration changes, *in situ* debugging of production code, tools for development of new code, and facilities for verification of proper operation. In fact, the farm must provide a comfortable programming environment with operating system tools comparable to that which exists on the popular minicomputers of today.

Trigger Designer's Tool Kit

The trigger designer today has a wide array of new and more advanced tools available for the task of building fast, powerful triggers. At the component level, programmable logic

is available with more versatile cells, larger scale integration, and advanced development (programming) tools. Gate arrays are available in a range of technologies, CMOS, BiCMOS, ECL, and GaAs, allowing optimization of speed and power. They now offer between 10^4 and 10^5 "usable" gates per chip, and will offer more in the future. Silicon compilation offers advanced cell libraries and development tools for semicustom designs, and design of full custom VLSI is possible where required.

For the fastest trigger processors memory look-up techniques will continue to be common for simple pattern recognition and fast mathematics. Content addressable memory, either commercial or custom, offers more efficient use of silicon for pattern matching.

Simple arithmetic processor chips, digital signal processors, and RISC processors can be chosen to match a combination of computational speed and programming flexibility to a task. Modern DSP's are programmable in high-level languages and have versatile operating systems. RISC processors are suitable for embedding in special-purpose devices as well as for general-purpose computing.

Processors with special architectures from outside HEP may also find roles as trigger processors. Image processors offer possibilities for pattern recognition, clustering, and similar tasks. Some of our local pattern recognition problems may be sufficiently simple to map onto neural nets of realizable scale. Alternatively, neural nets may serve as a paradigm for some application of massive parallel processing. Concurrent machines also offer a form of massive, fine-grained parallelism which may match the topology of some of our processing problems.

Special-purpose processors, such as traditional hardwired triggers, and general-purpose microprocessor farms often seem in competition as trigger processors. In fact, both types of processors have roles in the trigger. Special-purpose processors are necessary for speed at the first levels of prompt triggers, and can be designed to be programmable with respect to important parameters. General-purpose processors are required for flexibility at the last level of event selection. Furthermore, the distinction between special-purpose and general-purpose fades as DSP and RISC cores become embedded in custom circuits and as custom coprocessors are attached to general-purpose CPU's. The crucial issues in choosing technologies are: "How much processing power is required?" and "How much flexibility is needed?" Physics goals and detector design will determine the technology requirements.

Concluding Remarks

Although the trigger problems at future high luminosity colliders are challenging, they are tractable. Thresholds in prompt triggers can be chosen to satisfy both physics goals and data acquisition requirements. Event selection can be accomplished online with the same programmable flexibility available for offline physics analysis. Technology for electronics which can meet the processing challenges is rapidly developing.

Acknowledgments

This workshop contribution summarizes many contributions to previous workshops by other authors, who I would like to acknowledge here. This work was supported by Department of Energy contract DE–AC03–76SF00515.

Realities of Large Data Acquisition Systems

(Ph. Gavillet - CERN)

Introduction - Disclaimer

- Difficult to discuss problems instead of successes. Modesty is the rule.
- Wide, honest exchange of information is necessary as experiences vary from one system to another.
- To be judge and jury leads to biased opinion.
- Nevertheless, an objective observation of facts should help in :
  - Avoiding to do / repeat too many mistakes.
  - Design, construct and operate functional systems in optimum conditions.
  - Identify those sand grains and Achilla heels which can corrupt wonderful DAS systems.

The task of realising a functional DAS

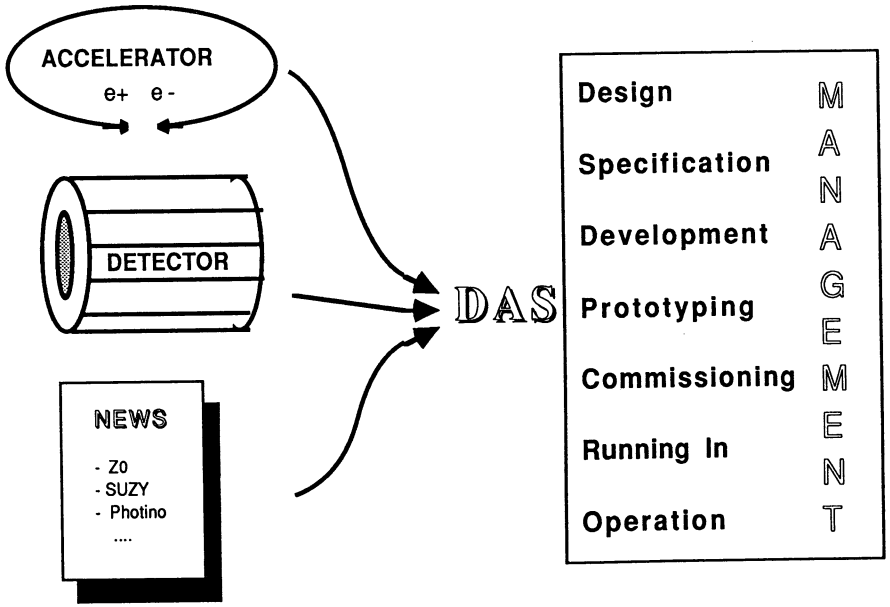

Several constraints : Time scale, technological, engineering, manpower and expertise, financial (DAS : 5% - Front End Electronics : 30% of detector cost).

Design Phase

- Exiting moment characterised by :
  - Random exchange of new ideas :
    HARDWARE : Architecture, Bus, microprocessors, ASIC, parallel processors, transmission media, computers, recording devices,...
    SOFTWARE : RT Operating Systems, languages, Expert Systems, graphic tools,..
  - Participation of various species of enthousiastic people :
    Physicists, "Data acquisitioners", computer scientists, electronicians,...

- Difficulty to :
  - Appreciate the relevant parameters (e.g the LHC/SSC actual trigger rate).
  - Form a team speaking the same language and prepared to converge on the specification of the system :
    Physicists : *" DAS is a service (Project ?) attached to the detector ".*
    Onliners : *" DAS is the chance to build a distributed multi-processor data acquisition network".*
    Electronician Developers :" *DAS is a nice motivation for frontier R&D projects".*

- Explanation : Contributors participate on a democratic basis. They come from scattered Institutes and are not really concerned by the System aspect (in particular : the financial).

- Reality : HEP DAS teams are very different from Design teams as setup in the industry for well defined projects.
  Some people say : *" They are more artist and less professional".*

- Lack of :

  - Methodology :

    Past experience on small scale systems of the previous generation cannot be extrapolated straight.
    Need for systematic approach e.g SASD.
    PROS: Logical, computerised approach do design.
    CONS : *"You do not get more than you put in ".*
    " It becomes a rigid bible - Real life is different".
    Pernicious example : SASD used aferwards to produce excellent docs.
    Feeling : It is the future, although, instead of a simple (pretentious ?) Top --> Down view, one should proceed iteratively : Top --> Down --> Top ... along the course of the project.

  - Simulation methods :

    a) Data flow simulation
    Done by a few LEP experiments (ALEPH, L3, DELPHI) on a limited scale.
    It should become systematic, based on commercial tools and be regularly refined during the realisation of the project.

    b) Trigger simulation
    Done in some experiments e.g DELPHI : 1st Level.
    Based on event generator and tracking through the detector elements, it is very useful to evaluate the best segmentation of triggers.
    Problem : It is especially required when designing the trigger, but at that time a substantial part of the input information is missing (detailed geometry, response functions, E, position accuracies,...).
    Nevertheless it is a tool which should be developed and upgraded during the project to ultimately serve to determine the trigger acceptance and to study new triggers for new experiments.

Specification Phase


The end of the design phase coincides with the definition of the DAS architecture and the adoption of hardware and software standards.

• **DAS Architecture :**

- Tree like oriented, imposed by the reality that individual detectors are built seperately in distributed Institutes and have to operate themselves as elementary DAS (Fig.1).

- The grouping of detectors in partitions is made according to their affinity.

- The integration of the partitions into a coherent system is achieved by a connecting network. All branches of the tree converge to a unique trunk (Central Partition) where the event is built and sent to a central online computer for data recording.

- Naturally : Control and processing (filter) elements are inserted at the distinct levels : Digitiser boards / Crate or cluster of crates / Partition / Event level.

  All constituants are identified :
  Connecting bus / Segments (crates, cables) / Interconnects / Controllers / Processors / Buffers / Interfaces / Host computers.

• **Standardisation choices :**

- Everybody agrees on the idea of stantardisation but problems arise when to decide which standards to choose.

  a) Hardware standards
  Simpler (?) : Standards are real in the sense that they correspond to official specifications following normalisation rules and/or are widely diffused and supported products.

  However a lot of problems :
  * Not always benchmarks available to decide on real performances versus needs.
  * Consultants are to be listened to prudently :
    Home experts recommand their favoured products.
    Industry can give futuristic advices e.g the announcements of fast magnetic tapes, optical disks, satellite data transfer to be of common use at the time LEP will start.
  * Too much theoretical and abstract considerations and too few interest to the future commissioning, operation and support of the system.

  Examples :
  * FASTBUS Choice : Nice standard especially designed for HEP, with all the necessary features and goodies.
    But : Very limited industry interest i.e expensive equipment, maintenance problem,...
    Severe weaknesses : Logical level fixed at 100mV on cable creates major difficulties in configuring distributed systems with long cables with several modules connected to them.
  * Development of microprocessor boards (Controller / Processor / Interface)
    Very interesting for a small competent team to develop a microprocessor board and later a few extension boards.
    Result : proliferation of good modules but some waste of effort and support problem.

* Choice of computer equipment
  Difficulty to define the best configuration of online computers and to match it with the packages offered by the constructors.
  Dilemma : Standardise and buy computer equipment to start development immediately or wait for better price / performance equipment.

  My advice : *Computer equipment purchase should be delayed as much as possible, especially if one has former models of the selected company. Never buy the first issue of a new series.*

b) Software standards

* Some easy choices e.g : when the computer family is selected, the choice of the Operating System and software tools normally follow.

* Microprocessor System : Everybody is going to multitasking systems.

* Dedicated and specialised softwares e.g VME, FASTBUS libraries, data bases, error handler, buffer manager, human interface,...
  The definition of standard is less clear as often one deals with products proposed by development teams attached to a computing department. In this situation the possible risks are :
  . The specification does not fit well the needs.
  . The collaboration developers / users is not close enough.
  . The product may not be ready when expected.
  . One has to partially debug packages written by others.
  . Each software module being developped as a very complete and universal package, the assembly of several modules leads to enormous packages even for limited applications.

Personal conviction:
One should have a precise opinion based (also) on pragmatic principles :
. Availability of the standard software from the development phase on.
. Simplicity, functionality immediately tested.
. Encourage the collaboration designer / user close to the experiment.
. Try to extract yourself the basic features that will make your software functional.

Development Phase

Nice period during which you do what you like to do. Good moment to :
- Setup properly your test bench (hardware and software) as it will be used for long... up to data taking runs.
- Appreciate the sort of tools you need :
  Hardware : Electronic CAD, Logic state analyser, universal programmer and accompagnying user software.
  Software : Basic libraries (VME, FASTBUS), human interface package,...

Facts :
- R&D projects are largely geographically distributed --> difficult to coordinate and to allocate priorities.
- Isolated in their labs, specialists, perfectionists may loose the goal and insist too much in providing the best, most universal product.

Some examples and remarks :

- Development of an electronic module ;
  * Necessity to associate from the very beginning, hardware and software experts in a development team.

  * Importance of the test software :
    . It is the basic tool to debug the hardware.
    . It should be developed close to the hardware specialists and iteratively from their requests.
    . However, it should be designed in order to be later integrated, at least partly in the form of libraries of routines, to the production software.

Personal experience :

- Nice general purpose test packages are not really used.
- One wonderful modern test package providing a graphical disassembling of FASTBUS transactions not frequently used.
- One simple, on the spot written and extended test program, largely used, exported and becoming a de facto standard. Reason : Simple of use (all in one screen), easy to modify and very close to the usual actions either at the module, crate or assembly of crates levels.

Deduction :

Test packages should be conceived as evolutive packages to become ultimately control packages. Below are summarised the important characteristics of such a package as a function of the successive phases of the project.

	Development	**Prototype**	**Production**
User Interface	Full interactivity	Procedure of commands	Automatised execution No interaction
Error processing	Fully interactive error handling at transaction level	Interactive error handling at command level	Error logging
Running conditions	Succession of independant sessions	Cold start Configurable system with context saving	Linear sequence of processes
Help Guidance	Built in Help facility	Intelligent Guide system	Comprehensive execution report

Prototyping Phase

Important phase : from a few modules to a few crates. One discovers that not everything works as expected.

- Run assembly of a few crates prefiguring a single partition DAS from the host mini-computer.
- Test / Control software should be versatile enough to :
  a) accomodate, changing, evolving hardware components.
  b) accept several users performing different series of tests.

Observations :

The more extensive use of modules in a prototype system reveals bugs, missing features of someone. It requires a close contact with the manufacturer starting the commercialisation of the modules.

Difficulty to :

- Decide on which hardware setup to start the test of the smal prototype system.
- Obtain a prototype version of the final data acquisition software.

Advice : Start as soon as a minimum set of hardware components exist to construct a small system. Push to get a first release of the DAS software.

Fortunately : The tests of detector elements in test beams puts a fixed time scale on the realisation of the prototype acquisition systems.

Construction - Commissioning

Hard, painful phase. It is never really discussed in workshops, conferences.
One realises the jump between small systems and the integration of 10 - 15 partitions of 10 - 20 crates each into a coherent system.

Preparation and order of equipment

- Final definition of detector, individual partition and central partition architecture.
- Final specification of the connectics : cable layout, choice of cable, connector, cable adaptor boards,...
- Precise accounting of all elementary components up to the tiny connectors.
- Choice of companies with second source if possible.
- Follow up of orders with the usual surprises : long delays, lack of components.

Validation of equipment

- Production and test of front-end electronics normally up to detector groups.
- DAS items : Hundreds of modules to test, of cable connector to mount and test.
- Ideally one should proceeds from module to partition in collaboration with detector teams.
- But difficulty to find the staff and the necessary experts although it is crucial to validate everything before and after installation at the experiment site.

Realisation of the Data Acqusition Center

In addition to the pure acquisition network, a complete data acquisition center includes :

Surface Control Room ---> Underground DAS counting room ---> Detector counting rooms

The infrastructure of rooms, the air conditioning, the water cooling system, the mounting of racks are normally commissioned at an early stage with the general infrastructure of the detector.

Observation : The working environment of counting rooms is not very ergonomic : limited space, noise,... DAS people should feel more concerned if they want good working conditions.

a) Surface Control Room
It usually comprises :
- A computer room housing the data acquisiton and operation computer(s) and their peripherals (disks, magnetic tapes, cassette units,..). It is the center of all communications.
- A control room with the necessary control and work stations.
- A conference and/or quiet room.
- A technical laboratory

b) Underground DAS Counting Room
It contains the data acquisition racks of the 10 to 15 partitions with for each of them the host mini-computer and console station.

c) Communication network

• **Backbone :**
- Communication racks concentrated in the computer room of the surface control room :
  ---> Arrival of all external communications (Accelerator, public network,..)
  <--- Distribution of all the surface and underground communications.
- Reserved cable path between the surface and the underground area for all the communication and control cables.
- Installation of communication nodes in the underground area to distribute all communications.

• **Communications :**
- Optical cable link for VME, FASTBUS data link, Ethernet, machine timing signals and video information.
- Ethernet network comprising the network of the Surface Control Room and the distribution of Ethernet in the underground area in the various nodes and counting rooms.
- Classical video links
  . Broad band video system to distribute the accelerator information in the surface and underground areas.
  . Surface <---> Underground camera control
- Intercom network
  . Surface <---> underground message broadcasting.
  . Point to point link in the underground area.

Problems :

- The task of installing the Data Acquisition Center is often underestimated and the expertise available is not entire.
- One has to face a lot of unforeseen events.
- Advice : *" On better handles it up to the minor details from the very beginning".* On the other hand it is rewarding as one learns a lot of things.

Running-In Phase

Short but frantic and sportive period. It consists of :

- Setting up each partition acquisition system using pulsed or cosmics triggers.

- Integrating one after each other the partitions into the Central Partition.

- Waiting with the largest configuration expected to work "reliably" for the first beams to come.

Realities :

- A lot of last minute, unforseen events to be handled (missing cables, architecture, layout reshuffling,...)

- It requires a very efficient crew with very good coordination and the ability to assert very short term plans with alternative issues.

- It demands specific qualities : Self control, resistance (almost 24h/day shifts) and fast reaction time with solid common sense. As such it looks as a commando type of operation.

Personal experience :

- One wants first to make the system work. Performance will follow.

- The life time of the system ranges from a few minutes to one hour,.. while its preparation can take hours.

- One experiences most of the Murphy's laws.

- The actual Run Control is limited to the minimum set of commands to prepare, start, abort and stop a run. This because :
  - One cannot rely on a safe run control strategy as it has also to be tested in situ.
  - The human errors become surprisingly high (people are nervous and tired) and therefore it is better to limit the system interactivity.

Parenthesis

It is a pleasure to mention the recent LEP Pilot Run.

Machine : Ready in time
Detectors : All with problems but all ready to take data.

Very good surprises :

Clean beams : Z0 events detected in real time
The four LEP detectors observing beautiful events.

Pay your effort: It works !!!

Operation - Support

• Running conditions

- Operation
  Organisation of shifts - Documentation - Training of shift leaders.
  An intelligent Run Control should rapidely be provided to guide the shift leader and prevent against most of human errors.
  Difficulty to find and keep a stable operating crew.

- Monitoring
  Acquisition : Full event display, graphical control of the data flow are the obvious controls to perform.
  Slow control of temperatures, pressures,.. although not discussed here is an important aspect of the monitoring of the experiment.

- Liaison with the accelerator
  Necessary to harmonise the conditions of running the experiments and the accelerator. It is usually based on exchange of critical parameters through computer networtk and direct personal contacts.

• Electronic support

- Financial aspect should be kept in mind (5% per year of detector cost)

- Given the variety of electronic items, the expertise is distributed. This complicates the organisation of the maintenance.

- The organisation of an Electronic Pool containing all equipments used in large quantities is a necessity.

• Computer support

- The optimisation of the computers architecture is a permanent preoccupation.

- The support of operating system experts is essential to help understanding the real time performances, the reason of hang ups, crashes,...

• Online software support

- Several problems :
  Turn over of collaborators
  Often not more than one specialist per critical software.
  Difficulty to intermixed development sessions with data taking periods.

Conclusions

• Apologies :

The slow control of the detector which is an integrant part of the DAS has not been discussed.

The management of a DAS project on its own justify a separated discussion.

• To realise a large HEP Data Acquisition System is always a challenging, pioneer, collective, sociological,... adventure.

• I would like to visit Research, high technology Data Acquisition Centers (ESA, NASA,...) to widen my experience.

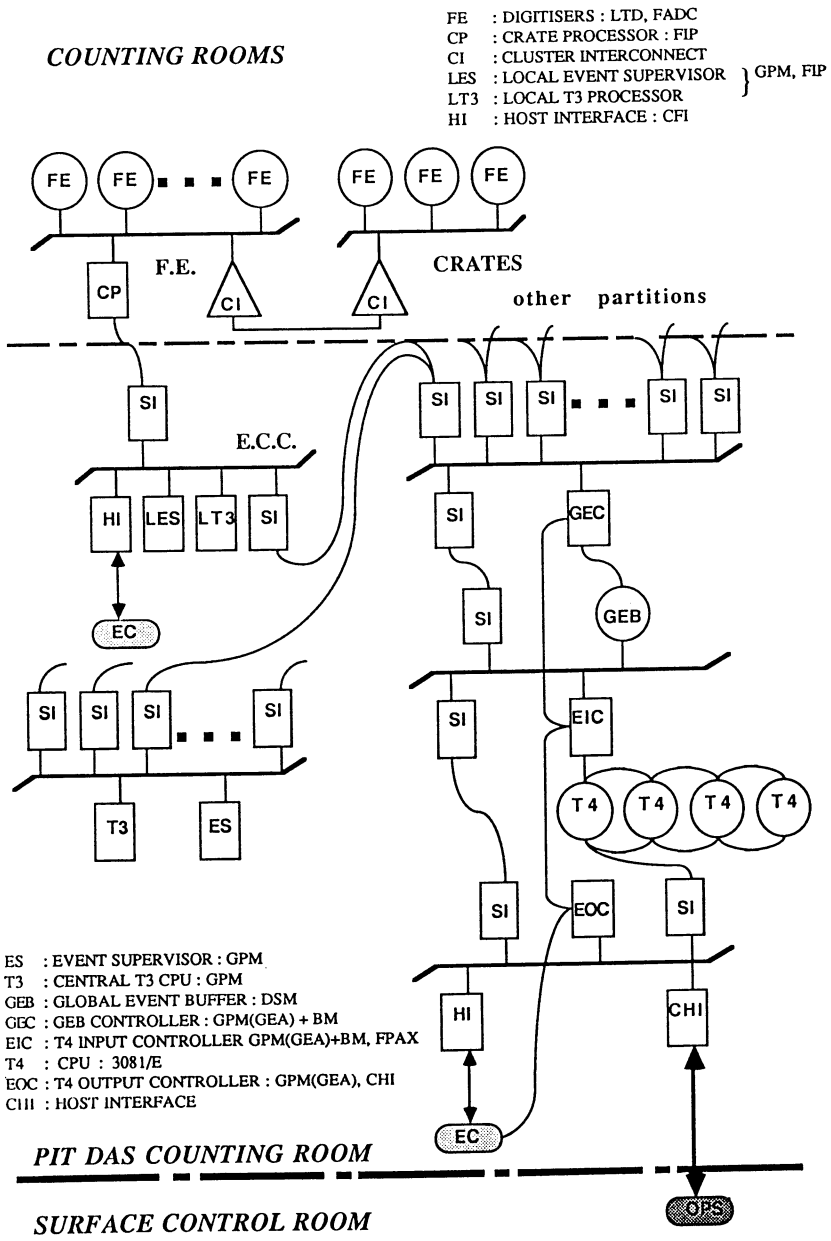

Fig.1 DELPHI Data acquisition Architecture

General Purpose Computers In Real Time

Joseph R. Biel
Fermilab Computing Division
September 18, 1989

Introduction

I see three main trends in the use of general purpose computers in real time. The first is more processing power. The second is the use of higher speed interconnects between computers (allowing more data to be delivered to the processors). The third is the use of larger programs running in the computers. Although there is still work that needs to be done, I believe that all indications are that the online need for general purpose computers should be available for the SCC and LHC machines.

More Processing Power

The history of computers is a history of vast increases of computing power with a simultaneous decrease in price. At present, the greatest contributor to the continuation of this trend is found in the development of RISC (Reduced Instruction Set Computers). One manufacturers projections of RISC performance are shown in figure 1.

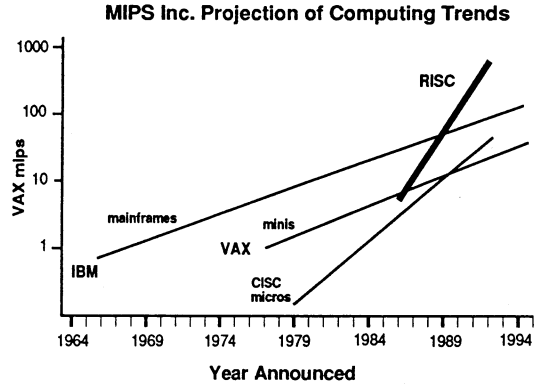

Figure 1. MIPS Computer Systems, Inc. Projections

The basic ideas behind RISC are to construct a microprocessor with

- A relatively small set of machine language instructions
- Machine instructions that provide needed functions only with no redundancy
- An instruction set that allows a simple, high speed implementation
- A highly optimized compiler well matched to the instruction set

A wide variety of RISC microprocessors have been designed. Among those available commercially are the MIPS R2000/R3000, the Sun SPARC, the Motorola 88000, the AMD 29000, the Intel 860, and the Intergraph Clipper. Among those companies with proprietary chips are Apollo, IBM , and Hewlett-Packard. Approximate performance values for some of these chips are

- MIPS R3000 (25 MHz clock) 20 VAX MIPS
- SPARC (16 MHz clock) 10 VAX MIPS
- Intel 860 (40 MHz clock) 14 - 17 VAX MIPS
- Motorola 88000 (20 MHz clock) 14 - 18 VAX MIPS

where a "VAX MIP" is the power of a VAX 780. Some of the complete computer systems using RISC microprocessors are manufactured by DEC, SUN, Apollo, and Silicon Graphics. It is rumored that IBM will soon make some major RISC product announcements. As a specific example of a RISC computer system, consider the Silicon Graphics model 4D/280S. One possible configuration for this machine is

- Eight cpu boards each containing a MIPS 25MHz R3000 RISC chip
- 64 MBytes of memory
- 256 KBytes local cache memory for each processor
- VME bus (10 MB/sec now, 30 MB/sec early 1990)

This configuration has a list price of about $230,000 which corresponds to about $1,400 per VAX MIP.

The Fermilab Computing Research and Development department is working on a RISC VME module. Like the Silicon Graphics machine, it also uses the MIPS R3000 microprocessor. It contains 8MB of memory, 32KB of both instruction and data cache, 256KB of EPROM, and a VME master/slave interface. It is constructed on two boards which together fit within a single width VME slot. A secondary data bus designed at Fermilab, called the "X bus", is also included. This provides an alternate DMA path into memory at a transfer rate of 40MB/sec. This can, for example, be used to implement a high bandwidth level 3 trigger. In such a system, a set of processors are sent events in parallel over their X buses. The total bandwidth for this event filling process is thus 40MB/sec times the number of processors being used. Each module examines the event stream that it receives and rejects the vast majority of them. If an event passes the trigger requirements, that event is read out over the much smaller bandwidth VME bus.

Plans for future enhancements of MIPS chips (not including gallium arsenide plans) include

- MIPS R3000
  - 33 MHz version in 1989
  - 40 MHz version in 1990
  - 60 MHz version in 1991
  - 100 MHz version in 1992
- SPARC
  - 33 MHz version in 1989

40-50 MHz version by 1990

- Intel i860
  50 MHz version soon
- Motorola 88000
  100 MIPS 5-chip set by 1991

Several gallium arsenide RISC implementations of RISC are also being worked on. TI and CDC have a chip that runs at 68 MHz and are working to get it running at 200 MHz. McDonnel Douglas Astronautics Corp. has a chip that runs at 60 MHz and are working to get it running at 200 MHz. Prisma, a startup company in Colorado, is working on a GaAs RISC system that will run at 250 MHz.

The TI/CDC and McDonnel Douglas chips both require external GaAs cache memories to allow 1 memory access every 5ns. Both also require clever compilers to keep pipelines full despite branches.

Higher Speed Interconnects

Computers constructed with the high speed RISC chips already being developed or being developed must also be faster than those currently in use. Fortunately, there are a number of new interconnection mechanisms that are being developed. The Scalable Coherent Interface (SCI) is a standard being developed to allow a 1GB/sec connection to be made between processors. The standard will allow up to 16K processors in a system. Future Bus is a new bus standard being developed. Current plans are to support transfers of 200MB/sec with a 32-bit wide data path and to support higher rates with wider data paths. Fermilab is working on an "event builder switch". This device has as its inputs, multiple streams of data -- each stream from a subdetector in an experiment. It has as its outputs multiple streams of assembled events -- each event sent directly into the memory of a processor. These processors are general purpose computers used as an upper level trigger farm.

Future Online Use Of General Purpose Computers

The expected event rates in the next generation of hadron colliders must be massively filtered to get to an acceptable event recording rate. One scenario for achieving this is shown in figure 2. This design uses a high level processor farm to provide a factor of 10 to 100 reduction in the event rate. The farm would accept 10,000 events per second which at an estimated event size of 1MB requires a bandwidth of 10GB per second. Current estimates for checking if an event passes the filtering requirements are 10 to 100 seconds on a processor with a power of 1 VAX MIP. The farm must, therefore, have a computing power of from 100,000 to 1,000,000 VAX MIPS. This is an impressive amount of general purpose computer power. There is at least one project already underway, the Intel/DARPA Touchstone project, to build a general purpose computer with a power of 100,000 VAX MIPS.

Even though it is theoretically possible to design a complete high luminosity hadron collider trigger without a large general purpose computer farm, there are important advantages in having such a farm. The programs running in the farm can examine the entire event using the full power of FORTRAN (or

any other desired high level language). These programs can exactly duplicate algorithms tested in offline computers. In fact, the experiment can use an offline farm that uses the same RISC microprocessor. In this case, moving a program between offline and online is especially easy. Another advantage is that the filtering algorithms can be discussed with the entire collaboration in terms of a FORTRAN program rather than some obscure trigger processor programming technique.

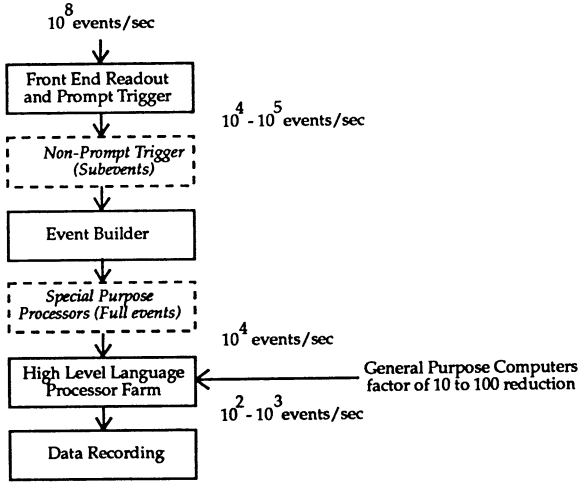

Figure 2. Possible Collider Scenario

In order to have an online farm of fully general purpose computers, it is necessary that the programs running in the computers have a complete operating system environment. In particular, the programs should have the usual FORTRAN access to disk files and terminal input/output. This allows program development to be done for an online farm the same way it is done for an offline computer. Initialization data files can be read from ordinary disk files using FORTRAN OPEN and READ statements. Programs can be debugged on the actual farm hardware by running a normal terminal session with a symbolic debugger. If a program crashes, the operating system can make its usual crash dump file. This file can then be examined later with a crash dump analysis program.

It is not necessary to have serial lines and disk drives connected to each processor. If the processors run UNIX, it is easy to make peripheral connections over a network. Serial connections can be established with telnet and disk connections can be established with NFS and ftp. For processors that share the same high speed bus (e.g VME) can make a network connection directly over that bus. For processors that do not share such a bus, a network connection can be established over Ethernet or FDDI.

There are some potential disadvantages to running a full operating system on the online processors. First, the processor modules will be somewhat more

expensive because they may need more hardware features to run the operating system. These features range from the simple (i.e. perhaps an onboard time-of-day clock chip) to the complex (e.g. a VME bus interface in order that VME disk and Ethernet controllers can be accessed). Second, more memory will be needed to hold the operating system. Third, the booting of the farm is likely to be more complex with a full operating system. Fourth, the operating system itself must be "ported" to the processor board. This includes getting the appropriate license for the operating system.

Larger Programs

The filtering programs running in an online processor farm will probably be longer and more complex than those being used now. How to write these long programs is a very important challenge. It will become more important that programs be properly designed. The tools of structured analysis and structured design (SASD) are one way to help write the programs. Another possibility is the use of new programing techniques such as "object-oriented programming" (OOP).

FORTRAN is still the most used language in HEP, but it may be of great benefit to switch to a more modern language. If UNIX is the operating system being used, the C language is a good choice because UNIX is written in C. Historically speaking, it has been easier to get a good C compiler for a new microprocessor than a good FORTRAN compiler. The use of C also allows a natural progression to be made to the object-oriented languages C++ and Objective C.

BUS AND COMMUNICATION STANDARDS FOR THE DATA ACQUISITION SYSTEMS OF FUTURE ACCELERATORS

Steve Quinton
Rutherford Appleton Laboratory, Chilton, OX11 0QX, UK

Abstract

This paper outlines the main bus and communication standards and their application to the data acquisition systems of future accelerators.

1) STANDARDS

1.1) VME (IEEE 1014)

VME is a well established single crate backplane standard. Continuing new developments and strong industry support maintain its popularity.

Up to 32 bit data transfers with 32 bit addressing are currently implemented. A new proposal offers 64 bit data words in block transfer mode by utilising the address lines for additional data bits. Other enhancements include an additional high performance memory bus (VSB), an intercrate standard (VIC) and an extension of VME designed for instrumentation (VXI) which offers card sizes up to 9U high, extra clock and analogue lines, and a low noise backplane design.

However VME uses old technology, a TTL driven bus and insufficient ground connections between the backplane and modules limit performance. With a 50nS slave response single cycle transfer rates reach 19 Mbytes/s and block transfers 21 Mbytes/s [1].

1.2) Futurebus+ (development of IEEE 896.1)

Futurebus+ is a new high performance 32 bit multiplexed asynchronous bus with extensions planned for up to 64 bit addressing, 256 bit data words. It offers broadcast or single slave protocols, geographical or logical addressing.

Unlike VME or Multibus, Futurebus+ is not a standard developed from a proprietary bus and is processor independent in the sense that it is not optimised for interfacing to particular microprocessors. It is technology independent because there are no time constraints built into the specification such as set up and hold times, and there are no central clocking or arbitration circuits. Thus the performance potential of any new high speed module developments can be fully exploited.

A significant feature of the bus is its BTL (Bus Transceiver Logic) drivers. A problem with TTL technology buses is the large output capacitance of the high current bus drivers. This reduces the loaded bus impedance requiring higher current drivers with even higher capacitance which then further reduces the bus impedance. BTL overcomes this problem by using open collector drivers with a series Shottky diode to buffer the driver transistor collector capacitance. In addition voltage swings are kept small, rise and fall times are well controlled and the receiver thresholds are tightly defined. A disadvantage is that the resulting output voltage swings are not TTL compatible, but the devices do run off a single +5V supply. Originally BTL was only available from a single supplier, National Semiconductor, it is now second sourced by Texas Instruments and other manufacturers are expected to manufacture and sell devices.

Of particular importance in multi-processor systems is the support of cache coherence protocols. The MOESI protocols, a superset of most commonly used protocols, is fully defined in the Futurebus+ standard document P896.2.

Futurebus+ is attracting a great deal of industry support and has been chosen both by the VME and Multibus manufacturers groups as their next generation architecture. Hardware and software 'bridge' products are under development to give continuity with these existing standards. It is this industry support which has provided the impetus behind the development of the original Futurebus standard into this new more widely accepted version. The variety of card sizes reflects these industry interests: 9U*400mm, 9U*280mm (the original Futurebus standard), 6U*220mm (Multibus II) and 6U*120mm (VME). The connector is likely to be the Dupont Metral with 2mm pitch pins.

Potential performance with 50ns slave response is 25 Mbytes/s for single cycle transfers, 44 Mbytes/s for block transfers with a 32 bit data word. because of the overhead imposed by the multiplexed address/data lines single cycle transfers are little faster than VME, however block transfer speeds show a factor of 2 improvement.

Basic protocol and physical layer definitions are at the draft stage. Prototype module are expected from industry in 1991 with volume production from 1993.

1.3) Scalable Coherent Interface (IEEE 1596)

The standard defines a point to point interconnection system which is scalable as the number of attached processors increases, provides a coherent memory system and defines a simple interface between modules.

The proposed physical implementation is a 16 bit connection with clock using 100k ECL balanced driver/receivers to provide 500 MHz (1 Gbyte/s) pipeline transfers. An optional optical fibre implementation offering 1-2 Gbit/s is also proposed. SCI networks will be implemented using rings for lower cost applications or switched networks for higher performance. Communication is packet based with a 64 bit address (16 bit module address, 48 bit offset within the module), 16-256 bytes of data and a CRC word.

Cache coherency will be provided. The normal broadcast and eavesdropping techniques are not applicable to large networks, instead a distributed directory scheme will be used where processors sharing cache lines (currently 64 bytes) are linked together by forward and backward pointers.

Mechanics will be Eurocard based with card sizes of 9U*400mm and 6U*220mm using, like Futurebus+, the Metral connector. A new approach is taken to power distribution by specifying only +/-24V supplies with on board DC-DC conversion for any other voltages required.

Progress towards SCI implementation is rapid with prototype systems expected in 1990 and general availability by 1992. A high priority is being placed on defining interfaces to other buses, in particular Futurebus+ where SCI is seen as a potential crate interconnect standard.

1.4) High Speed Channel

HSC is a point to point interconnect designed for use in a circuit switched environment which is being developed with strong computer industry backing. It is a simple high performance data link offering speeds of 100 or 200 Mbytes/s on 32 or 64 bit twisted pair copper cables of up to 25m in length. Future related standards will address issues such as transmission over greater distances. A completed standard is expected in 1990.

1.5) Fastbus (IEEE 960)

Fastbus was designed as a bus for data acquisition systems to meet the needs of physics experiments. It is a 32 bit, multiplexed, asynchronous bus offering broadcast or single slave protocols and geographical or logical addressing. Full multicrate capability is provided with crate or cable interconnections using the same protocols.

The ECL bus drivers give Fastbus better performance than Futurebus+, 25 Mbytes/s single cycle transfer and 55 Mbytes/s block transfer to 50ns slaves. 9U*400mm cards are housed in crates which provide good power and ground connections and air or liquid cooling. The engineering of the mechanics, the complexity of the interface and the requirements for ECL-TTL level conversion in most applications originally made Fastbus an expensive choice. The development ASICs for the interface and the higher production volumes for the crates have reduced this disadvantage.

The large Fastbus based data acquisition systems built for some recent experiments have yielded a lot of operating experience. Once debugged, systems have proven to be generally reliable with the exception of long cable segments

due to the relatively small drive signals. Developments in the direction of fibre optic based cable segments may provide one solution to this problem.

The performance of Fastbus systems in terms of data transfer rates has sometimes failed to meet the levels expected by the system designers. This prompted studies within the European Fastbus community which showed that although Fastbus modules could be designed to meet data transfer rate specifications at the hardware level the effects of the software overhead to generate those bus cycles could be considerable. This latter effect is of general interest because it is applicable to any bus system. There is a trade-off between ease of programming, for example with high level languages within a sophisticated operating system, and high performance with assembly language or hardware controllers which require longer development times. In the worst case calling a Fastbus routine from a complex operating system can add over a millisecond of overhead. These factors need to be taken into account when calculating system throughputs.

1.6) Fibre Optics

Fibre optic links have a number of advantages for the high energy physics environment. There is no electromagnetic pickup or radiation, there are no ground loop problems, and for equivalent performance they are smaller and lighter than copper.

With currently available technology data rates of 100 Mbits/s are achievable at reasonable cost using devices such as AMD's TAXI transmitter receiver chip sets. FDDI (Fibre Distributed Data Interface) is a new local area network standard employing a dual ring topology at these speeds. AMD supply 5 chip sets which handle the full protocol for $625, an IBM PC evaluation card is available for $6000. Plessey also have compatible driver receiver chips available.

While FDDI will be making links at this speed commonplace, components for 1 Gbit/s systems are becoming available such as Gazelle's GaAs parallel to serial interface. This chip is being proposed for the physical implementation of the Fibre Channel. Completion of this standard is expected within 4 years as a high performance replacement for computer industry interconnects such as HSC or SCSI.

2) APPLICATIONS

2.1) Detector I/O

Fibre optics solve many of the traditional problems in this area such as pick-up over long cable runs and ground loops. A disadvantage is the power requirement for on detector drivers for high speed fibre links. Lower power could be used if sufficient attention is given to the techniques required to overcome the resulting higher error rates.

The choice of protocol depends on the actual application. The distribution of real time clocks requires a system of dedicated links with no protocol. Data acquisition requires the highest possible data rate with a minimum encoding protocol, it may be possible to use chips from the lowest physical level of a standard such as FDDI. 'Slow controls', the downloading of test data, setting up parameters, and monitoring is less demanding on speed and could use the full implementation of a network standard, Ethernet or FDDI, gaining the benefits of using industry standard components and simple LAN connections.

2.2) Front End Readout

If the equivalent of front end crates exist, generally with a single master in a crate executing simple R/W operations, then as with many current data acquisition systems it is tempting to adopt a simple non-standard backplane protocol and a similar simple cable protocol to a readout module in a higher level of the system. Real time trigger and readout control signals require dedicated links, possibly in fibre for longer distances.

2.3) Higher Level DAQ

In architectures where the backplane is not in the DAQ path and is only used for downloading software and setting up the system it need not be of very high performance. In these cases standards such as VME are adequate and may give a cost advantage over newer more sophisticated systems. The data path itself could be custom designed using industry standard driver receiver chips or could based on the implementation of a standard such as SCI or HSC.

Where the data is read out through crate backplanes and the crate interconnects then higher performance standards such as Fastbus or Futurebus+ and SCI are applicable. Downloading and setting up could be through the same network in reverse or, as advocated by some system designers, through a separate network such as FDDI. As in the rest of the experiment, real time signals will need to be carried on dedicated links.

3) REFERENCES

[1] Paul Borrill, A Comparison of 32 bit Buses, IEEE MIcro.

Data-acquisition and triggering with transputer-like devices

J. C. Vermeulen and L.W. Wiggers
NIKHEF-H, P.O. Box 41882, NL-1009 DB Amsterdam

In the ZEUS-experiment the transputer microprocessor of INMOS will be applied in a substantial part of the data-acquisition and second-level triggering system [1]. Important features of the transputer - not found in other microprocessors - are: (i) 4 high-speed serial links (1.7 MByte/s per link) with associated DMA-controllers, and (ii) support for multi-tasking in micro-code, resulting in task-switching times of just a few µs. Moreover, the CPU of the transputer is powerful (for the 32-bits T800: 10 Mips, 1.5 MFlops). The OCCAM language provides direct support for parallel processing and for inter-process communication and synchronization.

About 45 % of the 260.000 electronics channels of the subdetectors of ZEUS will be read-out by transputers (fig.1 and 2), the other 55 % by Motorola 680x0 processors; but most of the data (80-90 %) will be transported by the transputer systems in the experiment. Two solutions are pursued for the backplane bus in the crates with a transputer read-out controller: (i) an extension of the external transputer bus for the Tracking Detector read-out, and (ii) the VME-bus for the Calorimeter read-out. The advantage of (i) is the simpler interface, of (ii) the more general potential. In fig. 3 the layout is sketched for the VME-based controller (2TP-module) for use in the Calorimeter read-out and second-level calorimeter trigger processing, the Event Builder and the Global Second-Level Trigger Box (GSLTB). For test set-ups a prototype series of 24 modules has been made, in spring of 1990 the final production modules will be available.

In the calorimeter read-out a 2TP-module handles the data of a crate. The full data is read-out and transported via the links of transputer Y to the Event Builder at an expected second-level trigger frequency of 100 Hz. The data of 36 read-out crates are sent from the collecting 2TP-modules over multiplexers, built around INMOS crossbar C004 Link Switches, to 3 2TP-modules in the subsystem crates of the calorimeter (fig. 4).

The X transputers in the front-end calorimeter crates search in parallel a subset of the full data read-out by the Y transputers, for local clusters of energy at an average event rate of 1 KHz. The results are combined in a tree structured network (fig. 5) and sent to the global second-level trigger. The total latency is about 3.5 ms, with a maximum processing time of about 1 ms for each of the three processing stages. For the Central Tracking Detector second-level trigger the processing transputers in the front-end crates form a linear chain. The track segments found are combined in a second chain of transputers (fig. 6) [2].

About 10 subdetectors are participating in the second-level processing. From every subdetector the data is broadcast to 10 transputers in 5 2TP-modules in the Global Second Level Trigger Box (fig. 7). One 2TP-module monitors the incoming data; the remaining transputers run different trigger algorithms. The results of the processing are sent over the VME-bus to a master processor, that takes the final decision. The decision is broadcast back to the subdetectors via the Event Builder.

Instead of building events centrally, data is sent from 2TP-modules in the subsystem crates via 48 links in parallel over 3 switches to six 2TP-modules in the third-level trigger crates (fig. 8). At most 12 events are built simultaneously in the third-level crates.

MicroVaxes controlling the subdetectors, are equipped with an Q-Bus to transputer link interface of CAPLIN Cybernetics Corporation. Monitor data is sent from the transputer systems to the MicroVaxes, displayed there and messages are sent to the main data-acquisition Vax for control and monitoring.

In the ZEUS experiment for the first time transputers are applied on a large scale in a trigger and data read-out system. Key features are: massive parallelism, pipelined processing combined with extensive data buffering, dynamically switched point-to-point links, effective use of multi-tasking and integration with standard minicomputers (i.e.VAXes). Therefore we consider the experience gained with this system to be of value in designing trigger and read-out systems for experiments at high luminosity hadron colliders, although higher speed processors with faster links (already in development) will be required.

References :

1. L. W. Wiggers and J. C. Vermeulen, Comp. Phys. Comm., to be published.
2. R. C. E. Devenish et al., OUNP-89-19 / ZEUS-89-76.

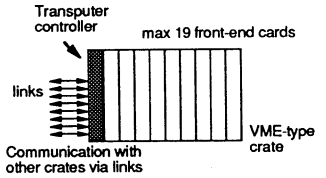

Fig. 1: Front-end crate with transputer controller

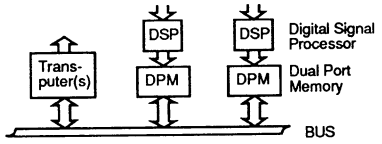

Fig. 2: Configuration inside a crate

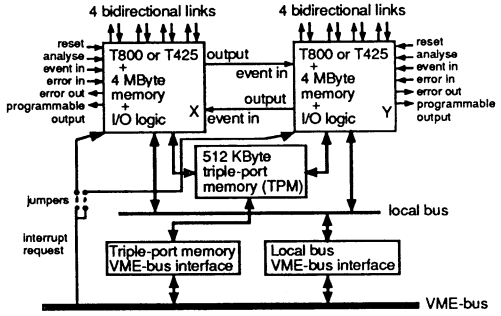

Fig. 3: The NIKHEF 2 transputer VME (2TP) module

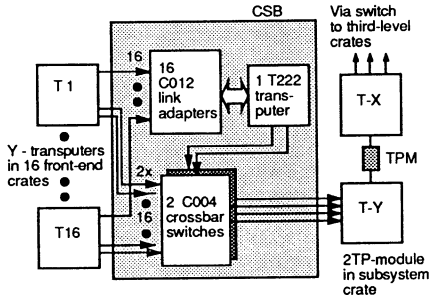

Fig. 4: Read-out of calorimeter data via the Control & Switch Box (CSB)

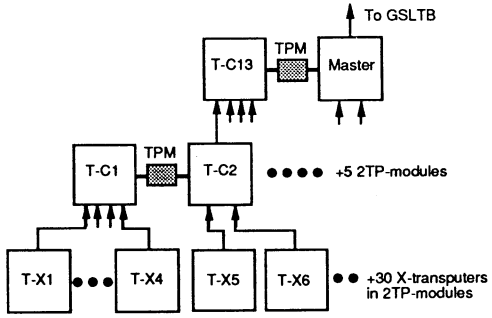

Fig. 5: Transputer network for calorimeter second-level trigger

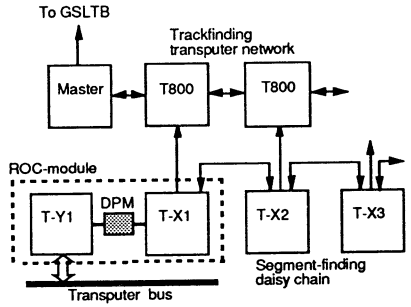

Fig. 6: Transputer network for Central Tracking Detector second-level trigger

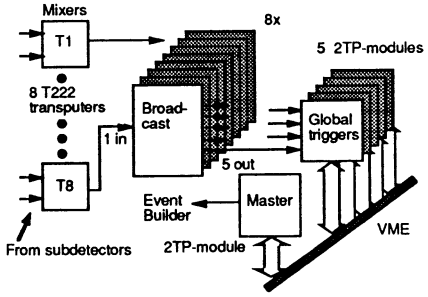

Fig. 7: The Global Second-Level Trigger Box (GSLTB)

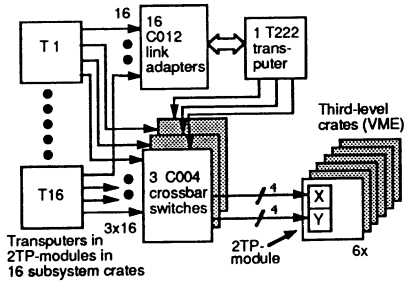

Fig. 8: The Event Builder transputer network

What did we learn in school today?

D. A. Tröster, Univ. of Basel, Switzerland

Abstract: From the first sketchy ideas to the last run of an experiment, errors will be committed. This is a summary of some crucial topics which appeared during the design, construction, and implementation of CP-LEAR (PS195). The conclusions are those of a small experiment of 100 staff members, and a low rate of 2MHz interactions, but maybe it can help you anyway?

Software
It is clearly necessary that a complex trigger system can be accessed from a decent mainframe or minicomputer to supply fast execution, reasonable menu or command line input, logging, multiple users, help facilities for less proficient users, and protection. Program documentation is a must.

An experience
We have developed some software to interact with the trigger processor. There are the following main tasks: debugging single modules, installation of a new trigger algorithm, reliability tests, single-stepping with monte-carlo data, programming Look-Up Tables, prescalers, comparators, and registers for constants, loading dead-wire maps, etc. A fancy program based on a table-driven parser to cover all future needs and possibilities was developed. Six months later, as the code was not yet functional, I have thrown together a small program just to do a few commands. This second program was quickly working and has been extended and improved ever since. The first one has become dusty and will never be used.

Another experience
The result of applying one's experience is usually only a new, much more complicated stupidity.

Documentation
Extensive in-line comments are a must, but the documentation should in fact be done before any code is written. This serves several purposes, namely: the specification of the software can be discussed with the future users and with other software writers. This helps to make code which behaves in a coherent way. You know the aim. This tells you when you are finished. If you get some help (usually the worst thing that can happen!), you can give something to read to this person. In the case of software maintenance, you can't do much without any documentation.

Expert system
An expert system would be the right thing to maintain such a complex hardware setup as our trigger processor. It should have been designed together with the hardware and grown with it. However, the request was not taken seriously in the early days, and now "we can't afford to commit a programmer or student for any two-year job" (end of quotation). Hence we have to face the fact that the complete trigger processor can not be tested automatically (nor manually, it's just too big).

Help
You as responsible software engineer are concious that non-specialists will use your program. Either you accept to answer the phone at 3 o'clock in the morning, or you provide context-sensitive help which follows the overall style of the manufacturer. The choice is yours. This help should appear in a decent structure, and might well be a by-product of a user's guide.

Language
Don't try to use fancy, machine and installation dependent language extensions unless it provides a dramatic improvement in program functionality, speed, and size. Of course, this code sections must be documented with special care to allow future programmers to transport the code. Clean and decent code can be written in any language, but this is preceded by clean and decent thinking. Such thinking is worth to be written down for future generations.

Protection
After prolonged use of the program it has turned out to be neccessary that users can allocate the resources for an indeterminate time. A test may go on for several weeks, running on one LORCOM board (see hardware, section on LORCOM), and intrusion must be logged. Similarly, the program must give a warning if run on a machine without access to CAMAC (risk of a crash).

Structure
Clean SASD and top-down program design are not goals for themselves, but help greatly to get manageable code. Since we live in a real world, it will sufficiently often be necessary to break the rules. However, you can fake rational design. And it is worthwhile to do so.

Testability
To build in some test features has proven to be a big value in the development of interactive programs. Even small programs with 4500 lines and 100 subroutines can behave odd. Built-in print statements which are activated through flags like VERBOSE (displays intermediate results, data, and flags) and TRACE (tells which subroutine is entered) help to debug new and modified code efficiently.

Work
Good, debugged, waterthight software is 80% of the complete work. Readable documentation is 25%, and the hardware another 15%. This is a rule of thumb, but the effort is systematically underestimated.

Hardware
It is not that easy to build state-of-the-art equipment. End users and workshops must collaborate thightly, the physicists should know some electronics, the engineers should know the purpose of their constructions, since there are several traps where one can fall into.

CAD
Electronic equipment is usually developed using CAD tools. Ours (PROTEL PCB) costed 2kFr, runs on a PC, is photoplotted in the CERN workshop and is fine for multilayer boards (8 layers, 70 ICs on 366mm * 160mm boards). Other CAD tools with higher sophistication will be more expensive, probably more powerful and surely more difficult to use. We are just happy.

Chips
Leading-edge electronics requires often the most recent chips available. Never start the development of a board before you have the chips. Some of them may well be found even in databooks but never be sold.

Crates
Due to the detector partitioning and based on efficient trigger algorithms, most triggger processor modules have about 100 signals to the front panel. Clearly, the front panel must be 9U high, like FASTBUS. Using essentially 100k ECL logic, 16cm deep prints are sufficient for virtually all needs. Hence we created the 'CPVME' ad hoc standard: FASTBUS high, VME deep.

Drawbacks: The crates will not be serviced by the pool. The depth is not sufficent for all needs. The height will be insufficient for some applications (Murphy's law).

Benefits: The crates, with power supply, are half the price of FASTBUS crates. The power supply uses a 2*32 indirect DIN connector of its own for heavy load and tailored voltages. Due to EUROmechanics, the crates are easy to get.

Comments: The brand new VXI standard, 'D' size, would be the obvious choice (9U * 34.0cm). FASTBUS was, is, and will be out of the discussion since it is not an industry standard.

Hint: Have a sufficiently big experiment and be rich enough, so what will you care about standards?

Equipment
A four track 350MHz oscilloscope and a logic analyzer with 18*100MHz + 36*50MHz channels, with adjustable threshold voltage, are the minimum equipment to develop fast electronics. Work with microprocessors requires a dissembler.

Ground
Probing high-frequency signals requires the presence of many GND pins on your board. We now even name these pins.

Interface
For fast private read-out we use differential ECL lines of the same type as the LeCroy definition. The VALID and ERROR bits are at the high end. It might be worthwhile for our community to settle down a standard which includes clock, handshake, valid, and reset lines in addition to 16 bit data and maybe parity.

LORCOM
Look-up Tables, pipeline registers and other such devices like counters, window discriminators or approximately equal comparators are quite complex equipment to debug, program, and check. LORCOM, the LOok-up table and Register COntrol Module, is a µP based interface between the host and the hardware processor of our make. The host computer simply sends a job with its data in DMA mode to LORCOM. The latter cares about the details of the serial data transfers to and from the hardware processor elements, and just reports when it has terminated. Termination status and other quantities, like number of iterations (of a test loop, for example), are returned. A particular cable and protocol have been chosen which can be emulated by a PC with centronix printer output port. Data are transmitted serially, while the 4 bit address and 4 bit command code are static. Transmission uses full handshake. This definition results in a very simple interface on the processor side (3-6 chips, simple TTL and PALs). Up to 16 hardware processor elements with up to 4 register sets each can be attached to one LORCOM. The LORCOM cable is a 13 pair flat cable, using TTL levels, and is tested up to 35m between the interface and the terminator. 10 such cables run in a plastic hose from the barrack to the zone, we experienced no problems of EM incompatibility.

Programability
We experienced that it is easier to nail a pudding on the wall than to get decent, finalized specifications from physicists. This usually results in programable devices which are more complex, more expensive, more error prone, and slower. On the other hand, programability can go along with testability, and then it is a big help.

Specifications
Again, top-down design and structured analysis, structured design (SASD) are the only way to get something within reasonable time that will work. Maybe, a bunch of chaotic, creative people can do a good job on a small task, but if the size increases, the method must be adapted. We have to learn from industry and at least fake their methods.

Speed
Our trigger processor runs with a variable clock of 30ns-105ns which caused no problems so far. The clock time is defined on a tick by tick basis, using the busy output of the slower modules.

For the reason of speed, even much logic of simple kind (coincidences, ORs) had been made in the own workshop. The devices turned out to be faster, cheaper, and denser than commercial equipment. This was a success.

Standards
Is it possible to adopt standards which don't enforce people to build camels instead of horses?

Testability
Money spent for testability is money saved. Our pipelined processor elements use a structure as shown in the figure. This construction allows fastest processing for live data and offers all diagnostic tools required: single stepping, analysis of intermediate results through the shadow registers and the serial data out (SDO) line, insertion of test data through the serial data in (SDI) line. Th LORCOM serial link also serves to program Look-Up Tables, registers, comparators, scalers and the like.

Testbed
For measuring device specifications, we have thrown the following testbed together. A programmable clock generator (30ns-105ns) sends its output to a 32 bit synchronous scaler. The scaler's output is fed to as many LUTs as neccessary which are programmed with test data and expected results from the output of the device under test. These output signals are sent to a window comparator where the upper and lower bound are equal. Its output can be used to trigger a logic analyzer or can simply be counted, or can be used to stop the clock generator.

Workshops
Workshops must get super clear specifications. I found it helpful to learn the whole construction process. Why shouldn't a physicist know how his things are made?

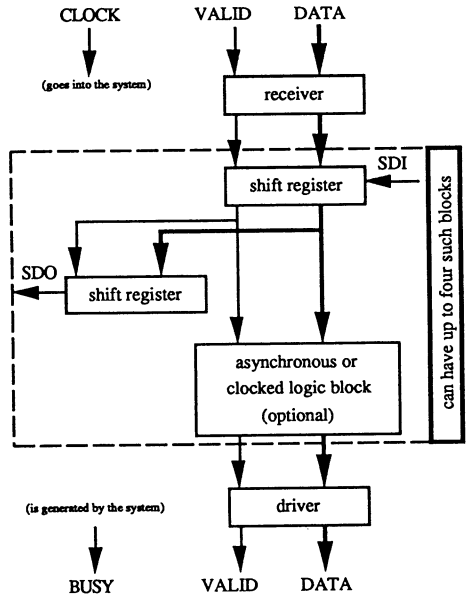

Figure: Generic testable pipeline processor structure

Uncertainty
The extended Heisenberg-Epstein uncertainty principle of a system in an R&D orbit must be remembered. The three parameters money, time, and result obey the following laws.

a) If the money to be spent and the amount of time alotted to a project are fixed, if is impossible to say up to which fraction of the task will be completed.
b) If both time and the result are determined, the cost will exceed any budget.
c) If the result and the financial frame are held constant, the time required to accomplish is completely undefined.
d) A system where all three parameters can reliably be determined is not in an R&D orbit.
e) Murphy's paradigm: more than one parameter can slip.

Data Acquisition and Triggering Systems (Summary Report Sessions P11/W11)

R.K.Bock (CERN), P.Le Du (Saclay)

Parallel Sessions

In the parallel sessions, much time was devoted to discussing the experience accumulated in experiments running now, and in extrapolating existing solutions to the future colliders' environment: the session *what have we learnt from the past?* was a success, within the limits in which people can be expected to talk about not only successes, but also misjudgements and detours. Some of the *industrial components* that will influence the design of future data acquisition systems, were looked at in detail, and extrapolations over the next decade attempted. And as *parallel architectures* of processing elements can be expected to play a major role in triggering and data flow control, this subject was also treated in a separate session.

What have we learnt from the past?

Reports on triggering solutions and problems encountered, all concerning active experiments, were given by D.Tröster (CPLear), J.Coughlan and K.Bos (UA1), J.Biel (CDF), P.Le Du (Opal), and Ph.Gavillet (Delphi). Some of their reports appear in condensed form as part of the present proceedings.

A remarkable consensus emerged from presentations and discussions: Even at the scale of today's experiments, with constraints much less stringent than expected for future hadron colliders, most experiments have suffered from integration problems. Data acquisition systems must be designed as *systems*, and not composed ad hoc as aggregates of *components*. All the same, *flexibility* and *modularity* must be built in, to cope with unforeseen requirements and fast technology evolution. Hardware and software components are both vital parts and highly interrelated, hence *software design* must be considered with equal rigour as hardware design, and together with it. Both should ideally use a single tool for modelling and detailed simulation. The specific tools around SASD (structured analysis, structured design), that have been used in some experiments, are an example of partial success: they were helpful where employed, but also demonstrated that we are far from a stable 'market' for such products, which one simply could learn about and utilize. *Industry standards and products* have proven to be invaluable, where they exist (example VME). In general, much caution was advocated for realistic engineering with established components, as opposed to state-of-the-art solutions, more challenging to design, but less predictable and eventually not cost effective.

Industry components and parallel architectures

These sessions were lively and useful; they are reported as part of the general discussion below, and the more substantive contributions are reproduced in extenso as part of these proceedings.

Architectural Discussion

The architecture of a data acquisition and trigger system is very dependent on a number of areas, only few of which can be taken for defined. Some of them establish *requirements* for data acquisition, like the accelerator parameters and the physics goals. Others offer and demand *choices* and decisions, like existing technology or available tools and system concepts. These are defined by the developments in the non-high energy physics world, and can be influenced by our needs and desires only to the extent that they overlap with other interests and thus constitute an interesting *market*.

The most direct coupling exists, of course, with the detectors that are to be the sensors of the data system. In particular, it is the *active* parts of a detector system that need to be designed and studied together with the electronics, trigger, and acquisition systems, i.e. those parts that contribute to real-time decision making. Multiple feedback loops exist, and an overall system design is necessary, including simulation using physics, detector, and readout modelling in reasonable detail.

We will now examine some of the more crucial system parameters of direct influence to the data acquisition system, in more detail. The input to this section comes from presentations at the present study week (sessions P10/P11, Hinchcliffe, Gilchriese, Brianti, and many others), but also from multiple previous discussions elsewhere (SSC trigger workshop Toronto, Jan 1989, CERN workshop on fast triggers, Silicon detectors, and VLSI, Nov.1988, SSC task force on triggering and data acquisition, etc.)

Intended Physics

Multiple workshops over the last years have well established the *expected* part of future physics, that must be discoverable at the next generation of hadron colliders: The Higgs particle(s), sequential heavy leptons and quarks (including, perhaps, the still undetected top quark), further gauge bosons, the limits in 'size' for constituents of the known quarks and/or leptons, and supersymmetric particles. Of course, it is likely that *unexpected* phenomena will also appear at the energy range of SSC/LHC – the criterion being that those must manifest themselves by signatures which the detector system is built for, i.e. those which are also characteristic for the expected physics. In other words, low-cross section signatures dominated by the known gauge bosons W and Z, and the known heavy quarks. In turn, they are discoverable by high-p_t leptons (e, μ, ν), by high-p_t jets, and varying isolation and correlation criteria.

Most signatures are found centrally (in a rapidity range ± 3), and not seriously overshadowed by soft background, but for some reactions with low-p_t signatures topological criteria like the number of tracks, or tracks from secondary vertices (B-lifetime) may also be needed.

Accelerators

In this interplay of different systems, the accelerator parameters act nearly as a welcome pole of stability: they have not changed dramatically since the first serious design studies were made public, and are definitely stable for the SSC. Needed to gain access to the low cross section of physics is a high *luminosity*: $L = 10^{33}\ cm^{-2}s^{-1}$ is thought feasible for accelerator design and detectors (resulting, at a total cross section of 100 mbarn, in 10^8 collisions/sec). The LHC may have a high-L option above 10^{34}. *Bunch separation* will be 15 to 20 nsec (16 for the SSC), giving a structure that may be possible to exploit in data taking by separating clearly crossings with no, single, or multiple interactions, for calibration and dead time purposes. Note that the probability of more than one interaction in a crossing at the SPS is 48%, and if restricting to crossings with at least one interaction, even 60% (see also A.Lankford, these proceedings). *Bunch length and width* will be about 30cm (full length) and 12μm (radius), which influences the vertex position's use in calculation and trigger.

Ways to extract interactions from multiple crossings will therefore have to be found, the detector response time becomes critical, and correct identification of 'time slices' throughout a complex detector will be a necessary and non-trivial part of data acquisition.

Detectors and Front-end Electronics

The detector parameters and the performance of the trigger/acquisition system are closely linked. As the most relevant parameters of a detector we see the following:

Granularity: the smallest spatially separated detector unit. The number of 'cells' or 'channels' determines directly the data volume to be stored, digitized, transmitted for each event or beam crossing. It also sets a limit to the execution of local algorithms for 'feature extraction': translation of raw data into quantities more meaningful for physics. These may then be used to form a trigger, reducing the number of events, or for compacting data, reducing the per-event data volume.

Occupancy: the probability of generating a signal in the smallest detector unit like wire, single cell, or fibre, on any given beam crossing, is directly related to the possibility of time integration of signals, hence relates to local storage of data in analogue or digital form, to multiplexing possibilities, and to synchronization questions between multiple local buffers.

Local Buffering: The physical overall detector size of tens of metres imposes a delay of the order of a μsec or more, before a detector-wide trigger can be formed and broadcasted to all local channels; at least for that time, a local storage capability must therefore be provided (latency). The technological limits of digitizing, perhaps not pushed to the ultimate limits today, determine subsequently which approach to take in processing data for local feature extraction: the popular approach for sparse data, 'zero suppression' and multiplexing, may be less performant than massively parallel 'iconic' processing.

Siting and Packaging: Several discussions at this study week raised the question as to *where* electronics has to be installed and how it has to be *logically decomposed* into suitable custom-made or commercial or technological units. For reasons of volume and cost, VLSI is the technique of choice for readout functions close to the detector, storage buffers, low-level decisions, and maybe further downstream, but little experience exists where to interface which functions. Radiation hardness and power consumption are further parameters proper to different technologies, and contribute to blur the picture which hitherto allowed to distinguish in a relatively simple way between 'front-end' and 'acquisition' modules.

Active Detectors

As will be seen in the architectural discussion below, it is a generally made assumption that at the end of the data acquisition system, before writing onto mass storage, a 'farm' of processors will exploit event parallelism, and allow decisions to be made about retention or rejection of events based on full event data. If we talk about active detector parts, however, we refer to such parts that provide information to lower-level triggers., Such information may be accumulated *globally*, i.e. for the entire detector, if it is coarse, whereas it is typically used *locally* for feature extraction, if we deal with fine-grain information. The detector must have fast response in order to be useable for triggering, and must be used in analogue form, or analogue-to-digital conversion must be feasible at the right time scale (and economically). The detector elements that are most frequently discussed as candidates for active triggering are

Calorimeters: they will provide electron identification (isolated, possibly as jet fragment) by lateral and/or longitudinal energy distribution, and by pre-shower devices; they will also provide information on hadronic jets (local clusters); summed globally, they will allow ν identification in a hermetic calorimeter, and may possibly provide a total $\Sigma|E_t|$ trigger (although this is adversely affected by multi-interaction crossings).

Tracking devices: they provide crucial supporting information to calorimeters in electron identification. They alone can provide high-p_t muon identification, in conjunction with shielding and, probably, a magnetic field. Trackers are needed to disentangle multiple-event beam crossings (although opinions diverge as to how that will be done). High-resolution tracking around the vertex may also be needed to identify (through secondary vertices) B-mesons.

Track identification: in past and present experiments this is confined to triggering in very simple topologies (e.g. threshold Cherenkov triggers), or to use in final analysis rather than real time. Track identification in future detectors may well play a more active role in real time: TRD-s or RICH detectors may be relevant contributions to, again, electron and muon identification, and possibly for tagging strange particles.

Overall Architecture of Data Acquisition and Triggering

Most discussions of the overall architecture evolve around diagrams as reproduced in fig.1, which concentrates on a number of *agreed concepts*:

Trigger decisions will have to be taken at various levels, starting with *fast and crude* 'algorithms', evolving to *finer-grain information* and hence more detailed information and its use in *local* processors, until eventually all information for an event is collected in an *event builder* and made available to fully programmable and commercial processors.

Due to the latencies in taking decisions at various levels, a hierarchy of local buffer memories must exist, in which events accumulate until rejected or accepted. Synchronizing them is one of the expected system headaches. The data flow through triggering processors is kept, as far as possible, separate from the flow of event data through buffer memories (an experience from the past).

Different kinds of *parallelism* may be exploited to speed up the execution of algorithms: the most obvious is event parallelism, which is exploited in 'processor farms' (see J.Biel, these proceedings), but may also be put to use at lower levels as speedup. Less experience exists with channel or detector module parallelism, strongly physics-, detector- and algorithm-dependent; this is perhaps the area in which progress need to be made most urgently for the SSC/LHC era.

Massive storage onto long-lived storage media (magnetic, if we believe J.Best, see these proceedings) is at the end of real-time operations, as in the past. Although detectors at future hadron colliders

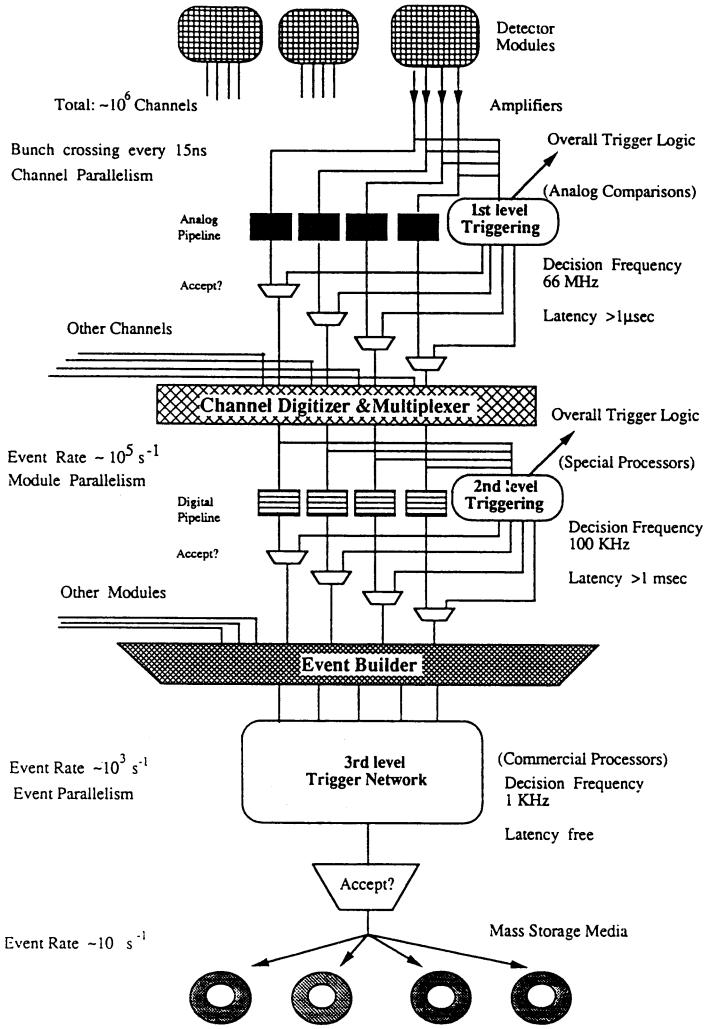

Figure 1: Schematic overall architecture for data acquisition

will (have to) set new scales for real-time data reduction, there are two rational arguments why storage media and the associated logistics will not be done away with entirely: First, the risk of taking cuts too close to (expected!) physics, in a detector that will be understood fully only on a timescale at which it is also being upgraded, will dictate moving even some of the algorithms well under control to an environment where repetition is possible. And secondly, there is a sociological argument: physics extraction will be a trade that is left to a multitude of often small institutes and universities, hence to young physicists. They will want to discover the physics in a loosely selected sample themselves – and may then get out more than what the professionals built it for.

Overall optimization of the architecture will be a delicate and iterative procedure. The advantages and disadvantages of local/global algorithms are compounded with questions of siting and packaging, of available technology, power and radiation constraints, calibration possibilities etc. To improve the understanding of these aspects will be one of the dominating tasks between now and the time when decisions on future systems have to be taken.

Technology, Tools, and Components

The various techniques to which the builder of a future Data Acquisition System will have to resort, were all discussed at this workshop. The following list may be incomplete and/or too general, but shows how many parameters will have to be narrowed down eventually.

VLSI, CAE, and simulation tools:

as one deals with *integrated* systems, the distinction between front-end electronics and data acquisition becomes blurred, and the same toolkit serves both. VLSI design platforms, gate arrays, standard cell and other manufacturer libraries, will therefore have to become standard items in the data acquisition designer's set of tools. Alongside with memories, programmable logic units etc, they serve to build look-up tables, content-addressable memories, or custom-made special-purpose processors.

Massively parallel systems:

even for 'algorithms' representing no more than simple sums or multiplications, the execution time depends critically on performing operations in parallel, particularly if one considers data transfers as just another operation. For more involved algorithms, some fine-grain systems (image processing systems with internal pipelines and SIMD systems) are under discussion and have been benchmarked; also, neural nets have recently contributed to the discussion. Generally, the projected number of parallel components is expected to be large enough to require fault-tolerant and densely packaged systems. The declared goals (M.Lea, these proceedings) are high performance per dissipated power (GOPS/W), per volume (TOPS/ft^3), and per cost (MOPS/$).

Connection technology:

a separate presentation (St.Quinton, these proceedings) concerned the expected evolution of the commercial data connection markets; fortunately, the signs are that industry has understood that customers hold standards in high value, and intra-crate as well as (point-to-point) inter-crate seem to be evolve towards bandwidths that set limits clearly superior to those of the present industry standard, VME. Also in optical connections, a standard (FDDI) is evolving, although low-level very high performance optical links (e.g. for ultimate speed in multiplexing) are, of course, not subject of a standard.

Computing and mass storage:

convincing evidence exists that industry will give us a variety of affordable choices when we move into the area of powerful processors (DSP-s and RISC-s) and mass storage media. Massively parallel MIMD systems can be built up from chips with individual high-performance parameters, with massive software support (Unix and compilers), some coming with standard interfaces to add special coprocessors. Transputers with their special connectivity and related software are well-known today (see J.Vermeulen's report, these proceedings), and are likely to have more powerful successors tomorrow. 10^5 Vax equivalents were proposed as the compute performance of the 'third-level farm', and there seems to be little doubt that this is possible. Complete parallel systems with software support suitable for our applications, on the hand, do not seem to become commercial items on a short time scale, and our own contribution in this area may therefore be required.

System simulation:

whereas computing tasks (third-level trigger) can be judged by computers' performances, lower-level system parts are inadequately described by MIPS or similar units. Overall optimization and design verification can only pass through extensive and detailed simulation. Commercial tools exist that have a good chance to be useable but insufficient experience is available in our community in their use.

Technology extrapolation:

in some of the areas under discussion (e.g. gate densities on chips, computing performances for RISC-s) the technology limits move fast. We should, however, beware of the danger of using extrapolation to the data of SSC/LHC first operation: A design for a complex data acquisition system will have to be frozen years before the system is turned on, and reliability will have to be given a much higher weight than the use of the ultimate technology.

Conclusions

A long road

Data Acquisition systems in future hadron colliders will be critical due toe the large data reduction factor needed: the information loss in triggers of various levels of complexity will be unprecedented. They will also be difficult to decide because relying on evolving technology. The lead time to build data acquisition systems will be long, and only some of the critical aspects begin to be understood in our community. On the shortest possible timescale of the LHC (1996/97), we stand no chance to implement a properly engineered detector and acquisition system. The study week may have shown that the present effort in Europe is not commensurate with the impact that future data acquisition systems are expected to have.

It thus seems urgent to mobilize efforts by focussing on selected pilot projects, and by starting serious overall simulation of model detectors and data flow architectures. There are some clearly missing links: identified were system simulation, neural network techniques for triggering, real-time data compaction and calibration techniques, ADC-related questions like parallelism or separating dynamic range from precision, and optoelectronics, to get access to the ultra-high speed available for transmission by optical fibres (even for analogue signals).

Industry

This study week has largely succeeded in bringing together physicists and industry representatives. In the discussions it has become apparent that, particularly for electronics and data acquisition, industry and the commercial market have a very serious role to play, as supplier of components and tools, as supplier of system parts, and as collaborator in R&D. In fact, it is widely believed that the available manpower and specialist knowhow in high energy physics will set severe limits to our own developments, which will have to concentrate on fields where our demands are not in overlap with any market. Industry does in fact offer many ready-made or adaptable solutions. Past experience shows that for systems much less complex than envisaged for future colliders, *single components, systems, standards, software, and support* should be taken from industry *wherever possible* (the S^5 rule). We hold that this will become even more true for the complex systems of tomorrow's colliders. A corollary is, of course, tahat the physics community should attempt to acquire complementary skills like interfacing and integration. This may correspond to a change in profile of staff in our institutes (see also N.DiGiacomo, these proceedings), and raises serious issues of (re-)training.

Session 12

RELATIONS WITH INDUSTRY

RICH MIRRORS FOR DELPHI AT LEP

A case of technology exchange between CERN and industry

By S. Walles, Bofors Aerotronics AB, S-181 84 Lidingö, Sweden.

(Bofors Aerotronics AB is a subsidiary of AB Bofors in Nobel Industries Sweden, a company with about 20,000 employees and a turnover of SEK M 20,000.)

The RICH mirrors are specified to have better than 80% reflectivity in the Vacuum Ultraviolet (VUV) wavelength region of 165-200 nm. The size is approximately 26 cm x 47 cm for the 300 concave, off-axis paraboloidal BARREL RICH mirrors and approximately 37 cm x 35 cm for the 125 concave, spherical FORWARD RICH mirrors delivered. The radius of curvature is approximately 80 cm for the former and 120 cm for the latter mirror type.

The precision slumping technique for obtaining concave mirror blanks from flat discs of float-glass was developed at CERN. Also developed at CERN was the vacuum evaporation procedure for obtaining a mirror coating of high reflectivity in the VUV. This technology was transferred to Bofors Aerotronics (BAAB), where it was implemented in existing production equipment. BAAB developed the technique for sawing trapezoidal mirror substrates out of the slumped blanks and the special packing needed during transportation and storage of these delicate components. Measurement of size, axis position, focal spot size, and reflectivity was done at BAAB before delivery and at CERN after arrival. In general, the measurement results agreed within the tolerance limits.

The collaboration between CERN and BAAB took place in 1983-1989. It was mediated by the Swedish Board for Technical Development, who also supported some early development work at BAAB. Soon, however, the frequent contacts between the scientists and engineers at CERN, and their counterparts at BAAB, developed into a self-propelled teamwork. The result was a production process, to which both parties had contributed, of a complexity necessary and sufficient from the points of view of cost and performance of the mirrors.

The following experience of the collaboration may be of general interest: 1) Since the slumping and the application of VUV mirror coatings were entirely new to BAAB, it was a great help to the company to obtain the technical solutions of these techniques from CERN. The cost savings can only be guessed at, but they must have been substantial. 2) BAAB has half a century of experience of optical components and instruments for industrial and military use, where the environmental requirements are typically thermal and mechanical, but not at all directed towards the type of environment existing in DELPHI (electrostatic fields, special chemical substances, particle radiation). Therefore, it was agreed that the detailed design specification, including all information on the drawings, would be CERN's responsibility, whereas BAAB's responsibility would be the production of the mirrors according to those drawings, using the production technology transferred from CERN. 3) The slumping moulds were developed by CERN and placed at BAAB's disposal free of charge. The idea of loaning tools to a supplier, who would otherwise have spent much time and money on an exacting problem that CERN had already solved during the experimentation phase, might be worth following. 4) Visits to all parties are important. Otherwise, various types of misunderstanding due to lack of imagination and comprehension may put the development at risk.

The collaboration appears to have created mutual advantages to CERN and BAAB. CERN had access to the sufficiently large and receptive production organization of BAAB. BAAB supplied a product which represented an inspiring challenge, an object of some publicity value, and a possible source of future business.

References

[1] P. Baillon et al., Nucl.Instr. and Meth. in Phys.Res. A277 (1989) 338.

[2] P. Baillon et al., Nucl.Instr. and Meth. in Phys.Res. A276 (1989) 492.

[3] S. Walles, "Collaboration between big science and industry", accepted for publication in Particle World (editor R. Klapisch, CERN).

OBSERVATIONS BY TWO TYPICAL INDUSTRY PARTICIPANTS

MICRON SEMICONDUCTORS LTD COLIN WILBURN
PHILIPS INTERNATIONAL B.V. ESSO FLYCKT
(Presented by Esso Flyckt as a before the dinner talk)

1. THE CLIMATE IN FAVOUR OF COOPERATION WITH INDUSTRY HAS IMPROVED SIGNIFICANTLY IN 10 YEARS:

At the ECFA International Conference on Experimentation at LEP, Uppsala, Sweden,1979,two industries participated: Scanditronix as local supporter,presenting their capabilities in Nuclear Physics accelerators and Philips Components on own initiative,presenting their Radiation Sensors. Both were very welcome, mainly to contribute to the costs of the conference coffee.

Now, 1989,at this ECFA Study Week on Instrumentation for High Luminosity Hadron Colliders here in Barcelona the ECFA organizers have been able to gather almost 50 industrial participants of about the right level and mixture of technological capabilities. To have hoped for more would have been too ambitious.

THERE IS HOWEVER,STILL A LONG WAY TO GO FOR FULL UNDERSTANDING OF INDUSTRIES PRIORITIES AND THOSE OF HEP TO REACH AN OPTIMAL COOPERATION.

2. TWO NEW ELEMENTS

- EUROPEAN R&D FUNDING?

This possibility has been discussed in HEP circles since long with no real actions or projects. The presentation of Mr White of SCIENCE must be seen as very positive and resulted in many discussions in the hallways, for and against;sceptical remarks from some industry participants claiming that the papers to fill-in made it almost impossible to make the flow of such money materializing.

It must also be taken into account that only 50% of the project is paid by Brussels, leaving the industry involved to risk some own money. Industry has thus still to be prepared to do so in competition with other non-HEP projects. The major problem to get projects funded is

FORMING OF THE OPTIMAL PROJECT PARTICIPANTS GROUP.

The organization of this may mean more and very small and very dedicated workshops focussing strongly on the goals of certain detectors. The time scale is short for forming the groups and strong people functioning as the organizational motors are needed. Who are they?

- PRIME CONTRACTORS?

The presentation by Digiacomo of Martin Marietta about prime contractors with system architecture responsibility for large HEP projects injected new material for the hallway discussions like a new wind. The acceptance of the idea was difficult by most Europeans because of PHYSICISTS MUST DEFINE THE PROJECT EARLY WITH DETAILED SPECIFICATIONS. HEP is not used to this and fears that "freezing" the project too early limits later possibilities of changing when new information becomes available. The discussions on this point will be very useful to analyse and prepare for the future very large projects.

3. INDUSTRIAL SPEAKERS

The speakers from industry are still too "commercial" and sometimes self-focused, giving no credit to the competitors, showing too many buildings and too much about todays products. As the climate changes one can hope for more information about R&D capabilities and also about capacity of certain products - a very important issue for the large quantities of the future. Few pointed out that HEP may help with the investments needed to produce these quantities or the capacity may not be there.

4. INDUSTRY'S WORRIES

- IS SSC REAL ??
- WILL LHC COME ???

) WHEN ?????

- ARE WE AT THE RIGHT CONFERENCE?

These questions are normal as we are still in an early phase of as well SSC as LHC detectors and caused by the

5. TOTAL CONFUSION

How will the final detectors really look?
There are many alternatives for each detector part as demonstrated in the parallel sessions. Many of these ideas involve new, inventive, hopeful ideas, sometimes looking like technological dreams. Moreover there are very many opinions about the realism of these ideas by too many oracles.

WHAT CAN THE NON-PHYSICIST INDUSTRIAL PARTICIPANT TELL HIS BOSS WHEN HE COMES HOME? HIS UNANSWERED QUESTIONS FROM THIS CONFERENCE ARE:

- CAN MY PRODUCT BE USED? If so
- WILL MY PRODUCT BE USED?
  The last question is certainly real as experience with the L3 BGO shows that none of the original scintillator suppliers could profit from the final order after the initial work and investments they did.We already hear that the BaF_2 can not cost $\$7/cm^3$ as predicted by the present industry, the hopeful price of $\$2/cm^3$ from USSR is already taken into the calculations. Should the European BaF_2 industry invest? This is only an example, whatever it is worth but illustrates the difficulty of the industrial participants and their bosses. This uncertainty will certainly be reflected in sample quotes for R&D products
- SHOULD WE COVER R&D COSTS FULLY NOW? THE LARGE ORDER MAY NEVER COME?

SOLUTION: INCREASE YOUR UNDERSTANDING AS INDUSTRY BY GOING TO MORE CONFERENCES, LISTEN WELL TO THE ORACLES AND SPEND A LOT OF EFFORT NOW TO FORM YOUR OWN OPINION.

6. FACTS

THE TOTAL MARKET LOOKS FANTASTIC WITH 1-10 MILLION PIECES OF EVERYTHING, ALMOST TOO FANTASTIC. WHEN?

INDUSTRY CAN OFFER RELIABILITY AND QUALITY CONTROL.

INSTITUTES CAN OFFER TO MEASURE ALL PARAMETERS, OFTEN FREE OF CHARGE AND WITH PHYSICS UNDERSTANDING.

QUANTITIES MEANS LARGE SCALE INDUSTRIAL PRODUCTION.
It is important that HEP learns more about industrial structure and conditions. Industry is not a big black hole out there that automatically produces what you can not make yourself. Industry has lead times, plan their capacity to long term planning methodes and has no sudden capacity for HEP just like that. As we talk about major quantities over several years for a large part of the components of the new collider detectors, such capacity will only be created against real HEP comitments and means a lead time.

THE PHYSICS COMMUNITY AND INDUSTRY MUST ANALYSE THEIR COMPLEMENTARY ROLES

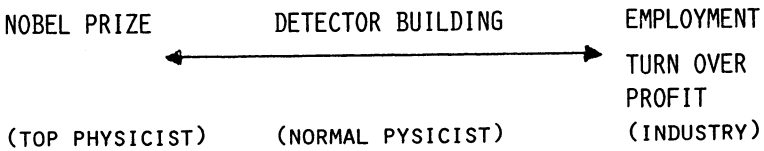

WE ARE SURE THAT THIS MEETING HAS STIMULATED INDUSTRIES TO DRAW THEIR OWN CONCLUSIONS OUT OF THE APPERENT CONFUSION AND POSITIVELY WILL DO THEIR BEST WITHIN THEIR LIMITATIONS TO MAKE THE COLLIDER DETECTORS MATERIALIZE.

WE EXPRESS OUR THANKS FOR A GOOD CONFERENCE TO THE ECFA ORGANIZERS AND ESPECIALLY TO THE INDUSTRIAL CONVEYORS, MARKUS NORDBERG AND OSCAR BARBALAT.

PHOTOTUBES FOR FUTURE COLLIDERS

Esso Flyckt
Philips International
Eindhoven, The Netherlands

Contribution to discussions in parallel sessions 4 and 8.

SUMMARY

Photomultipliers are wellknown to the HEP community and offer fast response in line with SSC and LHC demands. The situation today is presented with special attention to magnetic fields, multi-anode tubes, MCP tubes, shorter tubes, timing, image intensifier-CCD combinations, Si as anode, image delay, diode image intensifier-APD combinations, streak camera tubes and large tubes for water Cherenkov muon detection with indications where R&D could bring progress for SSC and LHC detectors.

1. INTRODUCTION

The extremly short time interval between bunch crossings in the future SSC and LHC hadron colliders presents a new problem resulting in the need to improve detector techniques in many ways. This conference bubbles of improved and maybe more interesting, of new futuristic techniques. It is likely that the final detectors will consist of a mixture of both. In that context it is interesting to look at phototubes with new eyes to judge where improvements and adaptions can be made in photomultipliers and other phototubes less wellknown to the HEP community. After a reminder about photomultipliers the other paragraphs cover a mixture of tube features and the application to some problems we have observed being of high specific interest lately; This survey is in now way complete but aimed at clearing up some misconceptions - trigger deeper

continous discussions. We also try to bring in some practical views and sometimes limitations of proposed ideas we are confronted with recently. Of course we also like to take the opportunity to promote phototubes as a well established technology offering safe solutions wherever applicable in the next collider detectors.

2. THE SITUATION TODAY

Except in a few cases,HEP has mainly been using the well known photomultiplier tube in quantity. Let us therefore concentrate on this tube first,recapitulating some of its advantages

+ large cathode area
+ low noise, high gain
+ nanosecond speed, sub-nanosecond time resolution
+ high blue and UV sensitivity
+ low price
+ well known by the community

and compare this with the disadvantages

- single channel device
- bulky
- high voltage needed
- bleeder power consumption
- sensitivity to magnetic fields
- non-perfect stability
- less green and red sensitivity than Si devices.

3. IMPROVEMENTS IN RECENT YEARS

A. General improvements

Multi-anode tubes are now on the market (see 3E).
Shorter tubes can now be made in new technology (see 3C).
The high voltage is still needed but the power consumption of the bleeders can be circumvented by distributed voltage supplies.
The magnetic field sensitivity is treated separatly in 3B.

The gain stability has been considerably improved for most tubes. It is still doubtful whether it can ever be improved to the demands of the next generation of large calorimeters asking for parts of a percent on all the stability parameters. One must count on sofisticated calibration systems also in the future but this will also be true for most competing techniques. Silicon devices e.g. will cause new problems and their low noise preamplifiers create other complications.
The green sensitivity has also been improved through new and better mastered photocathode processing. The red sensitivity could be improved a little more but is in no way close to Si. Other features like ns speed and area are however features that Si devices can not easily beat even in the red part of the spectrum.

B. Magnetic field sensitivity

Several special cases have been solved:

- The Vacuum Photo Diode (VPD) developed for a 0,3 T field directed up to 70^{o} off the tube axis for the CERN R808 experiment.
- The Vacuum Photo Triode (VPT), an offspring of the VPD, can work in a 1 T axial field offering a gain of about 10 and is now applied in the OPAL and DELPHI end cap electromagnetic lead glass calorimeters with good results. Compared with a solid state photo diode the VPT can offer a large area with low capacitance load on the preamplifier. Multi-segment VPTs can in principle be made with 10-50 channels, so far only explored in sample quantities. In a non-magnetic environment the VPT can offer a gain of about 20 resulting in a better energy resolution than a normal photomultiplier in high light level applications.
- One supplier offers a tube with a mesh multiplier structure offering a gain of 10^{3} in a 1 T axial field and a gain of some hundreds in a 2 T field. No solutions have been found so far for the 3 - 6 T fields discussed for the new detectors for SSC and LHC.

- A dedicated photomultiplier that works well in a perpendicular field of some hundred Gauss has been developed for the OPAL barrel lead glass electromagnetic calorimeter.

These developments are nice examples of how industry has tuned their capabilities to fit earlier HEP demands as soon as the projects were large enough and decently defined. To repeat the experience into 3-6 T situations looks hard.

C. Shorter tubes

When we discuss how to read out the next generation of calorimeters with maybe 50.000 photomultipliers the length becomes very important.
One supplier has developed a so called foil multiplier consisting of thin CuBe perforated blades allowing a very short multiplier package, comparable in size with the above mentioned mesh multiplier. Both concepts allow already now much shorter photomultipliers. Until now the good photocathodes all physicists want demanded a certain distance between the photocathode and the first dynode. This limits how short one can make the tube. However, but at a price of maybe a factor 5-10^{x} higher, very short tubes could be made in the so called transfer technology now applied for image intensifier tubes. To follow this way needs considerable new investments to produce tens of thousands of tubes and a 2-3 year lead time must be regarded as realistic.

D. Better timing

The best timing is today reached in several 2" tubes on the market already since many years. The normal competitor pressure slowly brings new versions and sizes from the major suppliers. This is mainly reached by improving older non-optimized input optics designs into modern ones.
Taking considerable steps into fully new, very optimised tubes with ultimate transit time jitter may be possible but are expensive and time consuming projects where some R&D contributions may be needed from HEP projects.

E. Multi-anode tubes

Two types with different designs and features exist:

- The above mentioned mesh multiplier that could work in a magnetic field. Used as multi-anode device it spreads the electron cloud by principle over many output elements. This means that the coordinates of a narrow input signal have to be found by centroiding over many output elements for each event. Designs of up to 256 elements are already offered today in sample quantities.

- The above mentioned foil multiplier, working only in very moderate magnetic fields, offers a very low cross talk between the last dynode output elements. Pencil beams of light perpendicular to the window give about 5% cross talk between adjecent element. For a fibre carrying the light one should probably count on more than 10% depending on the arrangement. The optical cross talk in the window could maybe be eleminated by focusing tricks and another way is to use a fibre optics window. The second solution is considerably more expensive and offers lower photo-cathode sensitivity, already now on the low side due to the proximity focusing design. Better cathode sensitivity can be reached in transfer technology but this again takes up the price to image intensifier levels. Sample quantities of a 64 element version are sold since some time.

Limitations for going to many more pixels are mainly in the dense arrangement of separate output pads/wires. A step to say 500 pixels in a 3-4" tube would cost a lot of R&D money and a lead time of say 2 years.

F. Micro Channel Plate photomultipliers

For every new generation of HEP detectors these devices attract renewed interest as the ultimate solution as well for extremly good timing as for multi-element tubes.
It is true that such tubes can be made with a very good transit time jitter and have low multiplier cross talk.
Such tubes are also sold in small quantities at high prices

for special markets. The problem is that their life is limited to about 0,1 - 0,5 C/cm^2 output charge making them unsuitable for most HEP situations.
Work has been going on for many years and is still going on to improve the life time of such tubes. Until now no real dramatic improvements have been reached and it is doubtful whether a break-through can be counted on for the time scale of the next detectors we discuss here.

4. MULTI-ANODE PHOTOMULTIPLIER TRACKERS

Understanding that the designs today aim at a modest scintillating fibre tracker of 5×10^6 fibres, i.e. 10^7 pixels if we want to read it out in both ends, we find a need for 20.000 x 500 pixel tubes. Let us guess that such a tube could be sold for $ 2000 each including the R&D and investments needed. Maybe it could cost less if some specification trade-offs can be reached but we still talk about 30-40M dollars. We understand that such numbers are regarded as almost acceptable for the next detectors if the tracker can do the job. The major problem is that the light levels are so low from the fibres that tubes must read them directly. This is certainly contradictory with a high magnetic field for the tracker. Moreover we should realize that at least 2 years extensive and expensive R&D effort is needed plus at least 2 years investments in the capacity needed to produce all the tubes. If this is a way to go it is thus necessary to make hard decisions within one year if the tubes should exist on the time scale planned for the SSC and LHC.
The question is whether clever ways can be found to couple several fibres to one pixel due to the low occupancy in the fibres. This assumes that it is enough to see the track, not necessarily each fibre signal in itself. If such a trade-off could be found multi-anode photomultipliers are at least not to be neglected for a tracker.

6. IMAGE INTENSIFIER TRACKERS

Being confronted with questions about 10^8 scintillating fibre trackers we do not see how multi-anode phototubes could do the job but start thinking about image intensifers.

The first fibre-image read out is demonstrated to work well in UA2 with three image intensifiers in series ending in a CCD read out. Although the tubes are quite expensive the price per pixel is attractive. The SSC will have time intervals between the beam crossings that are 250 times shorter. This would put difficult demands on the CCDs and on the phosphors available today.

Developing very fast CCDs for HEP is clearly an area where R&D cooperation with industry could be very fruitful and also have spin-offs into other markets.

The fastest phosphors today are P47 types with a decay to 1/e of about 40 ns with a tail out to 150 ns. This will lead to pulse pile-up etc. This is an other area where industry and HEP could try to work together in R&D. Such phosphors would also find a lot of other scientific non-HEP applications.
Image intensifier tubes would have to sit well outside any magnetic field and a rough calculation indicates a total cost of the same order as the smaller tracker above.

7. OTHER TYPES OF PHOTOTUBES

A. Si devices in photo tubes

As long as we talk about simple silicon diodes it is possible to put them into phototubes since many years. The renewed interest from one LAA project (Wigmans, Desalvo et. al.) is supporting R&D trials from at least three suppliers by sample orders. Such a tube could be made very short and the obvious feature is the long term possibility to put in Si diode arrays to get another type of multi-anode tube. Adding CCDs into phototubes is going on at the R&D level in several industry laboratories. HEP may profit from this on long term although the real commercialization may take several years.

B. Diode image intensifiers with APD read out

An diode image intensifier consists of a photocathode followed by a fast phosphor placed about 10-15 mm behind the photocathode with say 15 kV to accelerate the electrons onto the phosphor. Gains of at least 10 can be reached when followed by a photomultiplier. Followed by an Avalanche Photo Diode the gain could possibly be 20-30 depending on the wavelength of the emitted light from the phosphor.
The image intensifier can work in a high magnetic field and offers a "clean" gain before the APD takes on the signal. Such tubes can directly be made, would cost at least 1000 dollars in large quantity and need only limited lead time for creating production capacity. APDs exist from several companies in limited quantities.

C. Image delay tubes for a fibre tracker

We refer to the presentation by J-P Fabre at this conference. This device is very interesting although expensive and not only can it work in a magnetic field, it needs the field for keeping the image intact. Several questions will be answered by the prototypes now planned by LAA in investing R&D money for prototypes made by industry:

- Will the photoelectrons that return to the photocathode be absorbed or create new electrons?
- Will the tube really work as anticipated in theory?

If the tube works,it offers the very attractive possibility of direct data reduction very early - a very unique feature in the environment of the next collider detectors.

D. Streak Camera Tubes

Such a tube is in principle an image intensifier equiped with an intermediate electrode system to which a saw-tooth (fast) voltage is applied. The result is that signals from the input fibres placed in a horisontal row onto the input window are swept in vertical direction over the output phosphor screen by the saw-tooth voltage. The vertical

direction represents thereby a time signal with sub-nonosecond resolutions easily reached for single shots. Such tubes are thus faster by factors than the new colliders. As the signals enter only on one line of fibres at the photocathode, displayed in very many lines at the phosphor screen each displayed line can e.g. represent one bunch crossing. This could be a way to take down the data rate on each following CCD pixel with a factor 50 or so. The low occupancy in the fibres will also help to give a not too complex picture onto the CCD.
SCTs have several "negative" features:
- very expensive in todays excecutions
- very clumsy
- can only take a low number of fibres(one line)

Moderate R&D efforts could "downgrade" them to the timing range of interest here and in large quantities the prices and dimensions could certainly be adapted considerably.

A fibre tracker with 10^7 read-out elements will need some 20.000 such tube, probably in the price class of 5000 dollars each, or 100M dollars. Maybe these tubes are useful in lower quantities (at higher prices) in dedicated subdetectors. They do not work in a magnetic field due to the saw-tooth sweep - the principle of their function.

8. THE WORST CASE

If the inner parts of the detectors are not technologically feasible at the start of the SSC and the seriously proposed iron or uranium block has to be placed around the beam collision point, surrounded by a clean-water tank for the muon tracks the solution is certainly (large) phototubes.
Several versions exist:
- 20" with moderate timing and single electron resolution
- 16" " " " " " " "
- 15" with good timing and good single electron resolution
- several 8", 9" and 10" tubes with different mixtures of timing, single electron resolution and price. Larger tubes could be developed like the 25" for SUPERKAMIOKANDE.

These tubes are already developed and ready for series production for the large non-accelerator physics neutrino detectors. Adapting them for a specific SSC or LHC case would only ask for minor development and only some lead time. Although we should not aim for such a situation at this conference one can remark that this would probably be the cheapest detector proposal, using say 100.000 12" tubes at 1000 dollars each covering 50% of the outer wall.

9. CONCLUSIONS

Phototube technologies are well proven since decades. On top of the four photomultiplier manufacurers there is an entry seen by traditional image intensifier companies. The industrial base for phototubes is thus well underbuilt. Phototubes have certainly many limitations as discussed above and considerable R&D work has to be done to adapt them to the specific situations of the new colliders. Even so, adaptions are safer than totally new technologies and have a better chance to be ready on time. Phototubes are thus a decent possibility in several situations and they are one of the few concepts that directly can handle nanosecond signals by tradition.

MICRON SEMICONDUCTOR

SILICON DETECTORS OF THE 1990's

MICRON - C.D. Wilburn

SILICON DETECTORS FOR 1990's

with 'TECHNOLOGY DEMANDS'

MICRON SEMICONDUCTOR
1983 INCORPORATED

HEP DOMINATES MICRON BUSINESS

CURRENTLY 9 CONTRACTS CERN
8 CONTRACTS FERMI LAB

PRIVATE COMPANY U.K. BASED

PLUS U.S.A. MARKETING COMPANY

NO GOVERNMENT SUPPORT

TECHNOLOGY:

ION IMPLANTATION STRUCTURE

3" TECHNOLOGY (SILICON)

4" TECHNOLOGY (SILICON)

OTHER BUSINESS

HEAVY ION PHYSICS

SPACE PHYSICS

MICRON SEMICONDUCTOR

LATEST DEVELOPMENTS IN SILICON DETECTORS

U.K. BASED COMPANY / OPERATES FULLY TRACEABLE MONITORED QUALITY CONTROL

SUPPLIED APPROXIMATELY 50 DESIGNS TO PHYSICS MARKET

TECHNOLOGY 3" AND 4"

CAPABILITY: DETECTORS Several 100/Month. PHOTODIODES Several 1000/Month

Single Area: 0.1mm² - 25cm² (3")
0.1mm² - 50cm² (4")

Ring Counters with central hole to 9.6cm Ø

Gamma Transient Detectors
Microstrip Detectors

Pitch 10μ to 1cm
Channels 5 to 2000

Thickness 150μ, 300μ*, 500μ
Response Time < 10nS

* Leakage Current 6nA/cm² Capacitance 40pF/cm²

Single Sided and Double Sided

Integration with VLSI Electronics

Paralleled and Daisy Chained

FAN-OUT ON-CHIP / PCB / CERAMIC

Acceptance Levels: 99% - 100%

PIXEL Detectors
Ring Counter Format 384 Pads
Ceramic Overlay / Particles through back
Charge Injection Devices (Indium Bump)
256 x 256 (30μ PIXELS) and 12 x 66 (75μ PIXELS)
Designed to Interface Hughes RAM MICROCHIP with same pixel format

SILICON PHOTODIODES
0.1cm² - 2.5cm² Id 1nA/cm² tc 2nS
High Speed 1 Large Area / Low Series Resistance / Low Cost

MICRON SEMICONDUCTOR

PACKAGING / ASSEMBLY MATERIALS

FOR

SILICON DETECTORS

PCB MATERIAL G 10 or G 30

Minimum Track Width	40µm
Minimum Pitch	100µm
Maximum Size	40cm x 40cm

KAPTON

Minimum Track Width	70µm
Minimum Pitch	150µm
Maximum Size	40cm x 40cm

CERAMIC

Minimum Track Width	10µm
Minimum Pitch	20µm
Maximum Size	15cm x 15cm

KEVLAR

Minimum Track Width	70µm
Minimum Pitch	150µm
Maximum Size	40cm x 40cm

MICRON SEMICONDUCTOR

DETECTORS FOR 1990's

MICROSTRIP DETECTORS

SINGLE SIDED

	2048 Ch	25µ PITCH	300µ
*	520 Ch	10µ PITCH	150µ

Both Active and Inactive FAN-OUT

PROFILED DETECTORS (ZEUS)

Instead Straight Edge

Edge Termination

$\frac{X^2}{a} - \frac{Y^2}{b}$ (ELLYPSE)

SINGLE SIDED (HIGH RATE) CLOSE CUT

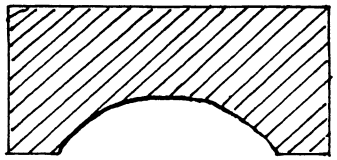

800Ch
45°

300µ

Edge < 500µ

ELECTRONICS - SANTA CRUZ
(Dielectric Isolated VLSI)

MICRON SEMICONDUCTOR

DOUBLE SIDED MICROSTRIP DETECTORS

for 1990's

5 DESIGNS TO DATE

1988	1.	RING COUNTER DESIGN S	Heidelberg / CERN
1988	2.	MICROSTRIP 40 x 40 x 1mm	LEAR / CERN
1988	3.	MICROSTRIP 50 x 50 x 3mm	Edinburgh / SERC Daresbury
1989	4.	MICROSTRIP 50 x 50 x (25μ & 50μ)	BCD / FERMI LAB
1989	5.	MICROSTRIP 16 x 32 x 2mm (A/c)	UA2 / CERN

Problems

Yield

Uniformity of Characteristics

Manufacturing Control

Silicon Handling

Interstrip Impedance on Ohmic Side

AC or DC Coupling

Radiation Effects

Testing

MICRON SEMICONDUCTOR

DOUBLE SIDED DETECTORS

Necessary to bias all strips during testing.

Assembling devices prior to Test too costly.

Micron have developed 'Double Sided' computerised probe station for coarse detectors and will enlarge this for fine strip devices.

Probe station gives rapid control and feedback of processing for these difficult devices.

Double Sided Microstrip Detectors are a
Triple Implant Device

(1) Junction Strips

(2) Ohmic Strip Isolation

(3) Ohmic Strips

MICRON SEMICONDUCTOR

SILICON PIXEL DETECTORS

During 1988 MICRON built 2 DESIGNS for SLAC for SSC DEVELOPMENT

(1) 10 x 64 120μ PIXELS

(2) 256 X 256 30μ PIXELS

Designed to Interface with HUGHES PIXEL ELECTRONICS built for INFRA-RED SYSTEMS and operate on U.C. Berkeley Test Facility.

STATUS

Both devices assembled via INDIUM BUMPING
Detectors at Berkeley, Space Science Lab.

10 x 64 resolving Minimum Ionising Betas (2MeV) with Oscilloscope S/N > 10:1

256 x 256 ready for first Beta Test.

Radiation Hardness

10 x 64 Claimed to be RAD HARD (1 M.RAD Co60?)

256 x 256 not RAD HARD, but RAD HARD version is now funded by SLAC to HUGHES (August 1989)

MICRON SEMICONDUCTOR

PIXEL DETECTORS

Pixel Electronics Studies EUROPE

CERN	Heinje/ Jarron	200μm
RUTHERFORD	Sharp / Seller	200μm

Pixel Collaboration U.S.A.

SSC Proposals

D. Nygren / N. Lockyer / G. Trilling / Hughes

Santa Cruz / Berkeley / Cornell

'Architecture for High Speed, High Rate Systems'

Limitations

Small Size 1cm² Indium Bump / Pressure Limits

Larger 'In'Solder Pads

Advantages

High Radiation Damaging Environments
Individual Pixels Damaged / Knocked out but sufficient numbers remain to collect and analyse data usefully. If damage rate high pixel should be small. S/N Min. Ionising needs to be high.

Future Physics

If successful EXPERIMENTS will most likely use some PIXELS along with MICROSTRIPS which will still carrry most of the AREA coverage.

MICRON SEMICONDUCTOR

RADIATION DAMAGE EXPERIENCE

EXPERIMENT CERN UA2
PHYSICIST: CLAUS GOSSLING
HADRONS: PROTONS with 15% NEUTRONS

OUTER DETECTOR	7 PAD ARRAY 6cm x 4cm 300µm
DESIGN I	LEAKAGE CURRENT (FD) 100nA typ.
1 METRE²	FULL DEPLETION (FD) 30 VOLTS
INNER DETECTOR DESIGN DD	16 Ch. ARRAY 16.4mm x 32mm 300µm
OPERATIONAL	1 Year with Off-Periods
Damage	1nA/cm² / 100 Rads
Total Dose	100K Rads
	Some Design I received 30K RAD during beam alignment
Electronics Inner	AMPLEX 16Ch CMOS VLSI IMEC (P. Jarron Design)
Outer	8 Ch. Hybrid. 0.8 µsec Shaping

EXPERIMENT E653

PHYSICIST BYRON LUNDBERG (Radiation mask

Reported Similar Damage results UA2

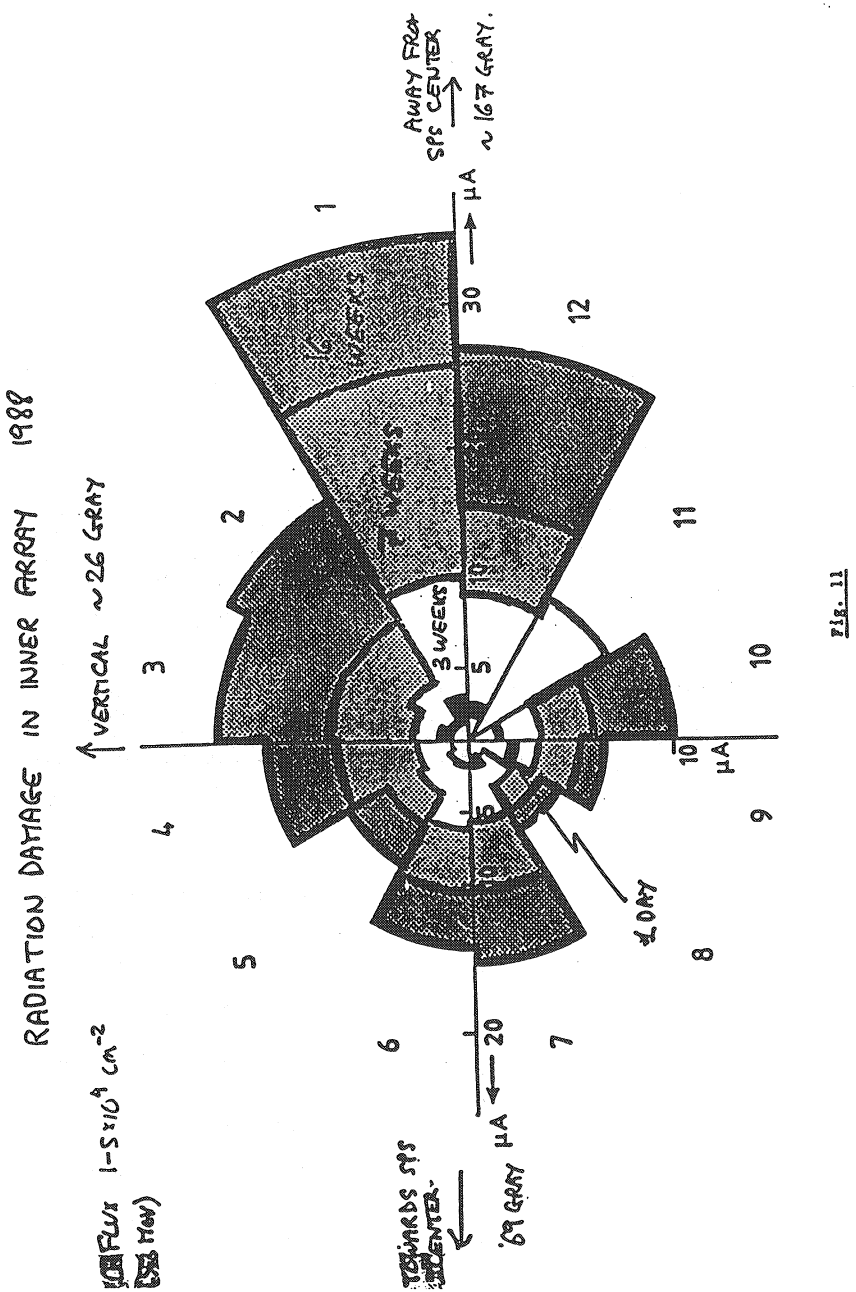

Fig. 11

MICRON SEMICONDUCTOR

CURRENT RADIATIION EXPERIENCE

NEUTRONS 10^{12}/CM²

REACTOR (14 MeV)

3 Test Detectors FD ≏ 50V OP.V. 80V

Exposure ≏10^{12} neutrons/cm² (≡ 1 Year SSC)

I LEAKAGE (BEFORE)	I (AFTER)	I(AFTER 3 MONTHS)
1.7nA	680nA	125nA
2.0nA	690nA	120nA
2.5nA	700nA	118nA

RISE TIME (B)	FALL TIME(B)	RISE TIME(A)	FALL TIME (A)
2.2nS	3.0nS	2.2nS	3.0nS
2.6	4.6	2.5	4.2
2.5	4.0	2.5	4.4

RESPONSIVITY (0.85µm) (B)	RESPONSIVITY (0.85µm) (A)
1	0.89

Capacitance and Breakdown Voltage

NO CHANGE

ANNEALING
85°C 80V

I LEAKAGE ≏ 50nA

MICRON SEMICONDUCTOR

RADIATION DAMAGE EXPERIENCE

EXPERIMENT: FERMI LAB E789

PHYSICIST: JOHN KAPUSTINSKY 'LANL'

LANL TEST AUGUST 1989

SILICON MICROSTRIP DESIGN B
5cm x 5cm
1000 Channels
50 Micron Pitch
Thickness 300µm
Full Depletion 40 Volts
Total Current 2µA

RADIATION

High Rate bursts of 300nS 800MeV PROTONS
Run Times 2 Hours and 12 Hours
Total Dose 1 x 10^{14} PROTONS
Event Rate: 5 x 10^{7} PROTONS/cm²/sec and 10^{8} PROTONS/Cm²/sec
Ambient AIR

DETECTOR (20°C)

Leakage Current / Strip increased 8nA - 200nA
Optimum Operating Voltage increased 60V to 150V
Additional Current only present when Beam on
Higher on Outer Strip and level proportion to Beam intensity

MICRON SEMICONDUCTOR LTD

SILICON STRIP BEAM TESTS AT LOS ALAMOS

(8/1 - 8/13/89)

MICRON TYPE B W / and Plane

10 HIGH INTENSITY EXPOSURES OF 800 Me V/C PROTONS

1.	1.82×10^{12}	2 Hrs	2.5×10^{8} Ptm^2 .5	ON
2.	1.86×10^{12}	2 Hrs	"	ON
3.	1.86×10^{12}	2 Hrs	"	OFF
4.	8.77×10^{12}	14 Hrs	1.7×10^{8}	ON
5.	9.29×10^{12}	14 Hrs	1.8×10^{8}	OFF
6.	9.29×10^{11}	5 Hrs	5.2×10^{8}	ON
7.	9.29×10^{11}	5 Hrs	"	OFF
8.	2.81×10^{13}	10 Hrs	8.0×10^{8}	OFF
9.	7.62×10^{13}	19 Hrs	1.0×10^{9}	OFF
10.	1.75×10^{14}	9 Hrs	5.4×10^{9}	OFF

4×10^{14} P/cm^2

10 Megarad Total Exposure

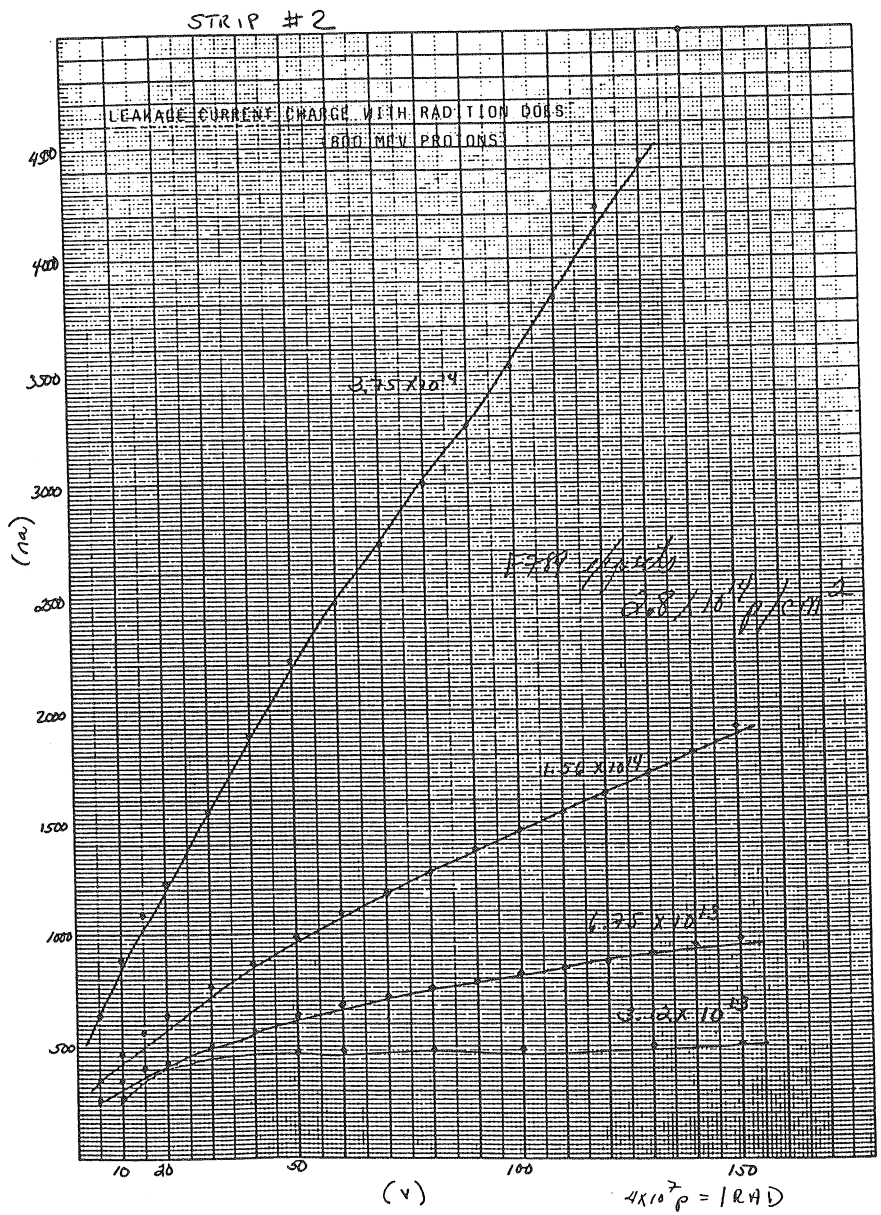

after irradiation 2×10^{13} p's/cm^2

Minimum Ionising Pulse to Applied Bias Voltage

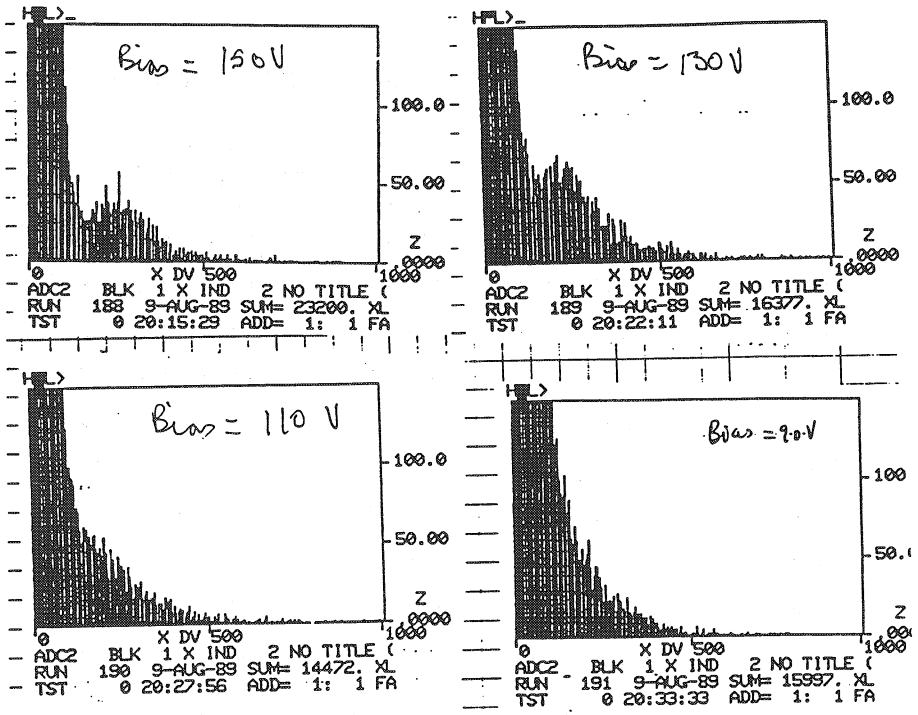

ADC of a single strip

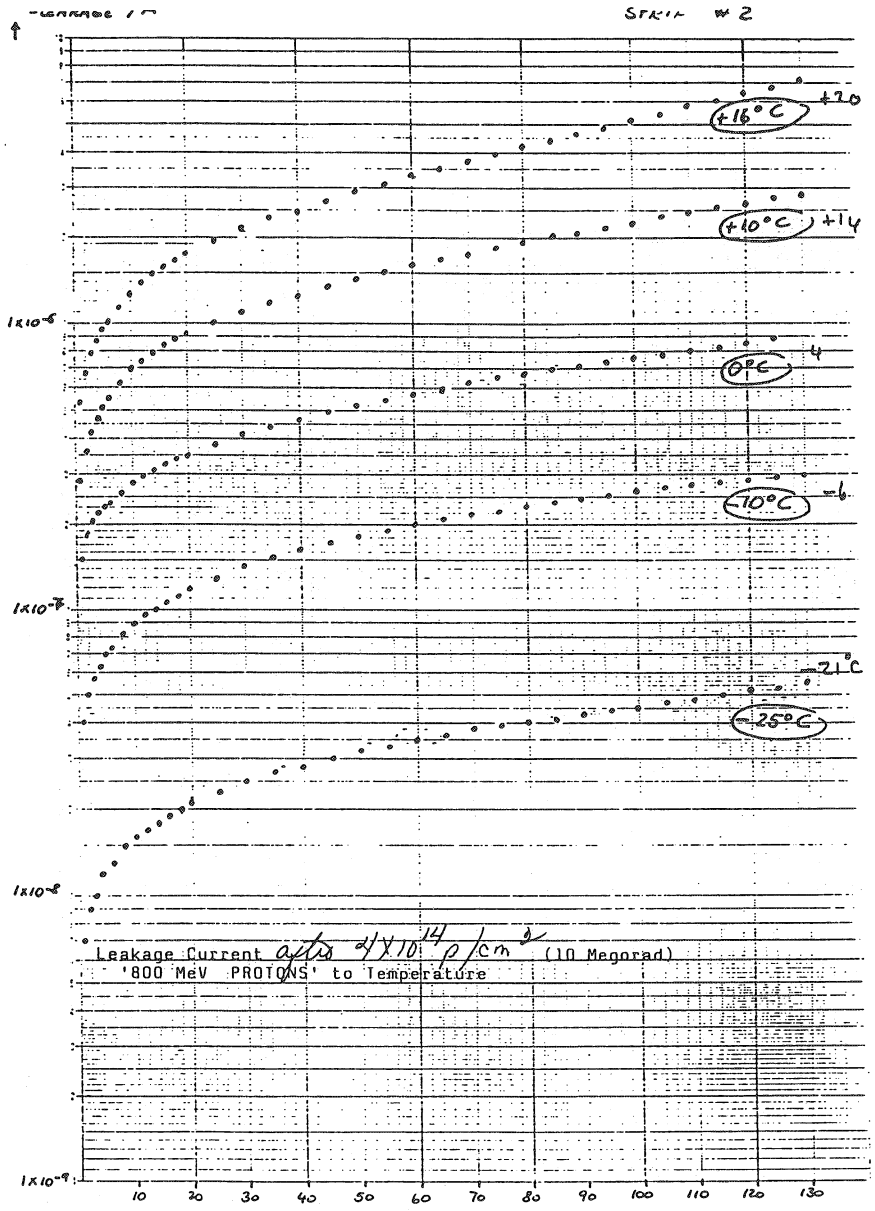

MICRON SEMICONDUCTOR

SILICON PHOTODIIODES

Micron Semiconductor is manufacturing a wide range of 'LOW COST' SILICON PHOTODIODES.

Standard and Thin Window Implants are shown.

The Standard Window is $\simeq$ 0.5µm

The Thin Window is $\simeq$ 0.1µm

Detector / Photodiode all depleted structure also available.

Typical Q.E. characteristic is shown next.

I dark Current - 1nA / cm²

Capacitance (150µm) $\simeq$70pF

Capacitance (300µm) $\simeq$40pF

Suitable for (Scintillation Interfacing'.

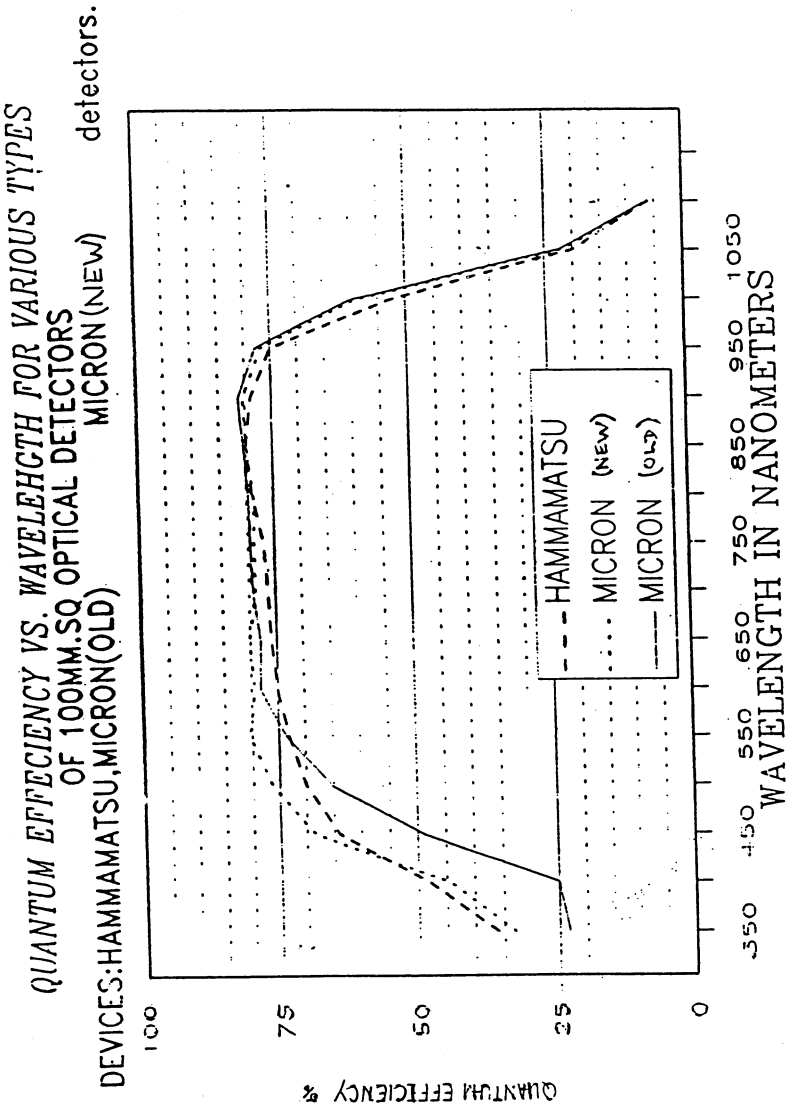

ONE VIEW OF INDUSTRY'S ROLE IN PARTICLE PHYSICS

N. J. DiGiacomo

Science Systems
Martin Marietta Astronautics
Denver, CO 80201
USA

INTRODUCTION

The scale of detector systems for the next generation of high luminosity hadron colliders demands, to some observers, a significant increase in industrial participation. We discuss here the various roles industry might play, and examine the case for more substantial industrial involvement in detector sub-system[1] design and fabrication. We then offer some observations on the cultural differences between the particle physics and industrial worlds. We present an example of an on-going effort in Superconducting Supercollider (SSC) detector sub-system design involving university, national laboratory and aerospace industry scientists and engineers, and consider this activity as a model for industrial participation in a major collider detector collaboration.

ROLES FOR INDUSTRY

It is clear that universities and national laboratories will continue to perform the detector physics R&D and prototype development as well, of course, as the particle physics research. The spectrum of other activities involved in the development, fabrication and commissioning of a large collider detector system can be divided so as to interest two types of industrial concerns: a) component fabricators and b) system builders and integrators. We consider each below.

COMPONENT FABRICATORS

It is useful to make the distinction between two classes of components, conventional and high technology.

- Conventional components include off the shelf items such as powers supplies, valves, computers, as well as standard build-to-print fabrication of metal structures, support and handling equipment, etc.
- High technology components include electronic devices, materials and advanced processes that are state-of-the-art or beyond. Such components often require significant technology R&D on the part of the vendor and/or the particle physics laboratory. It is important to recognize that the technology flow which occurs during the development of sophisticated components for particle physics is quite bi-directional, with techniques pioneered for commercial, space or defense applications contributing to particle physics detectors at the same time that novel particle physics technology developments are used in other arenas.

It is apparent to us that component fabrication is a well established industrial role in particle physics, and we anticipate a continued reliance on such industries.

SYSTEM BUILDERS AND INTEGRATORS

There is a class of companies that builds and integrates large, complex high technology systems. Such companies, examples of which include large aerospace contractors, can be responsible for the integration of a whole project as prime or associate contractors or for sub-system design and fabrication as associate or sub-contractors. The modus operandi is generally that of a number of companies (often grouped into teams) responsible to a program office in a government agency (e.g. DOD or NASA). The companies are integrally involved in projects from concept through commissioning, and have direct responsibility for the design, fabrication and commissioning of the entire project or of major sub-systems.

This approach is to be contrasted with the way in which particle physics detector systems have been built to date in the United States and Europe. The universities and laboratories design and fabricate the sub-systems (from components purchased in industry), while the accelerator laboratory generally leads the overall integration. Exceptions do exist, mainly in the form of large superconducting solenoids and associated cryogenics which have been acquired as complete sub-systems from industry. In addition, detector system development in Japan appears to proceed with rather more industrial responsibility for sub-system design and fabrication.

The involvement of industrial system builders and integrators in particle physics detectors is, as we will argue, necessary given the scale of future projects. How exactly to orchestrate and manage such industrial participation is not patently obvious. Before attempting to address this problem, we explore some of the cultural differences between the particle physics and industrial system-building worlds.

SOME CULTURAL DIFFERENCES

We discuss here some differences in the way particle physics and industrial system builders accomplish their goals. In considering the differences, it is interesting to note that an analogy can be made between the style of early space science projects and that of todays particle physics detector systems. Given that major changes in the structure and management of space science projects came in response to large increases in scale and cost, as well as more stringent reliability requirements, it is not unreasonable to consider the evolution of space science as a model for the way particle physics might be done in the future. In any case, we consider it likely that the development of the next generation of particle physics detector systems will result in a culture that is somewhere between the two characterized below.

REQUIREMENTS DEVELOPMENT

For *Particle Physics Detector Systems* the buyer (i.e. definer of the overall requirements), the builder and the user are generally the same people. This results in less need to fix the system requirements very early on in the development cycle.

Aerospace Systems, on the other hand, generally involve separate buyers, builders and users. For example, requirements for a space probe may be initially determined by an office of NASA, the probe built and launched by teams of companies, and later operated by a consortium of laboratories and universities. This sequence of segmented responsibilities is one reason that requirements need to be fixed very early in the project.

SYSTEM DESIGN VERSUS SENSOR TECHNOLOGY

For most *Particle Physics Detector Systems*, the sensor technology[2] is state-of-the-art. This is driven to some extent by the fact that those involved in sensor development are researchers, interested in breaking new scientific and technical ground, publishing original work, and generating interesting thesis work for students. Particle Physics detector systems are thus built of

sensors and sub-systems (tracker, calorimeter, muon system, etc.), with the integrated system design coming somewhat from the bottom up.

Aerospace Systems begin with an overall system design that focuses on high level requirements. Component (or sensor, where appropriate) technology is only as complex or sophisticated as necessary to fulfill requirements. This top-down approach leads to development of new technology only when clearly called for by the system design.

FLEXIBILITY

For *Particle Physics Detector Systems*, the changing physics goals require great system flexibility. Also, the relative ease of access to the system allows for less stringent reliability requirements and somewhat more adventurous designs.

Aerospace Systems, particularly those that are space-based and/or human-rated, require very high reliability and extensive verification. The lack of repair access to an interplanetary spacecraft, for example, demands designed-in reliability and independently verified performance long before the system is in its actual operating environment. This requires rather formal methods of configuration and change control, for example, as well as conservative initial designs (i.e. significant performance margins).

WHY SHOULD THINGS CHANGE NOW?

We offer here some reasons to consider increased industrial participation in particle physics detector sub-system design and fabrication, with the SSC as our particular example. We emphasize that the technical or managerial ability of the particle physics community to build future detector systems is never in question. The driving consideration is efficient use of limited resources to do the best science.

GOOD REASONS

- The scale and overall complexity of SSC detectors require more structured means of technical management and configuration control at system and sub-system levels. A strong emphasis on reliability is also called for, given the monetary and scientific expense of system down time. Industrial system builders have a large reservoir of experience and expertise that is clearly applicable.

- Universities and national laboratories cannot realistically increase their engineering and project management staffs to the level necessary to design and build all detector sub-systems for the SSC. The reason is simple: as detector systems get bigger and more complex, the ratio of builders to users becomes larger. In order, then, to avoid local boom-and-bust cycles, appropriate projects would have to appear with the proper timing to gainfully employ the university and laboratory-based system builders. Industrial system builders, on the other hand, are well versed in moving appropriately skilled personnel as necessary among a wide variety of projects.

- If NASA space science is any indication, increased political support for particle physics should result as widely-distributed industrial concerns become substantially involved in particle physics detectors and accelerators.

A BAD REASON: TECHNOLOGY TRANSFER

- Is is misleading, in our view, to argue that industry should be involved in basic science projects primarily on the promise of technology transfer. Particularly for large, industrial system builders, direct transfer of technology from basic research projects, if and when it occurs, is seen as a by-product - not the raison d'etre - of basic science. This view is not difficult to understand, since profit making organizations, accustomed as they are of thinking in terms of return on investment, are not easily convinced, for example, that building a multi-billion dollar accelerator is the best way to commercialize superconducting magnet technology. If soliciting industrial support for particle physics is the goal, much better then to tell the truth to an audience that is inherently appreciative of, and dependent upon, science: particle physics is a critical element of the scientific knowledge base upon which *your* company depends.

A corollary to the above is that industrial system builders can participate in the design, fabrication and commissioning of a particle physics project as team members, contributing their particular skills to the success of the project, with no particular desire (or need) to acquire technologies as such. With this in mind, particle physics detector system managers should construct industrial roles on the basis of technical qualifications and actual cost of work performed, and not expect industries to become involved simply to be "near" the technologies of particle physics.

BRIDGING THE CULTURES

We are presently engaged in a joint university-laboratory-industry (Stony Brook, Brookhaven and Martin Marietta) effort to perform a conceptual design of a major SSC detector sub-system. We describe this work here in the hope that some aspects of the collaboration may serve as a model for larger-scale industrial participation in detector system development.

The immediate objective of our work[3] is to quantitatively evaluate the feasibility of liquid argon calorimetery (LAC) for generic detector systems at the SSC. One of the primary challenges is to design and engineer a vessel and absorber support system whose structural and cryogenic elements have a minimal effect on overall calorimeter coverage and performance (i.e. do not compromise hermeticity). Progress has been such that it appears a proof-of-principle LAC design that meets the performance requirements of SSC is achievable.

Our primary focus has been on the creation of a design and analysis team that rapidly evaluates detector concepts from both engineering and physics performance perspectives. The functional composition of the design and analysis team is represented in Figure 1.

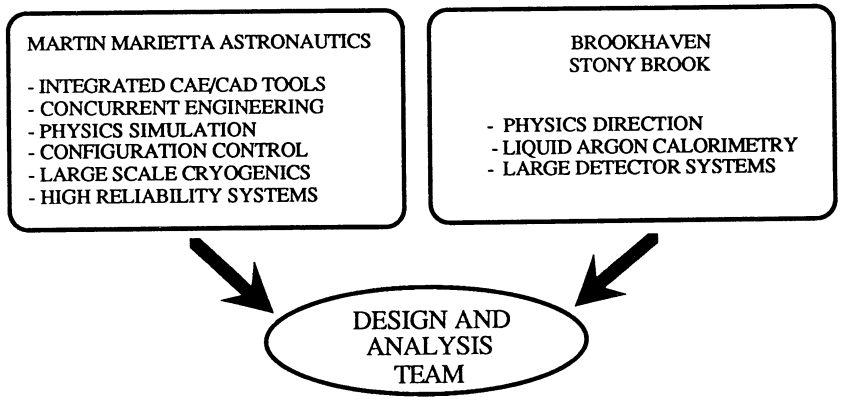

Figure 1. A schematic representation of the SSC calorimeter design and analysis team composition.

We list below some elements we view as key to the success of such a design team:

- *Participation by both physicists and engineers in the design work.* It is important that engineers understand the evolution of physics requirements and goals, and that the physicists grasp the engineering implications in "real time".
- *Integrated design, modeling, analysis and simulation.* This capability to rapidly examine detector concepts is built upon three cornerstones:
  - *Concurrent Engineering.* Engineering disciplines that communicate with each other daily and perform analyses in parallel.
  - *State of the art CAE/CAD tools:* 3-D modeling packages that allow fast, realistic design. The modeler is coupled to a flexible interface that allow models to be easily sub-divided and used for a wide spectrum of engineering analyses. The integrated CAE/CAD tools used by our collaboration are depicted in Figure 2.
  - *Integrated engineering and physics performance evaluation:* Physics simulation tools must be integrated with the modeler in order that the physics performance implications of engineering design changes can be quickly determined.

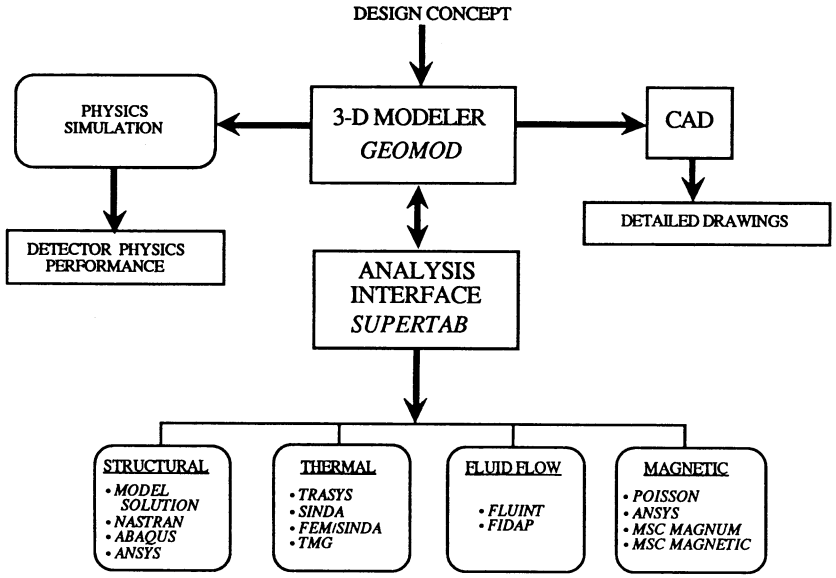

Figure 2. Detector design, modeling, analysis and simulation tools. The system is based in the I-DEAS[3] package, and incorporates a number of contemporary engineering analysis codes.

INDUSTRIAL PARTICIPATION IN A MAJOR DETECTOR COLLABORATION

The work outlined above is but one step toward a full-scale SSC detector collaboration in which industrial system builders play major roles. Nevertheless, it encompasses one very important requirement - industrial involvement in the conceptual design phase of detector system development. We anticipate extending this style of collaboration to prototype development, and ultimately to other appropriate areas in a major SSC detector system[5]. Because this approach breaks new ground, we cannot provide at this time an accurate road map. We do, however, offer observations on two areas of concern.

- Particularly in the concept evaluation and preliminary design phases, engineering and physics simulation resources must be available to all collaborators, be they small or large universities, national laboratories or industries. High speed computer communication networks that connect all collaborators are a must, in order that the necessary resource be available when and where it is needed. Figure 3 depicts a solution where institutions interested in simulation, for example, can access the appropriate sub-set of engineering data and necessary simulation tools.

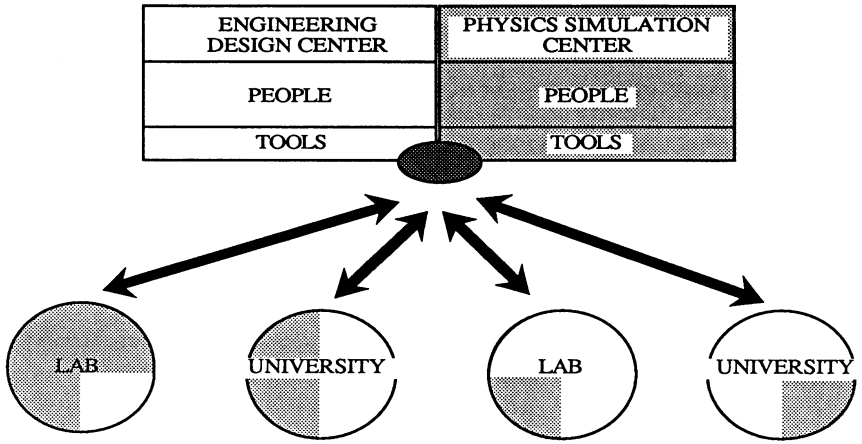

Figure 3. A schematic representation of an engineering design and physics simulation resource network. The shading emphasizes that institutions can interact with the engineering and simulation centers as appropriate for their particular interest(s).

- When universities and laboratories design, develop and integrate detector sub-systems, the issue of industrial competition is straightforward, since components and build-to-print elements can be acquired through normal procurement channels. It is not yet clear, however, how competition for substantial fabrication will be conducted in an environment where a number of industrial contractors have already been involved in concept development and engineering design within collaborations. Perhaps the competition between the detector system proposals for approval could be conducted so as to solve this problem. All interested parties must work towards a plan that encourages early participation and investment by industrial concerns in detector projects, without excluding those firms from later competition for major fabrication roles.

ACKNOWLEDGEMENTS

The author is grateful to Michael Davis and Michael Marx for stimulating discussions, and to James Gliozzi, Joe Pohlen and Glenn Guenterberg for critical reading of the manuscript. This work was supported by Martin Marietta Corporation.

REFERENCES

1) We note here, by way of definition, that a detector system is composed of a number of subsystems (vertex chamber, tracker, calorimeter, etc.), which in turn contain many sensors (BGO crystals, wires, straw tubes, etc.) with associated electronics, utilities, etc.

2) By sensor technology we mean the specific technique used for measurement (e.g. liquid argon versus warm liquid versus scintillating fiber calorimetry).

3) T.S. Adams et al., "Status Report on an Engineering Design Study of Hermetic Liquid Argon Calorimetry for the SSC", to be published in the Proceedings of the Workshop on Calorimetry for the Superconducting Super Collider, Tuscaloosa, Alabama (March 1989).

4) I-DEAS, Structural Dynamics Research Corporation, Milford, OH (1988).

5) M. Marx, "EMPACT - An Alternative Approach to a High P_T SSC Experiment, SSC-219 (May 1989).

CATALOGUE OF RESEARCH PROGRAMMES WITHIN THE FRAMEWORK PROGRAMME OF THE EUROPEAN COMMUNITY 1987 – 1991

(status 1 September 1989)

COMMISSION OF THE EUROPEAN COMMUNITIES
DIRECTORATE-GENERAL FOR SCIENCE, RESEARCH AND DEVELOPMENT
200, rue de la Loi - B-1049 Brussels
Tel Brussels 235.11.11 / 236.11.11 - Telex COMEU B 21877

PREFACE

This catalogue provides a summary of the specific R&D programmes within the Framework Programme for Community activities in the field of research and technological development 1987-1991. It includes existing programmes as well as those which the Commission has proposed to Council and Parliament.

The entry for each programme gives a brief description of its objectives, its duration, the name of the programme manager, and the amount allocated to it from the Community budget. It also gives an indication of the type of operation used to carry out the programme (see Glossary). The reference documents will be found in the Community's Official Journal (OJ) which may be consulted at any of Commission's Information Offices or European Documentation Centres in the Member States.

Whenever possible the next deadline relating to calls for proposals is indicated. Proposals should be prepared well in advance of this deadline in order to avoid last-minute problems. Proposers should consult the programme managers for advice on questions of presentation, and in those cases where the deadline has not yet been determined exactly.

The catalogue shows the status of programmes as at 1 September 1989. The main elements of the Commission's draft for a new Framework Programme (1990-1994) of 25th July 1989 are also attached.

A revised version of this catalogue will be produced in due course; at the latest when the new Framework Programme is adopted, hopefully before the end of the year.

Brussels, 1st September 1989

INDEX BY ACRONYM

Full explanations of acronyms are given in the text.

GLOSSARY

Call for Proposals:
This is an invitation for potential participants in a Community research programme to submit project proposals. It is published in the Official Journal (Series C). The deadline must be respected.

Official Journal:

The Official Journal (OJ) is published daily and contains all the formal announcements which the Commission is obliged to make. Series C contains Commission legislative proposals, calls for research proposals and expressions of interest. Series L contains the text of legislation adopted by the Council of Ministers. For the O.J. see addresses on p. 32.

Concerted Action:

This is a programme where the priorities and workplans are determined at Community level but the research is funded by Member States. The Community's role is concerned with the coordination of work and the exchange of research results.

Shared-cost Contracts:

This is the Community's principal instrument of research funding. Participants must fund part of the research from their own funds. The Community contribution is usually (though not always) half the cost of the project. The research may be carried out by Universities (or other establishments of higher education), public research institutes and private companies. Projects usually involve a consortium of companies and institutions. Details on contractual requirements are available on request.

Community research activities carried out within the Framework Programme are managed by a number of different Directorates-General; the entry for each programme indicates which one is responsible:

DG XII: Science, Research and Development (including overall science and technology policy)
DG XIII: Telecommunications, Information Industries and Innovation
DG VI: Agriculture
DG XIV: Fisheries

Commission address: 200, rue de la Loi, B-1049 Brussels

CURRENT FRAMEWORK PROGRAMME (1987-91)

		(million ECU)		%
1.	**Quality of life**		375	6,9
1.1.	Health	80		
1.2.	Radiation protection	34		
1.3.	Environment	261		
2.	**Towards a large market and an information and communications society**		2 275	42,3
2.1.	Information technologies	1 600		
2.2.	Telecommunications	550		
2.3.	New services of common interest (including transport)	125		
3.	**Modernization of industrial sectors**		845	15,6
3.1.	Science and technology for manufacturing industry	400		
3.2.	Science and technology of advanced materials	220		
3.3.	Raw materials and recycling	45		
3.4.	Technical standards, measurement methods and reference materials	180		
4.	**Exploitation and optimum use of biological resources**		280	5,2
4.1.	Biotechnology	120		
4.2.	Agro-industrial technologies	105		
4.3.	Competitiveness of agriculture and management of agricultural resources	55		
5.	**Energy**		1 173	21,7
5.1.	Fission: nuclear safety	440		
5.2.	Controlled thermonuclear fusion	611		
5.3.	Non-nuclear energies and rational use of energy	122		
6.	**Science and technology for development**		80	1,5
7.	**Exploitation of the sea bed and use of marine resources**		80	1,5
7.1.	Marine science and technology	50		
7.2.	Fisheries	30		
8.	**Improvement of European S/T cooperation**		288	5,3
8.1.	Stimulation, enhancement and use of human resources	180		
8.2.	Use of major installations	30		
8.3.	Forecasting and assessment and other back-up measures (including statistics)	23		
8.4.	Dissemination and utilization of S/T research results	55		
	Total		5 396	100

On July 27th, the Commission presented proposals for a new Framework Programme covering the period 1990-94. With these proposals the Commission aims to update its priorities for Community RTD, taking into account the pace and new directions of technological change.

According to these proposals the new Framework Programme would overlap with the current one. By doing this the Commission has extended the concept of 'rolling' programmes which take into account the dynamics of technological development today. Nevertheless, specific programmes launched under the current Framework Programme will be executed in full.

The shift in priority may be seen by comparing budget forecasts of the current and proposed Framework Programmes. In absolute terms, none of the activities of the current programme would be reduced. But the share of resources devoted to environmental research, biotechnology and human capital and mobility would rise significantly, while that devoted to energy research would be reduced. Industrially-oriented research (Enabling technologies) would rise only in absolute terms.

At this stage these proposals remain provisional, and may change during the course of discussions in the Council of Ministers and Parliament before the final decision is be taken.

Proposed Framework Programme (1990-94)

		(million Ecu)	%
I.	**Enabling technologies**		
1.	Information and communications technologies	3,000	38,9
2.	Industrial and materials technologies	1,200	15,6
II.	**Management of natural resources**		
3.	Environment	700	9,1
4.	Life sciences and technologies	1,000	13
5.	Energy	1,100	14,3
III.	**Management of intellectual resources**		
6.	Human capital and mobility	700	9,1
	TOTAL	7,700	100

EUROPEAN SCIENTIFIC AND TECHNICAL COOPERATION

THE SCIENCE PROGRAMME (DG XII)

Stimulation des Coopérations Internationales et des Echanges Nécessaires aux Chercheurs en Europe (SCIENCE)

This programme consists of a range of activities selected on the basis of their scientific and technical quality, which have as their aim the establishment of a network of scientific and technical cooperation and interchange at a European level. It aims to improve the efficacy of research in Member States and to help reduce the scientific and technical disparities between them. It covers all fields of the exact and natural sciences, such as mathematics, physics, chemistry, life sciences, earth and ocean sciences, scientific instrumentation and engineering sciences.

Programme Manager:	Louis BELLEMIN (Tel. Brussels 235.36.96)
Community budget	167 Mio ECU
Programme duration:	1988-1992
Call for proposals:	Every three months (applications received continuously)
Type of operation:	Bursaries, research allocations, grants for high-level courses encouraging the twinning of laboratories and operations contracts.
Reference document:	OJ L206 (1988)

THE SPES PROGRAMME (DG XII)

Stimulation Plan for Economic Science (SPES)

The programme will consist of a range of activities to establish a network of cooperation and interchange between economists of the highest professional quality at the European level. Possible research topics are issues related to the internal market of the Community, European integration economics, economic growth in Western Europe, systematic issues in the monetary areas and macroeconomic and fiscal policy coordination, trade policy, the role of Western Europe in the international division of labour and employment and social policy issues.

Programme Manager:	Louis BELLEMIN (Tel. Brussels 235.36.96)
Community budget	6 Mio ECU
Programme duration:	1989-1992
Call for proposals:	Announced 7 April 89, no deadlines
Type of operation:	Scholarships, research grants and subsidies for training courses and scientific meeting
Reference document:	OJ C109 (1988) and L44 (1989)

LARGE-SCALE SCIENTIFIC FACILITIES (DG XII)

The programme consists of a range of temporary financial support arrangements granted to scientific institutions in the Community having large-scale research and development facilities or installations which, in return for the Community contribution, agree to make these facilities or installations available to scientists and researchers working in universities, public research centres or industrial laboratories.

Researchers and scientists to whom facilities and installations have been made available will be able to benefit from research grants and funds provided for in the SCIENCE plan. The programme covers all fields of the exact and natural sciences, research and precompetitive technological development.

Programme Manager:	Louis BELLEMIN (Tel. Brussels 235.36.96)
Community budget	30 Mio ECU
Programme duration:	1988-1992
Call for proposals:	1 October 1989
Type of operation:	Shared-cost contracts, grants
Reference document:	OJ L98 (1989)

THE MONITOR PROGRAMME (DG XII)

The purpose of this programme is to contribute to the identification of new directions and priorities in the common research and technological development policy and to establish more clearly the relationships between it and the other common policies and to the improvement of evaluation of R&D programmes. It comprises three activities: Strategic Analyses in the field of Science and Technology (SAST); Forecasting and Assessment in Science and Technology (FAST); and the Support Programme for the Evaluation Activities in the field of Research (SPEAR).

The SAST activities consist of impact studies (technological, industrial, socio-economic, environmental) and analyses 'targeted' at a scientific field, technology or sector. The FAST activities include the study of scientific and technological changes and their many interactions with economic and social changes. The SPEAR activities concern the definition of practical and reliable procedures for the evaluation of R&D programmes and other methods of carrying out R&D. They also cover the means of support and management of research.

Programme Manager:	Herbert ALLGEIER (Tel. Brussels 235.40.55)
Community budget	22 Mio ECU
Programme duration:	1988-1992
Call for proposals:	Open
Type of operation:	contracts and grants
Reference document:	OJ C29 (1989), C161 (1989) and L200 (1989)

MODERNISATION OF INDUSTRIAL SECTORS

THE BRITE/EURAM PROGRAMME (DG XII)

Basic Research in Industrial Technologies for Europe (BRITE) European Research on Advanced Materials (EURAM)

This new single programme builds on the experience and the achievements already emerging in the first BRITE and EURAM programmes, and will cover cost-shared research projects concerning advanced materials technologies, design methodology and assurance for products and processes, application of manufacturing technologies and technologies for manufacturing processes. It will also carry out research aimed at the development of the European aeronautical technology base, including aerodynamics, acoustics, airborne systems and equipment and propulsion systems. The programme will include coordinated activities and feasibility awards aimed at assisting SMEs.

A separate research programme in aeronautics will be prepared to follow this pilot phase.

Programme Manager:	Willem van der EIJK (Production and Materials Technology) (Tel. Brussels 235.59.60) Joseph WURM (Materials Research) (Tel. Brussels 235.52.90) Herbert ALLGEIER (Aeronautics R&D) (Tel. Brussels 235.40.55)
Community budget:	499.5 million ECU
Programme duration:	1989-1992
Call for proposals:	12 May 1989; 9 June 1989 for aeronautics. Next call probably in first half 1990
Type of operation:	Shared-cost contracts
Reference document:	OJ L98 (1989)

INFORMATION AND COMMUNICATION MARKET

THE ESPRIT II PROGRAMME (DG XIII)

European Strategic Programme for Research and development in Information Technologies (ESPRIT)

Adopted in 1984, ESPRIT was conceived for a 10 year period with three main objectives: to help provide European IT industry with the technology base it needs to meet the competitive requirements of the 1990s, to promote European industrial cooperation in IT and to contribute to the development of internationally accepted standards.

For the second phase of ESPRIT (ESPRIT II) the sectors for support have been adapted to the rapid pace of technological development and consolidated into three sectors: Microelectronics and peripherals, Information processing Systems and IT Application Technologies. New emphasis is being placed on strengthening European capabilities in such areas as Application Specific Integrated Circuits (ASICS), high performance parallel processing computers and new office workstations, while ESPRIT II also includes a new component, Basic Research Actions, designed to complement the main industrial programme.

Programme Manager:	Ian COLLISSON (Tel. Brussels 236.20.67)
Community budget:	1 600 million ECU
Programme duration:	1988 — 1992
Call for proposals:	January 1990
Type of operation:	Shared-cost contracts
Reference document:	OJ L118 (1988)

THE RACE PROGRAMME (DG XIII)

Research and development in Advanced Communication in Europe (RACE)

RACE deals with the integrated broadband communications (IBC) of the future. It is designed to lay the foundations of the Community's communications infrastructure for the 1990s and into the 21st century, by combining the expertise of telecommunications researchers, manufacturers, administrations and broadcasting stations across European frontiers.

The programme covers IBC development and implementation strategies, IBC technologies and prenormative functional integration.

Contact Person:	Jürgen ROSENBAUM (Tel. Brussels 235.92.35)
Community budget:	550 million ECU
Programme duration:	June 1987 — May 1992

POSSIBLE SPIN-OFF FROM COLLABORATION BETWEEN INDUSTRY AND PARTICLE PHYSICS RESEARCH

Markus Nordberg, University of Helsinki (CERN)
Risto Orava, University of Helsinki

Abstract
Due to the demand of industrially produced technology in particle physics accelerator and detector systems, participation of industries has become an essential element in modern experimental physics.Out of this collaboration an interactive process with new technologies of high economical impact arise.
In this study possible spin-off areas are identified and some models for channeling technology transfer activities are suggested with a case-study of the University of Helsinki.

Introduction
Due to the demand for industrially produced technology in particle physics accelerator and detector systems, participation of industries representing areas such like electronics, special materials, communication and computer technologies has become an essential element in modern experimental physics.

Out of this interactive process, new technologies with high economical impact can arise; NMR-imaging, ion implantation, PET-scanning, high-efficiency energy storage, to name just a few. These are frequently called spin-offs, spill-overs or spin-outs describing the side-results of the primary research motivation.

In this article we identify possible spin-offs generated in experimental particle physic research centres, using CERN, the European Laboratory for Particle Physics, as a case-study.

Combining different motivations
While trying to identify possible spin-offs from any research and development work, the fundamental question is: what does the industry really need or want and what do the research laboratories have to offer in this respect? One has to bear in mind that the motivation of the industry differs significantly with that of a research centre like CERN. CERN is a basic research driven laboratory providing technological tools for the physicists in their quest for understanding the ultimate structure of the Universe. The industry, on the other hand, has a clear market-driven motivation.

Even though a research laboratory may create new technologies with a wide range of applications, it is usually not interested in transferring new innovations outside it's own needs.

Therefore high-potential market-driven spin-offs occur mostly in collaborative efforts where the industry sees the research laboratory as a "test-bench" for possible new components for their products and not so much as an "application spinner" of the particle physics R&D projects themselves.

There are a number of ways of combining these different perspectives inherent to industry and research. One could purely concentrate on existing commercial products (thus minimizing the implementation of new technological concepts by the research community) or on companies operating in that specific market (thus concentrating only on a limited amount of companies).
In this article our approach is first to attempt to identify the key technologies of the future with high economic impact and then see if and how these technologies are used today in a research laboratory like CERN. After that we suggest a method of cultivating spin-offs by using the activities of the Helsinki University as a case-study.

Emerging technologies of the future
The U.S. Department of Commerce published in 1987 a study identifying technologies with a high economic impact to the year 2 000 [1]. The study listed seven key technologies: advanced materials, electronics, automation, biotechnology, computing, medical technology and thin film technology. Since the benefits, applications and potential industrial users were indentified in this report as well, we will use it to illustrate an approach one could use in order to identify new spin-off areas from particle physics to industry.
We have added a fifth column, "used today by a HEP lab (CERN)", to give an example where the technologies in question are used today by a high energy particle physics laboratory (see Table 1.).

Out of seven identified key technology areas more than four are utilized by CERN today. By ranking them in economic importance (table 2, from the same study) one can see that they are mainly presented in groups A and B.

We conclude that the particle physics community does currently use and develop technologies with a high economical impact in the future.

Table 1
(SOURCE: EMERGING TECHNOLOGIES)

Technology	What does it do new or better?	Applied to what products or processes?	Used by what major industries?	Used today how by a HEP Lab (CERN)?
2. Electronics				
A. Advanced Microelectronics	Improved performance in speed,size	Semiconductor devices	Electronic & optical components & systems	Silicon detector ASIC-amplifiers(CMOS,GaAs)
	Improved magnetic properties	Information storage	Information processing	
	Higher efficiency photovoltaic conversion	Solar cells	Energy generation	"Hybrid photodiode" FADC
B. Optoelectronics	Improved performance in speed,size,capacity, and security	Electronic equipment, information processing	Communications & computers	Scintillating optical fibres
	Higher density information storage	Computer systems of all sizes	Computers	Fibre optic data links
C. Millimeter Wave Technology	When replacing radio systems it frees RF spectrum for other uses	Voice & data communication systems	Telecommunications carriers&corporate use for private circuits	HF sources RF cavities ?

784

Table 1
(SOURCE: EMERGING TECHNOLOGIES)

Technology	What does it do new or better?	Applied to what products or processes?	Used by what major industries?	*Used today how by a HEP Lab (CERN)?
1. Advanced Materials				
A Ceramics	Better high temperature strength-to-weight properties	Heat engine components, turbine blades, heat shields	Automotive & aircraft engines	Monolithic ceramics for fast pulsed magnets
	Better dielectric & optical properties	Electronic substrates, integrated optics	Electronic components	Ion Sources
B Polymer Composites	Higher strength-to-weight-ratio	Structural components	Aerospace,automotive, ind.const.	Insulating material for superconducting magnet coil & cables
	Design flexibility because of spatial asymmetry	Structural components	Aerospace,automotive,	Mechanical supports for delicate devices
C Metals	Improved strength& high-temperature performance	Structural components Superconducting components	Manufactured components	NbTi,NbSn3 in copper matrix (superconducting cables)
	Improved magnetic properties	Electro-magnetic equipment	Electrical machinery	Ferroelectric materials for electron emission

783

* = Column added by the authors

Table 1
(SOURCE: EMERGING TECHNOLOGIES)

Technology	What does it do new or better?	Applied to what products or processes?	Used by what major industries?	Used today how by a HEP Lab (CERN)?
4. Biotechnology				
A. Genetic Engineering	Improved diagnostic & therapeutic drugs	Health Service	Medicine, Pharmaceuticals	(Precision sensitive measurement techniques: silicon strip detectors?)
	Improved plants, pesticides & animal supplements	Food and pesticides	Agriculture Food processing	
	Neutralize pollutants	Environmental control processes	Chemical manufacturing & treatment	
B. Biochemical Processing	Improved control of chemical processes, outputs and yields	Chemical separations and reactions, biosensors	Chemical manufacturing	

Table 1
(SOURCE: EMERGING TECHNOLOGIES)

Technology	What does it do new or better?	Applied to what products or processes?	Used by what major industries?	Used today how by a HEP Lab (CERN)?
3. Automation				
A. Manufacturing	Flexible reconfiguration of production processes Integrated control of all production operations	All manufacturing processes	All Manufacturing	Particle acclerator control systems?
B. Business and Office Systems	Efficient information storage,retrieval & exchange	Networking, word processing & data base management	All organizations	Computer networks
C. Technical Services	Efficient high-volume information strorage, retrieval & exchange	Information retrieval & distribution, data base management, education & training	Financial services, electronic mail, telecommunications, professional service	Optical data strorage Automated cartridge library

Table 1
(SOURCE: EMERGING TECHNOLOGIES)

Technology	What does it do new or better?	Applied to what products or processes?	Used by what major industries?	Used today how by a HEP Lab (CERN)?
3. Medical Technology				
A. Drugs	Improved immunology and treatment	Health Services	Medicine, Pharmaceuticals	
B. Instruments & Devices	Improved diagnostics and therapeutic systems	Magnetic Resonance Imaging & CAT scanning radiation treatment	Medicine	Particle detectors (imaging chambers,MWPC, strip detectors...) Radiation sources

788

Table 1
(SOURCE: EMERGING TECHNOLOGIES)

Technology	What does it do new or better?	Applied to what products or processes?	Used by what major industries?	Used today how by a HEP Lab (CERN)?
5. Computing				
A. Computing Equipment	Faster, lower-cost computing	Information processing & computer control	Potentially all	On-line DAS (FASTBUS, VME,Futurebus,Transputer..)
B. Artificial Intelligence Techniques	Improved computer replication of human judgement	Information processing & computer control	All applications using computers	Lowel level triggers Particle track identification Accelerators control Robot remote control

787

TABLE 2

EMERGING TECHNOLOGIES RANKED BY ECONOMIC IMPACT

SYSTEM-LEVEL MARKETS ($ BILL)		
GROUP A (Highest)	>100	Advanced Materials; Composites Biotechnology; Genetic Engineering Electronics; Optoelectronics Electronics; Advanced Microelectronics Computing; Computing equipment Automation; Manufacturing
Group B	10-100	Automation; Business and Office Systems Biotechnology; Biochemical Processing Medical Technology; Drugs Advanced Materials; Ceramics Automation; Technical Services Computing; Artificial Intelligence Tech. Medical Technology; Devices
Group C	1-10	Thin Layer Technology; Membranes Advanced Materials; Metals Thin Layer Tech.; Surfaces & Interfaces Electronics; Millimeter Wave Technology

Source: Emerging Technologies

790

Table 1
(SOURCE: EMERGING TECHNOLOGIES)

Technology	What does it do new or better?	Applied to what products or processes?	Used by what major industries?	Used today how by a HEP Lab (CERN)?
7. Thin Layer Technology (for semiconductors, see Electronics)				
A. Surface & Interfaces	Improved control and yield of chemical reactions	Chemical catalysis	Chemical manufacturing of food processing	Titanium films onto ceramics
	New electronic & optical properties	Semiconductor devices, surface modifications and coatings	Electronic components, computers	Thin-metal (eg. Al, MgF_2) coating of mirrors, Wavelenght shifters, Photocathodes
B. Membranes	New chemical properties, better chemical separation techniques	Chemical separations	Chemical manufacturing, food processing	

780

The question still remains; how can such spin-offs be created in practise? To try to answer that, we need to take a look at the technology transfer mechanisms in particle physics.

Technology transfer mechanisms in particle physics

By technology transfer we mean a process in which technical information flows from one environment to another (for a more detailed definition, see e.g. reference 2,3).
Like in many other fields, in particle physics technology transfer is a two-way approach:

- from industry to particle physics (e.g. industrial manufacturing of components for accelerators and detectors)
- from particle physics to industry (e.g. spin-offs)

In this article, we will concentrate on the latter.

For effective technology transfer one requires at least:

- imaginative research scientists who are constantly looking for new and more efficient technological tools (like software, electronics, computers, materials science etc.) to carry out first-rate experimental physics.
  This naturally requires good contacts and recognized experience in a user-laboratory like CERN which acts as the common source of new technology
- people who understand the potential applications of the new tools used by the scientific community
- people who know what to do with the new ideas; how to organise collaboration with the right partners and get the projects started.
  This requires good contacts to the industry and a good understanding of the market trends
- an appropriately commercially and technologically oriented environment, e.g. a science park in the vicinity of a university
- people who can commit themselves 100% on these activities

Case-study: the University of Helsinki

The Department of High Energy Physics of University of Helsinki joined one of the LEP-experiments (DELPHI) at CERN in 1983. In 1987 the activity of the group was divided into two units;

- physics and hardware responsibilities at the University
- research and development (R&D) work for future experiments and industrially oriented spin-off activities at the Otaniemi Science Park.

The Otaniemi-unit carries out product-oriented R&D in collaboration with the industry. The aim is to contribute in future physics experiments

while finding new applications for the know-how gained in the process. The unit is financially self-sustained in the sense that the infra-structure of it's activities are covered by the industrial R&D-contracts.

The philosophy of the activities is illustrated in figure 1.

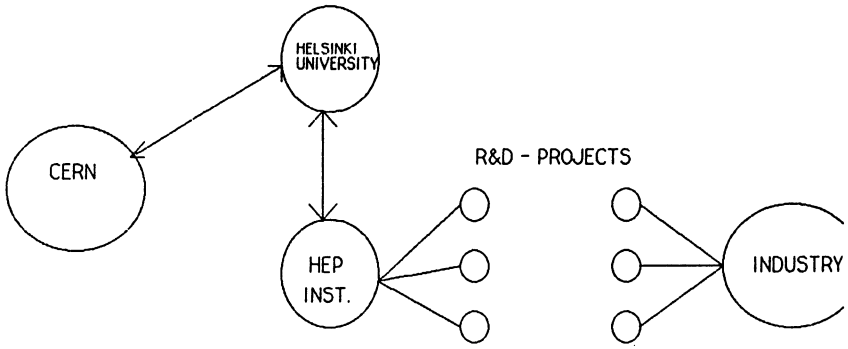

Seen from CERN or a research laboratory, the dominating motivation is basic research. On the other hand, seen by the industry, the motivation is market-driven (through the special R&D unit,which in the near future will transform into a separate high energy physics institute).

The Otaniemi-unit has and is carrying out a number of spin-off projects, such like:

- automation of fibre analysis for e.g. paper industry
- automation of computer monitors manufacturing
- designing and manufacturing of automatic gas calibration unit for gas chromatographs
- radiation sensors for paper thickness measurement for paper industry

It is intended in the future to form commercial-based joint venture companies for carrying out the R&D projects. In this model, the Otaniemi unit will share the equity with industrial partners having a buy-out option at a later stage where the presence of the research comminity is no longer necessary. This is felt necessary to ensure adequate interest from all parties involved.

Conclusions

While collaboration between the particle physics community and industry is beneficial for both parties and some key-spin-off areas can be identified, the following closing remarks should be made for all this to

work in practise, as well.
First, the research community should clearly know what it wants from the industry.
Second, the industry should fully understand that the research community is not primarly interested in the spin-offs themselves but that is willing to help creating them.
Third, priorities should be combined in a way to ensure a well-defined common goal thus avoiding possible conflict of interests.

References

1. The Status of Emerging Technologies: An Economic/Technological Assessment to the Year 2000.
U.S. Department of Commerce, June 1987
2. Rogers E M, The Diffusion of Innovation, Free Press, Glencoe, Illinois 1962
3. Jolly J A, Creighton J W, George P A, Technology Transfer Process Model and Annotated Selected Bibliography, Naval Postgraduate School Monterey, California 1978